

Chemo-mechanics of epoxy-asphalt

Apostolidis, P.

DOI

[10.4233/uuid:ec7eedb6-97a1-43a0-b7d9-46e78d0cd046](https://doi.org/10.4233/uuid:ec7eedb6-97a1-43a0-b7d9-46e78d0cd046)

Publication date

2022

Document Version

Final published version

Citation (APA)

Apostolidis, P. (2022). *Chemo-mechanics of epoxy-asphalt*. [Dissertation (TU Delft), Delft University of Technology]. <https://doi.org/10.4233/uuid:ec7eedb6-97a1-43a0-b7d9-46e78d0cd046>

Important note

To cite this publication, please use the final published version (if applicable).
Please check the document version above.

Copyright

Other than for strictly personal use, it is not permitted to download, forward or distribute the text or part of it, without the consent of the author(s) and/or copyright holder(s), unless the work is under an open content license such as Creative Commons.

Takedown policy

Please contact us and provide details if you believe this document breaches copyrights.
We will remove access to the work immediately and investigate your claim.

Chemo-mechanics of epoxy-asphalt

P. APOSTOLIDIS

Copyright © 2022 by Panos Apostolidis

All rights reserved. No part of the material protected by this copyright notice may be reproduced or utilized in any form or by any means, electronic or mechanical, including photocopying, recording or by any information storage and retrieval system, without the prior permission of the author.

Chemo-mechanics of epoxy-asphalt

Dissertation

for the purpose of obtaining the degree of doctor

at Delft University of Technology

by the authority of the Rector Magnificus Prof.dr.ir. T.H.J.J. van der Hagen

chair of the Board for Doctorates

to be defended publicly on

Wednesday 8 June 2022 at 17:30 hours

by

Panagiotis APOSTOLIDIS

Master of Science in Civil Engineering

Delft University of Technology, the Netherlands

born in Drama, Greece

This dissertation has been approved by the
promoters: Prof.dr.ir. S.M.J.G. Erkens and Prof.dr. A. Scarpas
copromotor: Dr. X. Liu

Composition of doctoral committee:

Rector Magnificus	chairperson
Prof.dr.ir. S.M.J.G. Erkens	Delft University of Technology, promotor
Prof.dr. A. Scarpas	Delft University of Technology, promotor
Dr. X. Liu	Delft University of Technology, copromotor

Independent members:

Prof.dr. A. Bhasin	University of Texas at Austin
Prof.dr. M.E. Kutay	Michigan State University
Prof.dr. L. Wang	Virginia Polytechnic Institute and State University
Prof.dr. S.J. Picken	Delft University of Technology

Reserve members:

Prof.dr.ir. M.A.N. Hendriks	Delft University of Technology
-----------------------------	--------------------------------

This research was funded by the Provinces of North Holland and Gelderland.

ISBN 978-94-6366-546-9

An electronic version of this dissertation is available at <http://repository.tudelft.nl/>.

Acknowledgments

I first owe my sincere gratitude to Prof. Tom Scarpas, who offered me the opportunity to conduct research at Delft University of Technology. Tom entrusted me to become a member of the group and provided me with the frame to develop myself. It is my honor to have been his student.

In the course of the doctoral program, I wish to thank Prof. Sandra Erkens and Dr. Xueyan Liu, who provided epoch-making feedback and kindly facilitated the completion of the present thesis. Sandra and Xueyan also followed the study with practical-oriented support, for which they are appreciated.

Special thanks go out to all my colleagues in the vibrant Pavement Engineering group, in particular Cor Kasbergen, Kumar Anupam, Katerina Varveri, Ruxin Jing, Peng Lin, Zhaojie Sun, and former colleagues Sayeda Nahar, Greet Leegwater, Santosh Srirangam, Tianchi Tang, Haopeng Wang and Hong Zhang, with whom I have had the pleasure of fruitful conversations. I am also indebted to Martin van de Ven for his invaluable contributions from the very beginning. The management support of Claudia Baltussen and Jacqueline Barnhoorn and the laboratory assistance of Michéle van Aggelen and Marco Poot are recognized.

The Provinces of North Holland and Gelderland are thankfully acknowledged for the grant, by which this program could be financed. By saying that, special thanks go to Dr. Paul Waarts, who believed in the group and continues to support it. The active involvement of Robbert Naus of Dura Vermeer Groep NV and John Bors of ChemCo Systems Inc also ensured the successful implementation of the program in the Netherlands, for which they are acknowledged.

In respect of the collaborations developing internationally on the topic, I would like to thank Dr. Jack Youtcheff of the Turner-Fairbank Highway Research Center, Federal Highway Administration. Jack also allowed me to interact with his team and, as such, the stimulating discussions with Dr. Michael Elwardany, Dr. Adrian Andriescu and Dr. David Mensching deserve special mention.

I finally want to thank my family. Not much of these would have been possible without you.

Panos Apostolidis
Delft, June 2022

Contents

TABLE OF CONTENTS

Acknowledgments	i
Contents	iii
1 Introduction	1
1.1 Background and Problem Statement	2
1.2 Thesis Research Objectives	3
1.3 Thesis Outline	3
1.4 References.....	6
2 Phase Behavior of Epoxy-Asphalt Binders.....	7
2.1 Introduction.....	8
2.2 Thermodynamics of Binary Blends.....	9
2.3 Phase Behavior of Binary Blends.....	12
2.4 Solubility of Binary Blends	15
2.4.1 Solubility of epoxy polymers	16
2.4.2 Solubility of epoxy polymers in asphalt binders.....	18
2.5 AFM Morphology of Epoxy-Asphalt Binders	20
2.5.1 Materials and preparation.....	20
2.5.2 Sample preparation and AFM setting.....	22
2.5.3 Assessment of microstructural characteristics	22
2.6 Summary.....	29
2.7 References.....	29
3 Determination of Curing Kinetics with Differential Scanning Calorimetry	37
3.1 Introduction.....	38
3.2 Curing Kinetics	39
3.3 Differential Scanning Calorimetry	42
3.4 Calorimetric Measurements of Epoxy-Asphalt Binders	43
3.4.1 Materials and preparation.....	43
3.4.2 Calorimetry setting.....	44
3.4.3 Temperature linear calorimetric measurements	45
3.4.4 Temperature modulated calorimetric measurements.....	49
3.5 Summary.....	53
3.6 References.....	54

4 Simulation of Curing Induced Hardening of Epoxy-Asphalt Binders.....	57
4.1 Introduction.....	58
4.2 Changes due to Curing	58
4.2.1 Glass transition temperature	61
4.2.2 Viscosity	62
4.3 Modeling of Chemo-Rheology	63
4.3.1 Model implementation	64
4.3.2 Influence of activation energy and reaction rate on viscosity development	66
4.3.3 Influence of temperature and reaction extent on viscosity development	66
4.4 Summary.....	69
4.5 References.....	69
5 Simulation of Diffusion-Reaction Phenomena in Curing Epoxy-Asphalt Binders.....	71
5.1 Introduction.....	72
5.2 Mass Transport due to Curing.....	72
5.3 Diffusion-Reaction Model	73
5.3.1 Model implementation	76
5.4 Mutual Diffusion-Reaction Model	79
5.4.1 Model implementation	81
5.5 Summary.....	85
5.6 References.....	86
6 Oxidative Aging of Epoxy-Asphalt.....	87
6.1 Introduction.....	88
6.2 Chemistry of Oxidative Aging in Asphalt Binders	88
6.2.1 Functional groups and fractions of oxidative aging.....	88
6.2.2 Kinetics of oxidative aging.....	90
6.3 Materials and Methods	91
6.3.1 Binders, filler and mastics	91
6.3.2 Fourier transforms infrared spectroscopy measurements.....	92
6.3.3 Dynamic shear rheometer measurements.....	94
6.3.4 Differential scanning calorimetry measurements	94
6.4 Chemical Compositional Changes	96
6.4.1 Kinetics parameters of carbonyls formation.....	101
6.5 Rheological Changes	104
6.6 Glass Transition Changes	110
6.7 Summary.....	117

6.8 References.....	119
7 Laboratory Tests on Epoxy modified Asphalt Concrete.....	125
7.1 Introduction.....	126
7.2 Epoxy-Asphalt as Surfacing Pavement Material.....	126
7.2.1 Laboratory experience.....	126
7.2.2 Field trials experience	131
7.3 Epoxy-Asphalt as Tack Coat.....	133
7.3.1 Laboratory experience.....	134
7.3.2 Recommendations for field trials.....	136
7.4 Summary.....	137
7.5 References.....	138
8 Conclusions	141
8.1 Conclusions.....	142
Summary.....	145
Curriculum Vitae.....	146

1

Introduction

1.1 Background and Problem Statement

Many governments have devoted significant resources to the deployment of high-quality roadway networks which subsequently demand adequate maintenance. Nowadays, most of national road budgets are spent on maintenance of existing roadways as the need for repair is more frequent. Regular repair operations, such as patching and sealing, implies increased maintenance costs for the road authorities and the inconvenience for road users due to the temporary disruption of normal traffic flows. Within this framework, the initial construction cost of a roadway pavement is often surpassed by the cost of its maintenance and reconstruction leading to very high life cycle costs.

In this context, roadway pavements of enhanced longevity would be expected to withstand very long-term traffic as well as varying environmental conditions reducing in this way the major maintenance needs. Considering also the adoption of long-term contracts by road authorities, long-life pavements have started to attract the interest of road contractors all over the world. New and relatively new binders specially designed to produce long-life pavements have been proposed to minimize the regular maintenance and reconstruction operations justifying their high initial costs. Among others, one quite promising technology is the epoxy modified asphalt, or epoxy-asphalt, which is able to lower the fracture sensitivity of pavement materials (Youtcheff et al., 2006; Kang et al., 2010 & 2015; Luo et al., 2015; Gong et al., 2019; Apostolidis et al., 2019; Chen et al., 2020), and have shown high aging resistance (Herrington and Alabaster 2008).

Historically, epoxy-asphalt has been applied as a premium surfacing solution for airfields and steel deck bridges (Lu & Bors 2015). While the epoxy-asphalt have been introduced in asphalt binders as a high-performance solution on high deflection bridges since the 1970s (San Mateo-Hayward Bridge in 1967 and San Francisco-Oakland Bay Bridge in 1969), recent studies have suggested the industrial transfer of this technology to roadway pavements under an OECD program (International Transport Forum 2017). Nevertheless, the primary concern that delay the wide use of this technology is the high initial material cost associated with the unknown chemistry of commercially available epoxy-asphalt binders. Although various epoxy resins have been used to modify asphalt binders, few epoxy products applicable for asphalt binders exist. Thus, an in-depth understanding of the epoxy modification mechanism in asphalt is needed to formulate durable epoxy-asphalt binders.

Another factor that prohibits the broader use of epoxy-asphalt is that contractors could face high risks of construction failures, because of the uncontrolled irreversible curing. For instance, the paving mixture may segregate due to the low viscosity when the curing of epoxy-asphalt is relatively slow (International Transport Forum 2017). Moreover, if the production and transport temperature of epoxy-asphalt is too high, then the material would cure before paving. One-step delay through the in-plant production or the mixture transport to the field may lead to undesired over-hardening causing paving, shaping and compaction issues. Therefore, it is critical to elucidate the curing mechanism of the epoxy-asphalt under certain energy conditions to avoid complications through the whole pavement manufacturing chain.

Finally, and despite the significant field data and performance histories of using epoxy-asphalt materials internationally, quantitative information on the oxidative aging resistance of these materials is still missing to prove their enhanced longevity benefits. Until now, predictions on the long-term material performance were with single-point lab data sets on the time scale at 130°C (Apostolidis et al., 2019), much higher than the actual pavement temperatures.

1.2 Thesis Research Objectives

The addition of polymers to asphalt binders can result in materials of inferior properties. Thermoplastic but mostly thermosetting polymers may not mix homogeneously in asphalt binders leading to immiscible or partially miscible binders, which are mostly phase-separated materials. The phase-separated epoxy-asphalt binders can become brittle and thus more prone to cracking, leading the pavements ultimately to fail. However, only a few proprietary protected epoxy products are applicable in asphalt binders, and thus, the knowledge of incorporating chemistry to develop miscible epoxy-asphalt binders remains unknown. For this to be the case, this thesis aims to provide a fundamental approach to elucidate the chemical and physical processes that bear miscible epoxy-asphalt binders.

Vital role in implementing the thermosetting epoxy-asphalt binders also plays the curing. To obtain fundamental insights into the material curing, multi-physics models and experimental methods mainly adapted by the polymer science are considered in this research to identify and assess the curing-induced changes of epoxy-asphalt. The development of physical and rheological properties that reflect the material workability are determined by laboratory experiments and used as input to multi-physics simulations.

As the ultimate scope of implementing the epoxy-asphalt is to increase the longevity of pavements, the oxidation-induced changes of epoxy-asphalt materials as a function of time are evaluated as well in this research to prove the high aging resistance of such materials for wearing surface courses. Within the same framework, emphasis is also given on the effect of epoxy-asphalt on the durability and mechanical performance characteristics of an asphalt concrete mix.

Details about the outline of the thesis are provided in the next section.

1.3 Thesis Outline

The thesis is composed of eight **chapters**.

In **Chapter 2**, the thermodynamic considerations regarding the miscibility of binary polymer blends are discussed in an endeavor to describe the phase behavior phenomena potentially operative in epoxy-asphalt binders. The objective of this **chapter** is to elucidate the mechanism that leads to phase separated binders and to understand the chemistry that bear miscible and homogeneous epoxy-asphalt binders. Experimental evidence of the microstructure morphology of a non-commercial epoxy binder formulation will be analysed in an atomic force microscopy (AFM) and compared with a proprietary protected epoxy binder.

In **Chapter 3**, the use of a differential scanning calorimetry (DSC) is discussed to evaluate the curing of epoxy-asphalt binders. The DSC analyses will be performed to asphalt binders

modified with various types of epoxy formulations to understand the relationship between the processing (e.g., during in-plant production and in-field construction of asphalt pavements) and the properties of studied binders. The determination of optimum curing conditions based on calorimetric measurements can guide the asphalt processing technologies to avoid the uncontrolled curing of epoxy-asphalt systems at large.

Since the epoxy-asphalt binders are thermosetting materials, it is of great importance to understand the phenomena that are involved to build-up their rheological properties during curing. Even though a lot of research has been performed on epoxy-asphalt the last decade, focus was given only on the material response after curing. In **Chapter 4**, the curing phenomena that lead to the formation of epoxy binders with certain rheological characteristics are discussed. In the same **chapter**, focus will be given also on a prediction model to simulate the thermo-hardening material behaviour. Within the same framework, the inter-diffusion phenomena that take place because of the chemical interfacial interactions of the two reactive components are explored in the **Chapter 5**. Two different models are proposed and tested in a multi-physics software and comparison of these two is performed to assess their effect on simulating the interfacial reactions.

In previous **chapters**, the impact of epoxy on asphalt binders is assessed providing fundamental understanding on the phase behavior and curing phenomena under certain energy conditions. Quantified knowledge of the oxidation mechanism of epoxy-asphalt is also needed for the reason discussed above. In **Chapter 6**, emphasis will be given on the impact of oxidation on chemical composition, physical and rheological characteristics of epoxy-asphalt materials. The oxidation kinetic parameters will be determined considering the carbonyls as the aging index in the studied epoxy and asphalt materials offering reliable predictions of the long-term performance of epoxy-asphalt pavements. Because the oxidative aging is accompanied by stiffening and embrittlement, Dynamic Shear Rheometer (DSR) and DSC studies have been performed to assess the oxidation-induced compositional dependence of the epoxy-asphalt materials.

Chapter 7 provides insight and recommendations for the large-scale surfacing application of an epoxy-asphalt concrete mix designed in the laboratory. The potential use of epoxy binder as tack coating will be explored as well by evaluating the interface shear strength of two-layer epoxy-asphalt concrete mix samples for different tack coats.

Finally, **Chapter 8** presents a summary of findings presented throughout the thesis.

Fig. 1.1 demonstrates the schematic flow diagram of the current work.

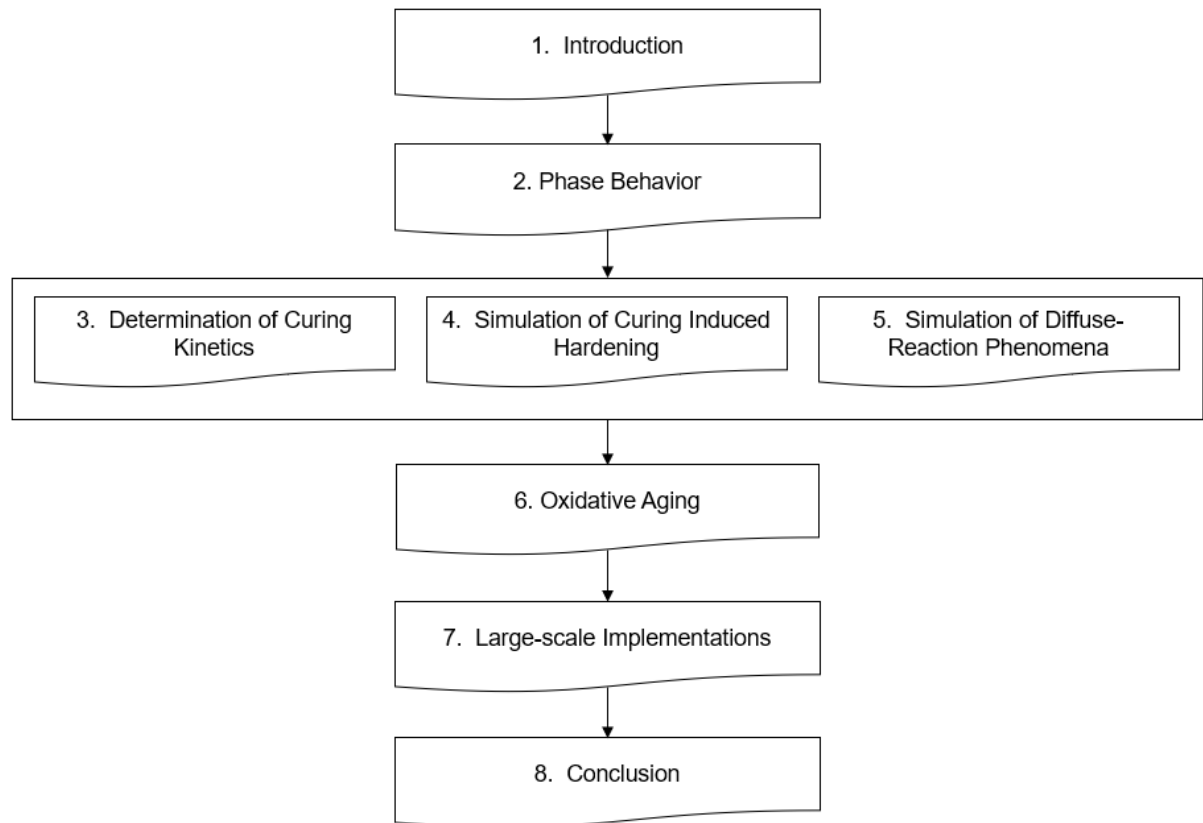


Figure 1.1 Schematic flow diagram of thesis outline.

1.4 References

- Apostolidis, P., X. Liu, S. Erkens, A. Scarpas. Evaluation of Epoxy Modification in Bitumen. *Construction and Building Materials* 208, 2019, pp. 361-368.
- Chen, C., W.O. Eisenhut, K. Lau, A. Buss, J. Bors. Performance Characteristics of Epoxy Asphalt Paving Material for Thin Orthotropic Steel Plate. *International Journal of Pavement Engineering* 21(3), 2020, pp. 397-407.
- Gong, J., Y. Liu, Q. Wang, Z. Xi, J. Cai, G. Ding, H. Xie. Performance Evaluation of Warm Mix Asphalt Additive Modified Epoxy Asphalt Rubbers. *Construction and Building Materials* 204, 2019, pp. 288-295.
- Herrington, P., D. Alabaster. Epoxy Modified Open-graded Porous Asphalt. *Road Materials and Pavement Design* 9(3), 2008, pp. 481-498.
- International Transport Forum. *Long-Life Surfacing for Roads: Field Test Results*. ITF Research Reports, OECD, Paris, France, 2017.
- Kang, Y., Z. Chen, Z. Jiao, W. Huang. Rubber-Like Thermosetting Epoxy Asphalt Composites exhibiting Atypical yielding Behaviors. *Journal of Applied Polymer Science* 116, 2010, pp. 1678-85.
- Kang, Y., M. Song, L. Pu, T. Liu. Rheological Behaviors of Epoxy Asphalt Binder in Comparison of Base Asphalt Binder and SBS Modified Asphalt Binder. *Construction and Building Materials* 76, 2015, pp. 343-350.
- Lu, Q., & J. Bors. Alternate Uses of Epoxy Asphalt on Bridge Decks and Roadways. *Construction and Building Materials* 78, 2015, pp. 18-25.
- Luo, S., Q. Lu, Z. Qian. Performance Evaluation of Epoxy modified Open-graded Porous Asphalt Concrete. *Construction and Building Materials* 79, 2015, pp. 97-102.
- Youtcheff, J., N. Gibson, A. Shenoy, G. Al-Khateeb. The Evaluation of Epoxy Asphalt and Epoxy Asphalt Mixtures. *Proceedings of the Canadian Technical Asphalt Association* 51, 2006, pp. 351-368.

2

Phase Behavior of Epoxy-Asphalt Binders

2.1 Introduction

The development of blends by mixing two or more polymers or polymer-like materials is an effective and relatively efficient method for preparing asphalt blends with improved mechanical properties and desired functions. Nevertheless, due to the thermodynamics of mixing, the majority of polymer blends, and thus systems like epoxy-asphalt binders, are immiscible (i.e., they do not form a homogeneous system). Differences in the chemical structure, molecular weight and polarity, and subsequently the solubility parameters, cause immiscible blends (Flory 1942; Huggins 1941). Partially miscible blends, as the immiscible one, are phase separated systems of heterogeneous structures. As phase separated blends are characterized by weak interfacial adhesion, the interfaces become the weak boundary between the polymer phases, leading mostly to inferior mechanical properties. To overcome this shortcoming, heterogeneous structures must be tuned to produce miscible systems.

The use of polymers like epoxy resins in asphalt binders to develop long-lasting pavement structures have gained increasing interest over the last years (Youtcheff et al., 2006; Herrington & Alabaster 2008; Lu & Bors 2015; International Transport Forum 2017). Unlike the pure epoxy thermosets which are inherently brittle once they are fully cured, epoxy-asphalt binders cure to rubbery systems of enhanced fracture toughness. Improved miscibility between epoxy resins and asphalt binders at microstructural level determines the long-term performance of epoxy-asphalt binders. In immiscible blends, the properties differ so much across the boundaries between the different phases that will probably lead to stress concentration on the interfaces, initiating micro-cracks. Once a micro-crack develops, the interfacial characteristics are insufficient to ensure the load transfer from one phase to another leading to the micro-crack propagation along interfaces. Therefore, the morphology at micro-level is normally employed in the characterization of polymer and asphalt binders with using various microscopy techniques.

Epoxy resins are immiscible in asphalt binders (Laval & Quivoron 1973; Laval & Brule 1974). Evidence of the immiscible phase behaviour of these materials has been reported by using techniques such as laser scanning confocal (Yin et al., 2015; Liu et al., 2017; Jiang et al., 2018; Sun et al., 2018; Gong et al., 2019) and fluorescence (Wei & Zhang 2012; Kang et al., 2015; Xu et al., 2018; Cong et al., 2018) microscopy. However, high-resolution microstructural analyses at the interface of epoxy polymers with asphalt binders have not been done yet.

The morphology of a binary polymer blend, or blend which consists of two polymers, is determined by phase separation occurring through the curing process. The morphology depends on the miscibility between the two types of polymers, the processing conditions, and others. Practically, the majority of polymer pairs are immiscible or partly miscible for thermodynamical reasons. Therefore, the thermodynamic considerations regarding the polymer miscibility will be discussed first in this **chapter**. The basic thermodynamic considerations of polymers' miscibility will be introduced including the phase behavior in heterogeneous polymer blends as discussed by Stary 2015. Then, experimental evidence of the surface morphology of different epoxy formulations in asphalt binder will be provided by conducting analyses in an atomic force microscopy (AFM).

2.2 Thermodynamics of Binary Blends

At a constant pressure and temperature, the thermodynamic equilibrium of a binary polymer blend corresponds to the minimum of Gibbs free energy of mixing (ΔG_{mix}), which is derived by Flory and Huggins theory for blends using a simple lattice model (Flory 1941; Huggins 1941; Flory 1953).

For a binary polymer blend, which consists of a liquid phase β with component B and an additional reactive liquid phase α with component A , the thermodynamic equilibrium is determined by the ΔG_{mix} . The ΔG_{mix} describes the energy difference between energy states as

$$\Delta G_{mix} = \Delta H_{mix} - T\Delta S_{mix} \quad (2.1)$$

where T is the absolute temperature [K], ΔS_{mix} is the change in entropy of mixing [$\text{J mol}^{-1} \text{K}^{-1}$], and ΔH_{mix} is the change in enthalpy of mixing [J mol^{-1}], which is the heat consumed ($\Delta H_{mix} > 0$) or released ($\Delta H_{mix} < 0$) during the mixing at constant pressure. To support miscibility and to form a homogeneous blend ($\Delta G_{mix} < 0$), the heat should be released during the mixing ($\Delta H_{mix} < 0$).

By assuming a binary polymer blend which consists of components A and B , the enthalpy of mixing (ΔH_{mix}) is expressed as

$$\Delta H_{mix} = \frac{V}{v_r} z w_{AB} \phi_A \phi_B \quad (2.2)$$

where V is the total volume of the system, v_r is the volume of the interacting unit (e.g., molecule), z is the coordination number (i.e., the number of neighbors of each interacting unit), w_{AB} is the internal interaction energy between components A and B , and ϕ_A and ϕ_B are the volume fractions of components A and B , respectively.

The internal interaction energy (w_{AB}) of the binary polymer blend can be defined as

$$w_{AB} = \frac{1}{2}(\varepsilon_{AA} + \varepsilon_{BB}) - \varepsilon_{AB} \quad (2.3)$$

where ε_{AB} is the contact energy (cohesive energy density) between components A and B (Flory 1953).

The interaction parameter (χ), or the interaction strength, is the ratio of the interaction energy and thermal energy and is expressed as

$$\chi = \frac{z w_{AB}}{kT} \quad (2.4)$$

where k is the Boltzmann constant. The interaction parameter is dimensionless and determines the change of enthalpy of each interacting unit (e.g., molecule or segment). In polymer blends, the interaction parameter depends on the temperature, composition and molecular weight of reactive components, and can be determined experimentally using the solubility parameter concept (Hilderbrand & Scott 1964), which will be discussed later.

By inserting **Eq. 2.4** into **Eq. 2.2**, the enthalpy of mixing (ΔH_{mix}) is expressed as

$$\Delta H_{mix} = kTV \frac{\chi}{v_r} \varphi_A \varphi_B \quad (2.5)$$

As mentioned earlier, the entropy corresponds to the randomness degree in the blend and can be determined using the Flory-Huggins lattice approach. As the entropy of pure components is assumed to be zero, the entropy of mixing (ΔS_{mix}) can be determined from the Boltzmann relationship as

$$\Delta S_{mix} = k \ln (\Omega) \quad (2.6)$$

where Ω is the total number of possible distinguishable space arrangements of N molecules and/or connected segments in the lattice. In this case, N is equal to the total volume of the system (V) and this represents also the total number of cells in the system. For a blend consisting of N_A molecules of component A and N_B molecules of component B ,

$$\Omega = \frac{N!}{N_A! N_B!} \quad (2.7)$$

and by using Stirling's formula ($\ln N! = N \ln N - N$) (Abramowitz & Stegun 2002), the entropy of mixing can be defined as

$$\Delta S_{mix} = -k(N_A \ln (\omega_A) + N_B \ln (\omega_B)) \quad (2.8)$$

where ω_A and ω_B are the molar fractions of components A and B , respectively.

Moreover, the parameters x_A and x_B determines the number of segments of components A and B having a volume equal to the volume of a cell (V_{cell})

$$x_A = \frac{V_A}{V_{cell}} = \frac{V_A N}{V} \quad (2.9)$$

and

$$x_B = \frac{V_B N}{V}$$

where V_A and V_B are the volume of components A and B , respectively. Assuming that one cell is occupied by one monomer unit, then x_A and x_B are the degrees of conversion. The degree of conversion is the number of monomer units in a macromolecule or polymer molecule.

Until now, it has been assumed that the molecule sizes of both components are equal (or of the same volume) and one cell is occupied by one molecule, which is reasonable for compounds of low molecular weight. Nevertheless, this assumption is not applicable to polymer blends, as the long macromolecules of polymers are much larger than a cell volume and thus one molecule will occupy more than one cell in the lattice.

Fig. 2.1 illustrates schematically a mix of low molecular weight solvents, a polymer solution and a polymer blend, respectively, and the volume fraction of two reactive components was assumed to equal (e.g., $\varphi_A = \varphi_B = 0.5$). For the lattice corresponding to the mix of solvents

(**Fig. 2.1a**), $N_A = N_B = 50$ and thus $\Omega = 10^{30}$ (10^{30} possible combinations). For the polymer solution (**Fig. 2.1b**), $N_A = 50$, $N_B = 5$ and thus $\Omega = 10^{16}$ (10^{16} possible combinations) and **Fig. 2.1c** illustrates a polymer blend with $N_A = 10$, $N_B = 5$ and thus $\Omega = 10^3$ (10^3 possible combinations). The addition of solvent molecules in a system like the depicted in **Fig. 2.1** could increase the randomness in the blend and consequently the entropy.

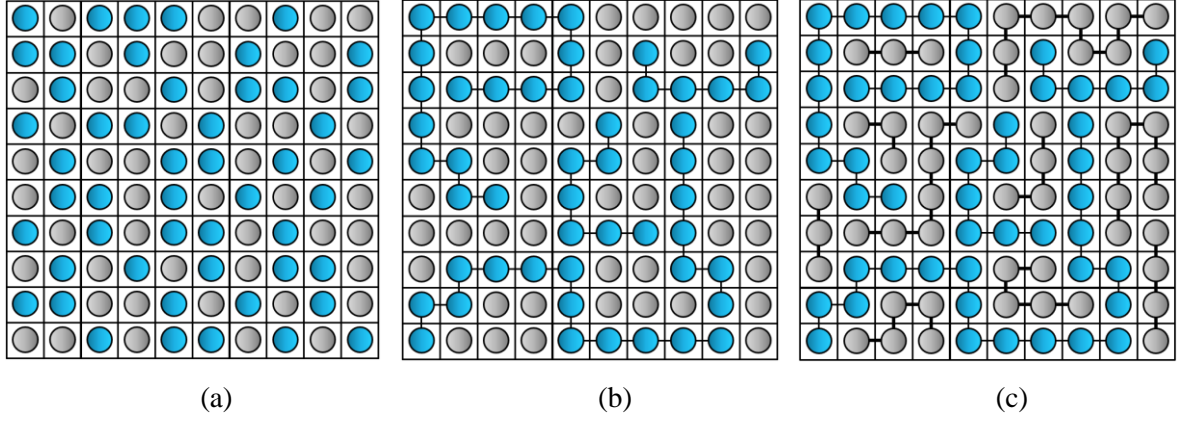


Figure 2.1 Schematic representation of a spatial arrangement of the lattice with random mixing of (a) two types of spheres (10^{30} possible combinations), (b) polymer and solvent (10^{16} possible combinations) and (c) two types of polymer chain (10^3 possible combinations).

When the number of molecules is not equal to the number of cells occupied by a component, the molar fractions in **Eq. 2.8** are substituted by the volume fractions as

$$\varphi_A = \frac{V_A N_A}{V}$$

and

$$\varphi_B = \frac{V_B N_B}{V}$$
(2.10)

After this substitution, and using **Eq. 2.9** or **Eq. 2.10**, the entropy of mixing in polymer blends becomes

$$\Delta S_{mix} = -kV \left(\frac{\varphi_A}{V_A} \ln(\varphi_A) + \frac{\varphi_B}{V_B} \ln(\varphi_B) \right)$$

or

$$\Delta S_{mix} = -kN \left(\frac{\varphi_A}{x_A} \ln(\varphi_A) + \frac{\varphi_B}{x_B} \ln(\varphi_B) \right)$$
(2.11)

The above discussed derivations of ΔH_{mix} and ΔS_{mix} are the parts of the Flory-Huggins theory that enable the determination of the ΔG_{mix} in polymer blends. By combining **Eq. 2.5** and **Eq. 2.11**, the equation of the Flory-Huggins theory can be expressed as

$$\Delta G_{mix} = kTV \left(\frac{\varphi_A}{V_A} \ln(\varphi_A) + \frac{\varphi_B}{V_B} \ln(\varphi_B) + \frac{\chi}{v_r} \varphi_A \varphi_B \right)$$
(2.12)

or by assuming that $v_r = V_{cell}$

$$\Delta G_{mix} = kTV \left(\frac{\varphi_A}{x_A} \ln (\varphi_A) + \frac{\varphi_B}{x_B} \ln (\varphi_B) + \chi \varphi_A \varphi_B \right) \quad (2.13)$$

where v_r is the volume of a chain segment and V_i is the volume of a macromolecule.

At a fixed concentration in unreacted blends, changes in **Eq. 2.13** are induced only by temperature variations and are limited to the entropic contribution, while enthalpy remains unaffected (Munk 1989). Nevertheless, through the curing of polymer blends, the ΔG_{mix} is controlled by the degree of conversion (x). As mentioned earlier, the term that drives the miscibility of blends is the ΔH_{mix} , which should be negative ($\Delta H_{mix} < 0$) to cause a negative ΔG_{mix} (Flory 1941). First, the two terms of ΔS_{mix} are negative and, thus, are favourable for mixing. As the molecular weight of the macromolecules rises, the number of possible spatial arrangements in the lattice decreases, leading to a lower ΔS_{mix} (**Eq. 2.11**).

2.3 Phase Behavior of Binary Blends

Phase diagrams, which are formed on the basis of the interaction parameter χ and the composition, provide a convenient way to illustrate the phase behaviour of heterogeneous blends. Two typical phase diagrams of binary blends are shown in **Fig. 2.2**. **Fig. 2.2a** indicates the dependence of ΔG_{mix} on φ_A as computed by the Flory-Huggins equation for a symmetric binary blend ($x_A = x_B = x$). In **Fig. 2.2b**, the curves are shown for different values of χx (asymmetric blends) as well.

Particularly, the ΔG_{mix} , which is a function of composition (φ_A), is negative with a minimum at $\varphi_A=0.5$ as shown in **Fig. 2.2a**. This means that miscibility occurs over the whole concentration range. Moreover, a change can be observed in the shape of curves for χx above a certain critical value (e.g., $\chi x = 2.5$), where a maximum rather than a minimum emerges at $\varphi_A = 0.5$. For very high positive χx values, the ΔG_{mix} is higher than zero over the whole composition range and the blend is immiscible. For asymmetric blends, or systems with different degrees of conversion of individual components ($x_A \neq x_B$), the concentration dependence of the ΔG_{mix} loses its symmetry and the positions of the extremes are shifted to lower concentrations of the component with the higher degree of conversion.

The general condition for a binary blend in thermodynamic equilibrium is the equality of chemical potential of components in each phase as

$$\mu_{A,a} = \mu_{B,b} \quad (2.14)$$

where $\mu_{A,a}$ is the chemical potential of component A in phase a and $\mu_{B,b}$ is the chemical potential of component B in phase b . The chemical potential is defined as the ΔG_{mix} change due to the addition of one molecule of component A or B while the whole system remains unchanged.

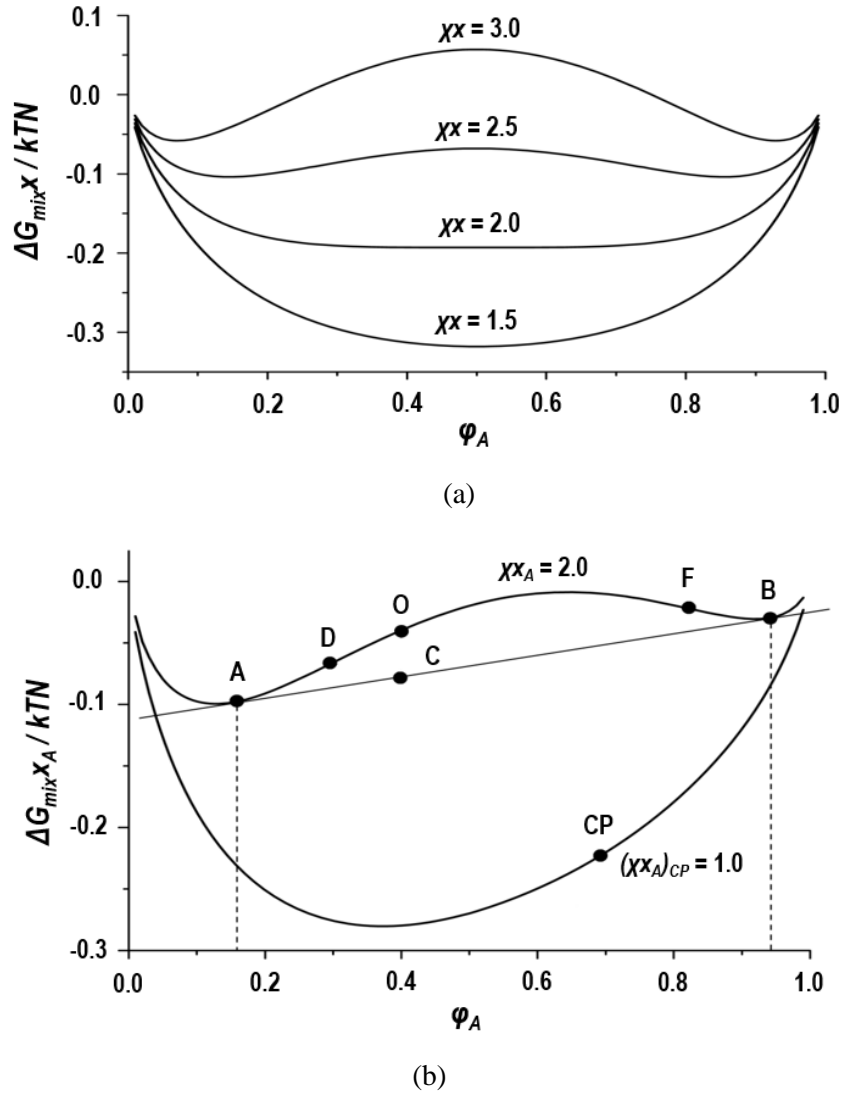


Figure 2.2 The Gibbs energy of mixing for a binary polymer blend as a function of its composition, (a) symmetric blend ($\chi_A = \chi_B = x$), (b) asymmetric blend ($\chi_A \neq \chi_B$).

When the two mixed phases a and b are in thermodynamic equilibrium, their exact composition can be determined. The relative amount of the phases a and b and the corresponding ΔG_{mix} can be determined using **Eq. 2.15** and **Eq. 2.16** as

$$\frac{\phi_A}{\phi_B} = \frac{|BC|}{|AC|} \quad (2.15)$$

$$\Delta G_{mix} = \phi_A \Delta G_{mix}^a + \phi_B \Delta G_{mix}^b \quad (2.16)$$

In the range of χx , where the composition dependence of ΔG_{mix} exhibits two minima, the final result of mixing depends on the initial blend composition. For low and high concentration values of ϕ_A , miscibility is observed, whereas a partially miscible blend is obtained. A homogeneous blend can be produced as the $\Delta G_{mix} < 0$, and two minima are present (points A and B in **Fig. 2.2b**). Therefore, according to **Fig. 2.2b**, the blends are not always miscible in

the whole composition range, and thus phase separation may take place in certain ranges. The phase separation processes also differ significantly in different composition ranges.

The following condition should be fulfilled for a miscible blend over the whole composition range

$$\frac{\partial^2 \Delta G_{mix}}{\partial \phi_A^2} > 0 \quad (2.17)$$

Nevertheless, a region, in which a homogeneous blend is always stable for any composition, and a region, in which two blended phases are more stable than a homogeneous system, are separated by the critical point (CP). The critical point is located at where the second and third derivatives of the ΔG_{mix} are zero in respect to the polymer volume fraction.

The critical value of the Flory-Huggins interaction parameter (χ_{CP}) and the location of critical point ($\phi_{A,CP}$) can be defined as

$$\chi_{CP} = 0.5 \left(\frac{1}{\sqrt{x_A}} + \frac{1}{\sqrt{x_B}} \right)^2 \quad (2.18)$$

$$\phi_{A,CP} = \frac{\sqrt{x_B}}{\sqrt{x_A} + \sqrt{x_B}} \quad (2.19)$$

For a symmetrical binary blend, the χ_{CP} shows the value of $2/x_A = 2/x_B$, and the $\phi_{A,CP}$ equals to $\phi_A = \phi_B = 0.5$.

On the basis of the phase behaviour shown in **Fig. 2.2**, the ΔG_{mix} increases and the blend tends to be phase separate over curing, or with increasing the degree of conversion (x). The same tendency can be seen with respect to the interaction parameter χ . For example, in endothermic mixing ($\Delta H_{mix} > 0$), a decrease in temperature leads to immiscible systems. The interaction parameter χ is inversely proportional of temperature. Also, as when specific interactions between the two polymer phases exists, the interaction parameter χ increases with temperature through the exothermic mixing ($\Delta H_{mix} < 0$). In this case, a lower critical solution temperature (LCST) behavior can be seen.

A phase diagram of a binary blend can be constructed in terms of χx_A and ϕ_A , or with the knowledge of temperature dependence of χ , as in **Fig. 2.3** by using **Fig. 2.2** and the corresponding equations. **Fig. 2.3** demonstrates the phase diagram of a symmetric binary blend with LCST, typical of miscible blends with specific interactions. The limits of miscibility are denoted by the binodal curve determined by the points of the tangent to the Gibbs energy curve, where the chemical potentials (μ) of the two coexisting phases are equal (see points A and B in **Fig. 2.2b**). Outside the bimodal curve, the blend is homogeneous and thermodynamically stable. Nevertheless, phase separation may occur in a stable blend when it is transferred inside the bimodal (e.g., temperature increase). For instance, if the composition of ϕ_A is 0.25 and the initial temperature of the blend is T_1 , then the corresponding point K lies in the homogeneous zone. Then, the blend is completely miscible at this temperature. The corresponding point A lies on the bimodal curve at T_2 , and the blend is at the metastable zone between the homogeneous and the two-phase separated zone.

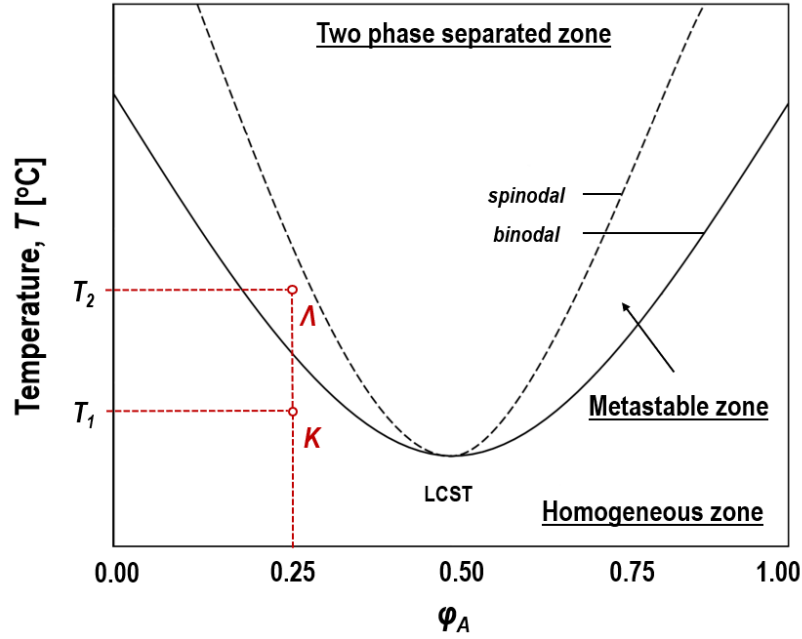


Figure 2.3 Phase diagram of a binary symmetric polymer blend with low critical solution temperature.

2.4 Solubility of Binary Blends

Cohesive energy (E_{AB}) is defined as the internal energy of vaporization (ΔE_v), or transformation, from liquid state to the ideal gas state. The values of cohesive energy of a component provide a measure of the intermolecular energy and can be expressed as

$$E_{AB} = \Delta E_v = \Delta H_v - p\Delta V \approx RT \quad (2.20)$$

where R is the universal gas constant, p is the internal pressure, ΔH_v is the molar heat of evaporation (at a given temperature). Thus, the cohesive energy can be defined as the increase in internal energy per mole of a component if all the intermolecular forces are eliminated [J/mol].

The Hildebrand solubility parameter (δ) [(J/cm³)^{0.5}] (Hildebrand & Scott 1964) can be expressed in relation to cohesive energy density (ϵ_{AB}) [J/mol³] as

$$\delta^2 = \frac{E_{AB}}{V} = \epsilon_{AB} \quad (2.21)$$

or

$$\delta^2 = -\frac{1/2 z w_{AB}}{v_r} \quad (2.22)$$

and thus, for binary polymer blends, the interaction parameter (χ), as defined in **Eq. 2.4**, can be accessible through the determination of the solubility of components A (δ_A) and B (δ_B) as

$$kT \frac{\chi}{v_r} = (\delta_A - \delta_B)^2 \quad (2.23)$$

or

$$\frac{\Delta H_{mix}}{V} = \varphi_A \varphi_B (\delta_A - \delta_B)^2 \quad (2.24)$$

As expressed by **Eq. 2.21**, the δ is defined as the square-root of cohesive energy density. As polymers cannot be evaporated, this parameter can be estimated from the swelling of a lightly crosslinked polymer or the intrinsic viscosity measurements in different solvents of known solubility values (Hilderbrand & Scott 1964). Then, the solubility parameter of the polymer is considered as the solubility parameter of the solvent in which the highest swelling ratio was reached, or as the solubility parameter of the solvent, which yielded the most viscous solution. Another possibility is to use other approaches (Small 1953; van Krewelen 1990; Coleman et al., 1990), in which the solubility parameter can be calculated as the sum of molar attraction constants of functional groups.

2.4.1 Solubility of epoxy polymers

The highly crosslinked (cured) epoxy resins are generally brittle polymers of high modulus. To avoid the generation of brittle epoxy polymers, specially functionalized block copolymers able to be co-polymerized with epoxy resins have been developed over the years to balance properties, such as strength and toughness (Thomas, Grohens & Jyotishkumar 2015). This can be achieved by functionalizing (terminating) the incorporating phases (i.e., epoxy and block copolymer) with specific precursors. For instance, copolymers, such as acrylonitrile-co-butadiene polymers, were functionalized with carboxyl (Rowe et al., 1970; Sultan & McGarry 1973; Visconti & Marchessault 1974) or amine (Rowe et al., 1970) end groups to react with the bisepoxide of DGEBA, and added in epoxy to promote toughness and miscibility. The functionalization of block copolymers could lead to rise of interfacial adhesion between the end-groups of block copolymers and epoxy, increasing thus the cohesive energy between the two components (Bucknall and Partridge 1986, Vechère et al., 1989; Thomas et al., 2008). **Fig. 2.4** illustrates the possible mechanisms for formulating miscible epoxy systems: (a) a functionalized liquid copolymer able to be co-polymerized with the epoxy or (b) by functionalizing the added epoxy.

Values of solubility parameter (δ , [(J/cm³)^{0.5}]) of some examples of block copolymers and epoxy precursors are given in **Table 2.1**. In accordance with **Eq. 2.20** and **Eq. 2.22**, the closer the solubility values of the two reactive components are, the more possible that they form a miscible blend ($\delta_A - \delta_B \rightarrow 0$). A characteristic example of predicting the miscibility of an epoxy polymer based on the values, which are provided in **Table 2.1**, is the incorporation of epoxidized polyisoprene (ePI, $\delta_{ePI} = 20.7$ (J/cm³)^{0.5}) of poly(butadiene-bisoprene-ran-epoxidized isoprene) with epoxy monomer (DGEBA, $\delta_{DGEBA} = 20.7$ (J/cm³)^{0.5}), and a homogeneous blend was produced (Grubbs et al., 2000).

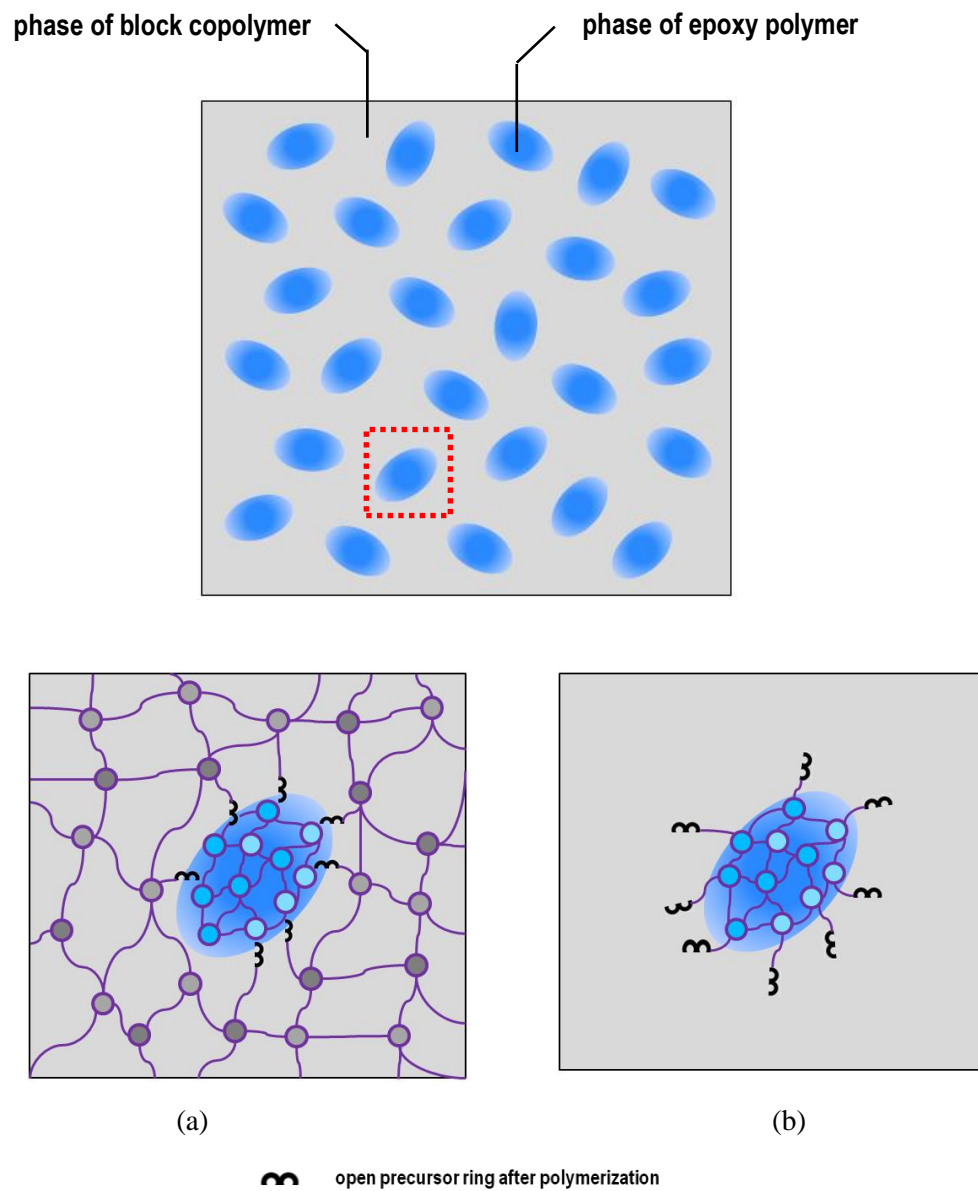


Figure 2.4 Schematic of highly grafted morphology: (a) epoxy in a functionalized block copolymer, and (b) functionalized-epoxy precursor in block copolymer.

Table 2.1 Solubility parameter values for different block copolymer and epoxy precursors reported in (Barton 1990; van Krevelen 1990; Ng & Chee 1997; Wohlfarth 2008; Parameswaranpillai et al., 2017).

Chemical substance	Solubility parameter $[(\text{J}/\text{cm}^3)^{0.5}]$
<i>block copolymers</i>	
polyethylene (PE)	15.8 - 17.1
polypropylene (PP)	16.8 – 18.8
polyisoprene (PI)	16.2 – 20.5
polybutadiene (PB)	16.6 – 17.6
poly(butyl acrylate) (PBA)	18.0 – 18.6
polystyrene (PS)	17.4 – 19.0
poly(methyl methacrylate) (PMMA)	18.6 – 26.2
<i>epoxy precursors</i>	
epoxidized polybutadiene (ePB)	20.0
epoxidized polyisoprene (ePI)	20.7
diglycidyl ether of bisphenol A (DGEBA)	20.7
diaminodiphenylsulfone (DDS)	23.5
Conversion factors: $1 [(\text{J}/\text{cm}^3)^{0.5}] = 0.49 [(\text{cal}/\text{cm}^3)^{0.5}]$; $1 [(\text{cm}^3/\text{mol})] = 10^{-6} [(\text{m}^3/\text{mol})]$; $1 [\text{J}/\text{mol}] = 0.24 [\text{cal}/\text{mol}]$	

2.4.2 Solubility of epoxy polymers in asphalt binders

In similar fashion with the miscible epoxy polymers, functionalized copolymers have been used as soluble modifiers in asphalt binders (Goodrich & Statz 1994; Kluttz & Erickson 1994; van der Werff 1996; Gallagher & Vermilion 1997; Prejean, Sanchez-Chavez & Babcock 1997; Planche, Turello & Lacour 2000; Planche et al., 2001; Prejean 2018). Despite the immiscible plastomers, such as polyethylene (PE, $\delta_{PE} = 16.0 (\text{J}/\text{cm}^3)^{0.5}$) and ethylene vinyl acetate (EVA, $\delta_{EVA} = 19.2 (\text{J}/\text{cm}^3)^{0.5}$) resins, the addition of epoxy-functionalized (e.g., glycidyl vinyl ester- or glycidyl butyl acrylate-terminated) ethylene in asphalt binders has resulted miscible polymer-asphalt binders of improved mechanical properties (Youtcheff et al., 2004; Polacco et al., 2004; Perez-Lepe, Martinez-Boza & Gallegos 2007; Jasso et al., 2015). Characteristic modifiers developed based on this material design approach are the Elvaloy® RET (e.g., ethylene/butyl acrylate/glycidyl methacrylate terpolymer) and Elvaloy® AC (e.g., ethylene/butyl acrylate copolymer). Moreover, a patent disclosed information about a commercial epoxy-asphalt binder (Fujitani et al., 2007), indicating that glycidyl grafted copolymers (e.g., ethylene, n-butyl and glycidyl (metha)acrylate) are chain copolymerized with maleinated polyolefins (e.g., polyethylene, polypropylene) within an asphalt binder. In all the above cases, a catalyst is also needed to accelerate the reaction of functionalized copolymers in asphalt binders.

Asphalt binders are characterized by high chemical complexity containing a large number of molecules, classified based on their differences in solubility and polarity into asphaltenes and maltenes (Lesueur 2009; Redelius & Soenen 2015). Previous studies have been performed to assess the solubility of asphalt binders with various polymers (Yang et al., 2002; Cong et al., 2008). Studies on the phase behaviour of asphalt binders and their fractions (e.g., asphaltenes)

have been conducted (Masson et al., 2003; Redelius 2004; Painter, Veytsman & Youtcheff 2014; 2015a; 2015b; Zhu, Balieu & Wang 2019) The solubility values of individual fractions are listed in **Table 2.2**. Certain fractions of asphalt binders have higher relevance with the promotion of miscibility in polymer modified asphalt binders (Masson et al., 2003; Masson, Polomark & Collins 2005; Zhu, Birgisson & Kringos 2014; Zhu, Balieu & Wang 2019). For example, improvement of polymer modified asphalt binder miscibility is reached when the aromaticity of maltenes decreased to certain values (Laval & Quivoron 1973). The miscibility of a certain polymer to asphalt binder is also affected negatively when a binder has high asphaltene content (Laval & Quivoron 1973). Thus, emphasis should be given to changing the reactivity of certain functional groups in binders to control their solubility with polymers.

Table 2.2 Solubility parameter values for asphalt binder fractions and different solvents reported in (Wloczynski, Vidal & Papirer 1997; Painter, Veytsman & Youtcheff 2014; 2015a & 2015b).

Chemical substance	Solubility parameter [(J/cm ³) ^{0.5}]
<i>asphalt binder fractions</i>	
saturates	14.3
aromatics	17.8
resins	19.4 – 20.1
asphaltenes	19.6 – 25.0
<i>solvents</i>	
diethyl ether	15.5
toluene	18.2
tetrahydrofuran	18.7
methyl ethyl ketone	19.0
cyclohexane	20.2
pyridine	21.8
quinoline	21.9
n-methyl pyrrolidone	22.9
dimethyl sulfoxide	26.3

Conversion factors: 1 [(J/cm³)^{0.5}] = 0.49 [(cal/cm³)^{0.5}]; 1 [(cm³/mol)] = 10⁻⁶ [(m³/mol)] ; 1 [J/mol] = 0.24 [cal/mol]

Variations in the asphalt binder composition strongly affect its chemical reactivity. The presence of heteroatoms (e.g., oxygen, nitrogen, and sulphur) in asphaltene and resin fractions introduce polarity in binders. These heteroatoms cause the amphoteric nature (i.e., the ability to react as both acid and base) of asphalt binders when reacting with other polar systems, such as polymers. The polarity of binder fractions can be altered by incorporating (ionic, non-ionic, steric or polymeric) surfactants (i.e., Lewis and Bronsted acids) (Barrett & Thomas 1969; Barrett 1973) and a reduction of the interface tension between binder and polymer ($\delta_{Binder} - \delta_{Polymer} \rightarrow 0$) can be achieved.

As mentioned earlier, epoxy resins are immiscible in asphalt binders and thus several attempts have been made to produce homogeneous binders of desired properties by incorporating various chemical substances. Especially, it has been reported in the literature that methyl tetrahydrophthalic of cyclic molecular structure, methyl hexahydrophthalic and tung oil

anhydrides have been used successfully to promote the system miscibility (Yu, Cong & Wu 2009; Zhou et al., 2011). However, the high volume of rigid benzene groups in epoxy-methyl tetrahydrophthalic systems could limit their applicability because binders of high viscosity can be developed (limited workability during construction). To address these issues, fatty acids were added to asphalt binders together with tung oil maleic tribasic acid (Li et al., 2014). In another research (Xu et al., 2018), a functionalized polyester with alkyl end groups was used as a toughening and miscibility promotor in an epoxy-asphalt binder. Lowering of the initial viscosity was noticed, which is an indication of improved solubility, together with an increase of curing time period. Similar performance was seen when epoxidized soybean oil was added in asphalt to produce a soluble phase in an epoxy resin even at 25°C (Si et al., 2018; 2019 & 2020). Stable binders of short polymer chains are produced as well when a binder is cured with maleated coupling agents, such as maleic anhydride (Herrington et al., 1999; Kang, Wang & Chen 2010). A polyetheramine has been used with polar ether groups to increase the stability between epoxy and binder without separated phases (Kang et al., 2016).

Overall, polymer and asphalt blends, such as the epoxy-asphalt binders, combine the properties and the functions of their individual components and unique characteristics can be possessed that cannot be achieved by utilizing the neat components only. Although extensive research performed to promote miscibility of modified binders, a high-resolution analysis is still needed to provide evidence about the final phase morphology and to reveal the interface formation of different epoxy-asphalt formulations. In this context, the morphology of two epoxy formulations in asphalt will be investigated in an effort to provide qualitative evidence on the miscibility of binders.

2.5 AFM Morphology of Epoxy-Asphalt Binders

Past studies have provided insight into the phase characteristics and phase behaviour of (neat and modified) asphalt binder by performing analyses in AFM (Loeber et al., 1996; Masson, Leblong & Margeson 2006; Masson et al., 2007; Schmets et al., 2010; Pauli et al., 2011; Fischer, Stadler & Erina 2013; Lyne et al., 2013; Nahar et al., 2013; Soenen, et al., 2014; Fischer, Dillingh & Hernse 2014; Allen et al., 2014; Pauli 2014; Menapace et al., 2015; Nahar 2016; Hofko et al., 2016; Nahar et al., 2016; Ramm et al., 2019; Ganter et al., 2020). Here, the assessment of surface morphologies and the interface characteristics of epoxy-asphalt binders will be carried out by performing a study in an AFM. Details of the AFM methodology and the results will be discussed as well.

2.5.1 Materials and preparation

The epoxy polymer which was used in this study was an under-development system, consisting of two liquid parts; (i) epoxy and (ii) hardener. The epoxy part consists of three elements; epichlorohydrin-bisphenol-A resin (molecular weight, $M_w = 700$ g/mol), epichlorohydrin-bisphenol-F-Harze ($M_w < 700$ g/mol) and benzyl alcohol (solvent). The benzyl alcohol was used as well in the mix of amine-type agents forming the hardener. The ratio by mass of epoxy and hardener was constant (epoxy : hardener = 71 : 29). A 70/100 pengrade asphalt binder was epoxy modified, using three different dilution ratios.

According to the supplier, the two parts of epoxy polymer were oven-heated for 1 hr at 70°C, and then stirred together for approximately 1 min. The epoxy polymer was produced ready to be diluted with the already pre-heated asphalt binder at 150°C. Three dilution ratios by mass (1:24 – EA24, 1:17 – EA17, 1:10 – EA10) were produced and studied.

To compare the microstructure morphology of the above binders, additional samples were prepared using a commercial epoxy-asphalt binder, which will be referred as EA_{ref}. The EA_{ref} is formulated from two liquid parts; (i) the Part A, which includes epichlorohydrin - bisphenol-A (DGEBA) (ChemCo Systems 2018a), and (ii) Part B (ChemCo Systems 2018b), which consists of a mix of a 70 pengrade petroleum asphalt binder with heavy naphthenic distillates and extracts. The exact chemistry of Part B is proprietary protected by the supplier and thus unknown. The EA_{ref} samples were prepared by mixing Part A and B at a weight ratio of 20:80. The two parts were oven-heated separately for 1 hr, to 85 and 110°C, respectively, and after that mixed for 20 s (ChemCo Systems 2018c). The basic properties of individual parts of EA_{ref} are provided in **Table 2.3**.

Table 2.3 Properties of EA_{ref} binder used in the research.

Property	Value
<i>Epoxy-based component (Part A)</i>	
Viscosity at 25°C [cP]	11,000-15,000
Specific gravity at 23°C	1.16
Boiling point [°C]	>260
<i>Asphalt-based component (Part B)</i>	
Viscosity at 100°C [cP]	140
Specific gravity at 25°C	0.99
Boiling point [°C]	288
Flash point, Cleveland open cup [°C]	232

All samples, with both epoxy types, were conditioned in an oven for 5 hrs at 100°C and then in a Pressure Aging Vessel (PAV) unit for 20 hrs at 2.1-MPa pressure, at 100°C (NEN-EN 14769), to ensure that the epoxy curing in asphalt binder was terminated and the samples were solid enough for microscopic analyses. The names and composition of studied binders are collected in **Table 2.4**.

Table 2.4 Name and composition of studied EA binders.

	epoxy [% wt]	hardener [% wt]	asphalt binder [% wt]
EA24	2.84 ¹	1.16 ²	96.00 ³
EA17	3.98 ¹	1.62 ²	94.40 ³
EA10	6.46 ¹	2.64 ²	90.90 ³
EA _{ref}	20.00 ⁴		80.00 ⁵

¹ epoxy component consists of (a) epichlorohydrin-bisphenol A ($M_w = 700$ g/mol) (CAS: 25068-38-6), and (b) epichlorohydrin-bisphenol-F-Hare ($M_w < 700$ g/mol) (CAS: 28064-14-4) and (c) benzyl alcohol (CAS: 100-51-6).

² hardener component consists of (a) amine-type agent (CAS: 1477-55-0, CAS: 2855-13-2, CAS: 98-54-4, CAS: 80-05-7, CAS: 109-55-7, CAS: 90-72-2, CAS: 25620-58-0, CAS: 1760-24-3), and (b) benzyl alcohol (solvent).

³ asphalt binder is a 70/100 pengrade binder.

⁴ epoxy component (Part A) of EA_{ref} consists of epichlorohydrin-bisphenol A (CAS: 25068-38-6).

⁵ asphalt component (Part B) of EA_{ref} consists of asphalt binder (<70% wt), heavy naphthenic residue, fatty acids and an unknown agent (CAS: 8052-42-4, CAS: 64741-53-3, CAS: 64742-11-6).

2.5.2 Sample preparation and AFM setting

The AFM instrument (Bruker, Dimension Icon), which was used for this research, has steel sample disks of 8-mm diameter as sample substrates. The samples were prepared on AFM steel substrate disks by heat casting on a heater plate at 100°C for 30 s to create a smooth thin film of binder (thickness: 300 to 400 μ) suitable for AFM probing. To ensure the same thermal history, the batch of samples were conditioned in the oven at 100°C for 15 min and ambient cooled. Then, the samples were stored in closed petri dishes on measuring the temperature of 21°C for 24 hrs prior to AFM. All measurements were performed at ambient conditions.

For tapping-mode AFM, RTESPA n-type antimony-doped silicon cantilevers having an aluminium reflective coating on the backside were used. This cantilever has a nominal resonant frequency, force constant and dimensions of 330 kHz, 40 N/m and 120 μ m \times 35 μ m \times 3 μ m respectively (Nahar 2016). In this initial AFM tapping mode study, a probe scan speed of 1.0 Hz (1 line/s) was applied over the surface at a scan size of 30 \times 30 μ m and also some high-resolution images. Height images are one of the output data sets of AFM tapping mode, providing the surface topography of the material surface.

2.5.3 Assessment of microstructural characteristics

The AFM tapping-mode measurements have been performed to acquire information on the potential association of epoxy and asphalt phases incorporated for producing miscible binders. The topography (i.e., relative height information) and phase (i.e., local modulus information) surface images disclosed for scans of 30 \times 30 μ m and 10 \times 10 μ m of studied binders are shown in the following figures. **Fig. 2.5** presents the microstructure of the base asphalt binder, EA24 and EA17. The base binder used to produce the EA24, EA17 and EA10 binders, shows a microstructure with unique feature of string like phases (**Fig. 2.5b**, light coloured strings connecting the light features), which does not resemble the global features of a neat asphalt binder. The string-like features were interconnected forming a network between domains (i.e., bees) and matrix.

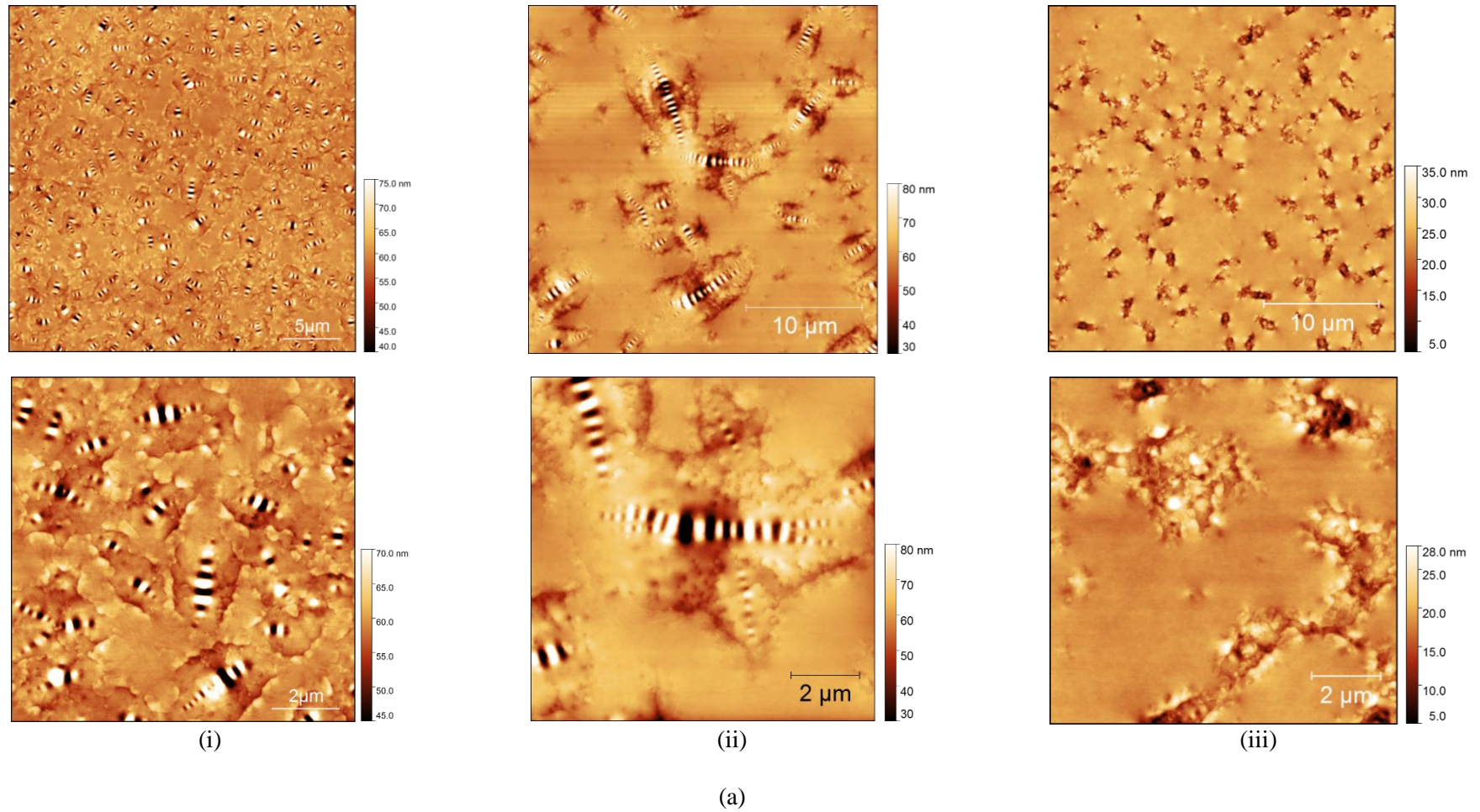
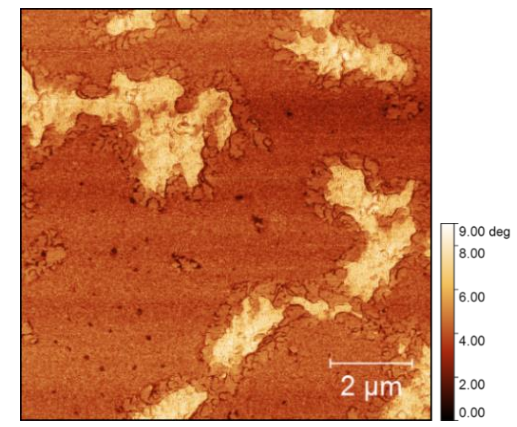
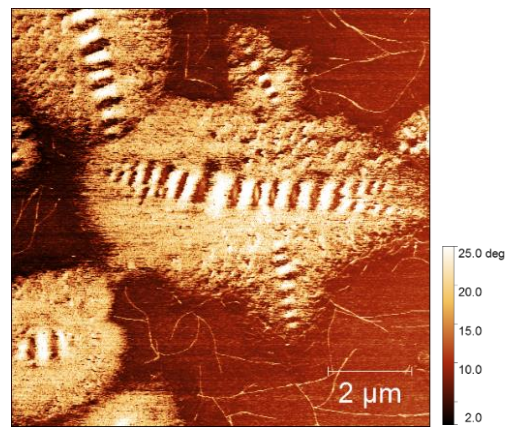
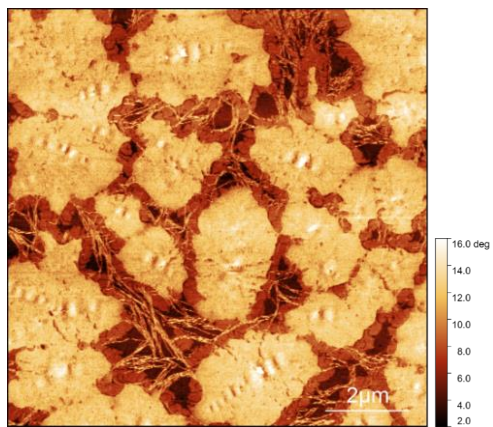
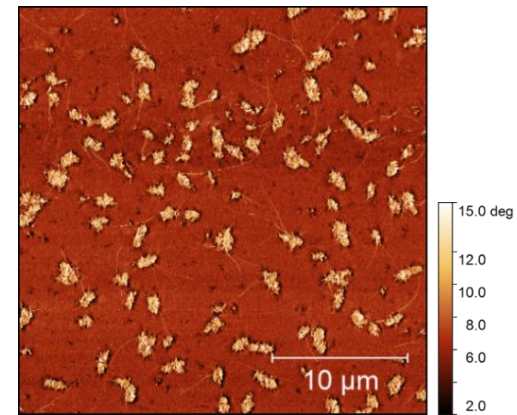
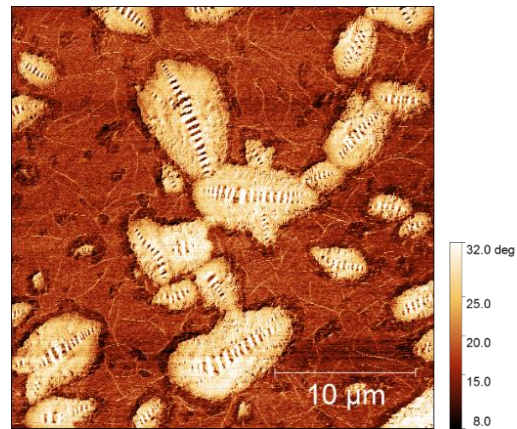
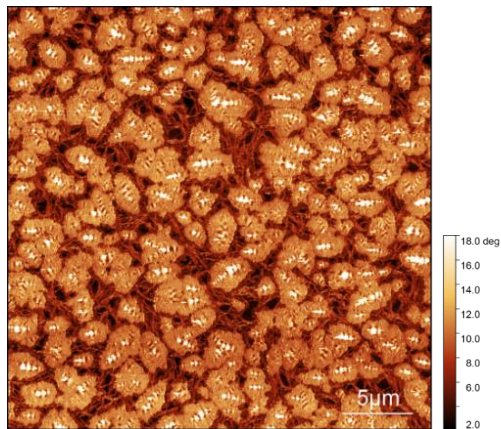


Figure 2.5 AFM tapping-mode (a) topography and (b) phase of 30x30 μm^2 (top) and 10x10 μm^2 (bottom) scan size images revealing the microstructure morphology of (i) base asphalt binder, (ii) EA24, and (iii) EA17 (*continued*)



(i)

(ii)

(iii)

(b)

Typically, three types of microstructure features have been observed on the surface of asphalt binders; the continuum phase called (a) para-phase, which embeds the (b) peri-phase and (c) catana-phase. The bee structures, which are patterns of pale and dark lines (Loeber et al., 1996) are considered as part of the peri-phase within the para-phase. Bee structures are associated with the presence of crystallizable wax fraction together with wrinkling or buckling of the surface (Pauli et al., 2011; Fischer, Stadler & Erina 2013; Lyne et al., 2013), even at small amounts of crystallizable waxes (Soenen et al., 2014). Here, the base asphalt and epoxy-asphalt binders of different dilution levels show bee structures, most probably due to the paraffinic nature of base binder. The completely isolated bee structures exist also in the case of asphalt binder with 1:10 dilution ratio (i.e., EA10), shown in **Fig. 2.6**, indicating that the epoxy resin does not affect greatly the bee structures originated from the asphalt binder. The EA17 binder shows a sharp interface indicating a separated phase of epoxy rich phase with limited bee structures, and asphalt rich phase with the increased amount of bee structures but without the string like structures.

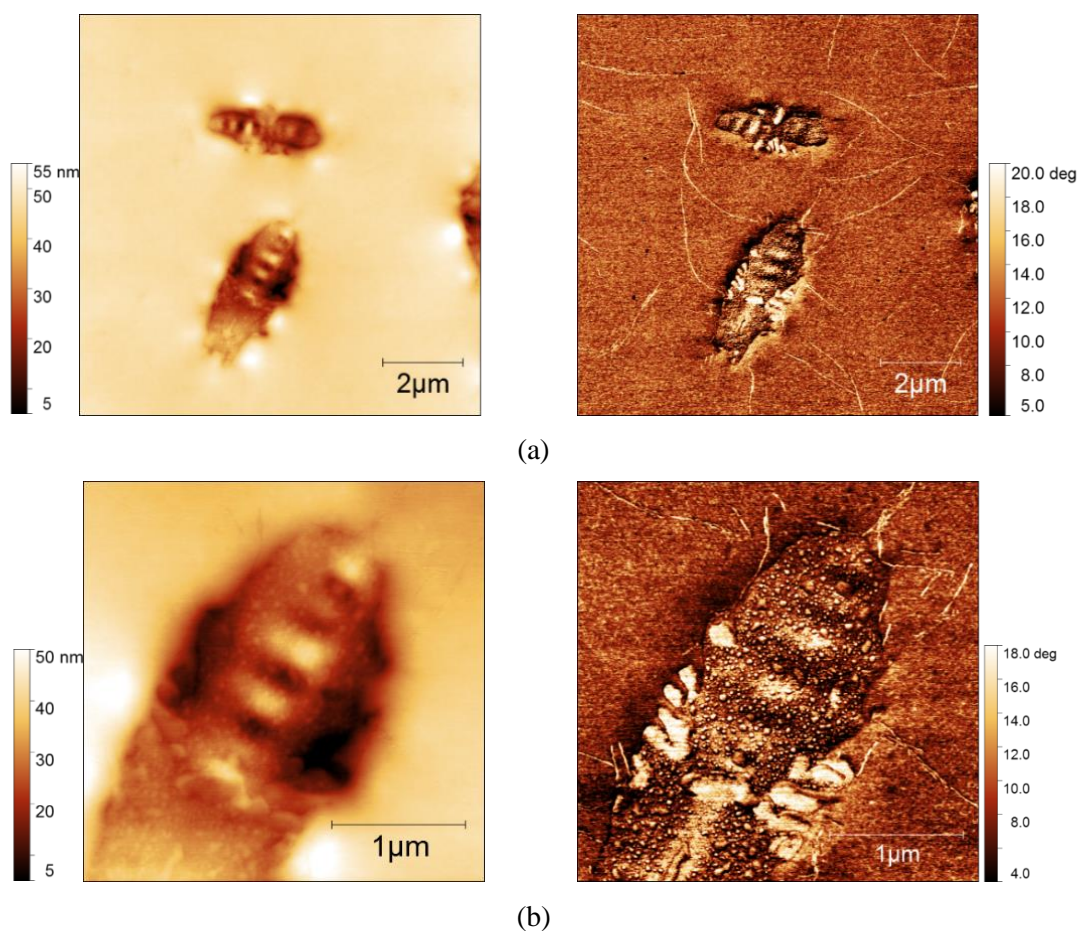


Figure 2.6 AFM tapping-mode results topography (left) and phase (right) of EA10; (a) 10x10 μm^2 , (b) 3x3 μm^2 scan size images.

According to the previously discussed thermodynamics of mixing of reacting polymer blends, it is known that the epoxy resin is of low molecular weight and soluble in asphalt binder at the beginning of curing and thus the epoxy-asphalt binders are homogeneous and initially form a single-phase regime. Phase separation is induced by the increase in the molecular weight of the

epoxy, resulting in hard domains and thus in a phase separated blend with well-defined interfaces as curing proceeds. The morphology of two-phase blends would be fixed at a certain stage of polymerization by gelation obtaining a phase-separated material. The gelation exists at the certain conversion extent at which branched molecules have infinite weight for first time. Once gelation occurred, the morphology is fixed. If these phenomena occur prior to separation, the epoxy polymer is trapped in asphalt binder while forming unconnected micro-domains in binder. Such observation has been shown in **Fig. 2.7**.

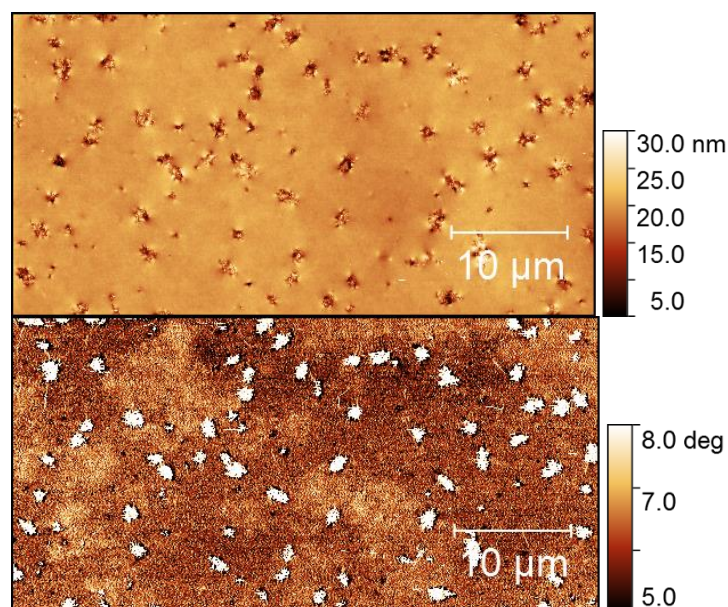


Figure 2.7 AFM tapping-mode results topography (top) and phase (bottom) of EA17.

From the phase AFM scans, the epoxy polymer obviously changed the matrix properties and a phase shift of matrix is observed in **Fig. 2.7**. The difference in local modulus or adhesion translates to a phase shift, and micro-domains of a brighter color were observed which represents areas of high modulus (Nahar 2016). In other words, **Fig. 2.7** depicts dispersed and unconnected micro-domains of the epoxy polymer trapped in asphalt binder. In case of EA17, epoxy domains into the asphalt binder were the bright elements compared to the soft matrix. Regions of higher contract and subsequently important difference of modulus within the continuous matrix were disclosed in AFM scans in **Fig. 2.7**.

A dedicated comparison of morphologies of EA17 of different resolutions at asphalt-epoxy interface zone was carried out to provide information about the extent of interfacial adhesion between the two incorporated phases. The asphalt-epoxy interface has been discovered with successive scans along a perpendicular line to this interface zone (**Fig. 2.8**).

A general observation from **Fig. 2.8** is that the region with more features (left sides of pictures) can be attributed to the base asphalt dominant region and the regions of the epoxy and asphalt phases are apparent. The topography (left) and phase (right) images along the presumed line of phases interface zone show a significant change of microstructure with limited dispersion of the epoxy phase throughout the asphalt one. A clear interface of different microstructures in low resolution scans (70 x 70 and 30 x 30 μm) is demonstrated in **Fig. 2.8(a-b)**. The sharp junction between the neighbouring phases corresponds to high interfacial tension and thus low

association between epoxy and asphalt binder (Loeber et al., 2000). This observation can be validated with high resolution images (3×3 and $1 \times 1 \mu\text{m}$) at the interface that do not display any phase-inverted microstructures and, thus, the phases co-association was limited (**Fig. 2.8(c-d)**). The chemical link of reactive species of asphalt and epoxy might be minimal.

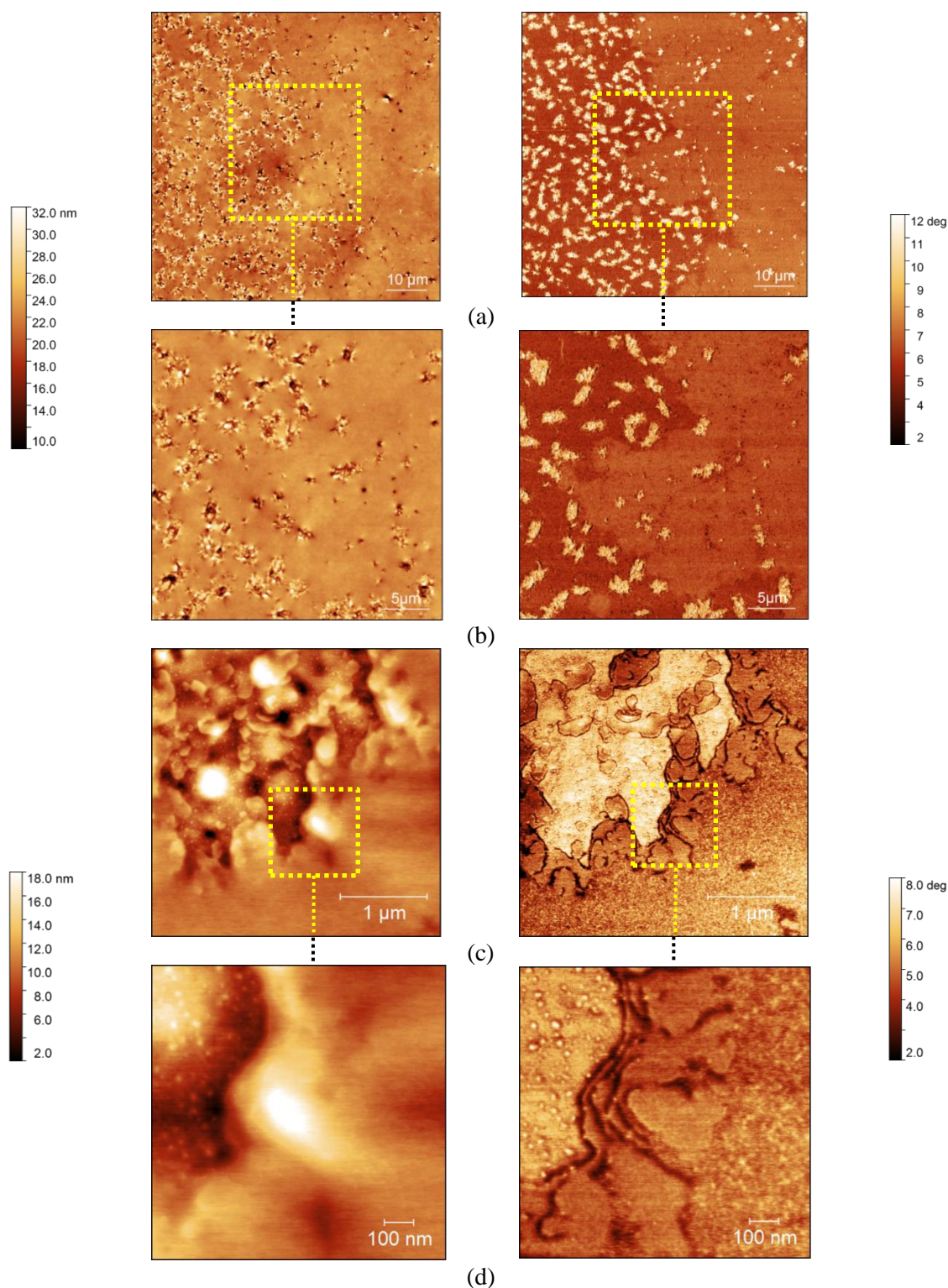


Figure 2.8 AFM tapping-mode results topography (left) and phase (right) of EA17; (a) $70 \times 70 \mu\text{m}^2$, (b) $30 \times 30 \mu\text{m}^2$, (c) $3 \times 3 \mu\text{m}^2$, (d) $1 \times 1 \mu\text{m}^2$ scan size images.

The microstructural characteristics of EA_{ref}, as shown in topography and phase AFM scans in **Fig. 2.9**, are not similar to an asphalt binder and totally different from the above discussed binders. The microstructure observed in this figure represents a homogeneous system with a relatively smooth and flat surface. This binder was produced after mixing epoxy resin with a black blend synthesized by naphthenic asphalt residues, fatty acids and an unknown agent. After curing and PAV-aging of EA_{ref}, the two mixed parts (i.e., Part A and B) were fully associated and co-polymerized formulating the homogeneous binder of a surface similar of a single-phase binder without bee structures, shown in **Fig. 2.9**.

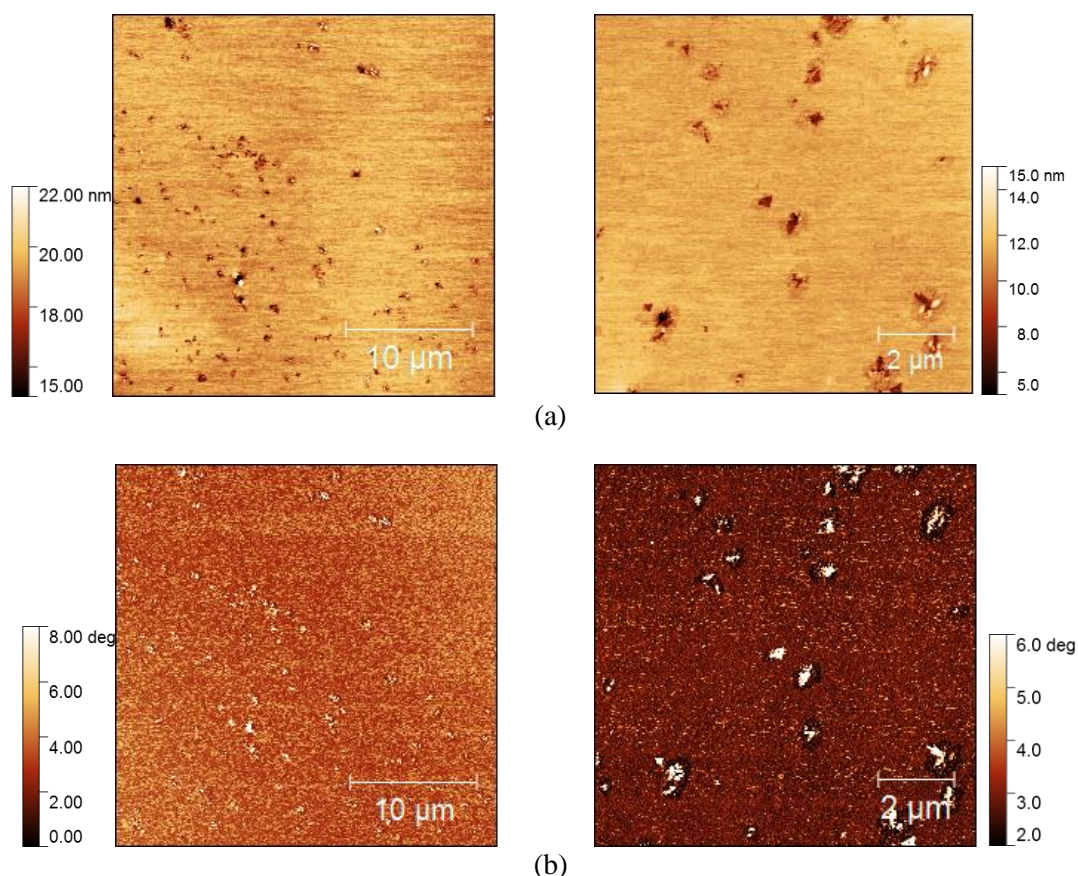


Figure 2.9 AFM tapping-mode results (a) topography and (b) phase of EA_{ref} binder; 30x30 μm^2 (left) 10x10 μm^2 (right) scan size images.

From the topographic and phase AFM scans, it seems that the two parts of EA_{ref} are miscible and thus once they were placed in contact at liquid state (before curing), inter-diffusion between the two parts occur. Normally, the efficiency of this process is determined by the thermodynamic interactions and the occurrence of certain interfacial reactions but the exact incorporating chemistry that results in such homogeneous systems as of EA_{ref} is unknown. However, bright spots, nano-particles, on the surface of EA_{ref} have been observed in phase scans (**Fig. 2.9b**). Surface microstructures of similar appearance have been seen elsewhere in epoxy-polymer blends formulated by co-polymerizing epoxy resin (i.e., DGEBA) and copolymer like a liquid carboxyl-grafted acrylonitrile-butadiene rubber in presence of piperidine (i.e., cure initiator) (Russell & Chartoff 2005). In this case, the carboxyl end groups of liquid rubber were reactive with the epoxy monomers. In a similar fashion, epoxy resins have been toughened with

triblock polymers as well (Larranaga et al., 2005) and shown nano-particles dispersion in a homogeneous matrix as of the EA_{ref} microstructure in **Fig. 2.9**.

2.6 Summary

Epoxy-asphalt binders are complex systems, and their thermodynamic stability depends mainly on the intermolecular interactions of different classes of molecules present in the phases. The purpose of this **chapter** was to provide the theoretical framework to produce miscible epoxy-asphalt binders. Hence, the thermodynamics of mixing and the phase behaviour of reacting systems were discussed and linked with previous studies on epoxy-polymer binders. Analyses of the morphological characteristics of asphalt binders with epoxy resins were carried out in an AFM showing evidence of a typical two-phase microstructure. Limited dispersion of the epoxy phase was observed throughout the asphalt binder. This observation coincides with the morphologies obtained at the asphalt-epoxy interface zone.

Ideally, a microstructure of co-continuous asphalt matrix or inverted structures should be obtained once the epoxy polymer is added, something which was observed by performing AFM scans in a proprietary protected binder (EA_{ref}). AFM analysis of the EA_{ref} exhibits to a single-phase system without wrinkling and typical asphalt features as noticed in epoxy-asphalt binders. The microstructure of this binder was homogeneous with a relatively flat and smooth surface. Solid nanoparticles were observed in EA_{ref} as well, resembling morphologies generated when epoxy resins are toughened by low concentrations of specially functionalized copolymers, as observed elsewhere. Overall, it can be concluded that the thermodynamic stability of epoxy-asphalt binders is strongly related to the incorporating chemistry of individual components, that allow the potential phase co-association.

2.7 References

- Abramowitz, M., I. Stegun. *Handbook of Mathematical Functions*. 2002.
- Allen, R.G., D.N. Little, A. Bhasin, C.J. Glover. The Effects of Chemical Composition on Asphalt Microstructure and their Association to Pavement Performance. *International Journal of Pavement Engineering* 15(1), 2014, pp. 9-22.
- Barton, A.F.M. *Handbook of Polymer-Liquid Interaction Parameters and Solubility Parameters*. CRC Press, Boca Raton, 1990.
- Barrett, K.E.J., H.R. Thomas. Kinetics of Dispersion Polymerization of Soluble Monomers. I Methyl Methacrylate. *Journal of Polymer Science Part A-1: Polymer Chemistry* 7(9), 1969.
- Barrett, K.E.J. Dispersion Polymerization in Organic Media. *British Polymer Journal* 5(4), 1973, pp. 249–332.
- Branthaver, J.F., M.W. Catalfomo, J.C. Petersen. Ion Exchange Chromatography Separation of SHRP Asphalts. *Fuel Science & Technology International* 10(4-6), 1992, pp. 855-885.
- Bucknall, C.B., I.K. Partridge. Phase Separation in Epoxy Resins containing Polyethersulphone. *Polymer* 24, 1983, pp. 639-644.
- Bucknall, C.B., I.K. Partridge. Phase Separation in Crosslinked Resins containing Polymeric Modifiers. *Polymer Engineering and Science* 26(1), 1986, pp. 54–62.

- Bucknall, C.B., A.H. Gilbert. Toughening Tetrafunctional Epoxy Resins using Polyetherimide. *Polymer* 30, 1989, pp. 213-217.
- Cabanelas, J.C., B. Serrano, J. Baselga. Development of Cocontinuous Morphologies in Initially Heterogeneous Thermosets Blended with Poly(methyl methacrylate). *Macromolecules* 38, 2005, pp. 961-970.
- ChemCo Systems, Inc. Epoxy Asphalt Resin, Part A. Safety Data Sheet. 2018a.
- ChemCo Systems, Inc. Epoxy Asphalt Binder, Type BIX. Safety Data Sheet. 2018b.
- ChemCo Systems, Inc. Construction Specification: Installation of Type IX Epoxy Asphalt Concrete Surfacing. 2018c.
- Coleman, M.M., C.J. Serman, D.E. Bhagwagar, P.C. Painter. A Practical Guide to Polymer Miscibility. *Polymer* 31(7), 1990, pp. 1187-1203.
- Cong, Y., W. Huang, K. Liao. Compatibility between SBS and Asphalt. *Petroleum Science and Technology* 26(3), 2008, pp. 346–352.
- Cong, P., W. Luo, P. Xu, Y. Zhang. Chemical and Physical Properties of Hot Mixing Epoxy Asphalt Binders. *Construction and Building Materials* 198, 2019, pp. 1-9.
- Corbett, L.W. *Composition of Asphalt Based on Generic Fractionation, using Solvent Deasphalting, Elution-Adsorption Chromatography, and Densimetric Characterization*. In 156th National Meeting of the ACS, Division of Petroleum Chemistry, 1968.
- Das, P., N. Kringos, B. Birgisson. Microscale Investigation of Thin Film Surface Ageing of Bitumen. *Journal of Microscopy* 254, 2014, pp. 95-107.
- Dickie, J.P., Yen, T.F. Macrostructures of Asphaltic Fractions by Various Instrumental Methods. *Analytical Chemistry* 39, 1967, pp. 1847-52.
- Dutta, P.K., R.J. Holland. Acid-base Characteristics of Petroleum Asphaltenes as Studied by Non-Aqueous Potentiometric Titrations. *Fuel* 63, 1984, pp. 197-201.
- Fischer, H., H. Stadler, N. Erina. Quantitative Temperature-Depending Mapping of Mechanical Properties of Bitumen at the Nanoscale using the AFM operated with PeakForce Mapping Mode. *Journal of Microscopy* 250(3), 2013, pp. 210-217.
- Fischer, H.R., E.C. Dillingh, C.G.M. Hermse. On the Microstructure of Bituminous Binders. *Road Materials and Pavement Design* 15(1), 2014, pp. 1-15.
- Flory, P.J. Thermodynamics of High Polymer Solutions. *The Journal of Chemical Physics* 10, 1942, pp. 51-61.
- Flory, P.J. *Principles of Polymer Chemistry*. Cornell University Press: Ithaca, NY, 1953.
- Fujita, H. Diffusion in Polymer-Diluent Systems. *Fortschr. Hochpolym.-Forsch.* 3, 1961.
- Fujitani, A., H. Hirayama, T. Kobayashi, A. Seo. *Asphalt-Epoxy Resin Compositions*. US Patent 2007/0185246 A1, 2007.
- Gallagher, K.P., D.R. Vermilion. *Thermosetting Asphalt having Continuous Phase Polymer*. US Patent 5.604.274, 1997.
- Ganter, R., S. Franka, V.V. Shvartsman, D.C. Lupascu. The Phenomenon of Bitumen ‘Bee’ Structures – Bulk or Surface Layer – A Closer Look. *International Journal of Pavement Engineering*, 2020.
- Gong, J., Y. Liu, Y. Jiang, Q. Wang, Z. Xi, J. Cai, H. Xie. Performance of Epoxy Asphalt Binder containing Warm-mix Asphalt Additive. *International Journal of Pavement Engineering*, 2019.

- Goodrich, J.L., R.J. Statz. *Polymer and Asphalt Reaction Process and Polymer-linked-Asphalt Product*. US Patent 5.306.750, 1994.
- Grubbs, R.B., J.M. Dean, M.E. Broz, F.S. Bates. Reactive Block Copolymers for Modification of Thermosetting Epoxy. *Macromolecules* 33, 2000, pp. 9522–953.
- Herrington, P.R., Y. Wu, M.C. Forbes. Rheological Modification of Bitumen with Maleic Anhydride and Dicarboxylic Acids. *Fuel* 78, 1999, pp. 101-110.
- Herrington, P., D. Alabaster. Epoxy Modified Open-graded Porous Asphalt. *Road Materials and Pavement Design* 9(3), 2008, pp. 481-498.
- Hildebrand, J.H. R.L. Scott. *The Solubility of Nonelectrolytes*. Dover, New York, 1964.
- Hofko, B., L. Eberhardsteiner, J. Fussl, H. Grothe, F. Hanke, M. Hospodka, D. Grosseegger, S.N. Nahar, A.J.M. Schmets, A. Scarpas. Impact of Maltene and Asphaltene Fraction on Mechanical Behavior and Microstructure of Bitumen. *Materials and Structures* 49, 2016.
- Hourston, D.J., J.M. Lane. The Toughening of Epoxy Resins with Thermoplastics: 1. Trifunctional Epoxy Resin-Polyetherimide Blends. *Polymer* 33(7), 1992, pp. 1379-83.
- Huang, P., S. Zheng, J. Huang, Q. Guo, W. Zhu. Miscibility and Mechanical Properties of Epoxy Resin/Polysulfone Blends. *Polymer* 38(22), 1997, pp. 5565-71.
- Huggins, M.L. Solution of Long Chain Compounds. *The Journal of Chemical Physics* 9, 1941.
- Jasso, M., R. Hampl, O. Vacin, D. Bakos, J. Stastna, L. Zanzotto. Rheology of Conventional Asphalt Modified with SBS, Elvaloy and Polyphosphoric Acid. *Fuel Processing Technology* 140, 2015, pp. 172-179.
- Jiang, Y., Y. Liu, J. Gong, C. Li, Z. Xi, J. Cai, H. Xie. Microstructures, Thermal and Mechanical Properties of Epoxy Asphalt Binder modified by SBS containing Various Styrene-Butadiene Structures. *Materials and Structures* 51, 2018, pp. 86.
- Iijima, T., T. Tochimoto, M. Tomoi. Modification of Epoxy Resins with Poly(aryl Ether Ketone)s. *Journal of Applied Polymer Science* 43, 1991, pp. 1685-92.
- Iijima, T., H. Hiraoka, M. Tomoi. Preparation of Epoxy-Terminated Poly(aryl Ether Sulfone)s and their Use as Modifiers for Epoxy Resins. *Journal of Applied Polymer Science* 45, 1992.
- International Transport Forum. *Long-Life Surfacing for Roads: Field Test Results*. ITF Research Reports, OECD, Paris, France, 2017.
- Kang, Y., M. Song, L. Pu, T. Liu. Rheological Behaviors of Epoxy Asphalt Binder in Comparison of Base Asphalt Binder and SBS Modified Asphalt Binder. *Construction and Building Materials* 76, 2015, pp. 343-350.
- Kang, Y., F. Wang, Z.M. Chen. Reaction of Asphalt and Maleic Anhydride: Kinetics and Mechanism. *Chemical Engineering Journal* 164, 2010, pp. 230-237.
- Kang, Y., Q. Wu, R. Jin, P. Yu, J. Cheng. Rubber-like Quasi-thermosetting Polyetheramine-cured Epoxy Asphalt Composites Capable of Being Opened to Traffic Immediately. *Scientific Report* 6, 2016, 18882.
- Kinloch, A.J., S.J. Shaw, D.A. Tod, D.L. Hunston. Deformation and Fracture Behavior of a Rubber-Toughened Epoxy: 1. Microstructure and Fracture Studies. *Polymer* 24, 1983.
- Kluttz, R.Q., J.R. Erickson. *Asphalt Composition containing Epoxidized Polymers*. US Patent 5.451.619, 1995.
- Larranaga, M., N. Gabilondo, G. Kortaberria, E. Serrano, P. Remiro, C.C. Riccardi, I. Mondragon. Micro- or Nanoseparated Phases in Thermoset Blends of an Epoxy Resin and PEO-PP-PEO Triblock Copolymer. *Polymer* 46, 2005, pp. 7082-93.

- Laval C, C. Quivoron. Mise en Evidence d'une Corrélation Entre le Rapport Hydrophile/Lipophile des Résines Epoxydes et leur Compatibilité Avec le Bitumen Routier. *C R Acad Sci Ilc* 256, 1973, 743–6.
- Laval, C., B. Brûlé. *Etude Expérimentale de la Compatibilité de Résines Epoxydes avec le Bitume*. Application à la Prévision de Systèmes Compatibles, Rapport LCPC 40, 1974.
- Lesueur, D. The Colloidal Structure of Bitumen: Consequences on Rheology and on the Mechanism of Bitumen Modification. *Advances in Colloidal and Interface Science* 145, 2009, pp. 42–82.
- Li, S., K. Huang, X. Yang, M. Li, J. Xia. Design, Preparation and Characterization of Novel Toughened Epoxy Asphalt Based on a Vegetable Oil Derivative for Bridge Deck Paving. *Royal Society of Chemistry* 4, 2014, pp. 44741-49.
- Liu, Y., Z. Xi, J. Cai, H. Xie. Laboratory Investigation of the Properties of Epoxy Asphalt Rubber (EAR). *Materials and Structures* 50, 2017, pp. 219.
- Loeber, L., O. Sutton, J. Morel, J.M. Valleton, G. Muller. New Direct Observations of Asphalts and Asphalt Binders by Scanning Electron Microscopy and Atomic Force Microscopy. *Journal of Microscopy* 182, 1996, pp. 32-39.
- Lyne, A.L., V. Wallqvist, M.W. Rutland, P. Claesson, B. Birgisson. Surface Wrinkling: The Phenomenon causing Bees in Bitumen. *Journal of Material Science* 48, 2013, pp. 6970-76.
- Manziona, L.T., J.K. Gillham, C.A. McPherson. Rubber-Modified Epoxies. I. Transitions and Morphology. *Journal of Applied Polymer Science* 26, 1981, pp. 889-905.
- Masson, J-F., P. Collins, G. Robertson, J.R. Woods, J. Margeson. Thermodynamics, Phase Diagrams, and Stability of Bitumen-Polymer Blends. *Energy & Fuels* 17, 2003.
- Masson, J.F., G. Polomark, P. Collins. Glass Transitions and Amorphous Phases in SBS-Bitumen Blends. *Thermochimica Acta* 436, 2005, pp. 96-100.
- Masson, J.P., V. Leblond, J. Margeson. Bitumen Morphologies by Phase-Detection Atomic Force Microscopy. *Journal of Microscopy* 221, 2006, pp. 17-29.
- Masson, J.P., V. Leblond, J. Margeson, S. Bundalo-Perc. Low-Temperature Bitumen Stiffness and Viscous Paraffinic Nano- and Micro-Domains by Cryogenic AFM and PDM. *Journal of Microscopy* 227, 2007, pp. 191-202.
- Mathew, V.S., C. Sinturel, S.C. George, S. Thomas. Epoxy Resin/Liquid Natural Rubber System: Secondary Phase Separation and its Impact on Mechanical Properties. *Journal of Material Science* 45, 2010, pp. 1769-81.
- McGarry, F.J. *Rubber-Toughened Thermosets*. Plastics Engineering, New York, 1996.
- Menapace, I., E. Masad, A. Bhasin, D. Little. Microstructural Properties of Warm Mix Asphalt Before and After Laboratory-Simulated Long-Term Ageing. *Road Materials and Pavement Design* 16(1), 2015, pp. 2-20.
- Mezzenga, R., L. Boogh, J.-A.E. Manson. A Thermodynamic Model for Thermoset Polymer Blends with Reactive Modifiers. *Journal of Polymer Science Part B-Polymer Physics* 38, 2000, pp. 1893-1902.
- Moschopedis, S.E., J.G. Speight. Oxygen Functions in Asphaltenes. *Fuel* 55, 1976.
- Munk, P. *Introduction to Macromolecules*. J. Wiley & Sons: Austin, Texas, 1989.
- Nahar, S.N., A.J.M. Schmets, A. Scarpas, G. Schitter. Temperature and Thermal History Dependence of the Microstructure in Bituminous Materials. *European Polymer Journal* 49, 2013, pp. 1964-74.

- Nahar, S.N., A.J.M. Schmets, G. Schitter, A. Scarpas. Quantifying the Thermomechanical Response of Bitumen from Microphase Properties. *Transportation Research Record 2574*, National Research Council, Washington, D.C., 2016, pp. 101-110.
- Nahar, S.N. *Phase-Separation Characteristics of Bitumen and their Relation to Damage-Healing*. PhD Thesis, Delft University of Technology, 2016.
- NEN-EN 14769. Bitumen and Bituminous Binders – Accelerated Long-term Ageing Conditioning by a Pressure Ageing Vessel (PAV). 2012.
- Ng, S.C., K.K. Chee. Solubility Parameters of Copolymers as Determined by Turbidimetry. *European Polymer Journal* 33, 1997, pp. 749–752.
- Painter, P., B. Veytsman, J. Youtcheff. Association Model for the Phase Behavior of Asphaltenes. *Energy & Fuels* 28, 2014, pp. 2472-80.
- Painter, P., B. Veytsman, J. Youtcheff. Asphaltene Aggregation and Solubility. *Energy & Fuels* 29, 2015a, pp. 2120-33.
- Painter, P., B. Veytsman, J. Youtcheff. Phase Behavior of Bituminous Materials. *Energy & Fuels* 29, 2015b, pp. 7048-57.
- Parameswaranpillai, J., N. Hameed, J. Pionteck, E.M. Woo. *Handbook of Epoxy Blends*. Springer, 2017.
- Pauli, A.T., R.W. Grimes, A.G. Beemer, T.F. Turner, J.F. Branthaver. Morphology of Asphalts, Asphalt Fractions and Model Wax-Doped Asphalts Studied by Atomic Force Microscopy. *International Journal of Pavement Engineering* 12(4), 2011, pp. 291-309.
- Pauli, A.T. *Chemomechanics of Damage Accumulation and Damage-Recovery Healing in Bituminous Asphalt Binders*. PhD Thesis, Delft University of Technology, 2014.
- Perez-Lepe, A., F.J. Martinez-Boza, C. Gallegos. High Temperature Stability of Different Polymer-Modified Bitumens: A Rheological Evaluation. *Journal of Applied Polymer Science* 103, 2007, pp. 1166-74.
- Planche, J.P., P. Turello, C. Lacour. *Bitumen/Polymer Compositions with Improved Stability and their Application in Carrying out Surfacing Operations*. US Patent 6.020.404, 2000.
- Planche, J.P., P. Maldonado, B. Neff, T. Senninger, A. Zins, S. Drouilhet. *Process for the Preparation of Functionalized Elastomer/Bitumen Compositions and their Use in Coatings*. US Patent 6.218.449 B1, 2001.
- Polacco, G., J. Stastna, D. Biondi, F. Antonelli, Z. Vlachovicova, L. Zanzotto. Rheology of Asphalts Modified with Glycidylmethacrylate Functionalized Polymers. *Journal of Colloid and Interface Science* 280, 2004, pp. 366-373.
- Prejean, G.W., F. Sanchez-Chavez, G.B. Babcock. *Composition comprising Asphalt and Epoxy (Meth)acrylate Copolymer*. US Patent 2007/0027261 A1, 2007.
- Prejean, G.W. *Epoxy Functionalized Ethylene Copolymer Asphalt Reaction Products*. US Patent 2017/0208769 A1, 2018.
- Raghava, R.S. Role of Matrix-Particle Interface Adhesion on Fracture Toughness of Dual Phase Epoxy-Polyethersulfone Blend. *Journal of Polymer Science: Part B: Polymer Physics* 25, 1987, pp. 1017-31.
- Ramm, A., N. Sakib, A. Bhasin, M. Downer. Morphology and Kinetics of Asphalt Binder Microstructure at Gas, Liquid, and Solid Interfaces. *Journal of Microscopy* 276, 2019.
- Redelius, P. Bitumen Solubility Model using Hansen Solubility Parameter. *Energy & Fuels* 18, 2004, pp. 1087-92.

- Redelius P, H. Soenen. Relation between Bitumen Chemistry and Performance. *Fuel* 140, 2015.
- Rowe, E.H., A.R. Siebert, R.S. Drake. Toughening Thermoset with Liquid. Butadiene/Acrylonitrile Polymers. *Modern Plastics* 47(8), 1970, pp. 110-117.
- Russell, B., & R. Chartoff. The Influence of Cure Conditions on the Morphology and Phase Distribution in a Rubber-Modified Epoxy Resin using Scanning Electron Microscopy and Atomic Force Microscopy. *Polymer* 46, 2005, pp. 785-798.
- Si, J., Z. Jia, J. Wang, X. Yu, Y. Li, F. Dong, R. Jiang. Comparative Analysis of Cold-Mixed Epoxy and Epoxy SBS-Modified Asphalts: Curing Rheology, Thermal and Mechanical Properties. *Construction and Building Materials* 176, 2018, pp. 165-171.
- Si, J., Y. Li, X. Yu. Curing Behavior and Mechanical Properties of an Eco-Friendly Cold-Mixed Epoxy Asphalt. *Materials and Structures* 52(81), 2019.
- Si, J., Y. Li, J. Wang, A.R. Niyigena, X. Yu, R. Jiang. Improving the Compatibility of Cold-Mixed Epoxy Asphalt based on the Epoxidized Soybean Oil. *Construction and Building Materials* 243, 2020, 118235.
- Small, P.A. Some Factors Affecting the Solubility of Polymers. *Journal of Applied Chemistry* 3, 1953, pp. 71-80.
- Schmets, A., N. Kringos, T. Pauli, P. Redelius, T. Scarpas. On the Existence of Wax-Induced Phase Separation in Bitumen. *International Journal of Pavement Engineering* 11, 2010.
- Soenen, H., J. Besamusca, H.R. Fischer, L.D. Poulikakos, J.P. Planche, P.K. Das, N. Kringos, J.R.A. Grenfell, X. Lu, E. Chailleux. Laboratory Investigation of Bitumen based on Round Robin DSC and AFM Tests. *Materials and Structures* 47, 2014, pp. 1205-1220.
- Stary, Z. Thermodynamics and Morphology and Compatibilization of Polymer Blends. In *Characterization of Polymer Blends: Miscibility, Morphology and Interfaces*. Edited by S. Thomas, Y. Grohens, P. Jyotishkumar. Wiley-VCH., 2015.
- Sultan, J.N., F.J. McGarry. Effect of Rubber Particle Size on Deformation Mechanisms in Glassy Epoxy. *Polymer Engineering and Science* 13(1), 1973, pp. 29-34.
- Sun, Y., J. Gong, Y. Liu, Y. Jiang, Z. Xi, J. Cai, H. Xie. Viscous, Damping, and Mechanical Properties of Epoxy Asphalt Adhesives containing Different Penetration-Grade Asphalts. *Journal of Applied Polymer Science* 2018, pp. 47027.
- Teng, K.-C., F.-C. Chang. Single-Phase and Multi-Phase Thermoplastic/Thermoset Polyblends: 1. Kinetics and Mechanisms of Phenoxy/Epoxy Blends. *Polymer* 34(20), 1993.
- Thomas, R., D. Yumei, H. Yuelong, Y. Le, P. Moldenaers, Y. Weimin, T. Czigany, S. Thomas. Miscibility, Morphology, Thermal, and Mechanical Properties of a DGEBA based Epoxy Resin Toughened with a Liquid Rubber. *Polymer* 49, 2008, pp. 278-294.
- van der Werff, J.C. *Method for Producing Asphalts containing an Epoxy-containing Polymer and Polyamine*. US Patent 5.574.095, 1996.
- van Krewelen, D.W. *Properties of Polymers*. 3rd Edn. Elsevier: Amsterdam, 1990.
- Varley, R.J., G.R. Heat, D.G. Hawthorne, J.H. Hodgkin. Toughening of a Trifunctional Epoxy System: 1. Near Infra-Red Spectroscopy Study of Homopolymer Cure. *Polymer* 36(7), 1995.
- Verchère, D., H. Sautereau, J.P. Pascault, S.M. Moschiar, C.C. Riccardi, R.J.J. Williams. Miscibility of Epoxy Monomers with Carboxyl-Terminated Butadiene Acrylonitrile Random Copolymers. *Polymer* 30, 1989, pp. 107-115.
- Visconti, S., R.H. Marchessault. Small Angle Light Scattering by Elastomer-Reinforced Epoxy Resins. *Macromolecules* 7, 1974, pp. 913-917.

- Yahyaie, H., M. Ebrahimi, H.V. Tahami, E.R. Mafi. (2013) Toughening Mechanisms of Rubber modified Thin Film Epoxy Resins. *Progress in Organic Coatings* 76, 2013, pp. 286-292.
- Wei, J., Y. Zhang. Study on the Curing Process of Epoxy Asphalt. *Journal of Testing and Evaluation* 40(7), 2012, pp. 1-8.
- Wieme, J., D.R. D'hooge, M.F. Reyniers, B. Marin. Importance of Radical Transfer in Precipitation Polymerization of Vinyl Chloride Suspension Polymerization. *Macromolecular Reaction Engineering* 3, 2009, pp. 16–35.
- Wohlfarth, C. *CRC Handbook of Liquid-Liquid Equilibrium Data of Polymer Solutions*. CRC Press, Taylor & Francis Group, 2008.
- Wloczyński, P., A. Vidal, E. Papirer. Relationships between Rheological Properties, Morphological Characteristics, and Composition of Bitumen-Styrene Butadiene Styrene Copolymers Mixes. II. A Thermodynamical Interpretation. *Journal of Applied Polymer Science* 65(8), 1997, pp. 1609-18.
- Xu, P., X. Zhu, P. Cong, X. Du, R. Zhang. Modification of Alkyl Group Terminated Hyperbranched Polyester on Paving Epoxy Asphalt. *Construction and Building Materials* 165, 2018, pp. 295-302.
- Yang, P., Q. Cong, K. Liao. Application of Solubility Parameter Theory in Evaluating the Aging Resistance of Paving Asphalts. *Petroleum Science and Technology* 21, 2003.
- Yen, T.F. The Charge-Transfer Nature of Bitumens. *Fuel* 52, 1973, pp. 93-98.
- Yin, H. H. Jin, C. Wang, Y. Sun, Z. Yuan, H. Xie, Z. Wang, R. Cheng. Thermal, Damping, and Mechanical Properties of Thermosetting Epoxy-modified Asphalts. *Journal of Thermal Analysis and Calorimetry* 115, 2014, pp. 1073–1080.
- Yin, H., Y. Zhang, Y. Sun, W. Xu, D. Yu, H. Xie, R. Cheng. Performance of Hot Mix Epoxy Asphalt Binder and its Concrete. *Materials and Structures* 48, 2015, pp. 3825-35.
- Youtcheff, J., K. Stuart, G. Al-Khateeb, A. Shenoy. *Understanding the Performance of Polymer Modified Binders*. Proceedings of the 3rd Eurasphalt & Eurobitume Congress, 2004.
- Youtcheff, J., N. Gibson, A. Shenoy, G. Al-Khateeb. The Evaluation of Epoxy Asphalt and Epoxy Asphalt Mixtures. *Proceedings of the Canadian Technical Asphalt Association* 51, 2006.
- Yu, J.Y., P.L. Cong, S.P. Wu. Laboratory Investigation of the Properties of Asphalt Modified with Epoxy Resin. *Journal of Applied Polymer Science* 113, 2009, pp. 3557-3563.
- Zhou, W., H. Zhao, J. Wen, F.C. Cai, N. Ma, T. Jiang. Study on Effects of Flexible Curing Agent on the Structure and Performance of Epoxy-Asphalt. *Journal of Wuhan University of Technology* 33(7), 2011, pp. 28-31.
- Zhu, J., B. Birgisson, N. Kringos. Polymer Modification of Bitumen: Advances and Challenges. *European Polymer Journal* 54, 2014, pp. 18–38.
- Zhu, J., R. Balieu, H. Wang. The Use of Solubility Parameters and Free Energy Theory for Phase Behaviour of Polymer-modified Bitumen: A Review. *Road Materials and Pavement Design*, 2019.

3

Determination of Curing Kinetics with Differential Scanning Calorimetry

3.1 Introduction

Polymers and polymer-like materials, such as asphalt binders, are in amorphous state at high temperatures and cooling of them demonstrates the transition from an amorphous to a glassy state. A stepwise increase of stiffness modulus, specific volume, and thermal expansion coefficient happen through the amorphous-to-glass transition, or glass transition. The glass transition region is the range of temperatures that correspond to this transition.

The glass transition temperature (T_g) is related to the overall chemical composition of materials. Based on past research, the T_g of asphalt binders of different performance grades and from different crude oil resources was shown to extend over the range between -60 and 0°C (Claudy et al., 1991; Claudy et al., 1992; Harrison et al., 1992; Bahia 1992, Jimenez-Mateos et al., 1996; Turner & Branthaver 1997; Planche et al., 1998; Anderson & Marasteanu 1999; Masson & Polomark 2001; Kriz et al., 2007; Qin et al., 2014; Frolov et al., 2017; Adams et al., 2019; Elwardany et al., 2019; Ding & Hesp 2021). The glass transition depends on the degree of aging as well, with the increase of T_g values to be associated with the increase of asphaltenes in binders (Turner & Branthaver 1997). From the mechanics point of view, the T_g can be used to interpret low temperature thermal cracking defects in asphalt pavements. Below the T_g binders exhibits brittle behaviour, while they are ductile at temperatures above T_g .

Differential scanning calorimetry (DSC) has been accepted as a robust instrument to determine the glass transition of asphalt binders as well as other enthalpy related transitions. With this device, the endothermic or exothermic heat flow of a sample can be monitored under a controlled temperature program. Moreover, the DSC has been proved as a powerful tool to evaluate the T_g of different copolymers as well as their miscibility with asphalt binders. As mentioned in **Chapter 2**, the miscibility, or lack of it, determines the performance of binders. On the one hand, a single T_g , otherwise a single blend-average T_g , indicates a single phase system, and on the other hand, blends of two T_g values manifest two phases systems. In asphalt binders, alterations of glass transitions manifest to changes of a single T_g . Many studies have been performed to evaluate the miscibility of various polymers in binders with the goal to link with other properties (Ho et al., 1997; Fawcett & McNally 2001; Kamiya et al., 2001; Varma et al., 2002; Masson et al., 2005a & 2005b; Adams et al., 2019; Kaya et al., 2020).

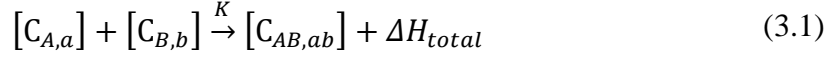
In epoxy-asphalt binders, it has been found that the bisphenol A diglycidyl ether (DGEBA), the main compound of epoxy resins, is immiscible with asphalt binders (Laval & Quivoron 1973; Laval & Brule 1974). Nevertheless, improved miscibility between epoxy polymers and asphalt binders is possible by applying specific formulations. Certain epoxy formulations may result in miscible binders and thus it is of high importance to evaluate their impact on the curing of epoxy-asphalt binders. The determination of optimum conditions during manufacturing flexible pavements will also assist the future binder formulations to avoid the undesired over-curing of thermosetting materials and thus the negative effect of reduced mix workability during construction.

In this **chapter**, the DSC is used to perform analyses of asphalt binders modified with various types of epoxy formulations to elucidate the curing behavior of new thermosetting systems. The parameters which will be determined in this **chapter** will be used as input in the chemo-

rheological model (see **Chapter 4**). The procedure to determine the kinetic parameters of curing epoxy-asphalt binders is described in the next section.

3.2 Curing Kinetics

As an epoxy-asphalt binder turns irreversibly into a crosslinked system, heat is released proportionally to the consumption rate of reactive components as



where $C_{A,a}$ and $C_{B,b}$ are the concentrations of the two reactive components in phases a and b (before reaction), $C_{AB,ab}$ is the concentration of component AB of the newly produced phase ab , or binder (after curing), K is the rate of reaction and ΔH_{total} is the total exothermic heat of reaction. Subscripts a , b and ab indicate the phases where A , B and AB components exist, respectively.

The exothermic heat of reaction ΔH up to time t can be calculated by

$$\Delta H(t) = \int_0^t \left(\frac{dQ}{dt} \right) dt \quad (3.2)$$

where dQ/dt is the rate of exothermic heat generation.

As shown in the heat flow signal in **Fig. 3.1**, the total heat of reaction (ΔH_{total}) is calculated based on a baseline constructed by connecting the two points at which the exotherm deviate from the relatively straight baseline. The area under the heat flow exotherm signal is integrated as a function of time to yield the ΔH_{total} .

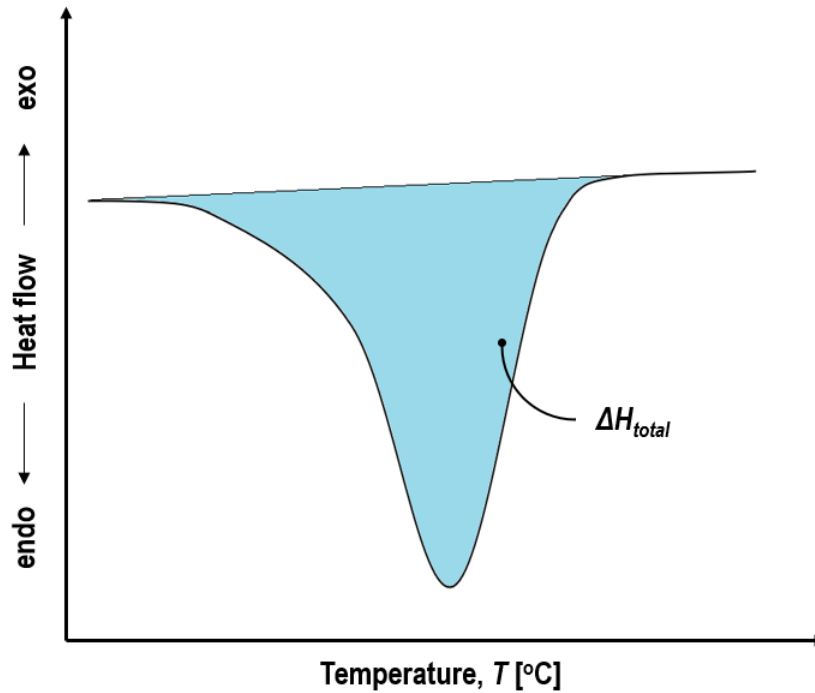


Figure 3.1 Typical thermograph through heating.

The total exothermic heat ΔH_{total} up to t_{total} is defined as

$$\Delta H_{total} = \int_0^{t_{total}} \left(\frac{dQ}{dt} \right) dt \quad (3.3)$$

where t_{total} is the time required to complete the reaction and ΔH_{total} is the amount of heat generated during the measurement until the completion of curing.

Non-isothermal measurements of reaction heat of binders as a function of time and temperature yield information about the degree of conversion (x). The degree of conversion is derived from the measured exothermic heating rates by dividing the rates by the total exothermic heat as

$$x = \frac{\Delta H(t)}{\Delta H_{total}} \quad (3.4)$$

where $\Delta H(t)$ is the partial area under a calorimetric measurement up to time t . The degree of conversion has the same meaning as the parameter x discussed in **Eq. 2.9** in **Chapter 2**. When the conversion degree equals 0 the material is uncured, without any crosslink between the reacting molecules. If it is 1, the material is fully cured.

The curing rate is a parameter proportional to the heat release rate which is defined as

$$\frac{dx}{dt} = \frac{1}{\Delta H_{total}} \left(\frac{dQ}{dt} \right) \quad (3.5)$$

where dQ/dt is the rate of heat generation and is provided by the calorimetric measurements.

The determination of reaction kinetics is crucial to develop a prediction scheme for the chemorheology of curing binders. The kinetic model allows to predict the conversion degree and the reaction rate as a function of time and temperature of reacting binder as

$$\frac{dx}{dt} = K(T)f(x) \quad (3.6)$$

where $K(T)$ is a temperature-dependent parameter, which is described by an Arrhenius equation, and $f(x)$ is a conversion function. The Arrhenius equation is defined as

$$K(T) = K_0 \exp \left(-\frac{E_a}{RT} \right) \quad (3.7)$$

where K_0 is the pre-exponential kinetic factor, E_a is the activation energy or the energy barrier to be overtaken to begin the reaction and R is the universal gas constant.

Based on the n^{th} order model which is defined as

$$f(x) = (1 - x)^n \quad (3.8)$$

the reaction rate, according to **Eq. 3.6**, can be expressed as

$$\frac{dx}{dt} = K(T)(1 - x)^n \quad (3.9)$$

and hence

$$\frac{dx}{dt} = K_0 \exp\left(-\frac{E_a}{RT}\right) \cdot (1-x)^n \quad (3.10)$$

where n is the reaction order, which is defined as the power dependence of rate on the concentration of all reactants. This parameter represents the number of species whose concentration directly influences the reaction rate.

An illustration of a typical exothermic energy diagram of a curing material is given in **Fig. 3.2**. In this figure, the peak of red line represents the transition state of a reaction of high activation energy. In this case, only few epoxy molecules can obtain enough energy to reach the transition state without the assistance of an agent to facilitate the reaction. The purple dotted line in the same figure illustrates the reaction of the same molecules but with the assistance of a hardening agent. In the presence of this agent, the required energy for transition is lower (or activation energy is lower) and thus the reaction can proceed faster to a fully cured system without influencing the overall energy change of the reaction, or the total exothermic heat of reaction (ΔH_{total}). The total amount of reacting and producing molecules are the same before and after the reaction, respectively.

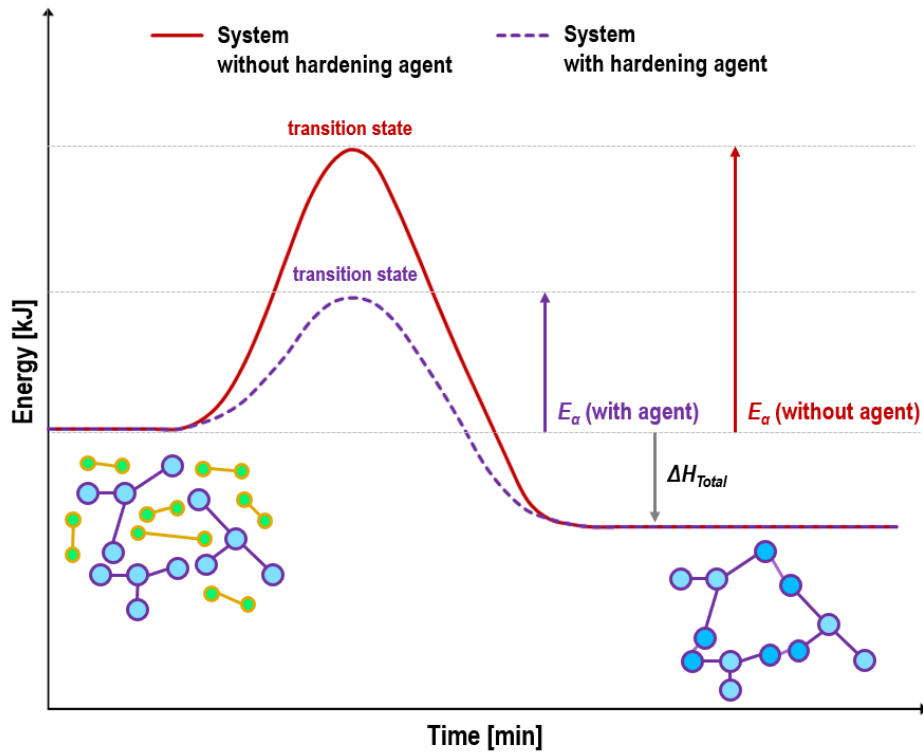


Figure 3.2 Exothermic energy diagram of a curing polymer with and without hardening agent. During the non-isothermal calorimetric analysis in a DSC, temperature varies linearly with time as

$$T - T(0) = \beta t \quad (3.11)$$

and

$$\beta = \frac{dT}{dt} \quad (3.12)$$

where T is the sample temperature, $T(0)$ is the initial temperature, t is time, and β is the rate of the temperature change.

For non-isothermal conditions, the theoretical shape of a calorimetric scan is expressed by

$$\beta \frac{dx}{dt} = K_0 \exp\left(-\frac{E_a}{RT}\right) (1-x)^n \quad (3.13)$$

Eq. 3.13 can be reduced to a linear form by taking the natural logarithm of both sides of the equation as

$$\ln\left(\beta \frac{dx}{dt}\right) = \ln K_0 - \frac{E_a}{RT} + n \ln(1-x) \quad (3.14)$$

A multi-linear regression is performed using $\ln[\beta(dx/dt)]$, $-1/RT$, and $\ln(1-x)$ as variables derived from DSC data to solve for K_0 , E_a , and n .

3.3 Differential Scanning Calorimetry

The use of DSC is based on a thermal analysis method that involves the measurement of heat flow (Q) and is utilized to determine the enthalpy related transitions of materials. The total heat flow signal (dQ/dt) from a calorimetry can be expressed as

$$\frac{dQ}{dt} = mC_p\beta + f(t, T) \quad (3.15)$$

where m is the sample mass, C_p is the baseline specific heat capacity of the sample and $f(t, T)$ is the heat flow due to kinetic processes, which is provided as a function of time (t) and temperature (T). Therefore, the total heat flow is composed of two parts; (i) the heat flow required to raise the sample temperature at a programmed heating (or cooling) rate, and (ii) the heat flow arising from the kinetic processes that may occur during the measurement. Phase change transitions, such as melting and crystallization, and second order transitions, such as glass transition and its associated enthalpy relaxation, are kinetic phenomena.

The C_p is the heat required to change the temperature of unit mass of a substance by one degree, therefore the temperature difference (ΔT) for a heat input (Q) is defined as

$$\Delta T = \frac{Q}{mC_p} \quad (3.16)$$

The C_p implies that it represents the heat capacity of a sample under equilibrium, which is mostly the case when the microstructure of a sample remains constant.

At constant pressure, where the heat input is equal to the enthalpy change, the operational definition of the C_p becomes

$$C_p = \frac{1}{m} \frac{dH}{dT} = \frac{1}{m\beta} \frac{dH}{dt} \quad (3.17)$$

where H is the enthalpy of the sample.

At the glass transition, the C_p increases from that of the glass to the amorphous in a sigmoidal way, as illustrated in the schematic in **Fig. 3.3**. In general, the T_g , C_p and heat capacity change at glass transition (ΔC_p) are obtained from the specific heat flow data during the calorimetric measurements. An equivalent endothermic heat flow increase also corresponds to the first term of **Eq. 3.15**. However, in some cases, small endothermic peak can be shown within the glass transition region, and these can be results of the relaxation behavior of a sample indicating the contribution of the second term in **Eq. 3.15**. The kinetic component in **Eq. 3.15** is linked with the thermal history of a sample, in other words the path by which a structural state is reached. The C_p of a sample depends always on the structural state in the transition region also considering the material thermal history.

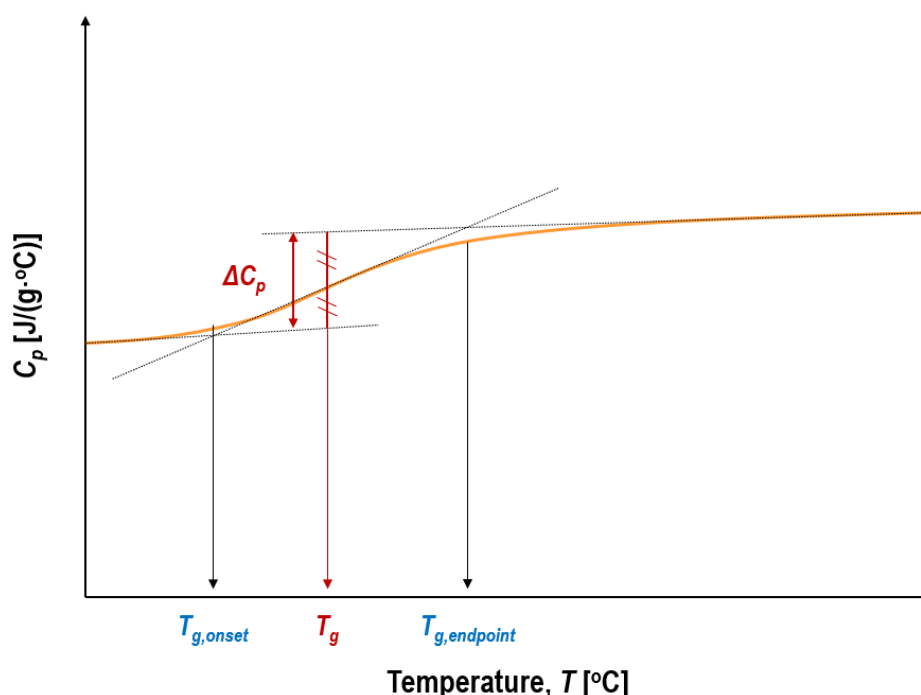


Figure 3.3 Schematic of specific heat capacity change at glass transition.

3.4 Calorimetric Measurements of Epoxy-Asphalt Binders

3.4.1 Materials and preparation

As discussed in **Chapter 2**, epoxy polymers for asphalt binders are normally binary reactive systems that enable the formation of a co-polymerized network under certain energy conditions. In this **chapter**, two epoxy polymers were selected, and their components used as received without any further purification. The polymers, named KD-HDP and KD-HYP, were formulated by two liquid parts; (i) the epoxy and (ii) the hardener. The part used as a hardener (i.e., B-KD) was an acrylonitrile-butadiene pre-polymer for both KD-HDP and KD-HYP, and the mix of KD-HDP and KD-HYP were named A-HDP and A-HYP, respectively.

To prepare the uncured samples for the calorimetric measurements, the two parts of KD-HDP were oven-heated first for 1 hr at 50°C, and then mixed manually together at weight ratio 61:39 (A-HDP : B-KD), according to the recommendations of the supplier. In a similar way, the two parts of KD-HYP polymer (weight ratio 50:50 of A-HYP and B-KD) were heated for

1 hr at 30°C in the oven, and immediately afterwards mixed together. In both cases, the two parts were mixed for approximately 20 s to minimize the curing during mixing. The freshly prepared samples were immediately placed in a freezer at -10°C.

For the formulation of an epoxy-asphalt binder with an equivalent amount of epoxy (20% wt resin of component A) for all studied cases, the uncured KD-HDP and KD-HYP polymers were mixed manually with an already pre-heated asphalt binder of 70/100 pengrade for 60 s at 170°C. The weight ratio of epoxy-asphalt binders (epoxy : hardener : asphalt) based on the before mentioned chemistries were 20:13:67 and 20:20:60, respectively.

To compare the material behaviour of all newly formed epoxy-asphalt binders, extra samples were prepared using the reference epoxy-asphalt binder (EA_{ref}) (see **Chapter 2**), which is formulated with amount equivalent to epoxy resin.

The compositions of studied formulations are collected in **Table 3.1**.

Table 3.1 Name and composition of studied EA binders.

	epoxy [% wt]	hardener [% wt]	asphalt binder [% wt]
KD-HDP	61 ¹	39 ²	0
KD-HYP	50 ³	50 ²	0
EA-HDP	20 ¹	13 ²	67
EA-HYP	20 ³	20 ²	60
EA _{ref}	20		80

¹ Part A-HDP consists of (a) bisphenol A – epichlorohydrin, dimer fatty acid polymer ($M_w = 320.814$ g/mol) (CAS: 68475-94-5), and (b) 2,3-epoxypropyl oleate ($M_w = 338.52$ g/mol) (CAS: 5431-33-4)

² Part B-KD consists of (a) 2-propenitrile polymer with 1.3butadiene, 1-cyano-1-methyl-4-oxo-4-[(2-(1-piperazinyl)ethyl)]amino]butyl-terminated ($M_w = 107.155$ g/mol) (CAS: 68683-29-4), (b) 9.12-octadecadienenoic(9Z,12Z)-dimer polymer, with 3.3-[oxybis(2.1-ethanediylloxy)]bis[1-propaneamine] ($M_w = 560.904$ g/mol) (CAS: 68541-13-9), and (c) phenyl-1-(3,4-dimethyl)phenylethane ($M_w = 210.32$ g/mol) (CAS: 6196-95-8)

³ Part A-HYP consists of (a) 2.2-[hexane-1.6-diylbis(oximethylene)]bis(oxirane) ($M_w = 230.152$ g/mol) (CAS: 16096-31-4), and (b) 4-tert-butylphenyl glycidyl ether ($M_w = 1.038$ g/mol) (CAS: 3101-60-8)

3.4.2 Calorimetry setting

In this study, the calorimetric measurements were performed on a power compensation DSC (Perkin-Elmer DSC). The enthalpy calibration in the instrument was conducted using the indium standard which has a well-known T_g (156.6°C) under a certain heating rate. Dry nitrogen was used as a purge gas. After the formulation of samples, they were sealed in aluminum pans (40µL), complying to ASTM E1356-08. Annealing was conducted before any measurement to remove any polar association existed in binders due to their thermal history.

It is important to note that heat transfer phenomena play crucial role in having accurate calorimetric measurements. The larger the mass of sample is, more non-uniform is the sample temperature distribution, and the larger the temperature phase angle between the sample and programmed temperature. The sample weights ranged from 10 to 15 mg to minimise the thermal lag. During the measurements, the DSC monitors the heat flow of samples under controlled conditions by having an empty pan as reference.

3.4.3 Temperature linear calorimetric measurements

To study the curing kinetics of epoxy-asphalt binders, their non-isothermal behaviour in an inert nitrogen environment was investigated using heating rates of 5, 10, 20 and 40°C/min in a temperature range from 0 to 300°C. Furthermore, non-isothermal measurements performed to determine the T_g evolution at different times over the curing of binders (two replicates per material). Samples were oven-conditioned at 130°C as well for different time intervals; from 0 to 3 hrs with a time step of 0.5 hrs and scanned from 0 to 300°C with 40°C/min heating rate.

As shown in **Fig. 3.4**, a single exothermic peak is demonstrated for all applied heating rates in EA_{ref}. Based on these scans, the total exothermic reaction heat (ΔH_{total}) of different binders was determined by the integration of TL-DSC signals at different heating rates (see **Eq. 3.3**). The shape of exothermic heat was almost the same for all binders independently on the epoxy formulation. The kinetic parameters of occurring reactions are calculated based on the theory discussed earlier (see **section 3.2**). The effect of different formulations on the curing of neat epoxy polymers and epoxy-asphalt binders is determined (see **Fig. 3.5**). The parameters of curing kinetics of studied materials are listed in **Table 3.2**, which includes also the calorimetric information obtained from the TM-DSC measurements.

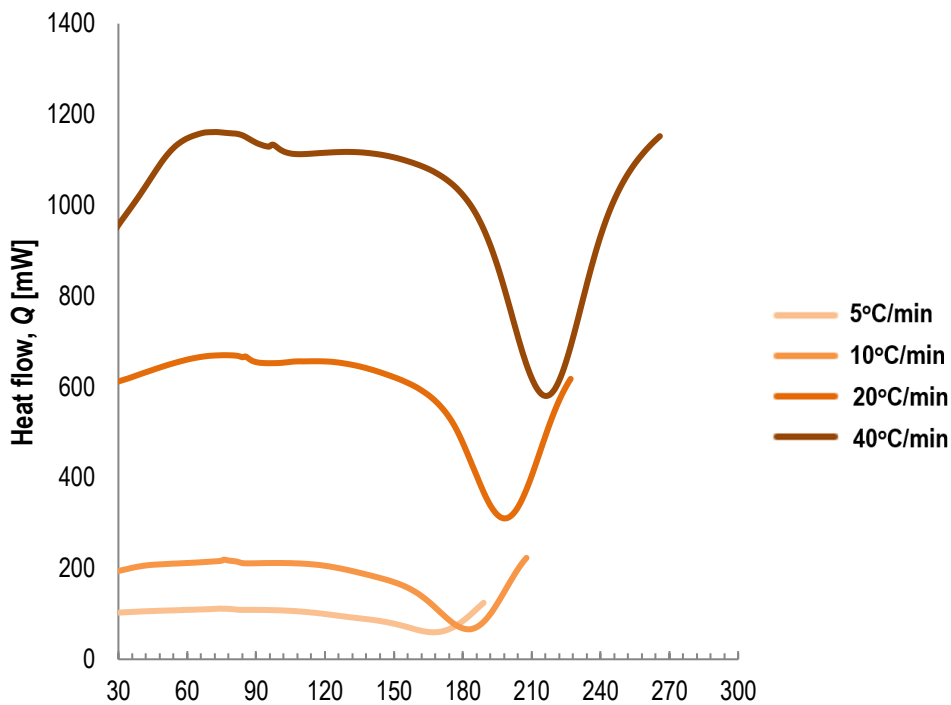
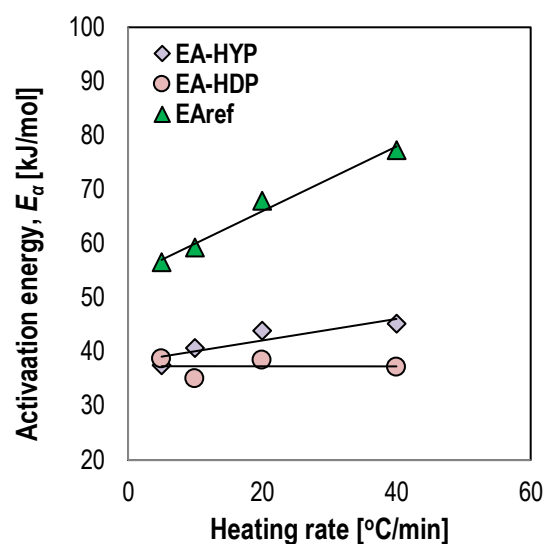
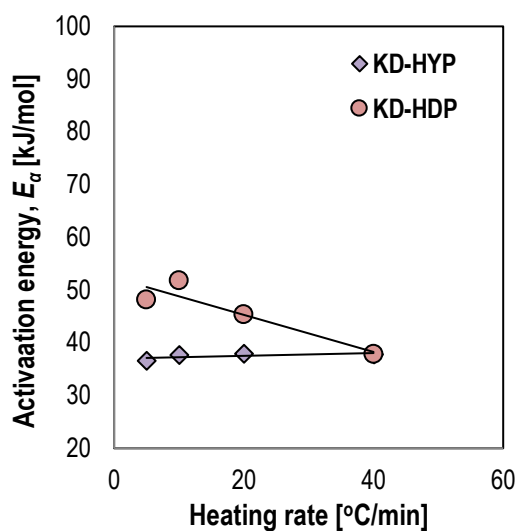
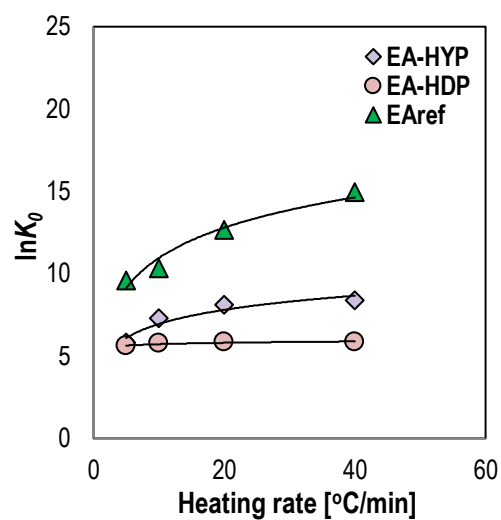
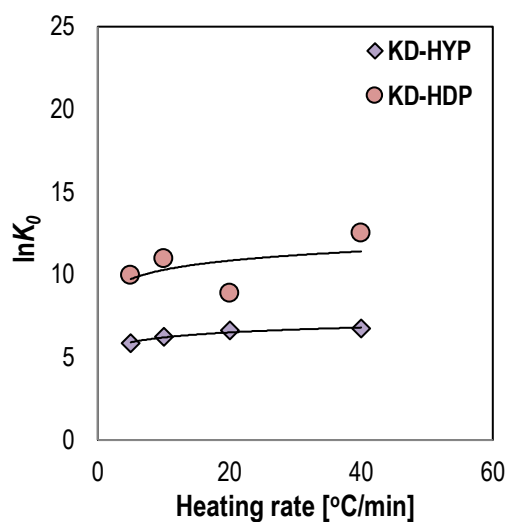


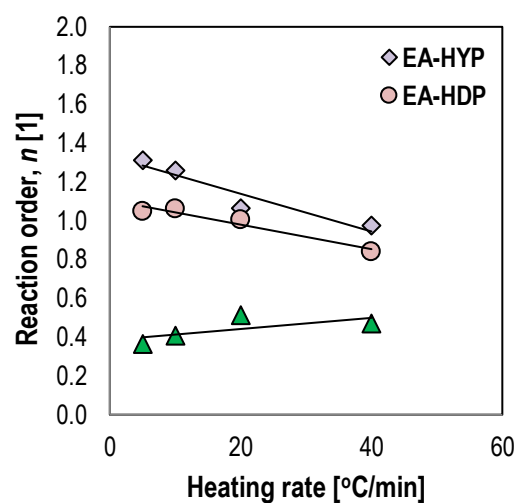
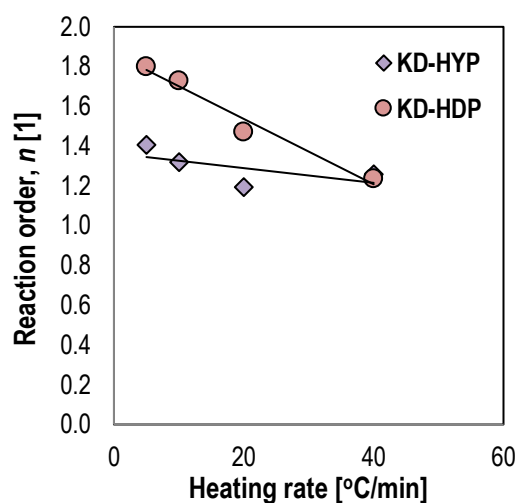
Figure 3.4 Standard non-isothermal TL-DSC measurements at different heating rates of EA_{ref}.



(a)



(b)



(c)

Figure 3.5 Kinetic parameters; (a) activation energy, (b) reaction rate and (c) reaction order corresponding to standard TL-DSC curve of each studied material.

The proportion of epoxy (i.e., 20% wt) and asphalt binder together with hardener (i.e., 80% wt) is fixed for all binders (see **Table 3.1**), only the formulation of the epoxy polymer was changed. It was expected that by changing the epoxy formulation, significant differences will be observed in the kinetic parameters of binders (i.e., E_a , K_0 , n).

As shown in **Fig. 3.5**, the activation energy (E_a), which is the energy barrier to be overtaken to initiate the curing reaction, is higher for EA_{ref} than EA-HDP and EA-HYP. Thus, the reference epoxy-asphalt binder demands higher applied energy levels to initiate the curing. However, once this binder overtakes this energy barrier, it cures faster (higher reaction rate) than the other binders. This observation is contradictory with previous studies on the topic but by assessing different binders and epoxy formulations (Yin et al., 2014; Li et al., 2014). Marginally lower activation energy values for epoxy-asphalt binder (46-49 kJ/mol (Yin et al., 2014) and 65 kJ/mol (Li et al., 2014)) than of their neat epoxy polymers (50 kJ/mol (Yin et al., 2014) and 78 kJ/mol (Li et al., 2014)) have been shown.

In addition to curing kinetic parameters, the T_g changes due to the curing of different binders are examined. The T_g is shifting to higher temperatures as curing proceeds and crosslinks are formed. A higher T_g corresponds to a greater degree of conversion. In other words, the T_g values rise with the material curing until achieving an ultimate value corresponding to the ultimate conversion degree at a given temperature.

Fig. 3.6 shows how the T_g changes as curing proceeds by the TL-DSC measurements of EA_{ref} at different time intervals emphasizing on the temperature range from -50 to 50°C.

The curing and increase of degree of conversion shift the T_g towards higher temperatures indicating more rigid molecular chains, and thus the high strength of forces between the molecules. Furthermore, the increase of T_g values reflects the rise of cracking susceptibility of binders due to the ductile to brittle transition behavior.

The T_g evolution over curing time (in the oven) of different epoxy polymers (i.e., KD-HDP and KD-HYP) is shown in **Fig. 3.7a**. Similarly, the T_g increase due to the curing of epoxy-asphalt binders (i.e., EA-HDP, EA-HYP and EA_{ref}) is demonstrated in **Fig. 3.7b**. The T_g studies after the non-isothermal measurements demonstrate a significant difference between the epoxy polymers and modified binders. By comparing **Fig. 3.7a** and **3.7b**, it is obvious that the epoxy cures faster than epoxy-asphalt binders showing that the asphalt binder hinders the interaction between the reactive components of polymers and thus slows down the reaction process. The difference in the extent of the T_g is observed when different polymers are cured. During curing, the KD-HYP demonstrates a higher extent of the T_g than KD-HDP (see **Fig. 3.7a**).

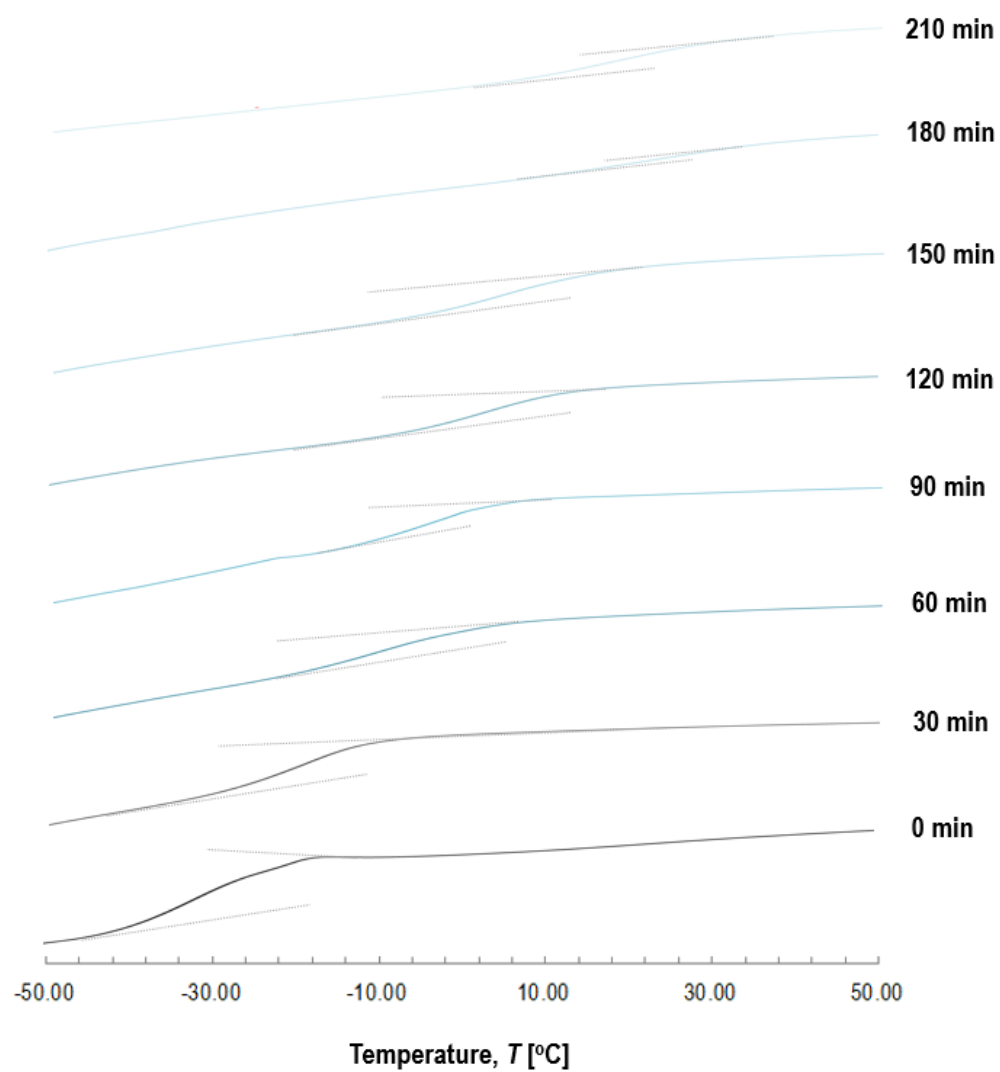


Figure 3.6 The T_g of EA_{ref} at different time intervals after standard non-isothermal calorimetric scans.

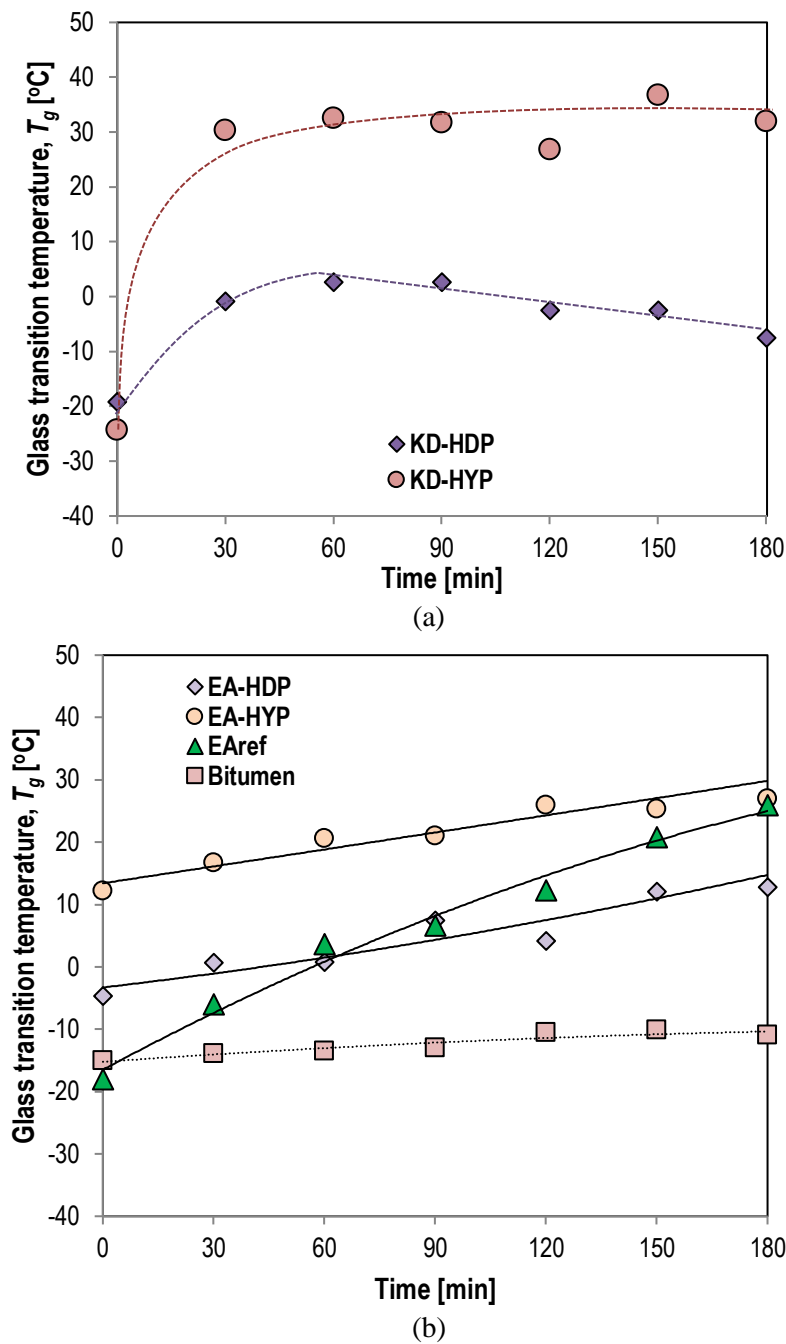


Figure 3.7 The T_g evolution during cure at 130°C of (a) epoxy polymers KD-HDP and KD-HYP and (b) epoxy-asphalt binders EA-HDP, EA-HYP, EA_{ref}, and bitumen (or asphalt binder), after standard non-isothermal calorimetric scans.

3.4.4 Temperature modulated calorimetric measurements

In addition to the standard temperature-linear DSC (TL-DSC), modulated calorimetric analyses were conducted for all binders as well. The temperature-modulated DSC (TM-DSC) is a powerful technique that has been used as a platform to assess both the reversing and non-reversing phenomena of polymers and polymer-like materials. A modulated temperature signal, which is superimposed on the linear heating or cooling temperature program, can be applied to elucidate the thermo-kinetic phenomena, such as cold crystallization, occurring

through thermal scanning (Gill et al., 1993; Schawe 1995; Reading 2001; Simon 2001). As it is less uncertain and ambiguous the definition and selection of baselines and end point in TM-DSC than in TL-DSC, the detection of different thermal events and enthalpic changes is more precise (Apostolidis et al., 2021).

In TM-DSC, the most implemented program is the sinusoidal temperature modulation of a frequency (ω) and amplitude (A_T) which is superimposed on a certain constant heating and/or cooling rate (β), with an initial temperature T_0 . With a sinusoidal temperature modulation, the temperature at any time t is provided as

$$T = T_0 + \beta t + A_T \sin \omega t \quad (3.18)$$

Here, a periodical step-scan signal is superimposed on the linear temperature changes yielding a heating profile, as shown in **Fig. 3.8**, with continuously non-linearly changes of average temperature of sample with time. After changing the sample mode, by 1°C at a certain heating rate, the heat flow rate can equilibrate again. Based on a Discrete Fourier Transformation, the measured amplitudes of modulation of temperature and heat flow are compared to a reference signal of the same periodic characteristics calculating thus the heat capacity. Thus, the TM-DSC method permits the calculation of the heat capacity of sample.

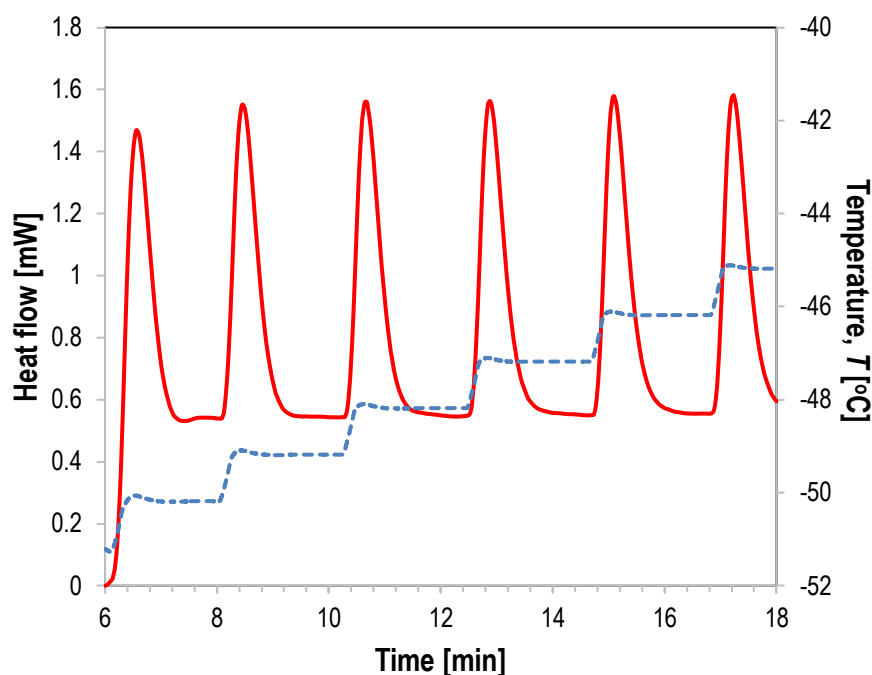


Figure 3.8 Typical temperature modulation profile and heat flow generated versus time in a TM-DSC measurement. The blue dotted line and orange line demonstrate the underlying temperature and heat flow, respectively.

The samples were cooled to -50°C, equilibrated at this temperature for 5 min, and then were heated to 200°C at a rate of 5°C/min with 1°C modulation amplitude every 120 s (modulation period). After reaching the set temperature of 200°C, the samples were kept at this temperature for 5 min to reach equilibrium. The modulated scans track the difference in heat flow between a sample and an inert reference pan as a function of time and temperature.

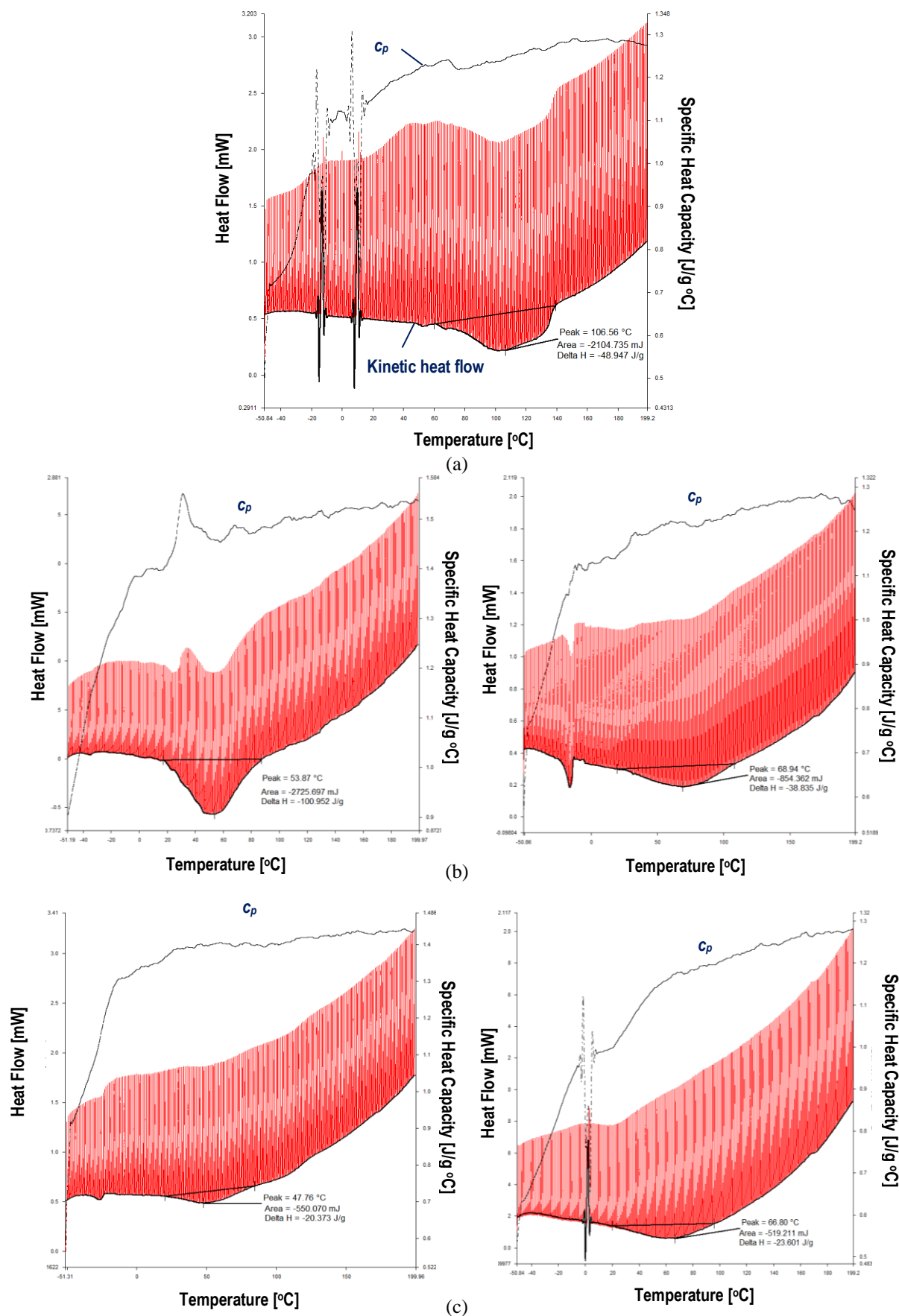


Figure 3.9 TM-DSC scans of (a) EA_{ref}, (b) KD-HDP (left) and EA-HDP (right) and (c) KD-HYP (left) and EA-HYP (right) including the heat flow (red line).

Table 3.2 Kinetic parameters corresponding to TL-DSC and TM-DSC measurements of studied materials.

	Heating rate [°C/min]	Activation energy, E_a [kJ/mol]	Reaction rate, K_0 [1/s]	Reaction order, n [1]	Total heat flow, ΔH_{total} [J/gr]
KD-HDP	5	48.08 ± 0.51	$2.1E04 \pm 3.0E03$	1.80 ± 0.01	-73.13 ± 1.54
	10	51.74 ± 0.60	$5.8E04 \pm 3.1E03$	1.73 ± 0.01	-127.70 ± 5.08
	20	45.28 ± 3.22	$7.0E03 \pm 5.2E03$	1.47 ± 0.02	-131.70 ± 8.38
	40	37.86 ± 3.45	$5.1E05 \pm 2.3E05$	1.23 ± 0.05	-55.17 ± 0.52
				TM-DSC	-100.95
KD-HYP	5	36.63 ± 0.34	$3.5E02 \pm 3.9E01$	1.41 ± 0.00	-47.10 ± 3.98
	10	37.63 ± 0.41	$5.1E02 \pm 1.3E01$	1.32 ± 0.01	-47.23 ± 0.64
	20	37.87 ± 1.17	$7.3E02 \pm 3.1E01$	1.19 ± 0.01	-47.52 ± 0.34
	40	37.86 ± 2.12	$8.4E02 \pm 2.8E01$	1.26 ± 0.01	-41.56 ± 0.67
				TM-DSC	-20.37
EA-HDP	5	38.66 ± 1.03	$2.3E02 \pm 4.2E01$	1.05 ± 0.03	-60.99 ± 2.94
	10	35.05 ± 1.15	$3.2E02 \pm 1.3E01$	1.06 ± 0.03	-39.57 ± 0.23
	20	38.47 ± 1.37	$3.4E02 \pm 1.2E01$	1.01 ± 0.04	-37.12 ± 0.29
	40	37.16 ± 2.30	$3.7E02 \pm 1.1E02$	0.84 ± 0.05	-25.03 ± 2.16
				TM-DSC	-38.84
EA-HYP	5	37.53 ± 1.38	$3.5E02 \pm 1.2E02$	1.31 ± 0.04	-28.39 ± 1.60
	10	40.76 ± 1.63	$1.6E03 \pm 8.4E02$	1.26 ± 0.06	-30.83 ± 1.56
	20	43.92 ± 1.87	$3.4E03 \pm 8.9E02$	1.06 ± 0.08	-12.38 ± 6.84
	40	45.22 ± 3.16	$4.8E03 \pm 4.7E02$	0.97 ± 0.09	-11.15 ± 0.30
				TM-DSC	-23.60
EA _{ref}	5	56.54 ± 2.19	$1.7E04 \pm 9.6E03$	0.36 ± 0.01	-27.86 ± 2.25
	10	59.27 ± 1.65	$3.3E04 \pm 1.5E04$	0.41 ± 0.01	-48.94 ± 3.33
	20	67.95 ± 7.52	$1.1E06 \pm 1.1E06$	0.51 ± 0.02	-51.58 ± 3.18
	40	77.24 ± 14.39	$6.8E07 \pm 6.8E07$	0.47 ± 0.16	-38.91 ± 3.60
				TM-DSC	-48.95

The graph in **Fig. 3.9(a)** shows the heat flow (red line) together with the specific heat capacity and kinetic curves of EA_{ref} after performing the calculation in the Pyris DSC software. Irregular peaks are shown in EA_{ref} which affect the precise positioning of the baseline tangents and thus the individual T_g values of epoxy and asphalt binder cannot be given. This issue is difficult to resolve for the uncured binders because they should be pre-heated at high temperatures and then cooled down with modulation before any measurement to remove any extraneous thermal effect. This pre-treatment before curing will result in crosslinks in the binders and thus the accuracy of kinetics will be lost. In such thermo-hardening binders, the TM-DSC measurements without this pre-treatment will also cause a lack of accuracy. Therefore, it is hard to determine the exact evolution of the T_g during the curing for a thermosetting binder by performing TM-DSC measurements. This also explains the change of the T_g position as the curing progresses and thus a broader glass transition region appeared, especially in the thermographs of neat epoxy polymers and epoxy-asphalt binders in **Fig. 3.9(b)** and **3.9(c)**. The broad glass transition region is shown having T_g values closer to those of fully cured binders.

Finally, the total exothermic heat flow determined from the two performed calorimetric methods shows similar values. For example, the total heat released from the curing EA_{ref} was -48.95 and -51.58 J/gr (see also **Table 3.2**) for the modulated and standard analysis (heating rate of 20°C/min), respectively.

3.5 Summary

In this **chapter**, two different epoxy formulations were used as asphalt binder modifiers by having a proprietary protected epoxy-asphalt binder as a reference, and their thermal behaviour under the standard TL-DSC and the TM-DSC measurements were observed. These measurements performed in a DSC provided insight into the processing parameters by considering the release of heat during the calorimetric measurements proportional to the progress of chemical reactions. Curing kinetic parameters and the T_g change were determined for the epoxy polymers and epoxy-asphalt binders under different conditions.

Particularly, the T_g is shifting to higher temperatures as curing progresses and crosslinks are formed, with the neat epoxy polymers to crosslink faster than the epoxy-asphalt binders. The asphalt binder also hinders the interaction between the two reacting epoxy components, and thus a reduction of the T_g evolution rate was obtained. The effect of applied energy on the curing of the studied materials was more pronounced on the neat epoxy compared to the asphalt binders modified with those polymers.

The insights provided by the TL-DSC were compared those obtained from the TM-DSC measurements as well. The modulated measurements offer higher precision in the determination of the T_g by isolating the scans from other thermal-driven events. Nevertheless, the exact evolution of the T_g of reacting materials by performing TM-DSC measurements was hard to obtain since a broad glass transition region was found. During the TM-DSC measurements, the binders were curing and hence the glass transition regions were shifting over scanning.

Overall, the determination of optimum curing conditions based on calorimetric measurements as performed in this **chapter** can assist to guide the design of epoxy-asphalt binder to avoid the negative effect of reduced mix workability during construction. In combination with the in-

depth understanding of the thermodynamics of thermosetting binders, the material designers would be able to control various curing induced phenomena (e.g., phase separation) by obtaining the appropriate calorimetric information.

3.6 References

- Adams, J.J., M.D. Elwardany, J.P. Planche, R.B. Boysen, J.F. Rovani. Diagnostic Techniques for Various Asphalt Refining and Modification Methods. *Energy and Fuels* 2019.
- Anderson, D.A., M.O. Marasteanu. Physical Hardening of Asphalt Binders Relative to Their Glass Transition Temperatures. *Transportation Research Record* 1661, 1999, pp. 27–34.
- Apostolidis, P., M. Elwardany, L. Porot, S. Vansteenkiste, E. Chailleux. Glass Transitions in Bituminous Binders. *Materials & Structures* 54:132, 2021.
- ASTM E1356-08. Standard Test Method for Assignment of the Glass Transition Temperatures by Differential Scanning Calorimetry, 2014.
- Bahia, H. *Low-Temperature Isothermal Physical Hardening of Asphalt Cements*. PhD dissertation. The Pennsylvania State University, 1992.
- Claudy, P., J.M. Letoffe, G.N. King, J.P. Planche, B. Brule. Characterization of Paving Asphalts by Differential Scanning Calorimetry. *Fuel Science and Technology International* 9(1), 1991, pp. 71-92.
- Claudy, P., J.M. Letoffe, G.N. King, J.P. Planche. Characterization of Asphalts Cements by Thermomicroscopy and Differential Scanning Calorimetry: Correlation to Classic Physical Properties. *Fuel Science and Technology International* 10(4-6), 1992, pp. 735–765.
- Ding, H., S.A.M. Hesp. Another Look at the Use of Modulated Differential Scanning Calorimetry to Study Thermoreversible Aging Phenomena in Asphalt Binders. *Construction and Building Materials* 267, 2021, 121787.
- Elwardany, M.D., J.P. Planche, J.J. Adams. Determination of Binder Glass Transition and Crossover Temperatures using 4-mm Plates on a Dynamic Shear Rheometer. *Transportation Research Record* 2673(10), 2019, pp. 247-260.
- Fawcett, A.H., T. McNally. Blends of Bitumen with Polymers Having a Styrene Component. *Polymer Engineering and Science* 41(7), 2001, pp. 1251-64.
- Frolov, I.N., T.N. Yusupova, M.A. Ziganshin, E.S. Okhotnikova, A.A. Firsin. Dynamics of Formation of Asphalt Microstructure according to Modulated Differential Scanning Calorimetry Data. *Petroleum Chemistry* 57(12), 2017, pp. 1002-06.
- Harrison, I.R., G., Wang, T.C. Hsu. *A Differential Scanning Calorimetry Study of Asphalt Binders*, Strategic Highway Research Program (SHRP), National Academy of Sciences: Washington, D.C., 1992, SHRP-A/UFR-92-612.
- Ho, R.M., A. Adedeji, D.W. Giles, D.A. Hajduk, C.W. Macosko, F.S. Bates. Microstructure of Triblock Copolymers in Asphalt Oligomers. *Journal of Polymer Science: Part B: Polymer Physics* 35, 1997, pp. 2857-77.
- Jimenez-Mateos, J.M., L.C. Quintero, C. Rial. Characterization of Petroleum Bitumens and their Fractions by Thermogravimetric Analysis and Differential Scanning Calorimetry. *Fuels* 75(15), 1996, pp. 1691-1700.
- Kamiya, S., S. Tasaka, X. Zhang, D. Dong, N. Inagaki. Compatibilizer Role of Styrene-Butadiene-Styrene Triblock Copolymer in Asphalt. *Polymer Journal* 33(3), 2001.

- Kaya, D., A. Topal, J. Gupta, T. McNally. Aging Effects on the Composition and Thermal Properties of Styrene-Butadiene-Styrene (SBS) Modified Bitumen. *Construction and Building Materials* 235, 2020, 117450.
- Kriz, P., J. Stastna, L. Zanzotto. Glass Transition and Phase Stability in Asphalt Binders. *Road Materials and Pavement Design* 9, 2007, pp. 37-65.
- Laval C, C. Quivoron. Mise en Evidence d'une Corrélation Entre le Rapport Hydrophile/Lipophile des Résines Epoxydes et leur Compatibilité Avec le Bitumen Routier. *C R Acad Sci IIc* 256, 1973, 743–6.
- Laval, C., B. Brûlé. Etude Expérimentale de la Compatibilité de Résines Epoxydes avec le Bitume. Application à la Prévision de Systèmes Compatibles, Rapport LCPC 40, 1974.
- Li, S., K. Huang, X. Yang, M. Li, J. Xia. Design, Preparation and Characterization of Novel Toughened Epoxy Asphalt Based on a Vegetable Oil Derivative for Bridge Deck Paving. *Royal Society of Chemistry* 4, 2014, pp. 44741-49.
- Masson, J.F., G.M. Polomark. Bitumen Microstructure by Modulated Differential Scanning Calorimetry. *Thermochimica Acta* 374, 2001, pp. 105-114.
- Masson, J.F., G.M. Polomark, P. Collins. Time-Dependent Microstructure of Bitumen and its Fractions by Modulated Differential Scanning Calorimetry. *Energy & Fuels* 16, 2002.
- Masson, J.F., S. Bundalo-Perc, A. Delgado. Glass Transitions and Mixed Phases in Block SBS. *Journal of Polymer Science: Part B: Polymer Physics* 43, 2005a, pp. 276-279.
- Masson, J.F., G. Polomark, P. Collins. Glass Transitions and Amorphous Phases in SBS-Bitumen Blends. *Thermochimica Acta* 436, 2005b, pp. 96-100.
- Planche, J.P., P.M. Claudy, J.M. Létoffé, D. Martin. Using Thermal Analysis Methods to Better Understand Asphalt Rheology. *Thermochimica Acta* 324, 1998, pp. 223–227.
- Reading, M. The Use of Modulated Temperature Programs in Thermal Methods. *Journal of Thermal Analysis and Calorimetry* 64, 2001, pp. 7-14.
- Qin, Q., M.J. Farrar, A.T. Pauli, J.J. Adams. Morphology, Thermal Analysis and Rheology of Sasobit Modified Warm Mix Asphalt Binders. *Fuel* 115, 2014, pp. 416–425.
- Schawe, J.E.K. A Comparison of Different Evaluation Methods in Modulated Temperature DSC. *Thermochimica Acta* 260, 1995, pp. 1–16.
- Simon, S.L. Temperature-Modulated Differential Scanning Calorimetry: Theory and Application. *Thermochimica Acta* 374, 2001, pp. 55-71.
- Stephens, R.F.T. ed. *Polymer Networks, Principles of their Formation, Structure and Properties*. Blackie Academic & Professional, London, 1998.
- Turner, T.F., J.F. Branthaver. DSC Studies of Asphalts and Asphalt Components. In *Asphalt Science and Technology*, Usmani, A., Ed. CRC Press: Boca Raton, FL, 1997, pp. 59–102.
- Varma, R., H. Takeichi, J.E. Hall, Y.F. Ozawa, T. Kyu. Miscibility Studies on Blends of Kraton Block Copolymer and Asphalt. *Polymer* 43, 2002, pp. 4667-71.
- Yin, H. H. Jin, C. Wang, Y. Sun, Z. Yuan, H. Xie, Z. Wang, R. Cheng. Thermal, Damping, and Mechanical Properties of Thermosetting Epoxy-modified Asphalts. *Journal of Thermal Analysis and Calorimetry* 115, 2014, pp. 1073–80.

4

Simulation of Curing Induced Hardening of Epoxy-Asphalt Binders

4.1 Introduction

During mixing, paving and compaction of asphalt mixes, the rheological properties of asphalt binders, and particularly the viscosity, play key role. High production temperatures decrease the viscosity of asphalt binder allowing the effective wetting of aggregate surface. During construction, the asphalt mixture should be workable enough as well, or the binder to have low enough viscosity, to prevent segregation without also causing a material of pre-mature cracks. In accordance with AASHTO M320, the binder viscosity should not exceed 3 Pa·s at 135°C to allow sufficient workability for the paving mixes. Nonetheless, the processing of thermosetting epoxy-asphalt (EA) binders is more complicated.

Higher temperatures accelerate the epoxy curing and lower the time window for the transport and compaction of thermosetting mixes. The uncontrolled irreversible curing of such materials before compaction and during the early traffic period remains the main technical issue that prohibits the wide use of this technology, even though it has been implemented in various bridges and highways internationally (Lu & Bors 2015; International Transport Forum 2017).

On the one hand, the relatively slow curing of EA could lead to paving mixtures that may segregate after compaction due to the low material viscosity, lower than that of standard asphalt binders at the onset of compaction. On the other hand, if the in-plant production and transport temperature of EA is too high, the material could be fully cured before paving which will make the material compaction impossible. Therefore, it is crucial to control the whole production chain of EA materials to ensure the development of roads with the desired properties and subsequently performance characteristics.

Within the framework of this thesis, the focus of this **chapter** is on developing a model to simulate the thermo-hardening behaviour of a thermosetting EA binder (or more strictly the chemo-rheology) under certain energy conditions, or constraints in temperature and time for production and construction. As the development of physical (i.e., glass transition temperature) and rheological (i.e., viscosity) properties plays a role to characterize the EA workability, the curing induced changes of these properties will be determined by conducting laboratory experiments. These parameters will be used as input for the chemo-rheological model as well.

4.2 Changes due to Curing

A rigid three-dimensional polymer network is formed when the epoxy molecules react chemically with a set of hardeners. This phenomenon is called curing and it starts with the formation, branching and, finally, the crosslinking of epoxy molecules. As curing proceeds, the molecular weight and viscosity increase toward infinite, and the gel point is reached when the molecular weight becomes theoretically infinite. The kinetically controlled material transition from viscous liquid to a viscoelastic gel is called gelation. Prior to gelation, the epoxy molecules are soluble in appropriate solvents and the polymer is at a liquid state. The viscosity of the initial liquid polymer will increase together with the glass transition temperature over curing. Once the gel point reached, the epoxy molecules have interacted together, branched molecules are created, and an initial macromolecular network is formed. The stiffness modulus grows continuously at the post-gelation regime indicating the densification of the polymer network.

In general, the epoxy polymers are viscoelastic materials demonstrating temperature and time dependent behavior. In **Fig. 4.1**, a schematic of relaxation curves at different degrees of conversion are illustrated indicating the effect of the molecular weight of a thermosetting binder, and subsequently the conversion degree on stress relaxation modulus. Specifically, the viscoelastic behavior also including the impact of increasing the molecular weight and thus the degree of conversion (i.e., crosslink density) on the modulus at different temperatures is schematically illustrated in **Fig. 4.1**. As discussed earlier, the thermosetting polymer gradually transforms from liquid state into a viscoelastic solid with a relatively high stiffness modulus. The modulus is almost zero before the gelation. In the range from x_1 to x_7 , the modulus exhibits a very short plateau, like a viscous liquid, indicating the material behavior at the pre-gel regime. On the basis of the schematic of **Fig. 4.1**, the gelation (x_{gel}) occurs between the degree of conversions x_7 and x_8 . At the post-gel regime (x_8 , x_9 and x_{10}), the amplitude of rubbery plateau dominates the material response at high temperatures, or at long times.

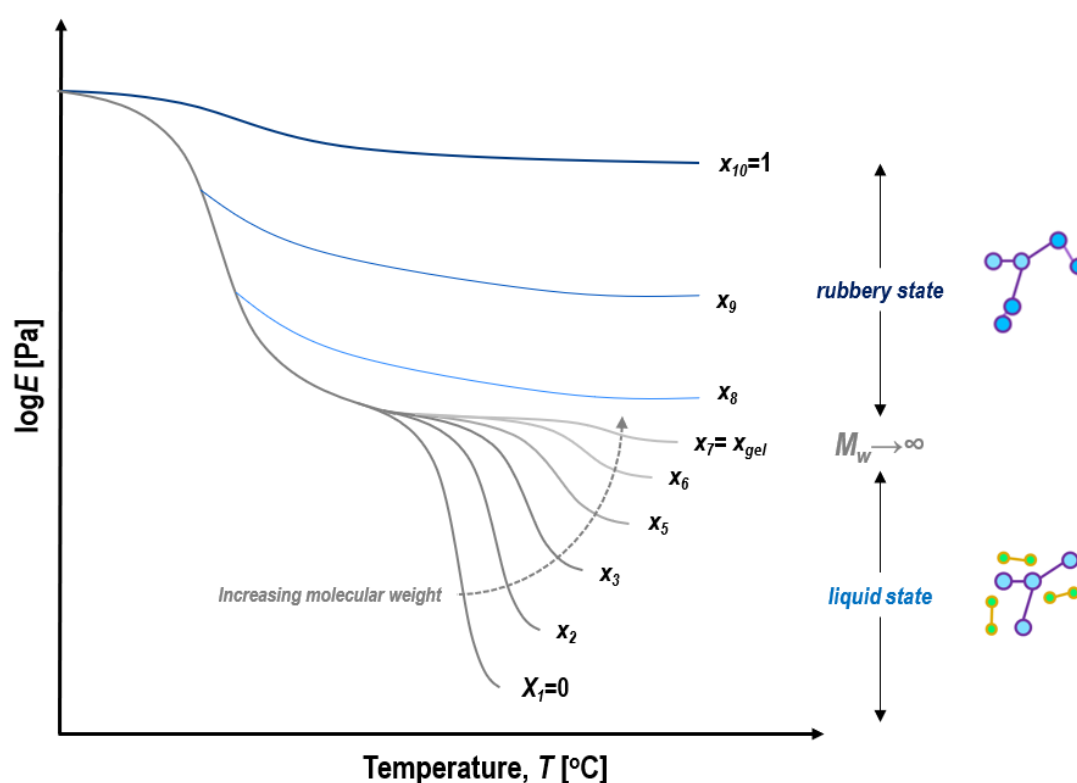


Figure 4.1 Schematic of the effect of molecular weight and degree of conversion ($x_1 < x_2 < \dots < x_{10}$) on stress relaxation modulus.

The curing reactions of polymers are dependent on the externally applied energy in the form of temperature and/or pressure and these reactions generate internal heat making the curing process exothermic. During curing, the properties of an epoxy polymer vary remarkably as a function of the degree of conversion (x) and the glass transition temperature (T_g).

A schematic of conversion-temperature transformation is shown in **Fig. 4.2** to describe the main curing related transformations in a thermosetting binder. The binder is at liquid state at the beginning of curing, and the T_g is located below the applied temperature (curing temperature). As the curing proceeds and the conversion degree (x) increases, the T_g increases as well. If the curing temperature is lower than the T_g at fully cured state ($x = 1$ and $T_g = T_{g\infty}$), then

polymerization of the incompletely cured binder occurs. In this case, the material becomes fully cured only when a temperature close to or higher than $T_{g\infty}$ is applied.

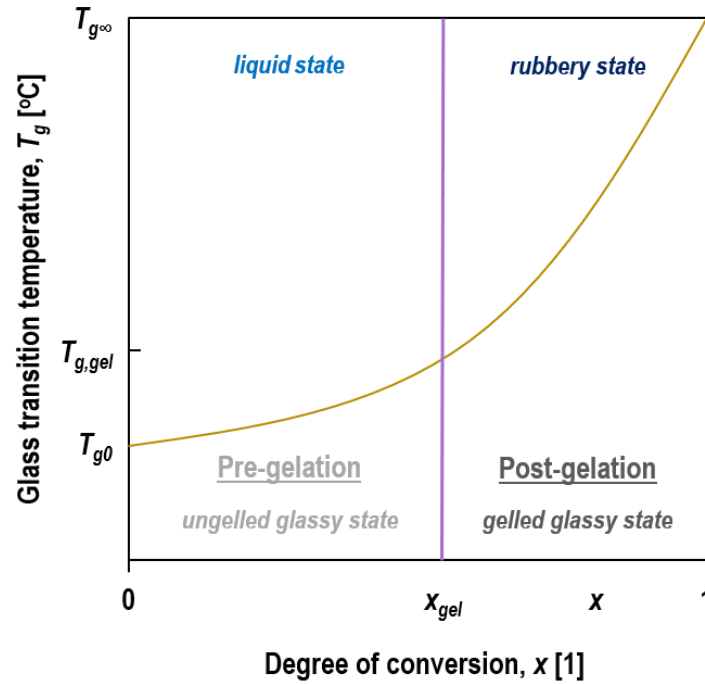


Figure 4.2 Schematic of the main conversion-temperature transformation during curing.

The parameters that determine the curing kinetics, such as the activation energy and the reaction rate, have been studied for pure epoxy resins (Babayevsky & Gillham 1973; Matsuoka et al., 1989). On the basis of curing kinetics, extensive studies have been conducted to develop models to link the chemistry with the rheology of epoxy resins (Kamal & Sourour 1973; Ryan & Dutta 1978; Halley & Mackay 1996; Yousefi & Lafleur 1997). Among various phenomenological and mechanistic models, the autocatalytic models have been successfully applied to various epoxy resins. Models developed based on n^{th} order kinetics can also describe sufficiently the curing induced hardening of thermoplastic binders, such as asphalt, of a relatively low amount of epoxy resins (Yang et al., 1997; Blanco et al., 2004).

From the above, it is realized that the curing of thermo-hardening materials, such as EA, is influenced by several factors, such as the amount and the properties of epoxy polymer, the production temperature and time. However, limited is the research on the curing induced hardening of EA binders although the evolution of rheological properties during the curing of epoxy resins has been explored extensively.

In this **chapter**, the behavior of EA binders prior to gelation will be investigated by giving emphasis on the viscosity changes induced by the increase of the conversion degree. The EA binder, used earlier and referred as EA_{ref}, was used as the model binder here. Constitutive relations for the curing binders before gelation are discussed as well to simulate the pre-gelation behaviour of this binder. These relationships will be discussed in the following section.

4.2.1 Glass transition temperature

The T_g is a physical property that corresponds to the temperature at which the sudden change of free volume of a polymer is occurred due to the transition between a glassy and an amorphous state (Stepto 1998). Therefore, a stepwise change in the specific volume of polymer happens at the T_g . The T_g is influenced by material factors, such as the polymer structure, crystallinity and the molecular weight of the material, and processing factors. In polymer industrial applications, the properties of polymers, such as density, specific heat, stiffness modulus or strength, can be determined at this transition temperature which increases with the degree of conversion.

According to DiBenedetto 1987, the T_g evolution due to changes in the degree of conversion of polymers and blends, such as the epoxy-asphalt binders, can be defined as

$$\frac{T_g(x) - T_{go}}{T_{g\infty} - T_{go}} = \frac{\lambda x}{1 - (1 - \lambda)x} \quad (4.1)$$

where x is the degree of conversion, T_{go} is the T_g of the uncured polymer, $T_{g\infty}$ is the T_g of the completely cured polymer and λ is a material constant.

Several criteria can be used to characterize the T_g in epoxy polymers. As discussed earlier in this thesis, the evolution of the T_g due to curing is evaluated at different time intervals as a measure to quantify the degree of conversion. The data obtained from the non-isothermal TL-DSC measurements in **Chapter 3** (see **Fig. 3.6** and **Fig. 3.7b**) are used here to build the relationship between T_g and the degree of conversion fitted to the **Eq. 4.1**.

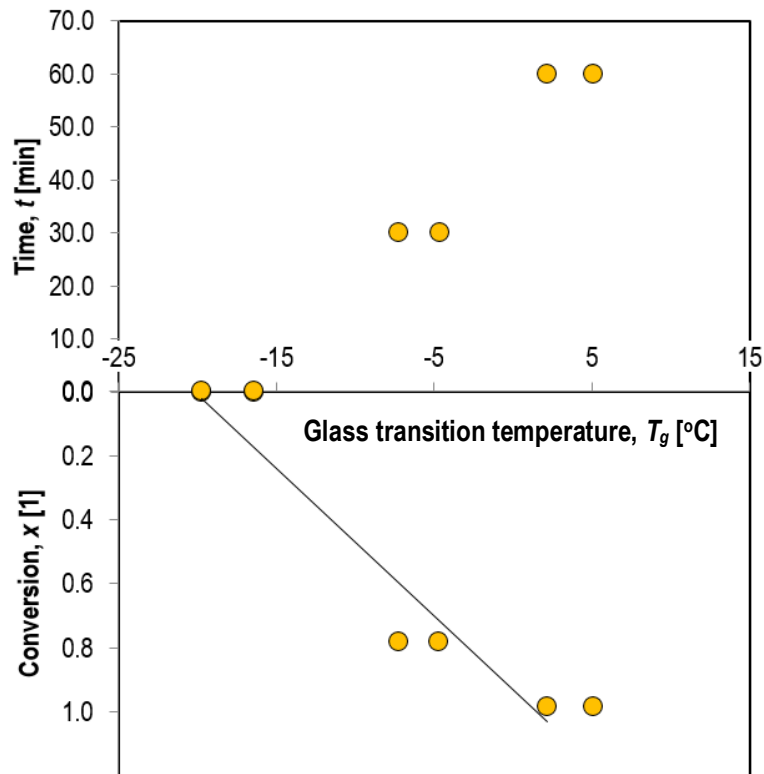


Figure 4.3 Degree of conversion and glass transition temperature of EA_{ref} versus time at 130°C.

The activation energy, reaction rate and reaction order of EA_{ref} have been determined and presented (see **Table 3.2** in **Chapter 3**). The plot of the conversion degree as a function of time at 130°C is shown in **Fig. 4.3**. As shown in the same figure, the T_g increase as a function of time is plotted. The values of T_{g0} , $T_{g\infty}$ and λ of studied binder, which have been determined on the basis of the current results, are -18.07°C, 3.63°C and 0.45, respectively.

4.2.2 Viscosity

To link the conversion degree with the viscosity, various predictions schemes have been developed (Kamal & Sourour 1973; Ryan & Dutta 1978; Castro & Macosko 1980; Halley & Mackay 1996; Yousefi & Lafleur 1997). In this study, the curing induced viscosity changes of EA_{ref} are expressed on the basis of the Castro & Macosko 1980 model as

$$\eta^*(T, x) = \eta^*_{gel} \cdot \exp \left[-\frac{C_1 (T - T_g(x))}{C_2 + T - T_g(x)} \right] \cdot \left(\frac{x_{gel}}{x_{gel} - x} \right)^{n_r} \quad (4.2)$$

where x_{gel} is the degree of conversion at the gel point, $T_g(x)$ is the glass transition temperature as a function of the conversion, η^*_{gel} is the viscosity at the gel point, n_r is a material-dependent constant, C_1 and C_2 are material-dependent and temperature-independent constants obtained from the rearranged William-Landel-Ferry (WLF) equation. The above equation, which is a combination of the WLF equation (Williams, Landel & Ferry 1955) and the conversion degree, and it describes the chemo-rheology of binder ($x < x_{gel}$).

The rheological measurements of EA_{ref} were performed using a Brookfield rotational viscometer under a shear rate of 20 rotations per minute (rpm). After placing the binder into the viscometer, measurements were immediately started to avoid any reaction in samples before testing. Isothermal measurements were taken at several temperatures (i.e., 100, 130 and 160°C) for the viscosity measurements and the tests were terminated at the gel point (defined as a vertical asymptote in the viscosity measurement) (see **Fig. 4.4**).

The gelation time varied from few minutes (i.e., 10 min) to about 240 min, depending on the applied temperature. At lower temperatures, such as 100°C, the viscosity still increases exponentially, as described in **Eq. 4.2**, but slower than at 130 and 160°C. Also, the starting value of the viscosity is slightly higher at 100°C than at the higher temperatures. By considering 130°C to be the actual production temperature of epoxy-asphalt in the plant (ChemCo Systems 2016a & 2016b), the experimental viscosity results at this temperature are fitted to **Eq. 4.2**. As the T_g and the degree of conversion were discussed in **Chapter 3**, they have been used here to model the chemo-rheological behaviour according to **Eq. 4.2**. DSC and viscosity measurements were taken at the same temperature (i.e., 130°C) to apply data into the fitting algorithm and to calculate the unknown parameters. The values of x_{gel} , C_1 , C_2 and n_r parameters are 0.97, 35, 20 and 1.5, respectively. It should be mentioned also that the observed viscosity trends coincide with analogous chemo-rheological responses discussed elsewhere (Yao et al., 2019; Luo et al., 2019; Chen et al., 2020).

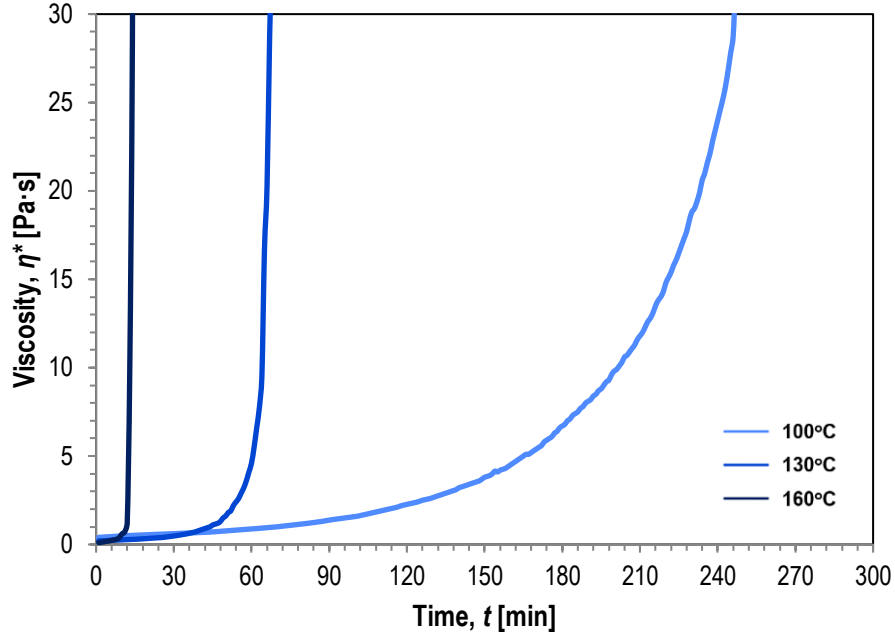


Figure 4.4 Isothermal measured viscosity of EA_{ref} binder at 100, 130 and 160°C ($x < x_{gel}$).

4.3 Modeling of Chemo-Rheology

Continuous monitoring of curing reactions of thermosetting binders is highly important to obtain the desired end-product performance. The curing induced hardening of EA binders involves the heat transfer, the curing kinetics and the material rheology (see **Fig. 4.5**). Thus, this section presents the numerical predictions of viscosity of binders under certain energy conditions.

The curing kinetics allow to predict the conversion degree (x) and the reaction rate as a function of time and temperature as

$$\frac{\partial x}{\partial t} = K(T) \cdot f(x) \quad (4.3)$$

where $K(T)$ is a temperature-dependent parameter, which is described by an Arrhenius equation, and $f(x)$ is a function of conversion. The same equation is discussed in **Chapter 3**, as **Eq. 3.6**. The shape of the $f(x)$ shows the reaction performance of the system and is determined by the n^{th} order kinetics. The change rate of the conversion degree is described as

$$\frac{\partial x}{\partial t} = K_0 \exp\left(-\frac{E_a}{RT}\right) \cdot (1-x)^n \quad (4.4)$$

where K_0 is the pre-exponential kinetic factor, E_a is the activation energy, R is the universal gas constant and n is the reaction order upon the curing mechanism.

The transient heat conduction within the EA binder is described by

$$\rho C_p \nabla T - \nabla \cdot (k \nabla T) = Q \quad (4.5)$$

where ρ is the mass density of binder, k denotes the thermal conductivity, C_p is the heat capacity, T is the temperature, Q represents the exothermic heat source. Here, it was assumed that the convection and radiation heat do not have an important impact on the energy balance of the system.

As EA cures, heat is released (exothermic chemical reaction). The heat releasing rate is proportional to the consumption rate of reactive elements in the EA. Assuming no heat flow, the volumetric heat source Q accounts the exothermic effect and is described by

$$Q = \rho \Delta H_{exo} \frac{\partial x}{\partial t} \quad (4.6)$$

where ΔH_{exo} is the exothermic reaction heat. The reaction rate gradients generated by the temperature gradients affect the temperature profile in the binder.

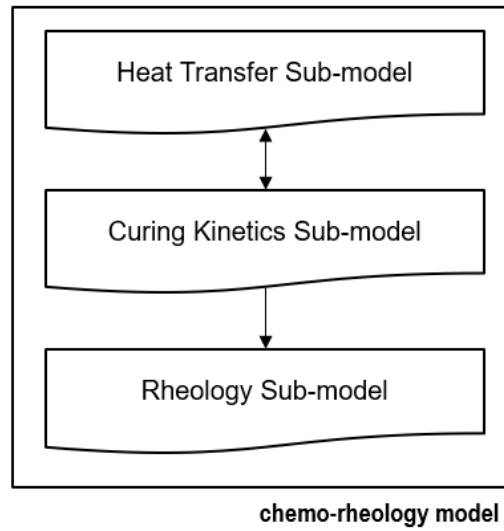


Figure 4.5 Chemo-rheology modelling approach.

4.3.1 Model implementation

For qualitative numerical analyses, one three-dimensional cubic finite-element mesh of $1.0\text{E-}9 \text{ m}^3$ mesh volume ($1.0\text{E-}3 \times 1.0\text{E-}3 \times 1.0\text{E-}3 \text{ m}^3$) and of 16535 total number of tetrahedral elements was created. The proposed chemo-rheology model was implemented in COMSOL Multiphysics to simulate the viscosity evolution during curing as a measure of reaction progress. For these analyses, heat capacity ($920 \text{ J/kg}\cdot\text{K}$) and thermal conductivity ($0.45 \text{ W/m}\cdot\text{K}$) were assumed to be constant. The exothermic reaction heat (ΔH_{exo}) was considered constant (30 kJ/kg) as well (see **Table 4.1**). It is also assumed that the gelation of the unreacted binder occurs at a fixed conversion degree. The imposed thermal field at the top boundary of the finite element cube is shown in **Fig. 4.6** with the rest boundaries to be thermally insulated. The model predictions are demonstrated at a point located in the cubic centre.

By varying the different parameters (see **Table 4.1**), insights are gained into the effect of each of them on the overall chemo-rheological response of a binder with thermo-hardening characteristics, as the EA binder.

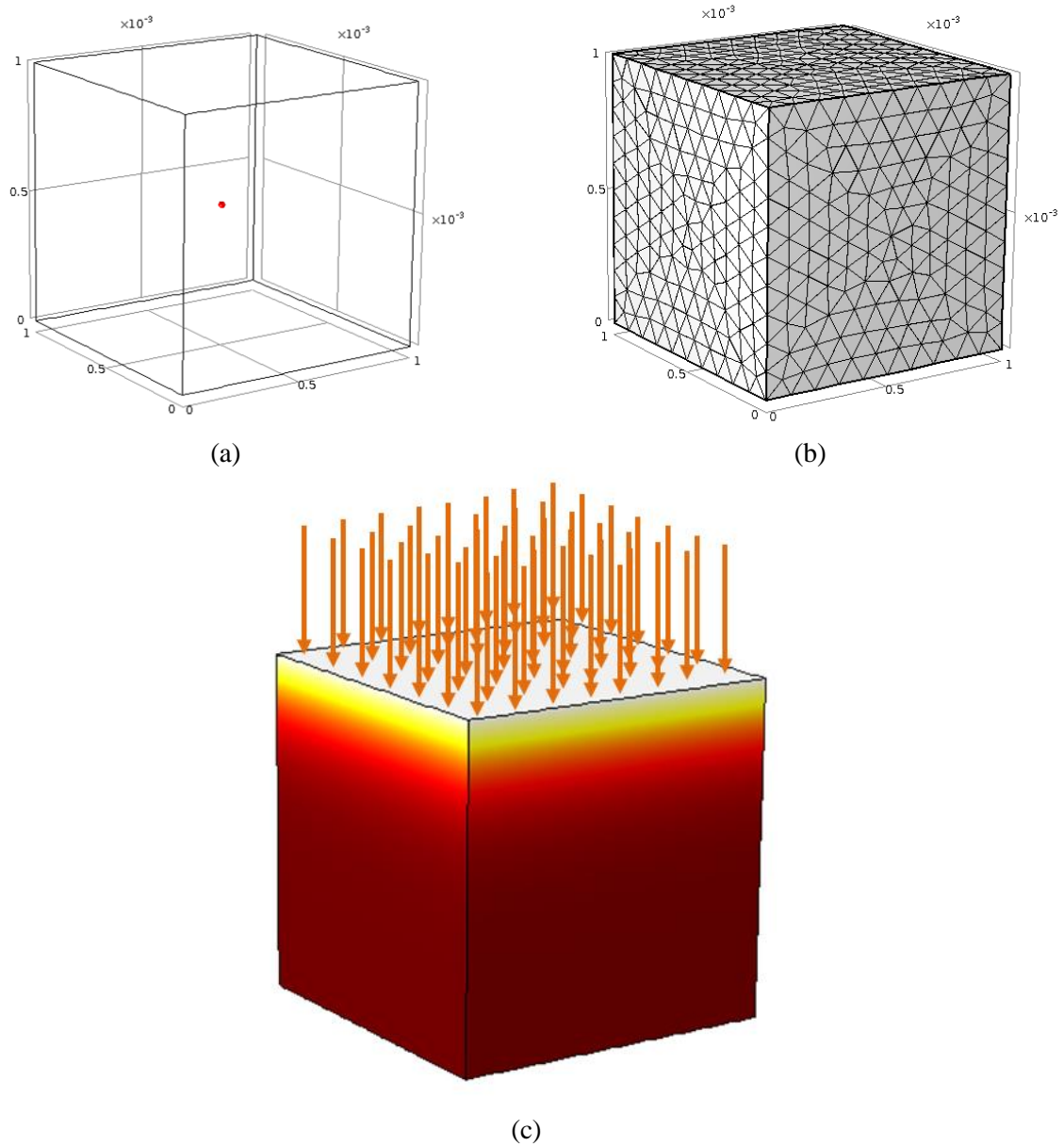


Figure 4.6 Finite element cubic geometry: (a) location of output point in the centre of cube; (b) mesh and (c) direction of the applied thermal field at the top boundary.

Table 4.1 Model parameters used in the finite element analyses.

Parameters	Values
heat capacity, C_p [J/(kg·K)]	920
thermal conductivity, k [W/(m·K)]	0.45
exothermic heat, ΔH_{exo} [J/g]	30
activation energy, E_a [kJ/mol]	50, 55, 60
reaction rate, K_0 [1/s]	200, 400, 600, 800, 1000
material-dependent constant n_r [1]	2.0, 2.5, 3.0, 3.5, 4.0
temperature, T [°C]	90, 100, 110, 120, 130
conversion at gelation, x_{gel} [1]	0.3, 0.4, 0.5, 0.6, 0.7, 0.8, 0.9

4.3.2 Influence of activation energy and reaction rate on viscosity development

The operational time window from plant to field will affect the workability of thermosetting materials. In this sub-section, the effect of reactions kinetics on the curing induced changes of viscosity are discussed.

The results that illustrate the effect of activation energy are presented in **Fig. 4.7a**. As demonstrated in this figure, the activation energy has a strong impact on the viscosity evolution under isothermal conditions (130°C). By decreasing the activation energy from 60 kJ/mol to 50 kJ/mol, the viscosity increases exponentially very fast. This response indicates that a more reactive system can be attributed to lower the energy demands to facilitate the epoxy curing. Note that the EA mixes are produced and compacted at a temperature range substantially lower than conventional asphalt mixes resulting in a decrease of the material production energy (ChemCo Systems 2016a & 2016b).

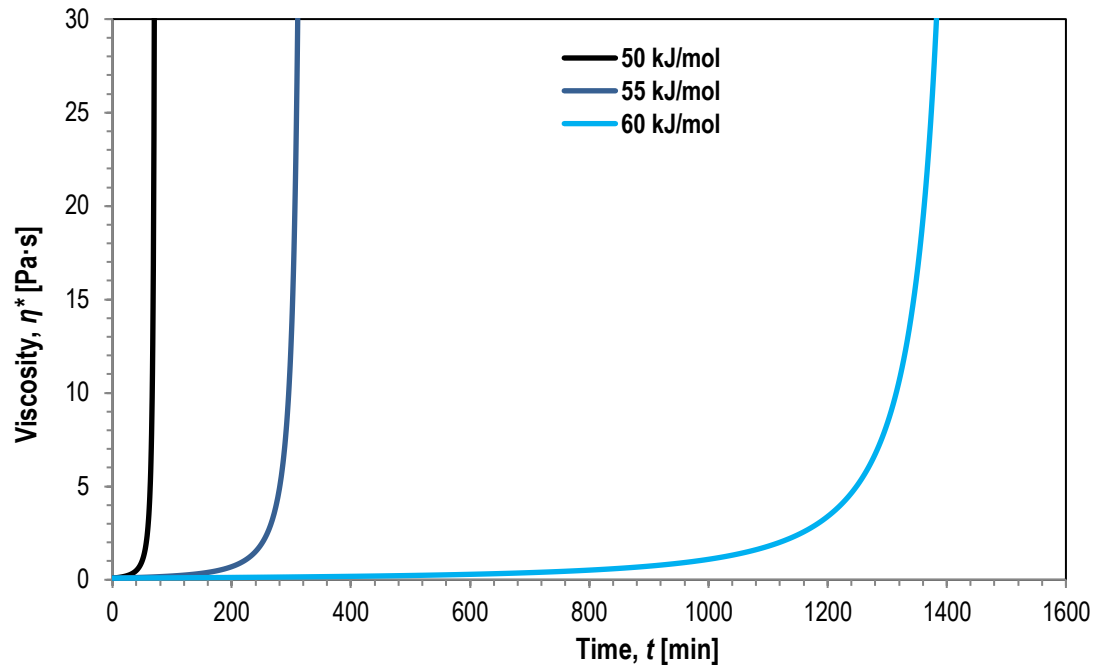
Similar viscosity predictions were observed when various kinetic factors were tested. The impact of the kinetic factor on viscosity development appears in the isothermal hardening curves of **Fig. 4.7b**, confirming that the highly reactive binders harden faster.

4.3.3 Influence of temperature and reaction extent on viscosity development

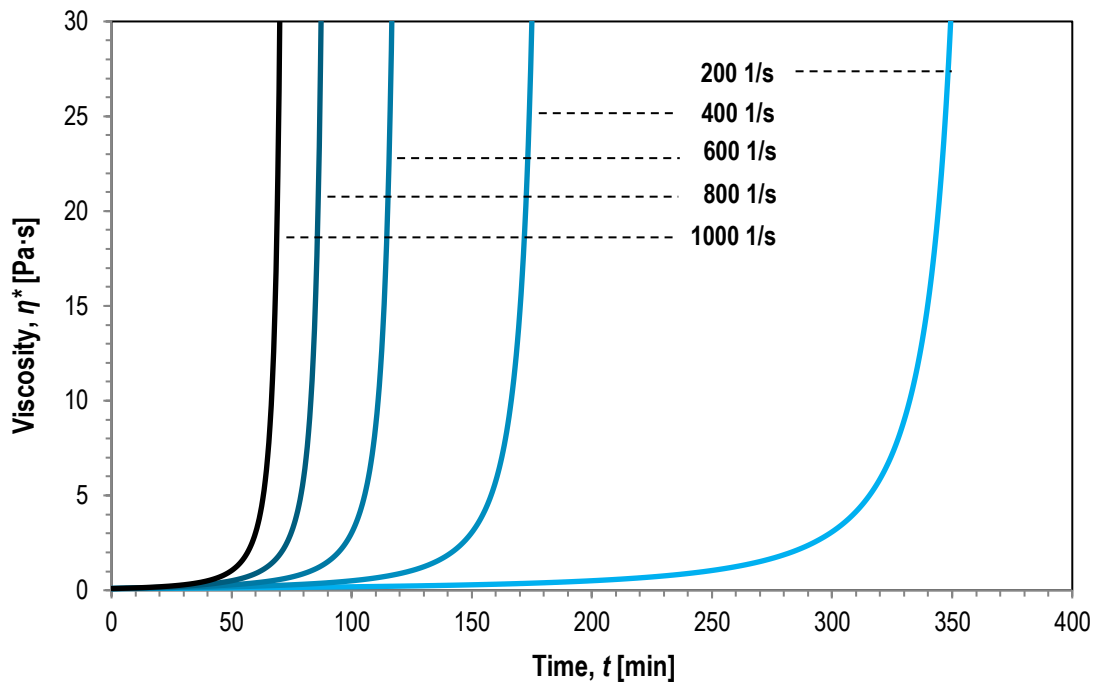
To investigate the impact of temperature on the viscosity evolution, different isothermal studies were considered as well (i.e., 90, 100, 110, 120, 130°C). The numerical analyses performed by varying the conversion degree at the gel point (x_{gel}) from 0.3 to 0.9 (step 0.1).

Fig. 4.8 demonstrates the influence of temperature on the gelation time. Significant decrease in the predicted gelation time was achieved by increasing the temperature. At isothermal conditions, the computed results illustrate the role of applied temperature on the material curing, and the gelation. The trend above was also observed in the experimental section of this **chapter**.

Analogous trend was observed for x_{gel} , as a material parameter linked with the gel point of epoxy, on building the viscosity of binders (see **Fig. 4.8**). For example, for all the predefined applied temperatures, the achieved viscosity was higher when the x_{gel} decreases from 0.9 to 0.3. As a result, the intermolecular interactions between the components produce a composite with a lower value of the conversion degree until the gelation.



(a)



(b)

Figure 4.7 Predicted viscosity development of binder of different (a) activation energy and (b) reaction rate levels ($E_a=50$ kJ/mol, $n=0.4$, $T=130^\circ\text{C}$).

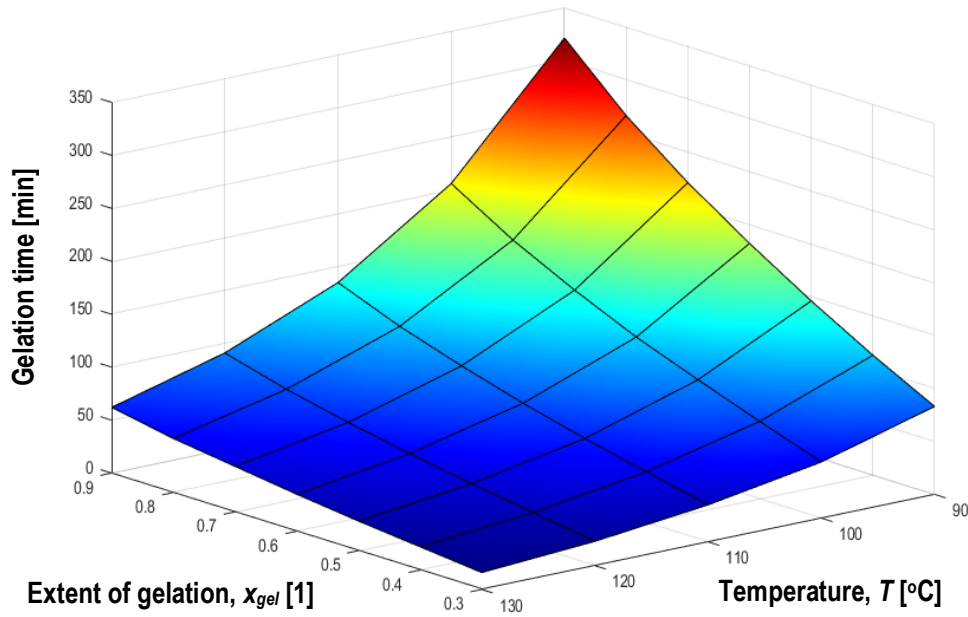


Figure 4.8 Predicted viscosity development of binder for different x_{gel} at various temperatures ($E_a=50$ kJ/mol, $n=0.4$, $K_0=1000$ 1/s).

Finally, the influence of the constant n_r is depicted in **Fig. 4.9** showing the importance of this parameter on providing realistic numerical predictions. The rate of viscosity development was found to increase with increasing value of n_r from 2 to 4 with a step of 0.5 for the initially un-reacted EA having as consequence a faster hardening. Thus, for the ranking of the individual components, it was important to identify experimentally these factors since they contribute vitally to the material performance.

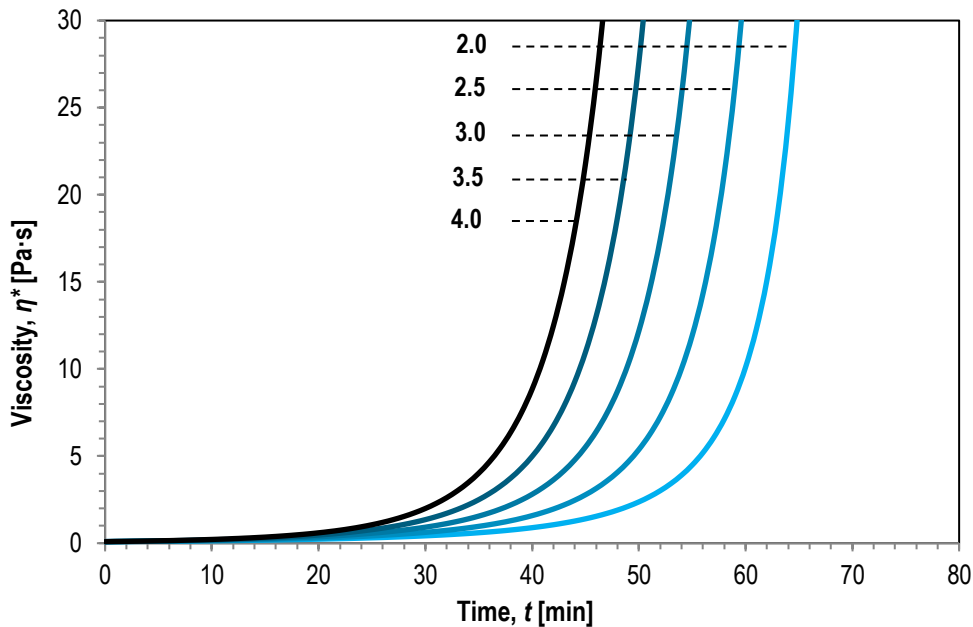


Figure 4.9 Predicted viscosity development of binder for different n_r at 130°C ($E_a=50$ kJ/mol, $n=0.4$, $K_0=1000$ 1/s).

4.4 Summary

Normally, the hot-mixed asphalt materials are applied at high temperature, which could lead to reduction of operational time window in the case of EA. By increasing the production or transport temperature of epoxy asphalt paving materials, shorter time windows are needed for the epoxy system to gel irreversibly. This **chapter** presents the curing induced changes and the subsequent predictions of viscosity evolution of EA binders via performing laboratory experiments and numerical analyses to understand the way these binders are hardening due to curing.

The time-dependent chemo-rheology model used in this work can provide hardening predictions by linking the degree of conversion with the viscosity. A simple rheological analysis of a thermosetting binder has been performed capturing the typical exponential increase of viscosity. The numerical analyses also showed the impact of the curing kinetics parameters on the hardening of epoxy binders. Lower levels of activation energy increase the rate of viscosity development. The numerical sensitivity analyses have shown that with the increase of temperature the material viscosity increased, as the curing rate is highly dependent on the temperature. Overall, the binders of different reactivity characteristics could show different flow and thermo-hardening behaviour under certain energy conditions.

4.5 References

- Babayevsky, P.G., J.K. Gillham. Epoxy Thermosetting Systems: Dynamic Mechanical Analysis of the Reactions of Aromatic Diamines with the Diglycidyl Ether of Bisphenol A. *Journal of Applied Polymer Science* 17, 1973, pp. 2067-88.
- Blanco, I., G. Cicala, O. Motta, A. Recca. Influence of a Selected Hardener on the Phase Separation in Epoxy/Thermoplastic Polymer Blends. *Journal of Applied Polymer Science* 94, 2004, pp. 361-371.
- Bogetti, T.A., J.W. Gillespie. Process-induced Stress and Deformation in Thick-Section Thermoset Composite Laminates. *Journal of Composite Materials* 26(5), 1992, pp. 626-660.
- Castro, J.M., C.W. Macosko. Kinetics and Rheology of Typical Polyurethane Reaction Injection Molding Systems. *Society of Polymer Engineers Technical Paper* 26, 1980.
- ChemCo Systems, Inc. Batch Plant Operator Information for Production of Epoxy Asphalt Paving Mix. 2016a.
- ChemCo Systems, Inc. Construction Specifications Installation of Type IX Epoxy Asphalt Concrete Surfacing. 2016b.
- Chen, C., W.O. Eisenhut, K. Lau, A. Buss, J. Bors. Performance Characteristics of Epoxy Asphalt Paving Material for Thin Orthotropic Steel Plate Decks. *International Journal of Pavement Engineering* 21(3), 2020, pp. 397-407.
- Halley, P.J., M.E. Mackay. Chemorheology of Thermosets-An Overview. *Polymer Engineering and Science* 36(5), 1996, pp. 593-609.
- International Transport Forum. *Long-life Surfacing for Roads: Field Test Results*. ITF Research Reports, OECD, Paris, France, 2017.
- Kamal, M.R., S. Sourour. Kinetics and Thermal Characterization of Thermoset Cure. *Polymer Engineering and Science* 13(1), 1973, pp. 59-64.

- Lu, Q., J. Bors. Alternate Uses of Epoxy Asphalt on Bridge Decks and Roadways. *Construction and Building Materials* 78, 2015, pp. 18-25
- Luo, S., Z. Liu, X. Yang, Q. Liu, J. Yin. Construction Technology of Warm and Hot Mix Epoxy Asphalt Paving for Long-Span Steel Bridge. *Journal of Construction Engineering and Management* 145(12), 2019.
- Matsuoka, S., X. Quan, H.E. Bair, D.J. Boyle. A Model for the Curing Reaction of Epoxy Resins. *Macromolecules* 22(10), 1989, pp. 4093-98.
- Ryan, M.E., A. Dutta. Kinetics of Epoxy Cure: A Rapid Technique for Kinetic Parameter Estimation. *Polymer* 20, 1978, pp. 203-206.
- Williams, M.L., R.F. Landel, J.D. Ferry. The Temperature Dependence of Relaxation Mechanisms in Amorphous Polymers and Other Glass-Forming Liquids. *Journal of the American Chemical Society* 77(14), 1955, pp. 3701-3707.
- Yang, Y., H. Fujiwara, T. Chiba, T. Inoue. Morphology Development in a Thermoset/Thermoplastic Blend: DAP/PPE System via Apparent Two-step Spinodal Decomposition. *Polymer* 39(13), 1998, pp. 2745-50.
- Yao, B., C. Chen, K.J. Loh. Performance Characteristics of Diluted Epoxy Asphalt Binders and their Potential Application in Chip Seal. *Journal of Materials in Civil Engineering* 31, 2019.
- Yousefi, A., P.G. Lafleur. Kinetic Studies of Thermoset Cure Reactions: A Review. *Polymer Composites* 18(2), 1997, pp. 157-168.

5

Simulation of Diffusion-Reaction Phenomena in Curing Epoxy-Asphalt Binders

5.1 Introduction

The phase behavior of two polymers, which include components of specific interactions, were discussed in **Chapter 2**. Evidence about the interphase characteristics of different epoxy-asphalt formulations was also provided in the same **chapter**. Nevertheless, the properties at the interface between different phases are not easy to be determined experimentally, mainly due to the fact that the composition of interfacial layers of two interacting phases differs significantly from the composition of the bulk phases. Reacting species of low molecular weight tend to be concentrated at the interface while the exact composition of product species at the interface are usually unknown.

Once the two reactive components are placed in contact, inter-diffusion of miscible parts occurs at the interface. Through this process, the diffusion rates of components depend on their conversion and subsequently on the local molecular weights distribution. Thus, the diffusion rate of a binary polymer blend of two contacted phases depends on the production rate of a third phase, named interphase. In other words, the diffusion rate depends on the degree of conversion, and it is locally controlled by the Flory-Huggins interaction parameter (χ) and the molecular weight of interacting components.

In this **chapter**, the effect of governing chemical and physical parameters is explored by simulating the inter-diffusion phenomena that take place due to the chemical interfacial interaction of the two reactive components. Two different models are proposed and tested in a finite element software to assess the effect on reactivity and diffusivity parameters that determine the interfacial reactions and subsequently the desired properties of multiphase blends, as epoxy-asphalt binders.

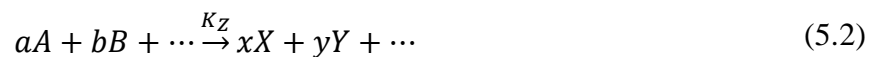
5.2 Mass Transport due to Curing

The time-dependent mass balance per component (species) or their transport through diffusion mechanisms, solves the mass conservation equation for one or more components I as

$$\frac{\partial [C_{I,i}]}{\partial t} + \nabla \cdot (-D_{I,i} \nabla [C_{I,i}]) = R_{I,i} \quad (5.1)$$

where $[C_{I,i}]$ is the concentration of the component I [mol/m³] in phase i , $D_{I,i}$ is the diffusion coefficient [m²/s] of the component I in phase i , and $R_{I,i}$ is the reaction rate of the component I [mol/(m³·s)] in phase i . The first term on the left side of **Eq. 5.1** corresponds to the consumption of the components. The second term accounts for the diffusive transport, accounting for the interaction between the perfectly mixed dilute components and the solvent-phase.

Modeling the reactions is based on the mass action law. The general formula of an irreversible transformation which consists of Z reactions and involves I number of components is given by

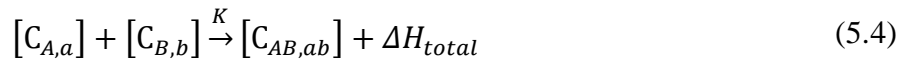


All irreversible reactions contribute to the time rate of change of $C_{I,j}$ corresponding to the chemistry as

$$\frac{d[C_{I,j}]}{dt} = K_Z \prod_I [C_{I,j}]^{-\tau_Z} \quad (5.3)$$

where K_Z denotes the irreversible rate constant, the stoichiometric constant is denoted as τ_Z and is defined as being negative for reactants and positive for products.

Most reactions consist of many simple sub-steps where only pairs of reactants need to be considered. For simplification, the one-step irreversible reaction of component A with B to form a new component AB is considered as a perfect stoichiometric system (i.e., 1:1 mol/mol), then



where subscripts a and b indicate the phases where components A and B exist, respectively.

To describe the chemical reactions, the temperature dependence of the reaction rate is included through Arrhenius expressions for the reaction rate constants

$$K = K_0 \exp \left(-\frac{E_a}{RT} \right) \quad (5.5)$$

where K_0 is the pre-exponential, or for first order kinetic reactions, frequency factor, T is the temperature [K], E_a is the activation energy of intrinsic reaction [J/mol] and R is the ideal gas constant 8.314 [J/(mol·K)].

The reaction rate of a one-step irreversible reaction as described by **Eq. 5.4** is expressed as

$$R_{A,b} = R_{B,a} = -K [C_{A,a}][C_{B,b}] \quad (5.6)$$

In this study, phases are considered as reacting liquids which are incompressible, ideally mixed and of constant volume.

5.3 Diffusion-Reaction Model

As a reactive component concurrently diffuses into and reacts with another one, bonds are formed establishing an interphase (i.e., the intermediate phase between two reacting phases). The size of interphase is controlled by the available free volume within the system, the kinetic parameters, and the diffusion coefficients of two reacting components. In particular, the diffusion coefficient of molecules is related to their chain length and weight. In reacting epoxy-asphalt binders, the curing reactions lead to the formation of crosslinks, which results in an increase in the molecular weight over time. The diffusivity of reacting components decreases as the degree of conversion increases until the molecular weight is so large as to prevent diffusion.

A way to model this phenomenon of reducing the diffusivity is the free volume theory. The free volume theory has been introduced to predict the mobility-related properties of reacting systems (Cohen & Turnbull 1959, Turnbull & Cohen 1961). Molecules are bound by their neighbour molecules or molecular chains for most of the time and their ability to rearrange their position depend on the existence of sufficient volume to move. As free volume decreases, there is less and less volume for the molecules to move and they tend to collide more frequently with their neighbours. Thus, the mobility of chain segments is reduced, and the reaction is limited in a thin film thickness.

According to the Fujita free volume theory (Fujita et. 1960), the fraction free volume (V_f) in a liquid is described by **Eq. 5.7** in which the volume increases due to thermal expansion without phase change

$$V_f = V - V_0 \quad (5.7)$$

where V_0 is the occupied volume by molecules of an equilibrium liquid and V is the total volume taken up by the liquid.

To consider the free volume (f) as non-dimensional, the following equation is used (DiBenedetto 1987)

$$f = \frac{V_f}{(V_0 + V_f)} = \frac{V_f}{V} \quad (5.8)$$

and the Arrhenius diffusion coefficient can be expressed in terms of free volume theory as

$$D = D_0(T) \exp \left(-\gamma \frac{V^*}{V_f} \right) \quad (5.9)$$

where $D_0(T)$ is the Arrhenius diffusivity, γ is a factor needed to correct the overlap of free volume ($1/2 < \gamma < 1$), and V^* is a critical volume (i.e., minimum local free volume necessary for the motion of a substance to occur). The critical volume is a quantity close to V_0 (Macedo & Litovitz 1965), and using this in combination with **Eq. 5.7** and **5.8**, **Eq. 5.9** can be rewritten as

$$\begin{aligned} D &\cong D_0(T) \exp \left(-Z \frac{V_0}{V_f} \right) = D_0(T) \exp \left(Z \left(1 - \frac{1}{f} \right) \right) \\ &= D_0 \exp \left(-\frac{E_a}{RT} \right) \exp \left(Z \left(1 - \frac{1}{f} \right) \right) \end{aligned} \quad (5.10)$$

where D_0 is a constant and Z is a constant for a single substance.

The concept of the free volume theory on diffusion is illustrated in **Fig. 5.1**. A concentration of a reactive component (i.e., C_A) is set at the left boundary condition of a phase/domain with different diluted component (i.e., $C_{B,b}$). The diffusion of C_A largely occurs through the free space in the phase. As curing proceeds, the curing phase becomes increasingly rigid as the T_g

shifts to a higher temperature and the mobility of molecules decreases. The increasing T_g of the polymer due to curing reflects the decrease in its free volume, or the amount of voids that are available for diffusion.

To link the T_g and degree of conversion, or $x=(C_{AB}-C_{AB,0})/C_{AB,0}$, over the curing process, the DiBenedetto relation is utilized (DiBenedetto 1987). This relation, which is also discussed in **Chapter 4**, is defined as

$$T_g(x) = T_{go} + \frac{\lambda x}{1 - (1 - \lambda)x} \cdot (T_{g\infty} - T_{go}) \quad (5.11)$$

where T_{go} is the T_g of monomer, $T_{g\infty}$ is the T_g of fully cured material and λ is a material constant.

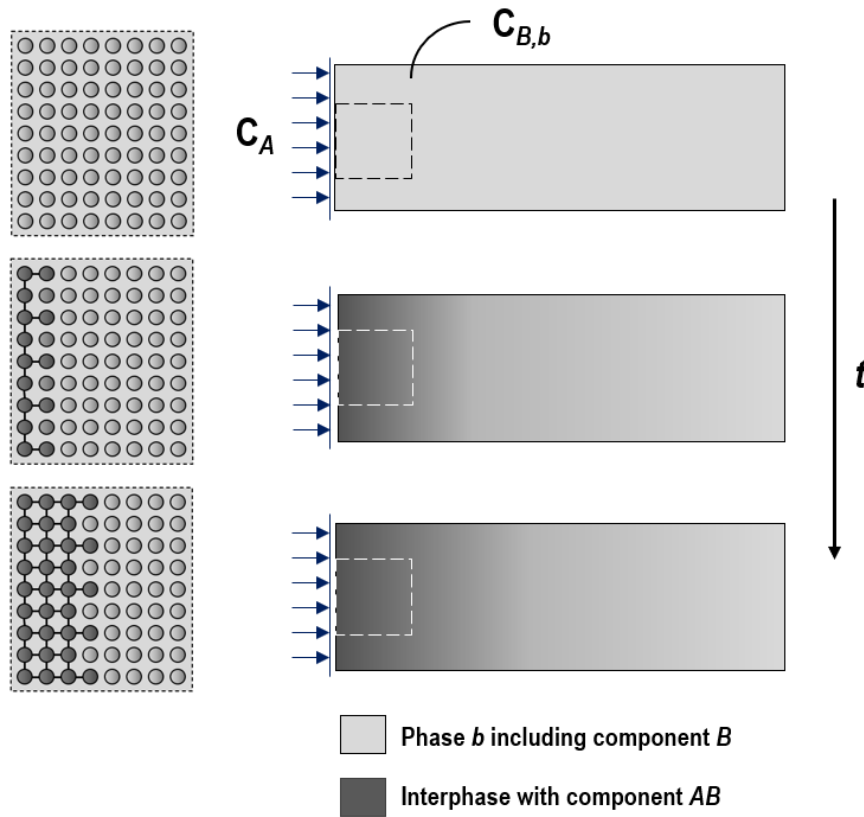


Figure 5.1 Schematic of diffusion-reaction concept based on free volume theory.

The fractional free volume is linearly dependent on temperature, with a discontinuity at the T_g (William, Landel & Ferry 1955)

$$\frac{\partial f}{\partial T} \cong \xi \quad (5.12)$$

and

$$f = f_g + \xi(T - T_g) \quad (5.13)$$

where f_g is the fractional free volume at the T_g , and ξ is the thermal expansion coefficient of the free volume. Typically, ξ is $4.8E-4 \text{ K}^{-1}$ and $4.8E-5 \text{ K}^{-1}$ for temperatures greater than the T_g

and lesser than the T_g , respectively. The value of ζ in **Eq. 5.13** is valid for thermosetting materials in the temperature range of T_g to $T_g + 100^\circ\text{C}$, at the first stage of cure as the T_g increases but is smaller than the imposed temperature (William, Landel & Ferry 1955).

By inserting **Eq. 5.11** in **Eq. 5.13** and using **Eq. 5.10** to express the diffusivity, the diffusion coefficient of the reactive components can be described as

$$D = D_0 \exp \left(-\frac{E_a}{RT} \right) \exp \left(Z \left(1 - \frac{1}{f_g + \xi (T - T_g(x))} \right) \right) \quad (5.14)$$

The parameters f_g , ξ and Z have been determined by (William, Landel & Ferry 1955) and can be considered constant throughout the curing (f_g : $2.5\text{E-}2$, ξ : $5\text{E-}4 \text{ deg}^{-1}$, Z : 1.5).

5.3.1 Model implementation

The proposed diffusion-reaction model, which has been discussed before, was implemented in COMSOL Multiphysics to simulate the interaction of two reactive components without considering the effect of mixing. A two-dimensional finite element mesh of $5.0\text{E-}9 \text{ m}^2$ mesh area ($1\text{E-}4 \times 5\text{E-}5 \text{ m}^2$) and 5000 total number of quad elements was created (see **Fig. 5.2**). The single domain formed considering the resolution of AFM analyses discussed in **Chapter 2** to simulate the phase *b* at diluted regime with free species of component *B* ($M_{WB} = 107.155 \text{ g/mol}$) in a solvent, assumed to be asphalt binder ($M_{wb} = 1000 \text{ g/mol}$, $\rho = 1010 \text{ g/mol}$). From previous research (Rajagopalan et al., 2000), the diffusion coefficient of epoxy into a thermoplastic polymer including a hardener was about 1.5 and $2.5\text{E-}14 \text{ m}^2/\text{s}$, and the initial diffusion coefficient of component *A* in phase *b* was assumed $1\text{E-}14 \text{ m}^2/\text{s}$. An initial concentration of component *A* (i.e., C_A) was set $3\text{E-}4 \text{ mol/m}^3$ at the left boundary condition, as shown in **Fig. 5.2**.

Fig. 5.2 demonstrates the variation of concentration field of the reacting component *B* and the newly produced component *AB* in phase *b* after diffusion and reaction (total reaction time: 60 min). To be more specific, this figure clearly shows the continuous decrease of the concentration of component *B* from the left boundary to the bulk of the solvent phase *b*.

Fig. 5.3 demonstrates the concentration of component *AB* along the horizontal axis (*x*-coordinate) over time. Obviously, due to the free volume theory, the highest concentration of component *AB* is formed at the left boundary where abundant components *A* and *B* are available to react resulting in the highest reaction rate. However, the concentration of component *AB* decreases along the length of the studied domain (phase *b*).

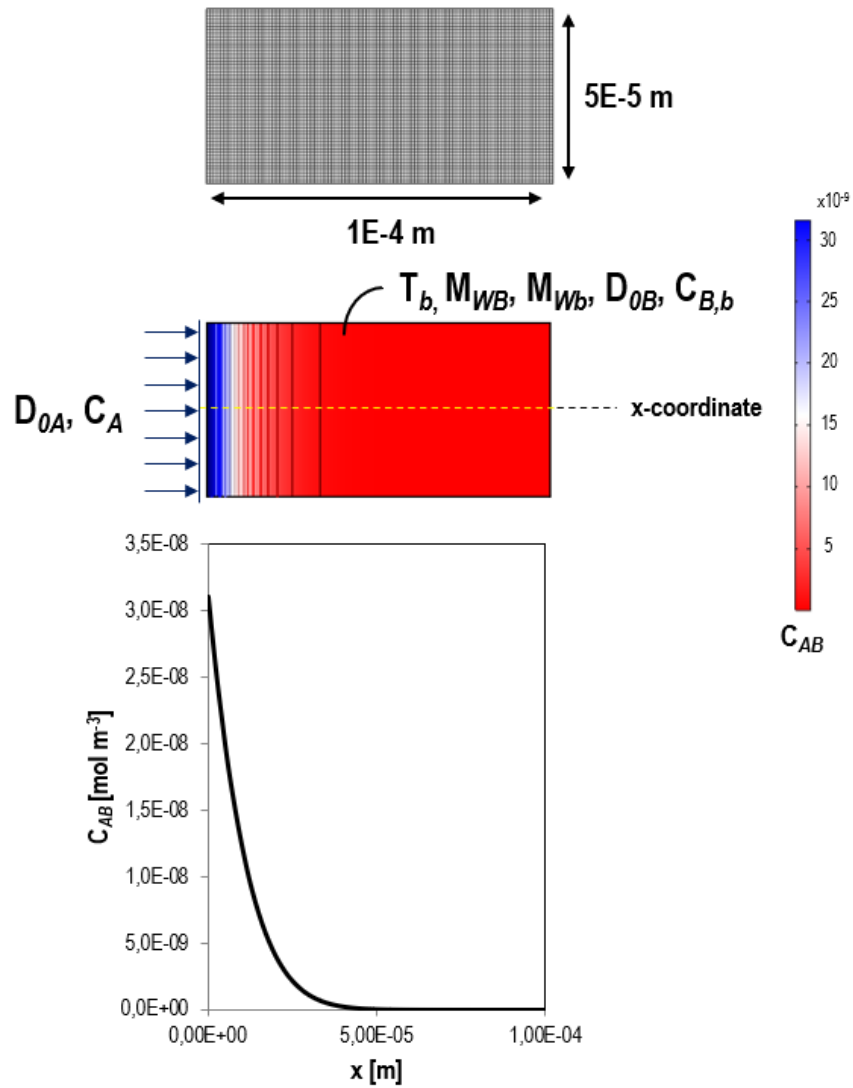


Figure 5.2 Finite element geometry and mesh of single domain, and concentration predictions of component AB along the x-coordinate of geometry.

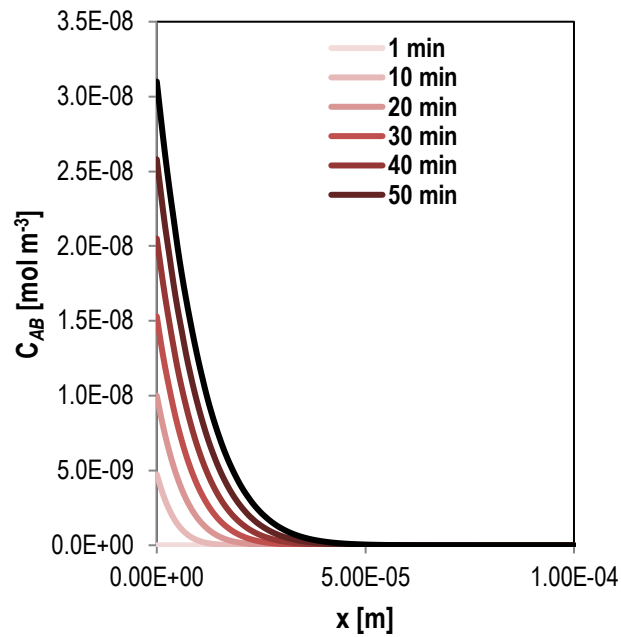


Figure 5.3 Predicted variation of concentration of producing component *AB* along the horizontal axis at different time intervals ($E_a=56$ kJ/mol, $K_0=2000$ 1/s, $T=130^\circ\text{C}$).

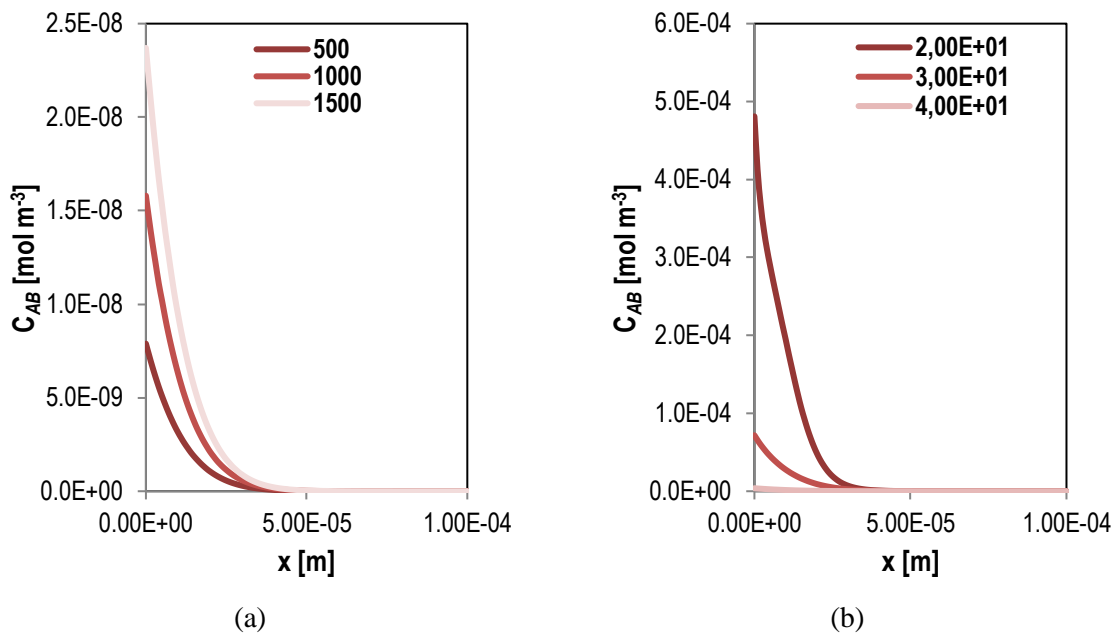


Figure 5.4 Effect of (a) reaction rate (500, 1000 and 1500 1/s with constant 56 kJ/mol) and (b) activation energy (20, 30 and 40 kJ/mol with constant 2000 1/s) on the extent of product concentration of two reacting components.

In addition, a sensitivity analysis was performed using different reaction rates (K_0 : 500, 1000 and 1500 1/s) and activation energies (E_a : 2E1, 3E1 and 4E1 kJ/mol), respectively, to assess their influence on the concentration of reaction products. The concentration profiles of producing component *AB* along the length of the studied domain (*x*-coordinate) at an instant time for different values of reaction rate and activation energy of the chemical reaction are plotted in **Fig. 5.4a** and **5.4b**, respectively. Lower values of activation energy result in the acceleration of reaction and higher concentrations of component *AB* close to the left boundary.

Based on the plots in **Fig. 5.4**, the activation energy is more important than the reaction rate on facilitating the diffusion of reactive species over curing. It could be also expected fast evolution at significantly higher reaction rates at higher temperatures easing thus the mass diffusion. Along the x-coordinate, the shape of concentration distribution was the same for all case scenarios.

5.4 Mutual Diffusion-Reaction Model

As discussed in **Chapter 2**, the lack of interactions at the interface results in phase separated blends. The thermodynamic stability of reacting phases in binary systems, as the epoxy-asphalt binders, is ultimately influenced by the inter-diffusion related compositional alterations. Improvement of the simulation of interfacial phenomena can be achieved by increasing the number of reacting phases. In principle, the reaction rates of interfacial reactions depend on local concentrations of reactant, and thus formed species (reaction products) affect significantly the size of interphase. Therefore, a mutual diffusion-reaction model is discussed in this section to increase the number of interfacial interactions and the interacting phases and potentially to provide more accurate predictions.

Between the contacting/interacting phases (i.e., phases a and b) as shown in **Fig. 5.5**, the chemical driving force of mutual diffusion process is determined by the chemical potential difference for their interacting species (i.e., components A and B) at the b - a interface and expressed as

$$\Delta G_m = \sum_i^n \varphi_i^0 [\mu_{A,a}(\varphi_{A,a}^{\Gamma_{b-a}}) - \mu_{B,b}(\varphi_{B,b}^{\Gamma_{b-a}})] \quad (5.15)$$

where φ_i^0 is the concentration of interacting components (I) transferred over the interface, n is the number of different interacting components, $\varphi_{A,a}^{\Gamma_{b-a}}$ and $\varphi_{B,b}^{\Gamma_{b-a}}$ are the molecular fractions of interacting species of phases a and b at the interface b - a (denoted as Γ_{b-a}), respectively, $\mu_{A,a}$ and $\mu_{B,b}$ are the chemical potentials of components A and B in phases a and b , respectively.

The general condition for two phases a and b to be in thermodynamic equilibrium is the equality of chemical potential of the components. In thermodynamic equilibrium, the chemical potential of reacting components is equal at Γ_{b-a} and it is expressed as

$$\mu_{B,b}(\varphi_{B,b}, T, p) = \mu_{A,a}(\varphi_{A,a}, T, p) \text{ at } \Gamma_{b-a} \quad (5.16)$$

In the complete binary case ($\varphi_{A,b} \neq 1$), there is also a relation similar to **Eq. 5.16** for the other component.

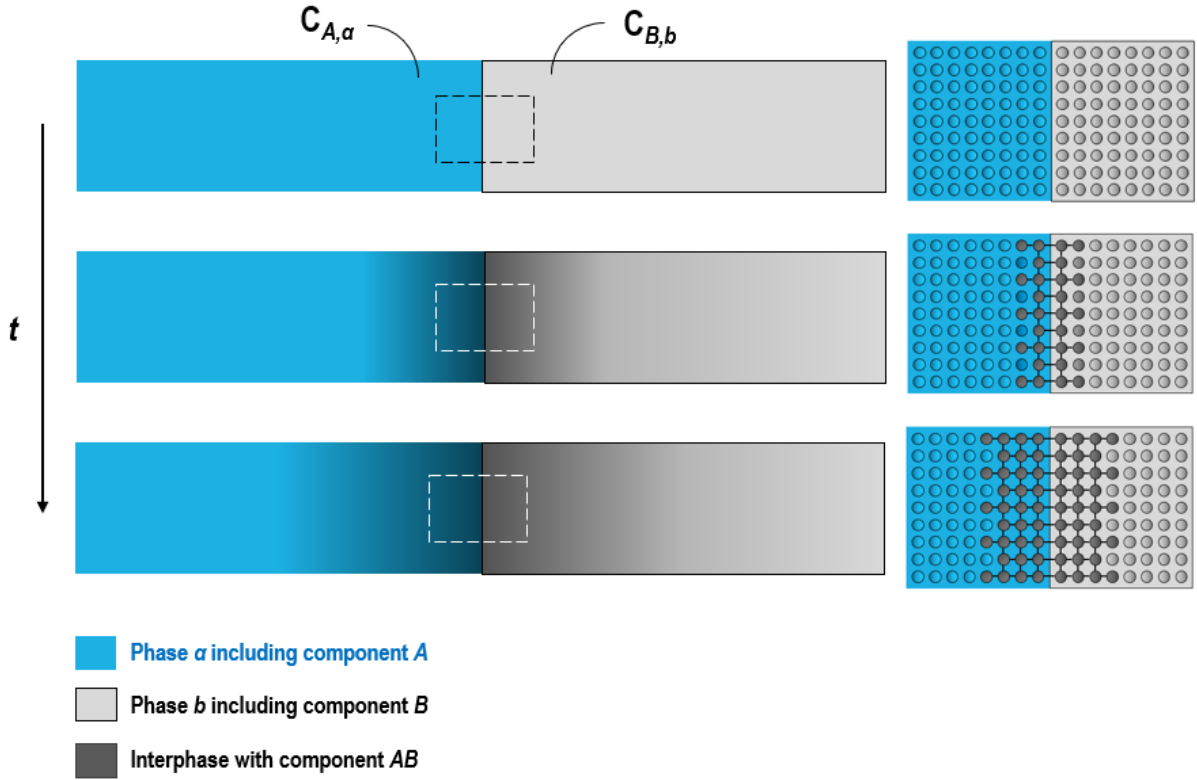


Figure 5.5 Schematic of interface mutual diffuse-reaction concept.

For the case under consideration, both phases a and b are immobile. The mass balance equations for components A and B in the solvent phase are

$$\frac{\partial(\rho_b \varphi_{A,b})}{\partial t} - \nabla \cdot (\rho_b D_{A,b} \nabla \varphi_{A,b}) = 0 \quad (5.17)$$

$$\frac{\partial(\rho_b \varphi_{B,b})}{\partial t} - \nabla \cdot (\rho_b D_{B,b} \nabla \varphi_{B,b}) = 0 \quad (5.18)$$

where ρ_b is the density of solvent, $D_{A,b}$ is the liquid binary diffusion coefficient, $D_{B,b}$ is the self-diffusion coefficient of solvent.

The mutual diffusion-reaction process is controlled by thermodynamic equilibrium at the interface and is translated into a simple Dirichlet condition. Therefore, an equilibrium concentration (φ_{eq}) for component (species) A at the polymer-solvent interface is expressed as

$$\varphi_{A,b} = \varphi_{eq} \text{ at } \Gamma_{b-a} \quad (5.19)$$

The mass balance equation for components A and B at the interface $b-a$ gives

$$(\rho_b D_{A,b} \nabla \varphi_{A,b}) \cdot \mathbf{n}_{ba} = (\rho_a \varphi_{A,a} \mathbf{w}) \cdot \mathbf{n}_{ba} \text{ at } \Gamma_{b-a} \quad (5.20)$$

$$(\rho_b D_{B,b} \nabla \varphi_{B,b}) \cdot \mathbf{n}_{ba} = (\rho_a \varphi_{B,a} \mathbf{w}) \cdot \mathbf{n}_{ba} \text{ at } \Gamma_{b-a} \quad (5.21)$$

The total mass balance at the interface $b-a$ gives

$$\rho_b \mathbf{w} \cdot \mathbf{n}_{ba} = \rho_a \mathbf{w} \cdot \mathbf{n}_{ba} \text{ at } \Gamma_{b-a} \quad (5.22)$$

where \mathbf{w} is the velocity of the interface $b-a$. The set of balance equations presented above are sufficient to solve the physical problem, provided that the overall surrounding boundary conditions are given as

$$\mathbf{n}_{ba} \cdot \mathbf{w} = \mathbf{n}_{ba} \cdot \left(\frac{\rho_b}{\rho_a(1-\varphi_{A,b})} D_{A,b} \nabla \varphi_{A,b} \right) \text{ at } \Gamma_{b-a} \quad (5.23)$$

$$0 = \mathbf{n}_{ba} \cdot \left(\frac{\rho_b - \rho_a}{\rho_a(1-\varphi_{A,b})} D_{A,b} \nabla \varphi_{A,b} \right) \text{ at } \Gamma_{b-a} \quad (5.24)$$

The diffusion coefficient of two components in corresponding phases is described by **Eq. 5.14**.

5.4.1 Model implementation

A two-dimensional finite element mesh of 10E3 total number of quad elements was created consisting of two contacting domains of 1E-3 m width and 5E-4 m height each (**Fig. 5.6**). The two domains represent the interacting phases a and b . Particularly, the phase a (left domain) is considered as a single-component (component A) phase at a concentrated regime. Component A is assumed to be a free reactive epoxy species ($M_{WA} = 320.814$ g/mol). Similar to **section 5.3**, phase b (righthand domain) is considered at a diluted regime with free species of component B ($M_{WB} = 107.155$ g/mol) diluted in a solvent/asphalt binder ($M_{Wb} = 1000$ g/mol, $\rho = 1010$ g/mol). It should be mentioned again that the two-domains (i.e., two contacting phases) system are considered at a perfect stoichiometric condition in thermodynamic equilibrium ($\varphi_{Ab} = \varphi_{Ba} = \varphi_{Aa} = \varphi_{Bb}$).

The typical results of the current model and of reactions between the two domains are shown in **Fig. 5.6**, in where the concentration change of component A ($C_{A,a}$) and B ($C_{B,b}$) at the interface of two domains demonstrates the new component (C_{AB}). A general observation is that the concentration of solvent species (i.e., component A) gradually decreases while the concentration of producing species (i.e., component AB) gradually increases as reaction proceeds.

To quantify the effect of reactivity parameters on the interaction of two domains, parametric analyses have been performed (E_a : 2E1, 3E1 and 4E1 kJ/mol; K_0 : 500, 1000 and 1500 1/s). The predicted results of these analyses (concentration profiles along x-coordinate) are shown in **Fig. 5.7a**. The concentration of the reaction product reached the highest level after 60 min of curing reaction between the two domains when 1500 1/s reaction rate was used. Higher reaction rates or lower activation energies lead to the fast growth of new species resulting in sharp interfaces. Comparing **Fig. 5.7a** and **7.5b**, the impact of activation energy on the concentration level achieved after the two domains reaction was more significant than of reaction rate (**Fig. 5.7b**), a phenomenon which is also noticed in the single domain model in **sub-section 5.3.1**. For all case scenarios, the shape of concentration distribution was the same along the x-coordinate, as the initial diffusion coefficient of both domains remains the same for all analyses (5E-14 m²/s).

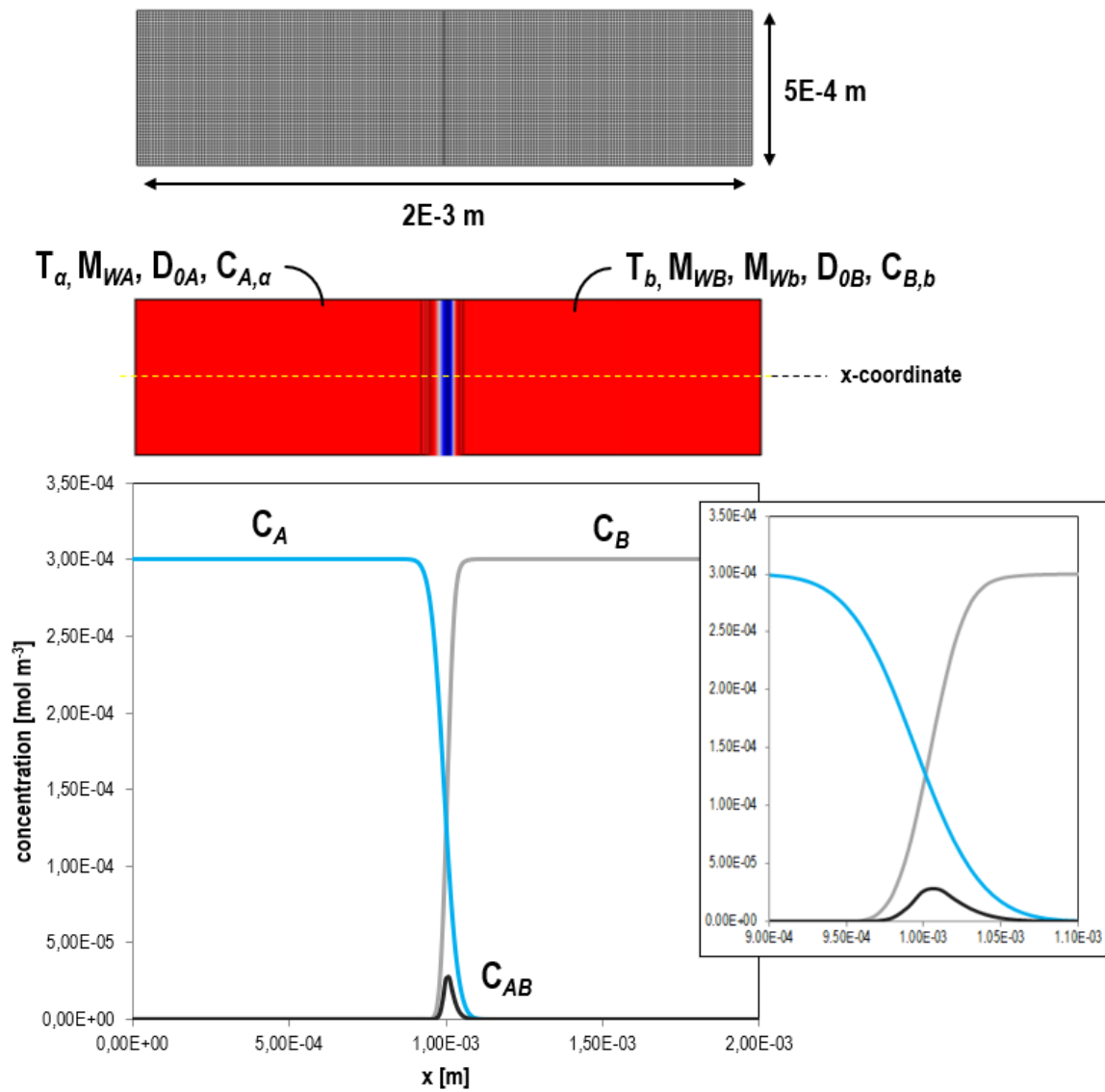
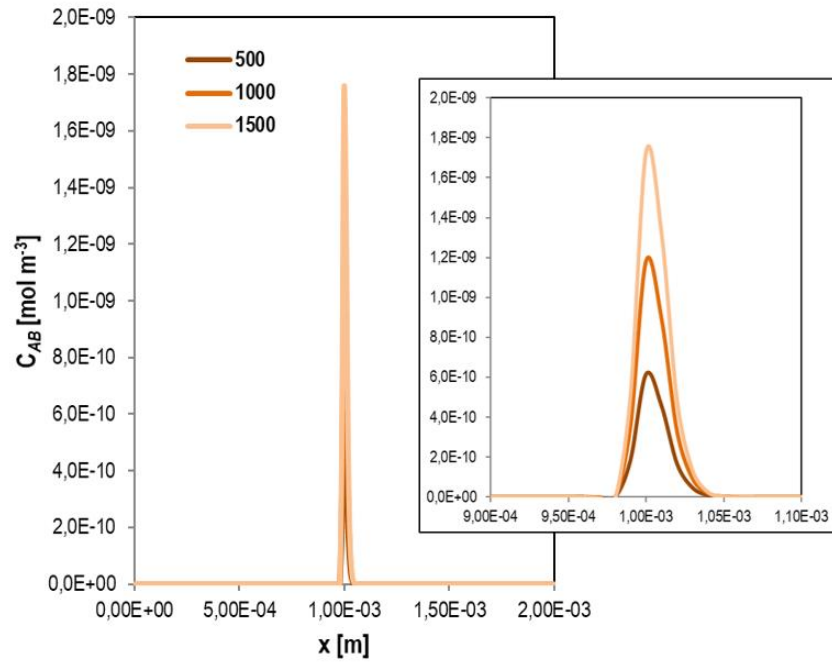
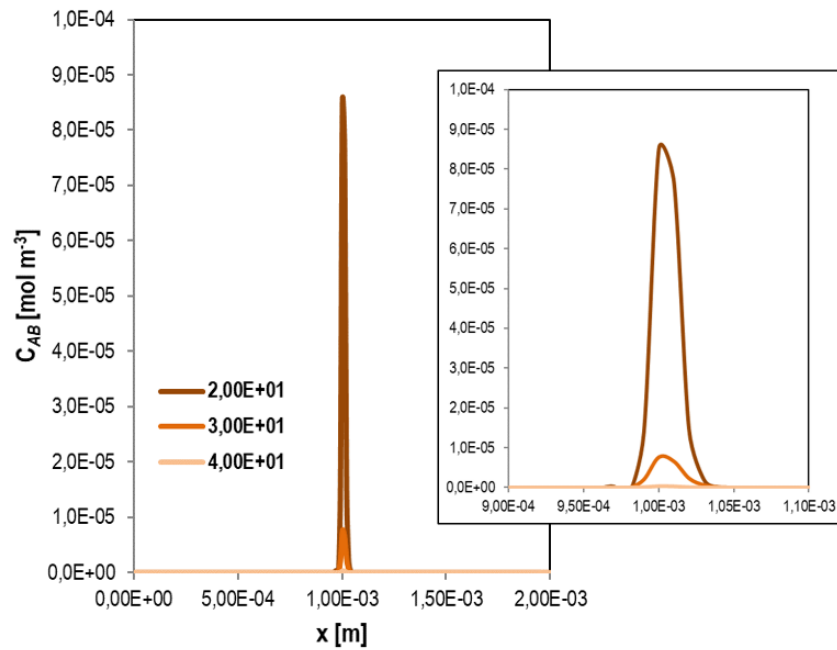


Figure 5.6 Finite element geometry and mesh of two contacting domains, and concentration predictions of different reacting components along the x-coordinate of geometry.

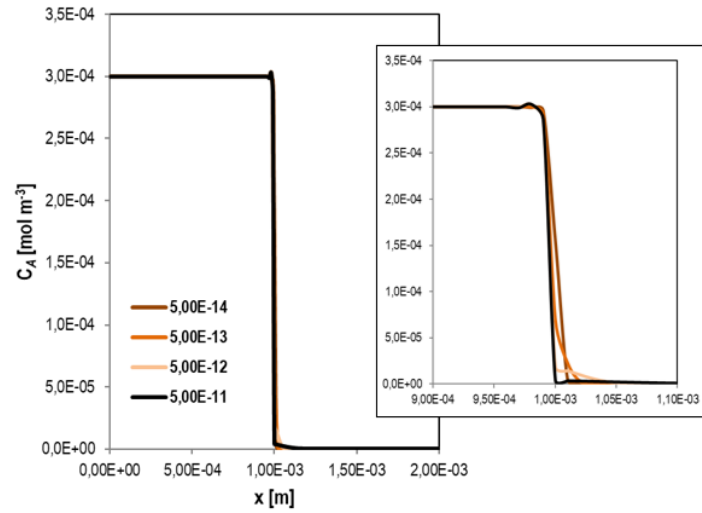


(a)

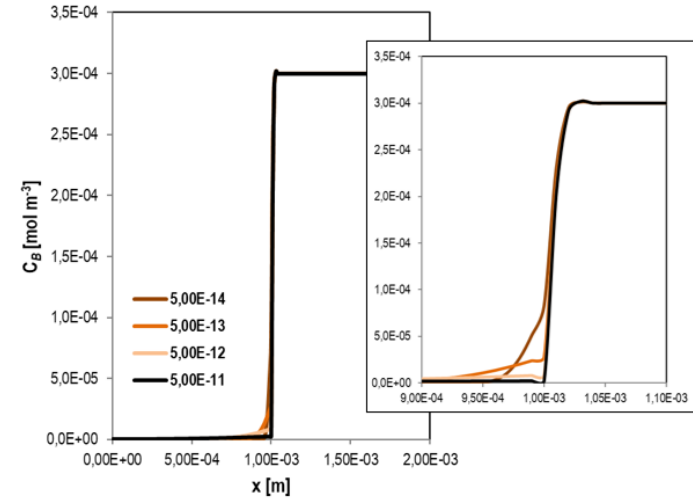


(b)

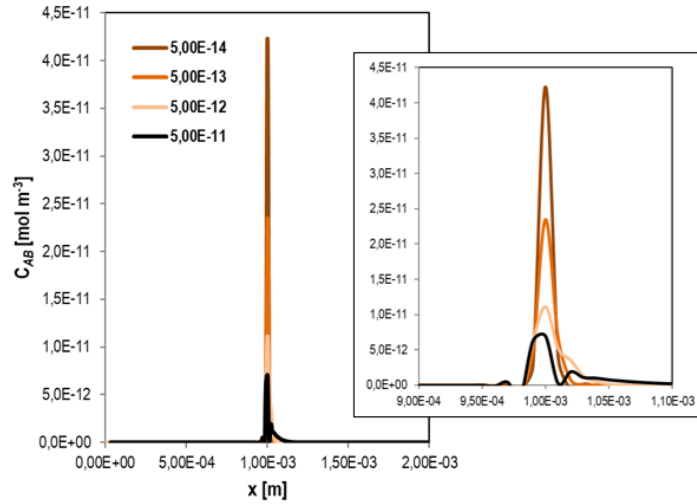
Figure 5.7 Effect of (a) reaction rate (500, 1000 and 1500 1/s with constant 56 kJ/mol) and (b) activation energy (20, 30 and 40 kJ/mol with constant 2000 1/s) on the extent of product concentration of two reacting components (D_{0A} and D_{0B} : 5×10^{-14} m²/s).



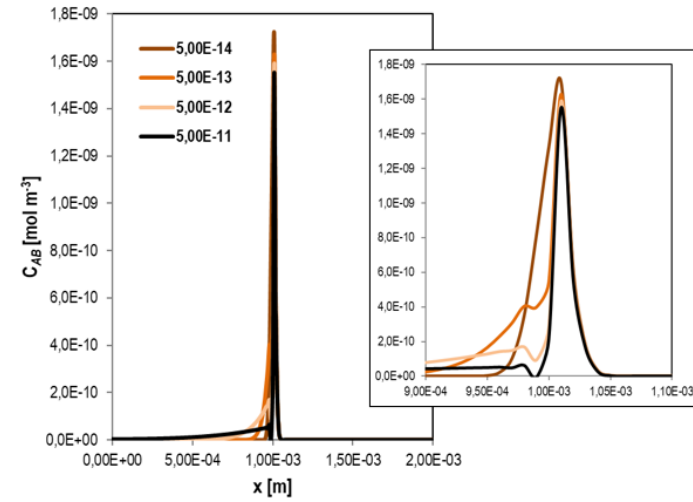
(a-i)



(a-ii)



(b-i)



(b-ii)

Figure 5.8 Effect of the diffusion coefficient of component (a-i) A in phase b and (a-ii) B in phase a on the concentration variation of (b-i and b-ii) component AB along the horizontal axis at the end of reaction (D_0 : 5E-11, 5E-12, 5E-13 and 5E-14 m²/s, with constant $E_a=56$ kJ/mol, $K_0=2000$ 1/s, $T=130^\circ\text{C}$).

The plots of concentration of components *A*, *B* and *AB* at the end of reaction for different diffusion coefficients are given in **Fig. 5.8**. Especially, the simulation results when D_{0A} (diffusion coefficient of *A*) and D_{0B} (diffusion coefficient of *B*) vary in phases *b* and *a* are shown in this figure. The concentration gradient depicts the generated inter-diffusion profiles predicting the concentrations levels and rates of formed component *AB* when the two phases inter-react. The concentration profile of component *AB* differs from low to high D_0 showing the level of diffusion. Higher values of diffusion coefficient result in lower concentrations of newly produced species at the interface. For example, as shown in **Fig. 5.8a-i**, when the D_{0A} was $5\text{E-}11\text{ m}^2/\text{s}$, then the diffusion of component *A* in phase *b* was considerably low comparing the lower D_0 values, causing subsequently lower concentrations of component *AB* at the interface (see **Fig. 5.8b-i**). The same phenomenon was noticed in the predicted profiles of components *B* and *AB* by varying the values of D_{0B} (see **Fig. 5.8a-ii** and **Fig. 5.8b-ii**). In all cases, the concentration profiles of component *AB* show the highest localized concentrations always at the interface.

5.5 Summary

In the case of binary polymer blends, as epoxy-asphalt binders, accurate predictions of the composition at the interface between different phases are needed to obtain a mechanistic picture of diffusion-reaction of interacting species. In this **chapter**, a model based on the free-volume theory is implemented in a multi-physics tool to simulate the curing induced diffusion phenomena. Numerical predictions have shown that lower values of activation energy result in the acceleration of curing process, as discussed in **Chapter 4** as well, leading to higher concentrations of newly produced species at the interface. The impact of activation energy on facilitating the diffusion of reactive species over curing was more significant than of reaction rate in both cases (i.e., single domain and two contacting domains). Furthermore, higher values of diffusion coefficient result in lower concentrations of newly produced species at the interface. More and more species *A* diffuse into phase *b* over curing, particularly at lower initial diffusion coefficient values, causing an overall concentration increase of species *AB* at the interface, decrease of diffusion coefficient, hindering the further species transport.

The presented model in this **chapter** can be applied as a powerful tool for understanding the reaction mechanisms to produce homogeneous blends reducing the number of trial-and-error experiments. In turn, the reliable quantitative description of process kinetics can be a decisive tool for the design of optimal reaction paths. Binders with chemical species of certain reactivity and diffusivity characteristics could be able to co-associate with the epoxy groups producing thus partially or fully miscible systems under certain energy conditions. Nonetheless, the energy conditions play crucial role in this process, as indicated also in the previous **chapters**, and thus they should be selected carefully to control the quality of epoxy-asphalt binders.

5.6 References

- Cohen, M.H., D. Turnbull. Molecular Transport in Liquids and Glasses. *The Journal of Chemical Physics* 31, 1959, pp. 1164-69.
- DiBenedetto, A.T. Prediction of the Glass Transition Temperature of Polymers: A Model based on the Principle of Corresponding States. *Journal of Polymer Science: Part B: Polymer Physics* 25, 1987, pp. 1949-69.
- Flory, P.J. *Principles of Polymer Chemistry*. Cornell University Press: Ithaca, NY, 1953.
- Fujita, H., A. Kishimoto, K. Matsumoto. Concentration and Temperature Dependence of Diffusion Coefficients for Systems Polymethyl Acrylate and n-Alkyl Acetates. *Transactions of the Faraday Society* 56, 1960, pp.424-437.
- Macedo, P.B., T.A. Litovitz. On the Relative Roles of Free Volume and Activation Energy in the Viscosity of Liquids. *The Journal of Chemical Physics* 42, 1965, pp. 245-256.
- Rajagopalan, G., J.W. Gillespie, S.H. McKnight. Diffusion of Reacting Epoxy and Amine Monomers in Polysulfone: A Diffusivity Model. *Polymer* 41, 2000, pp. 7723-33.
- Turnbull, D., M.H. Cohen. Free-volume Model of the Amorphous Phase: Glass Transition. *The Journal of Chemical Physics* 34, 1961, pp. 120-125.
- William, M.L., R.F. Landel, J.D. Ferry. The Temperature Dependence of Relaxation Mechanisms in Amorphous Polymers and other Glass-forming Liquids. *Journal of the American Chemical Society* 77(14), 1955, pp. 3701-07.

6

Oxidative Aging of Epoxy-Asphalt

6.1 Introduction

The impact of epoxy polymers on the oxidative aging performance of asphalt binders was evaluated in various studies (Herrington & Alabaster 2008; Apostolidis et al., 2019). However, fundamental understanding of the oxidation mechanism of epoxy-asphalt binders is needed because of the significantly different nature of these binders comparing the conventional one. Quantitative information on the rate of chemical, physical, and mechanical changes of epoxy-asphalt as a function of time is important to precisely predict the evolution of material properties through service life. This is also true for conventional binders, but it becomes even more important in the case of epoxy-asphalt because of their extremely long potential lifetime.

The scope of this **chapter** is to provide understanding on the oxidative aging of epoxy-asphalt binders and mastics by performing laboratory analyses. Fourier Transform Infrared (FTIR) spectroscopy is used to track carbonyls and sulfoxides of studied materials at different temperatures over time. The oxidation kinetic parameters of epoxy-asphalt binder and mastic have been determined to quantify their aging sensitivity. As the oxidative aging is accompanied by stiffening and embrittlement of binders contributing to the overall deterioration of asphalt pavements, special attention is also given to assess these characteristics of epoxy-asphalt materials due to oxidative aging. Especially, Dynamic Shear Rheometer (DSR) studies have been performed to assess the changes of stiffness modulus and phase angle and ultimately to analyze the oxidation-induced stiffening of epoxy-asphalt materials. Analysis of the dependence of the glass transition temperature, T_g , on the initial composition of the materials has also been conducted using differential scanning calorimetry (DSC). Below the T_g , asphalt binders exhibit brittle behavior while they are ductile at temperatures above the T_g . Hence, the T_g could be used as an alternative parameter to quantify the influence of epoxy in asphalt, as discussed in **Chapter 3**, and ultimately to elucidate the mechanism of oxidation-induced embrittlement.

The background of oxidative aging in asphalt binders will be discussed in the next section.

6.2 Chemistry of Oxidative Aging in Asphalt Binders

Asphalt binder is composed of an extremely large number of different types and sizes of organic (hydrocarbon) molecules ranging from paraffins to alkyl polyaromatics containing trace elements of nitrogen, oxygen, sulphur and traces of metals such as vanadium and nickel. These molecules are separated into categories based on the chemical reactivity and the polarity of organic molecules. In the next sections, the chemistry of oxidative aging of asphalt binders is discussed together with the main factors influencing the oxidative aging process.

6.2.1 Functional groups and fractions of oxidative aging

A lot of effort has been given to get information on the organic molecular groups in virgin and aged asphalt binders where new functional groups are formed due to the chemical interaction mainly between oxygen and the organic molecules of asphalt binders. Among other groups, the heterogeneous functional groups in binders have been mentioned with the largest impact on rheological properties (Petersen 1984). The larger of the heteroatom-containing groups in

asphalt binders (i.e., asphaltenes) were identified as highly polar and more interacting groups. These are made-up mainly from large organic molecules; (i) carboxylic acids, (ii) anhydrides, (iii) ketones, (iv) 2-quinolone types, (v) sulfoxides, (vi) pyrrolic and (vii) phenolic types. Sulphur is the most present polar atom, and it is displayed as sulphides, thiols and sulfoxides. Oxygen and nitrogen heteroatoms are the next most common after sulphur. Oxygen has appeared in the form of ketones, phenols, and carboxylic acids. Pyrrolic, pyridic and 2-quinoline structures are formed based on nitrogen. Functional groups formed naturally in asphalt binders are sulphur, carboxylic acids, phenolic, pyrrolic and 2-quinolone-type groups which are hydrogen bonding functional groups.

Additional oxygen-containing chemical functional groups are formed during oxidative aging after reaction of oxygen with highly polar molecules. Less reactive molecules with low polarity or nonpolar elements suffer less due to oxidation. Mainly sulfoxides (Petersen 1981) and ketones (Dorrence et al., 1974) are produced with a lesser number of dicarboxylic anhydrides and carboxylic acids at a later aging time (Petersen et al., 1975). Sulfoxides are formed at a much faster rate than ketones (Petersen 1981). Ketones are formed at the benzylic carbon position, and hydrogen on the tertiary benzylic carbon is very reactive and thus easily removed during oxidation (Dorrence et al., 1974; Mill & Test 1990). Previous works on chemical reactions of aromatic molecules in binders also reported that in most of the cases the oxidation reaction is finished with the complete formation of ketones.

Studies were carried out to analyze the chemical composition and the functional groups in asphalt binders using different techniques, such as FTIR, ultraviolet spectroscopy, mass spectroscopy and nuclear magnetic resonance proved that difficulty (Petersen 2009). Techniques able to identify different elements according to their molecular size, reactivity, solubility, and polarity are introduced as well. One of them is SARA (saturates, aromatics, resins and asphaltenes), which separates fractions using ion exchange chromatography, and molecular groups based on their polarity into SARA using liquid chromatography and nonaqueous potentiometric titration methods (Branthaver et al., 1993). The molecular weight of the fractions increases as saturates \leq aromatics \leq resins \leq asphaltenes.

The saturate part of an asphalt binder is non-polar, linear, branched and/or cyclic saturated hydrocarbons. The aromatic fraction is more polar than saturates owing to the contained aromatic rings. Similarly, resins and asphaltenes are polar. Resins are soluble with n-heptane or n-pentane while asphaltenes are insoluble in n-heptane. The fractions of saturates (i.e., paraffins, naphthene and mix of two), aromatics (i.e., mix of paraffin, naphthene and aromatics with sulphur components) and resins (i.e., multi-ring aromatics structures and heteroatoms) consist of one category which is named maltenes and together represent the medium solution of asphalt. The non-soluble fraction is the asphaltenes with different molecules (i.e., paraffins, naphthenes and polycyclic aromatic structures). Asphaltenes, which are the most polar components of asphalt binders, have been identified as the major responsible factor for the viscosity increase. Studies of different fractions of binders show that, on the one hand, saturates, being nonpolar molecules, display weak interaction forces leading a collection of those molecules to demonstrate low viscosity (Petersen 2009). On the other hand, aromatic ring systems are usually polar, and their molecular interactions are strong explaining thus the loss

of sufficient mobility of molecules and the relatively high viscosity of a material consisting solely of asphaltenes and aromatics.

The amount of polar functional groups in asphalt binders increases over aging, resulting in a reduction of molecular flow and kinetics. However, the composition of molecules differs among different binders and, hence, studies were conducted to identify which is the most important element correlated with the viscoelastic properties of asphalt binders. It was concluded that asphaltenes (Plancher et al., 1976) and ketones (Martin et al., 1990; Lau et al., 1992; Lin et al., 1995; Petersen et al., 1993; Branthaver et al., 1993) display good correlations between their content and the viscosity, and the asphalt becomes brittle with increased stiffness modulus and reduced phase angle (Vallerga 1981; Lu & Isacsson 1998; Siddiquie & Ali 1999; Lamontagne et al., 2001; Glover & Doke 2005; Durrieu et al., 2007; Lu et al., 2008; Mouillet et al., 2009; Wu et al., 2009; Wu & Airey 2009; Farrar et al., 2013; Glaser et al., 2013; Liang et al., 2019; Jing et al., 2019a; 2019b; 2019c & 2019d).

6.2.2 Kinetics of oxidative aging

Due to the fact that the oxidation-induced compositional changes of asphalt binders are dependent on the material type and source, it is important to consider the oxidation reaction kinetics of the asphalt binders. As mentioned before, major products at the initial stages of oxidation of asphalt binders are ketones and sulfoxides. The rate of formation of these products is characterized as less at later stages when carboxylic acids and dicarboxylic anhydrides being formed (Lee & Huang 1973; Petersen et al., 1975; Lau, et al., 1992; Branthaver et al., 1993; Petersen 1998). It has been reported that the formation rate of sulfoxides during the initial stage of oxidative aging is higher than ketone formation rate at ambient temperatures (Lau et al., 1992; Petersen et al., 1996; Petersen 1998; Petersen 1998). Note that the total concentration of sulfoxides and ketones at the end of the initial oxidation stage, which was determined using the FTIR spectroscopy, is about the same regardless of the temperature and the relative amounts of each component (Petersen 2009).

Studies on oxidized binder examined the correlation of ketones and sulfoxides during aging with the current fraction of maltenes and asphaltenes in asphalt. When the material was oxidized, the fraction of maltenes decreased and that of asphaltenes increased, respectively. Furthermore, the highest amount of ketones formed during oxidation were derived from resinous fractions forming large parts of polar aromatics. Sulfoxides, which are derived from the oxidation of sulfides, are the less polar fractions and no correlation was found with the formation of asphaltenes. After initial oxidation, it is believed that the increase of viscosity is not associated by the polarity of molecules with the large, agglomerated domains formed because of the polarity changes of these groups. These agglomerated domains have been recognized as products causing insufficient mobility (Petersen et al., 1996).

The asphalt oxidation is distinguished in two phases, a non-linear fast-rate reaction, and a linear constant-rate reaction phase (see **Fig. 6.1**) (Van Oort 1956; Liu et al., 1996; Jin et al., 2011; Glaser et al., 2013; Liu & Glover 2015; Herrington 2012; Herrington et al., 2017; Jing 2019). Previous works focused on constant-rate kinetics of aging asphalt binder as well because the duration of the fast rate period is relatively short and of small impact on the long-term asphalt

performance (Liu et al., 1996; Domke et al., 1999). The oxidation reactions as aliphatic sulphide to sulfoxide and benzylic carbon to carbonyls have been indicated as the main reaction pathway of oxidative aging in asphalt that dominates the material stiffening (Petersen et al., 1993; Petersen & Harnsberger 1998). Several models and mechanisms were also proposed through the years to predict the reaction rate to describe the oxidative aging kinetics (Bateman & Hargrave 1954; Martin 1966; Knotnerus 1971; Petersen 1984; King 1993; Herrington 1995; Petersen 1996; Petersen 1998).

Overall, the state of molecular dispersion within the asphalt alters with oxidative aging and new molecules are produced. In the present research, emphasis was given on assessing the development of polar molecules in the form of sulfoxides and carbonyls using the FTIR spectroscopy. As the dispersion of polar organic molecules in a medium of less polar molecules and their interaction are highly associated with the performance-related properties of asphalt, stiffening and embrittlement of materials were evaluated as well by conducting DSR and DSC tests, respectively. The materials used, and the conditioning and testing protocols implemented for this research part are discussed in the following section.

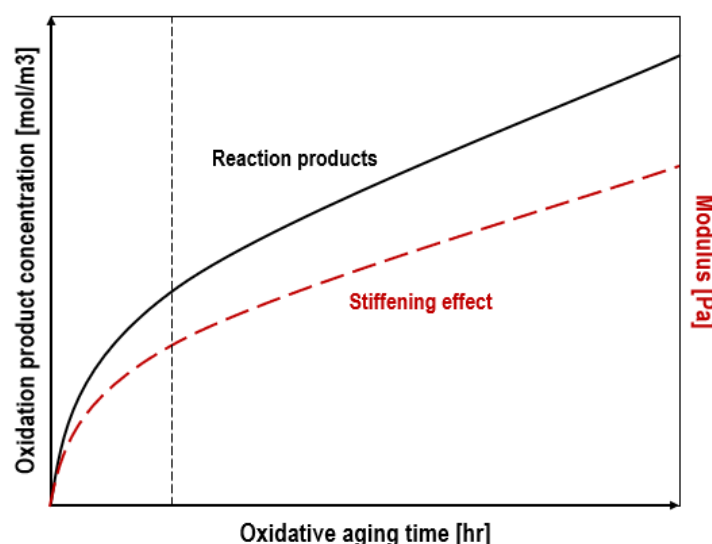


Figure 6.1 Schematic illustration of typical asphalt oxidation in-service conditions.

6.3 Materials and Methods

6.3.1 Binders, filler and mastics

The idea to dilute the epoxy binder with a conventional asphalt binder has been adopted in New Zealand as a feasible method to produce durable pavement materials under relatively long operational time windows (Herrington & Alabaster 2008; International Transport Forum 2017). Here, a 70-100 pengrade binder was diluted with the epoxy binder (EA_{ref}). Immediately after preparing the EA_{ref} as described in **Chapter 2**, the epoxy was mixed with the pre-heated 70-100 pengrade binder at 120°C with a weight ratio of 20:80 and 50:50 of epoxy (100:0) and neat asphalt binder (0:100), respectively.

Asphalt binders are always in conjunction with mineral particles (i.e., filler and aggregates) of different sizes in asphalt mixes. Filler particles together with the binder form the mastic which

is the binding material between the aggregates. The fillers used were pure limestone particles (main minerals; dolomite and calcite) (density: 2.77 gr/cm³; BET specific surface area: 13.25 m²/gr) passing through the 0.075-mm sieve.

The mastic samples were prepared by mixing fillers (pre-heated for 60 min at 120°C) with the newly formulated binders. The weight ratio of filler and binder was 56:44. This weight ratio corresponds to the asphalt mastic part of a stone mastic asphalt (SMA-NL 8B, RAW-2015), which will be discussed in **Chapter 7**. To assess the effect of filler particles on the oxidation kinetics of the studied materials, the neat asphalt and EA_{ref} binders were aged as well. Before mixing filler and binders, filler particles were pre-heated in the oven for approximately 60 min at 120°C. Mixing fillers and binders performed manually for 5 min to ensure the production of homogeneous mixes without migrated particles at the bottom of the can. Four mastic samples were prepared of different weight ratios of epoxy and asphalt binder (EAF0); 20:80 (EAF20), 50:50 (EAF50) and 100:0 (EAF100) (see **Table 6.1**). Samples were placed in a refrigerator at -10°C to minimize further curing.

Table 6.1 Name and composition of studied materials.

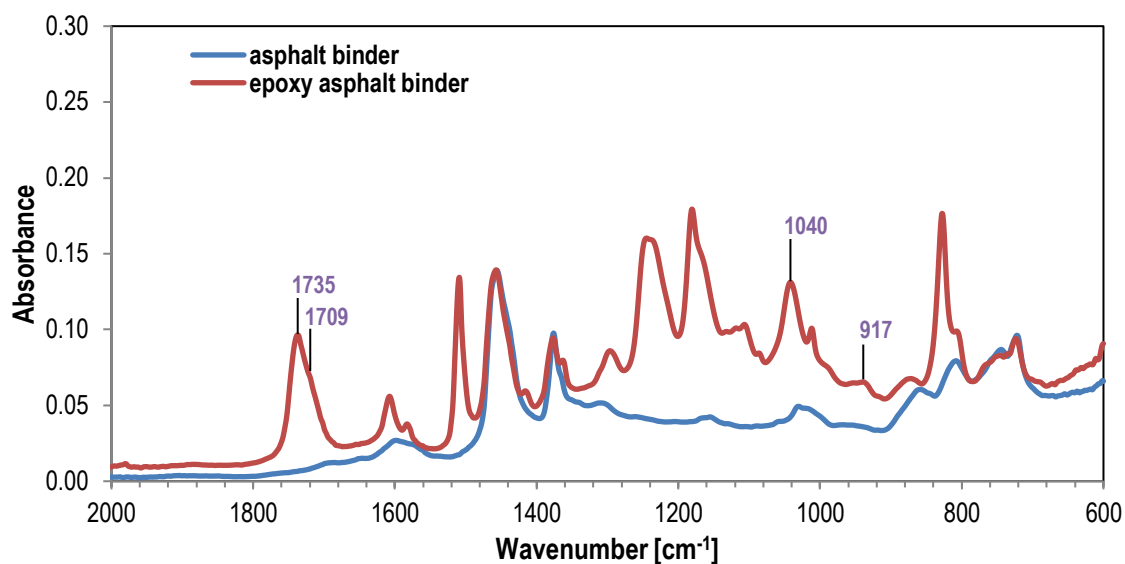
Material	Asphalt binder [% wt]	Epoxy binder [% wt]
EA0	100	0
EA100	0	100
EAF0	100	0
EAF20	80	20
EAF50	50	50
EAF100	0	100

*F denotes the inclusion of filler particles. Weight ratio of filler and EA binder: 56:44.

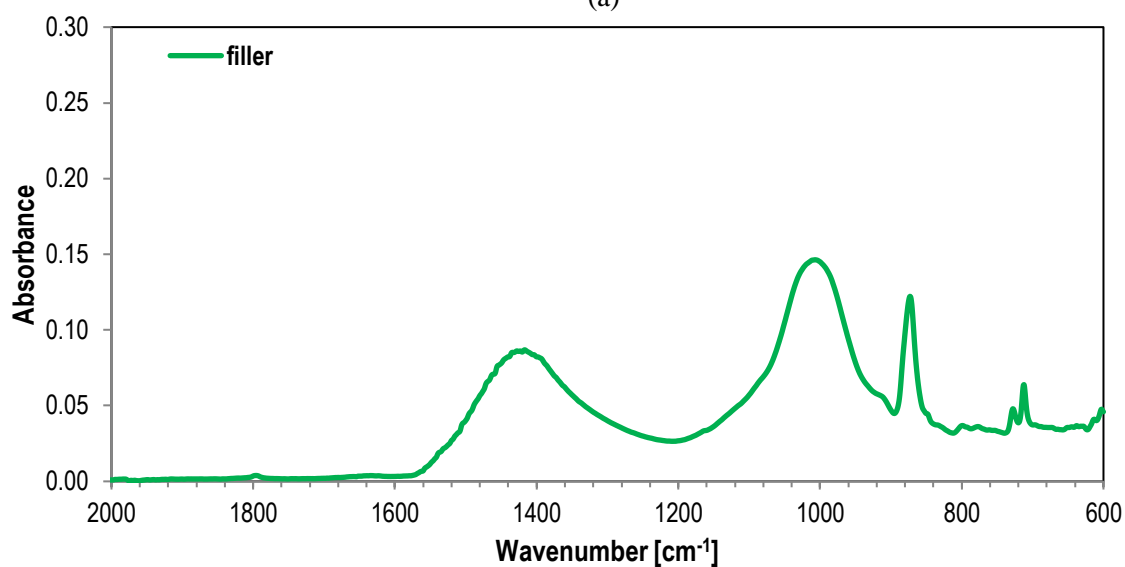
6.3.2 Fourier transforms infrared spectroscopy measurements

To assess the effect of oxidative aging on the chemistry of binders and mastics, samples were subjected to oven-conditioning (atmospheric pressure) and the evolution of carbonyls and sulfoxides was tracked by FTIR spectroscopy equipped with an Attenuated Total Reflectance (ATR) fixture. Particularly, samples were subjected to oven-conditioning (0.1-MPa) over 2, 5, 8, 24, 120, 240 and 480 hrs lengths of time at 80, 90 and 100°C. After each isothermal period, the chemical composition changes were measured as a function of time. Because the oxidation rate of a binder is affected by the material chemistry, film thickness and temperature, all samples were obtained from the top surface of materials to avoid measuring samples of different aging levels at different depths.

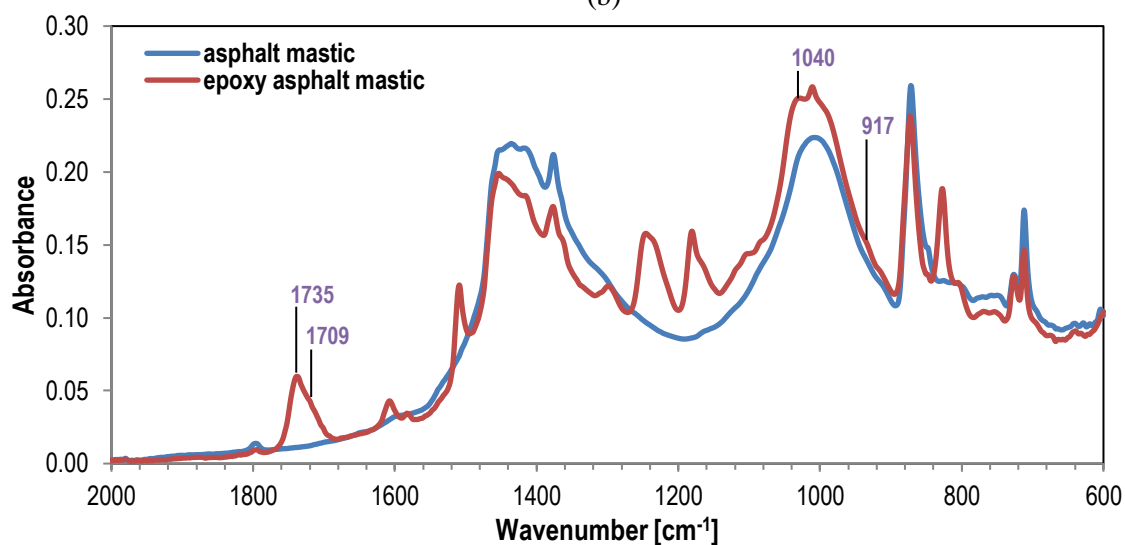
Infrared spectra with wavenumber from 4,000 to 600 cm⁻¹ were recorded and collected for all samples. A certain amount of material was placed directly on the ATR crystal pedestal and pressed with a constant force to ensure proper contact to the surface. A minimum of three sub-samples was investigated for each sample and 20 scans per sub-sample were performed with a fixed resolution of 4 cm⁻¹. Typical spectra of functionalities of neat asphalt and EA_{ref} binder are shown in **Fig. 6.2a**. **Fig. 6.2b** and **Fig. 6.2c** demonstrate the IR spectra of filler and of mastics, respectively.



(a)



(b)



(c)

Figure 6.2 IR spectra of (a) asphalt and EA binder, (b) filler and (c) asphalt binder with filler, or asphalt mastic, and EA mastic (after oven-conditioning at 100°C for 480 hrs).

Once Part A is mixed with Part B, the curing reaction of epoxy in Part A with the specific functionalities in Part B occurs in presence of acid-based reaction catalysts/initiators giving ether and ester compounds and producing the epoxy binder (Herrington & Alabaster 2008; Wei & Zhang 2012; Apostolidis et al., 2019). Specifically, oxirane groups (at 917 cm^{-1}) react with the carbonyl acid group (at 1709 cm^{-1}) resulting into ester (at 1735 cm^{-1}) and ether (at 1040 cm^{-1}). Hence, loss of carboxylic acid (at 1709 cm^{-1}) and oxirane (at 917 cm^{-1}) groups, and the corresponding increase of ester (at 1735 cm^{-1}) and ether (at 1040 cm^{-1}) groups happens. Due to the curing of EA materials is beyond the scope of this research part, the extent of oxidative aging of studied materials was evaluated by calculating the carbonyl (CO) and sulfoxide (SO) aging indices by using the area method. The CO and SO aging indices are defined as the integrated peak area from 1753 to 1660 cm^{-1} and from 1047 to 995 cm^{-1} , respectively. Details on how these indices were calculated provided by Ruxin 2019d.

6.3.3 Dynamic shear rheometer measurements

To quantify the oxidation-induced stiffening in mastics, frequency sweep measurements were conducted using DSR. The effect of aging on the performance of the frequency-dependent properties (i.e., complex shear modulus defined as the total resistance of samples to deformation under different frequencies and phase angle indicated the viscous performance of samples) of mastic samples at different epoxy modification levels and oven-aging time periods (i.e., 2, 5, 8, 24, 120, 240 and 480 hrs) at 100°C was determined here. DSR testing frequency sweep measurements (0.1 to 10 Hz , 0 to 50°C at temperature steps of 10°C) were performed to quantify the aging effect on the viscoelastic properties of mastic. The parallel plate testing geometry (plates of 8-mm diameter with a 2-m sample gap) was used and the samples were reshaped to fit between the parallel plates. The master curves were produced with the time-temperature superposition model at a reference temperature of 30°C .

6.3.4 Differential scanning calorimetry measurements

Glass transition is the glass to amorphous non-equilibrium transition occurring in all material types. Although the glass transition of asphalt binders is a well-established research topic (Apostolidis et al., 2021), systematic analyses of the glass transition of polymer modified asphalt materials using DSC is still needed, to obtain information about the miscibility and the potential oxidation-induced embrittlement of such materials. The knowledge of T_g as a function of composition reflects miscibility or lack of it. The determination of composition relationship with the T_g and its deviation can be used as indicators of the thermodynamics of mixing of amorphous systems, with the positive enthalpy of mixing to be associated with the T_g deviations and the formation of immiscible binders.

The composition dependence of the T_g in several binary polymer blends has been reported along these lines, showing positive, negative, and zero deviations from the ideal mixing rule (Lesikar 1976; Painter et al., 1991; Murthy & Tyagi 2002; Pinal 2008; Gupta & Mauro 2009; Wang et al., 2011). Various relationships that describe the glass transition-composition dependence have been proposed in various binary polymers (Gordon & Taylor 1952; Fox 1956; Couchman & Karasz 1978; Kwei 1984), and all are represented as minor variations of the following expression

$$T_{g,mix}^{eq} = \frac{\phi_A T_{gA} + k \phi_B T_{gB}}{\phi_A + \phi_B} \quad (6.1)$$

where $T_{g,mix}^{eq}$ is the predicted glass transition temperature of the amorphous mix, the subscripts A and B denote the individual components A and B , respectively, ϕ_i is the concentration (in mole or weight fraction) of component i (e.g., component A or B) and k is a physical parameter whose interpretation depends on the underlying model used.

The Gordon and Taylor (GT) model is proposed to predict the T_g based on the volume additivity of basic properties (ideal volume of mixing) and the linear change in volume with temperature (Gordon & Taylor 1952), and expressed as

$$T_{g,mix}^{eq} = \frac{w_A T_{gA} + k w_B T_{gB}}{w_A + k w_B} \quad (6.2)$$

where w is the weight fraction of each component in the mix, and k is a parameter depending on the change in thermal expansion coefficient (α) of the components as they change from glassy to amorphous form, or $k = (V_B/V_A)(\Delta\alpha_B/\Delta\alpha_A)$, where V is the specific volume at the corresponding T_g , and $\Delta\alpha_i = (\alpha_{melt} - \alpha_{glass})_i$ are increments at T_g of the isobaric thermal expansion coefficients of the individual components.

Another expression which is empirical since it was derived on the basis of amorphous systems with T_g values of S-shaped profiles (Kwei 1984) is defined as

$$T_{g,mix}^{eq} = \frac{w_A T_{gA} + k w_B T_{gB}}{w_A + k w_B} + q w_A w_B \quad (6.3)$$

where k and q are both fitted parameters related to the intermolecular interactions between the individual components of amorphous systems (Lin et al., 1989; Schneider 1997).

Whether simple physical forces (e.g., van der Waals forces) are the only intermolecular interactions functioning between the constituents, the simple Flory-Huggins theory can explain the phase behavior of binders (see **Chapter 2**). Nevertheless, strong interactions are not considered in this theory, and its simple approximations do not sufficiently elucidate the miscibility in binders. On the one hand, binders of strong, attractive forces might show large and negative ΔH_{mix} together with T_g deviations from the ideal mixing mode (ideal binders or binders without intermolecular forces) (Pinal 2008; Lesikar 1976; Kalogeras 2010). On the other hand, the ΔS_{mix} provides information about the constitutive differences of intermolecular forces in materials. For instance, the intermolecular forces of ideal binders are equal between every pair of molecules. This is the reference case to evaluate the mixing of non-ideal binders, such as the polymer modified asphalt binders. However, the change of ΔS_{mix} is not included in the above expressions, although it is a notable feature of the glass transition of amorphous mixes (Kauzmann 1948).

Once two or more components of different compositions and under internal equilibrium are mixed without chemical reaction, the ΔS_{mix} attributes the rise in the total entropy (or chaos) when the new system reaches a new thermodynamic state. The ΔS_{mix} at a finite heating/cooling rate, for example, over scanning with calorimetry, consists of the following two parts

$$\Delta S_{mix} = \Delta S_{mix}^c + \Delta S_{mix}^r \quad (6.4)$$

where ΔS_{mix}^c is the entropy of mixing accessible to the amorphous, or the configurational part, and ΔS_{mix}^r is the entropy of mixing in the vitrified mix or the residual part. As real amorphous mixes exhibit significant vibrational differences in relation to their glasses, the main characteristic of the ΔS_{mix}^r is inaccessible to amorphous when mix vitrifies. Such unavoidable ΔS_{mix}^r at the glass state limits the possibilities of having a mix of the same entropy equal to the summation of its entropies.

In this study, the contribution of the accessible part of the entropy of mixing, or S^c , is considered the defining parameter for the glass formation of amorphous mixes. The increase of T_g values manifests the smallness of the accessible configurational energy (S^c) (Adam & Gibbs 1965), or the glass transition is a phenomenon that occurs by vanishing of S^c . Considering the kinetic nature of the material, the configuration of glass remains stable over infinitely long time periods at low temperatures. The glass state configuration changes as the glass transition proceed with a minimal rate towards reaching an equilibrium state.

According to (Pinal 2008), the ΔS_{mix}^c values are predicted by using the following equation

$$\Delta T_{g,mix} = T_{g,mix}^{eq} \left[\exp \left(- \frac{\Delta S_{mix}^c}{\Delta C_{p,mix}} \right) - 1 \right] \quad (6.5)$$

where $\Delta C_{p,mix}$ is the difference in the heat capacity of a binder from glass to amorphous.

All samples were aged in a pressure aging vessel (PAV) unit for 20, 40, and 80 hrs at 100°C (2.1 MPa) as well. The 20 hrs PAV protocol is thought to simulate the binder aging during the first five years of asphalt pavement service life, but this hypothesis is still debatable (NCHRP 871, 2017). It is believed that an extended PAV could mimic sufficiently the in-field aging of materials with long-lasting characteristics. Thus, for comparison purposes, the samples were also oven-conditioned for 480 hrs at 100°C, and their glass transition was assessed.

To minimize the effect of the kinetic nature of studied materials, the temperature modulated scanning protocol was implemented in DSC. Nitrogen was used as a purge gas. Samples after placing them in pans were heated for 5 min at 165°C to erase their earlier thermal history and then cooled down to -50°C with 2°C/min fixed rate. The modulated temperature signal was 1°C at a modulation period of 120 s. After equilibrating the samples for 5 min at 165°C, a heating cycle was performed under the same modulation with 2°C/min rate. The calorimetric quantities for the studied materials are determined from the C_p curves, where the change of C_p occurs sigmoidally over the glass transition, as illustrated in **Fig. 3.3** in **Chapter 3**.

6.4 Chemical Compositional Changes

The content of carbonyls and sulfoxides was calculated as a function of time at constant temperatures. The evolution of carbonyls and sulfoxides in binders over time at different temperatures is demonstrated in **Fig. 6.3**. The total amount of carbonyls and sulfoxides in these binders did not change dramatically at 80°C, however remarkable effects of temperature were noticed by increasing the applied temperature to 100°C. This trend is also shown when fillers

were added in binders, as shown in **Fig. 6.4**. These compounds increase as aging proceeds in all binders with and without filler.

Both **Fig. 6.3** and **6.4** depict a decreasing trend of carbonyls and sulfoxides of EA_{ref} materials at the first 24 hrs of oven-conditioning at a constant temperature, due to the epoxy curing (Apostolidis et al. 2019). At 80 and 90°C, sulfoxides remain almost unchanged through the aging of asphalt binder and mastic as well. However, the sulphur reacting species of studied materials have shown an obvious increasing trend at 100°C (see **Fig. 6.3a** and **6.4a**), in similar fashion with the increased attribute of sulfoxides in EA_{ref} at 130°C, evaluated elsewhere (Apostolidis et al., 2019). Sulfoxides continuously decrease at 80 and 90°C and through the early conditioning time lengths at 100°C. Through the later conditioning time lengths, the formation rate of sulfoxide of all mastics shows an increasing tendency at 100°C. The increase of sulfoxides with temperature led to hypothesize a different oxidation pathway in where the sulfides agglomerates dissociate at high temperatures producing free sulfur species available to form more sulfoxides over oxidative aging.

Another observation is that the actual carbonyls measured in the infrared spectrum have been significantly higher in the epoxy binder (EA_{ref}) than in the neat asphalt binder (EA0), as demonstrated in **Fig. 6.3b**. Similarly, high carbonyl values were measured in the epoxy binders with filler (see **Fig. 6.4b**). The epoxy resin, or Part A, is composed of monomers (i.e., building blocks) with an epoxide group at either end. Part B includes free acids able to react with the epoxide groups of Part A formulating new groups mainly composed of carbonyls. This can be the primary reason why both EA_{ref} binder (EA100) and mastic (EAF100) demonstrated remarkably higher carbonyls than of neat asphalt binder (EA0) and mastic (EAF0). Carbonyls in asphalt also increased more rapidly than in epoxy systems during oxidative aging.

For quantitative reasons, the incremental values of carbonyls, demonstrated in **Fig. 6.3** and **6.4**, were calculated to estimate the oxidation kinetics parameters of carbonyls in studied materials. According to **Fig. 6.5**, the extent of incremental values of carbonyls (i.e., $\Delta(\text{CO}) = (\text{CO}_i - \text{CO}_0) / \text{CO}_0$) of EA_{ref} binder with and without filler increased, in a similar fashion with the carbonyls in asphalt. The incremental values of carbonyls have been used as well to determine the oxidation kinetics parameters of studied materials. The oxidation kinetic parameters as a function of time and temperature are important to assist on predictions of the long-term material performance. The methodology for estimating the oxidation kinetics parameters is discussed in the following section.

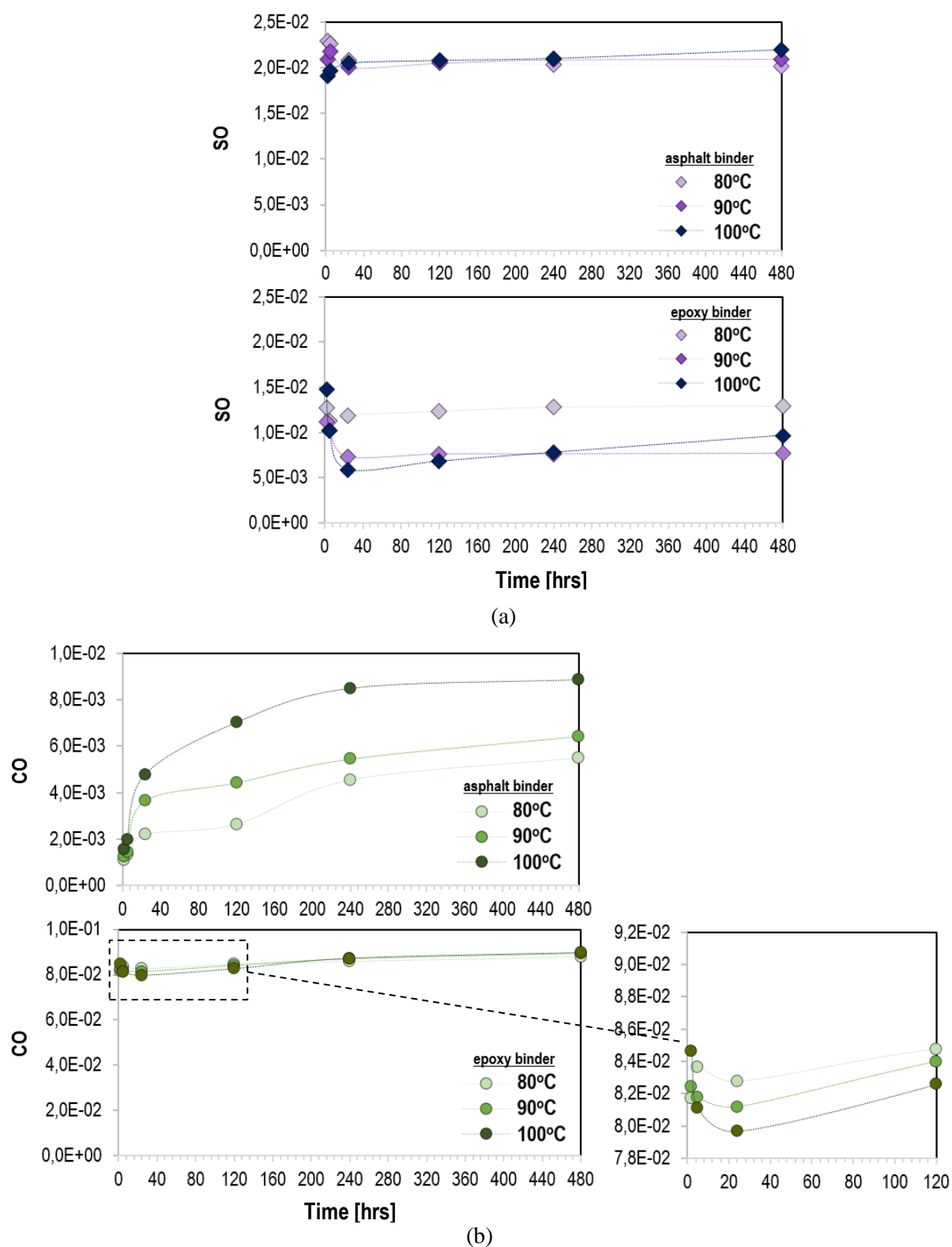
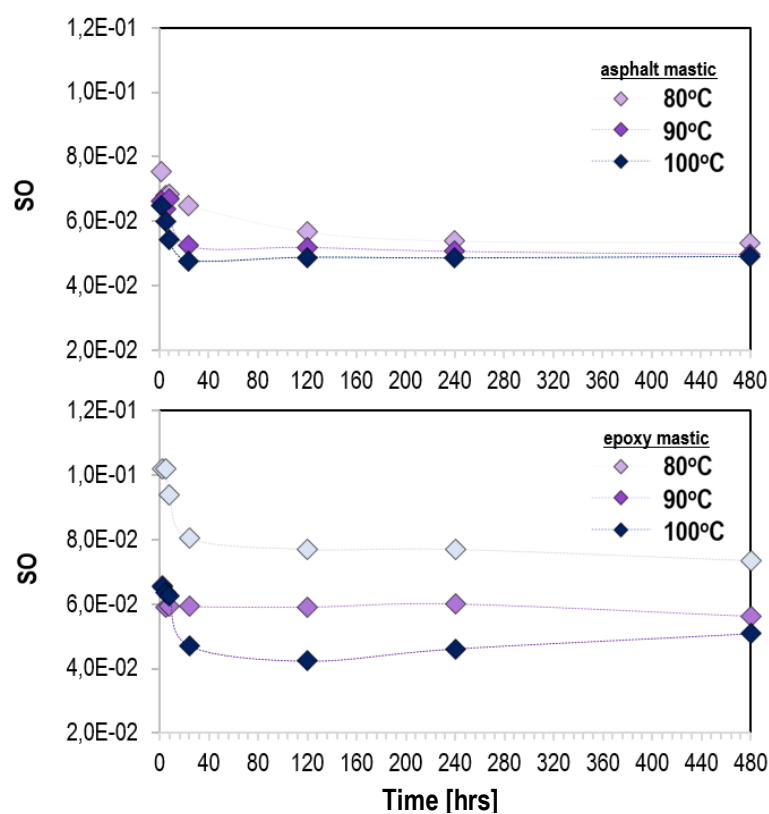
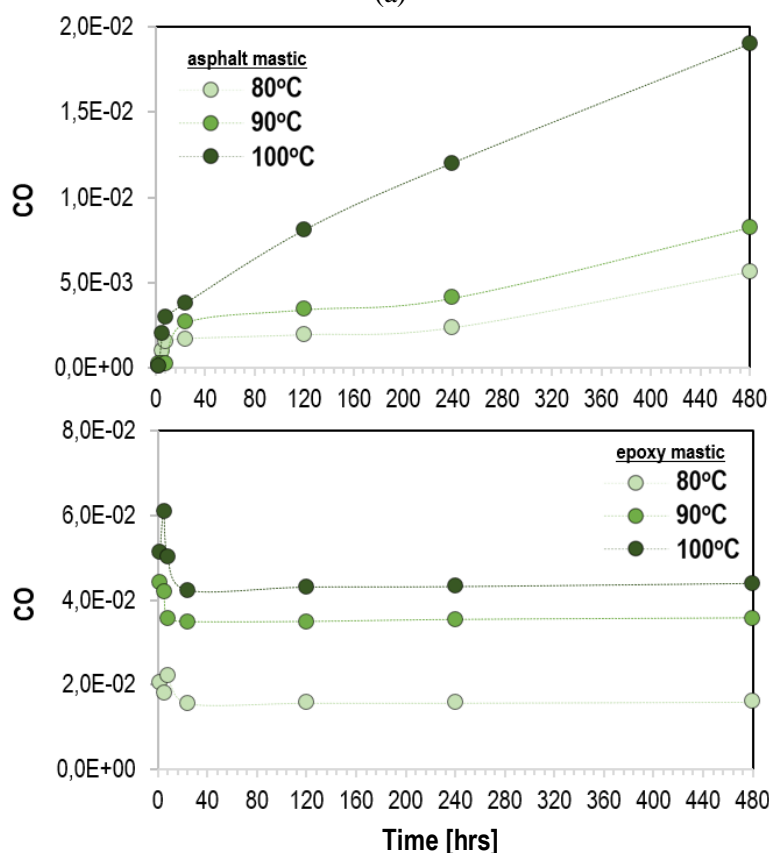


Figure 6.3 Change of (a) sulfoxide and (b) carbonyl compounds of asphalt (top) and EA_{ref} binder (bottom) over oven-conditioning at 80, 90 and 100°C.

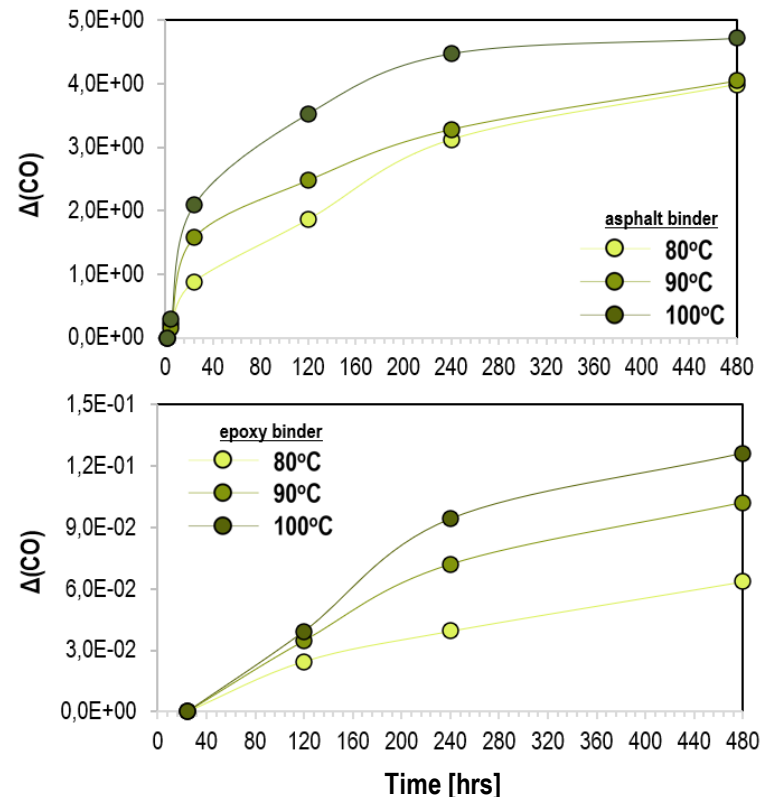


(a)

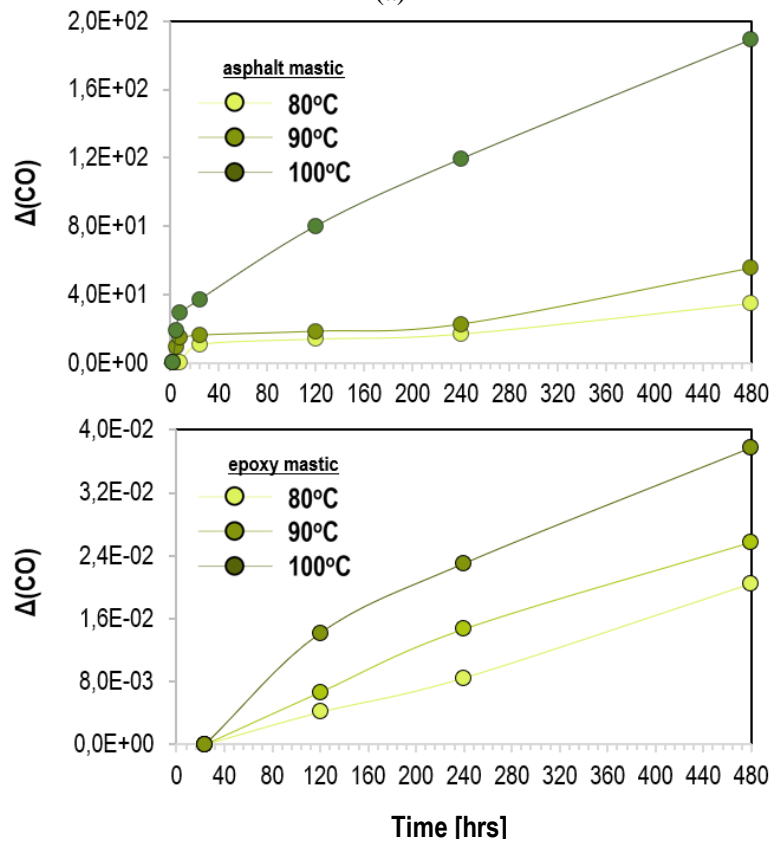


(b)

Figure 6.4 Change of (a) sulfoxide and (b) carbonyl compounds of asphalt (top) and EA_{ref} mastic (bottom) over oven-conditioning at 80, 90 and 100°C.



(a)



(b)

Figure 6.5 Incremental values of carbonyl compounds asphalt (top) and EA_{ref} binder (bottom), (a) without and (b) with filler particles, over oven-conditioning at 80, 90 and 100°C ($\Delta\text{CO}_i = (\text{CO}_i - \text{CO}_0) / \text{CO}_0$).

6.4.1 Kinetics parameters of carbonyls formation

The chemical reaction process of carbonyls formation in asphalt binder is expressed as

$$\frac{\partial x}{\partial t} = K(1 - x)^n \quad (6.6)$$

where x is the reacted carbon at different aging times, K is the reaction rate coefficient and n is the reaction order number.

In **Eq. 6.6**, it has been assumed that the chemical reaction of carbonyls formation was independent of oxygen concentration and the changes in the measured carbonyl peak area in the spectra were entirely due to oxidation. Thus, the first-order rate expression of reaction kinetics is as

$$\frac{\partial x}{\partial t} = K(1 - x) \quad (6.7)$$

and by calculating its integral, it can be written as

$$\ln(1 - x) = \ln(1 - x_0) - Kt \quad (6.8)$$

where t is the aging time and x_0 is the initial carbonyl content.

Because the conditioning temperature affects the oxidation reactions and the transformation rate of carbon species to carbonyls, these effects can be incorporated into the reaction rate coefficients by using the Arrhenius approach as

$$\ln K = \frac{E_a}{RT} + \ln K_0 \quad (6.9)$$

where E_a is the activation energy, R is the universal gas constant, T is the absolute temperature and K_0 is the reaction factor.

Based on the data generated by the incremental values of carbonyls in both binders and mastics, **Fig. 6.6** plots the relationship between $-\ln(K)$ and $1/T$. **Table 6.2** lists the E_a and K_0 values obtained from **Eq. 6.9**. From **Eq. 6.9** and **6.8**, the final form of the oxidation kinetics equation of materials becomes as

$$\ln(1 - x) = \ln(1 - x_0) - K_0 \exp\left(\frac{E_a}{RT}\right) t \quad (6.10)$$

The values of kinetics (Arrhenius) parameters (i.e., activation energy and reaction rate) were fit by utilizing the linearization of the natural log of the rate constant plotted against $1/RT$ and the curve-fitting results are demonstrated in **Fig. 6.6**. Based on the relationships given above, the Arrhenius parameters were calculated and provided in **Table 6.2**. In **Fig. 6.6**, the reaction rates of materials illustrate a reasonable fit to the Arrhenius temperature dependency in isothermal conditions. The Arrhenius plot of asphalt and epoxy binder and of respective

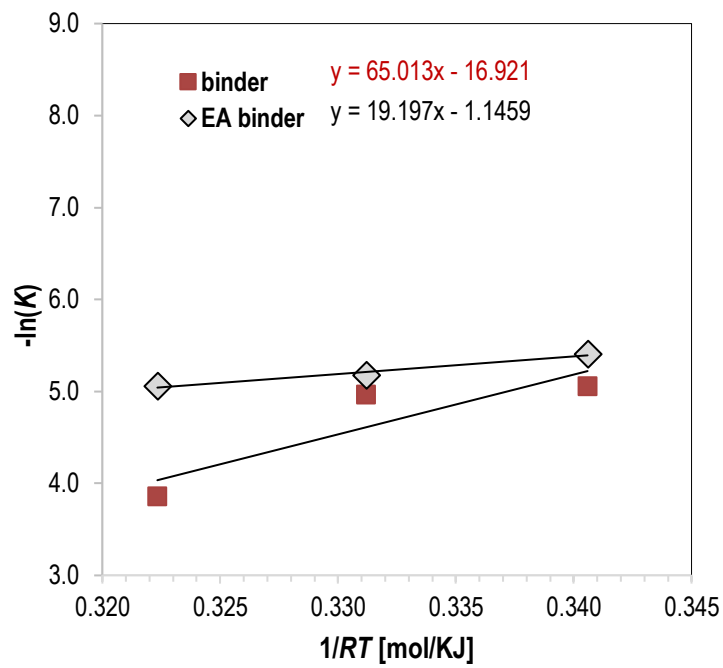
mastics are shown in **Fig. 6.6(a)** and **6.6(b)**, respectively. The datapoints provided in these graphs were the average of three replicates and the variations observed in some cases might be associated with the existence of more than one reaction steps over aging.

Data in **Table 6.2** show that the increase of epoxy proportion in asphalt binder, with and without filler, leads to a decrease of activation energy (E_a) and reaction rate (K_0) of carbonyls formation, and thus to materials of high temperature sensitivity and slow reaction rate over aging, respectively.

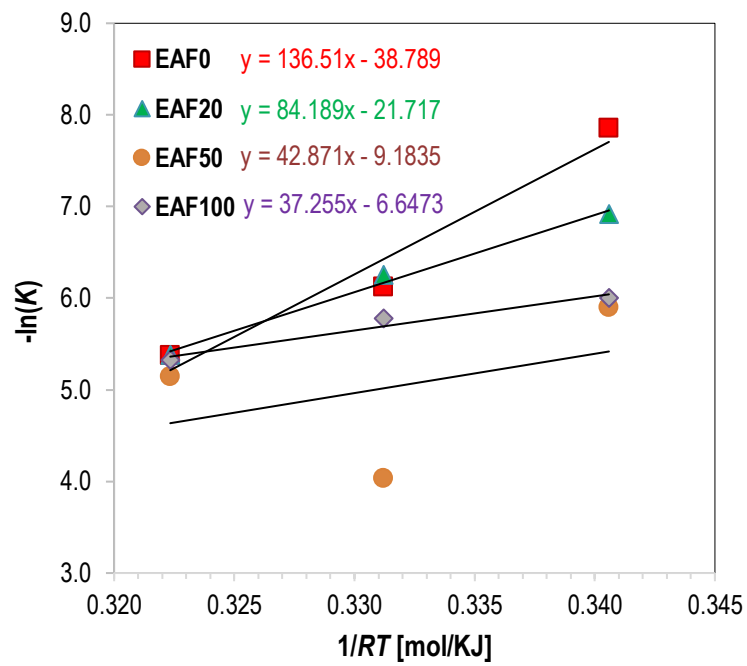
Especially, the temperature sensitivity of the formation process of carbonyls over oxidative aging is represented by the values of activation energy. The latter is the energy threshold for a reaction to occur. Hence, the lower values of the activation energy of carbonyls formation in aging EA binders correspond to systems of higher temperature sensitivity over oxidation comparing the neat asphalt binders. In other words, materials of lower E_a values mean that the oxidation reaction of carbon species takes place easier under equal conditions than of materials of higher E_a values. Furthermore, the proportional increase of epoxy part in asphalt led to lower the oxidation reaction rates and thus carbonyls of lower reactivity, indicating the generation of materials with slow reacting carbon species, or materials of enhanced aging resistance.

An increase of activation energy of carbonyls formations in both asphalt and epoxy binders was noticed as well with the addition of fillers, as given in **Table 6.2**. Specifically, an increase of the energy levels to initiate the formation of carbonyls in asphalt and epoxy-asphalt binders is indicated with the addition of filler at any given temperature. These phenomena can be confirmed by previous studies on the topic of oxidative aging in asphalt. The impact of fillers, such as the hydrated lime, demonstrated a reduction in the oxidation rate and subsequently improvement on the aging resistance (Petersen et al., 1974; Plancher et al., 1976; Petersen et al., 1987; Elder et al. 1985; Johansson et al., 1995 & 1996; Lesueur & Little 1999; Huang et al. 2002; Little & Petersen 2005; Huang & Zeng 2007; Lesueur et al., 2013 & 2016; Moraes & Bahia 2015a & 2015b).

Overall, lower activation energies and reaction rates of carbonyls formation are exhibited on binders of higher epoxy proportions in asphalt including filler particles. The present observations confirm that the incorporation of polymer modifiers, such as styrene-butadiene-styrene (Jin et al., 2011; Liu et al., 2019), leads to the generation of binders of reduced oxidation reaction rates. In the future, the oxidation kinetics parameters could be used to provide reliable predictions on the oxidative aging rates of pavement materials at road conditions without performing expensive long-term oxidation tests in the laboratory.



(a)



(b)

Figure 6.6 $-\ln(K)$ versus $1/RT$ through oven-conditioning for the studied (a) binders and (b) mastics.

Table 6.2 Kinetic parameters of studied materials.

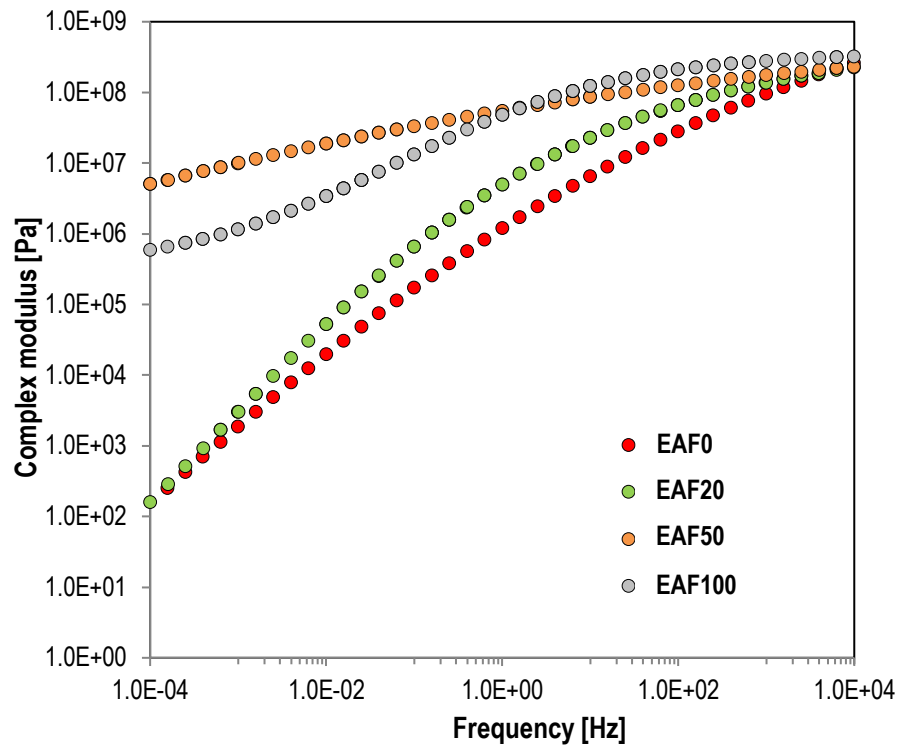
Percentage of EA	K_0 [1/hrs]	E_a [kJ/mol]
EA0	2.23E+07	65.01
EA100	3.15E+00	19.20
EA0	7.01E+16	136.51
EA020	2.70E+09	84.19
EA050	9.74E+03	42.87
EA0100	7.71E+02	37.26

6.5 Rheological Changes

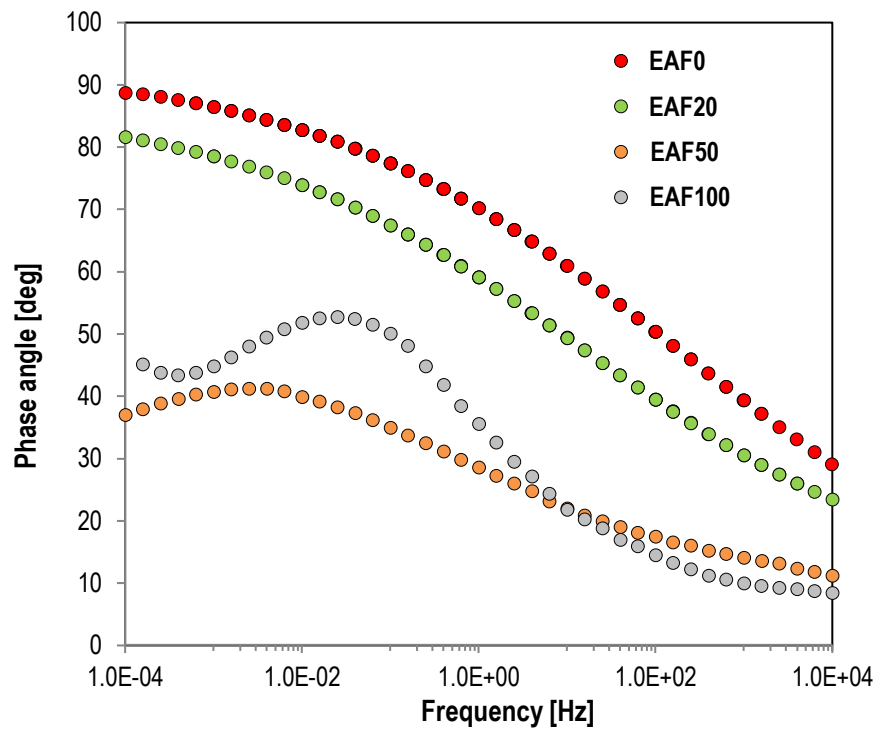
Fig. 6.7 shows the master curves of complex modulus and phase angle of oven-conditioned samples (i.e., EAF0, EAF20, EAF50 and EAF100) after 480 hrs at 100°C. These materials are already fully cured. EAF20 and EAF50 have shown higher values of stiffness modulus over the analyzing frequency range than the unmodified mastic, or EAF0, indicating the generation of stiffer materials by substituting asphalt binder with epoxy. The EA binder with filler, or EAF100, is a material of high modulus, higher than of EAF0 and EAF20, indicating that the latter has shown the stiffer material among all studied mastics (i.e., all modification levels).

Another observation from the **Fig. 6.7** is that EAF100 mastic has shown a low frequency dependency of stiffness modulus over the studied frequency range implying that this material is more elastic than the unmodified one. With the proportional substitution of asphalt binder with epoxy, epoxy mastics have been produced of similar frequency dependency as of EAF100, and particularly EAF50 has demonstrated this elastic behaviour. EAF20 is shown a similar shape of complex modulus and of phase angle as of EAF0, leading to the conclusion that the role of asphalt binder in mastic is more dominant in EAF20. The S-shape of phase angle of both EAF50 and EAF100 illustrates the presence of a strongly crosslinked polymeric network and the rubbery characteristics of these materials at the whole frequency range. Similar response is observed in polymer modified asphalt binders (Lu & Isacsson 1998; Airey 2003; Airey et al., 2008).

Fig. 6.8 shows the master curves of complex modulus (part (i) of **Fig. 6.8**) and phase angle (part (ii) of **Fig. 6.8**) of EAF20, EAF50 and EAF100 after different time periods of oven-aging at 100°C. The influence of aging on the viscoelasticity of epoxy mastics is apparent in **Fig. 6.8**. The complex modulus increases rapidly with the oven-conditioning time. In the case of EAF50 and EAF100, the phase angle at low frequencies is dropped dramatically from 2 to 5 hrs of oven-conditioning at 100°C and generating the S-shape phase angle which indicates the strongly crosslinked network in asphalt.

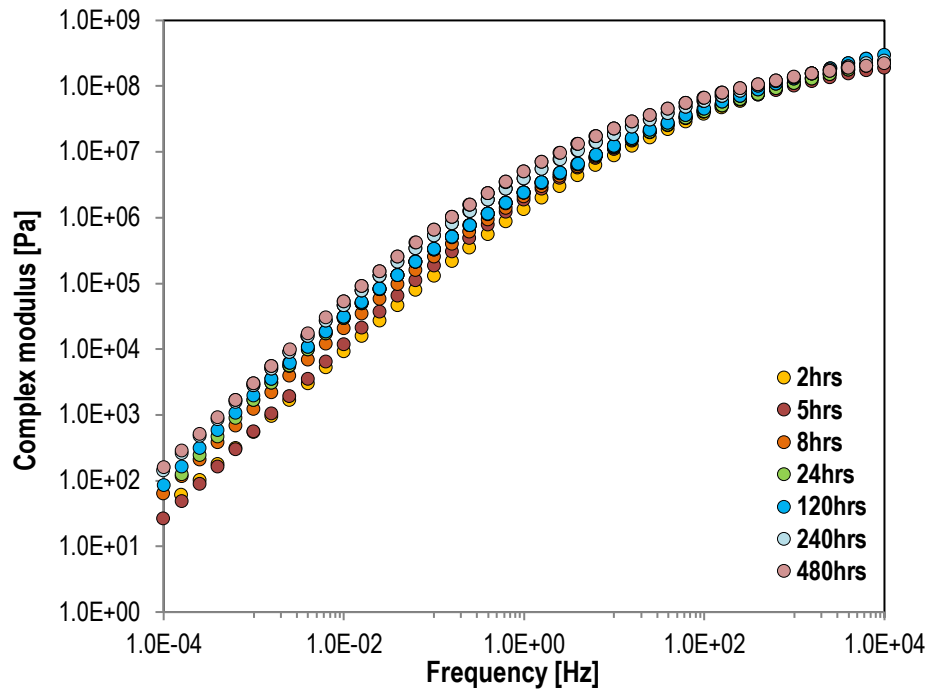


(a)

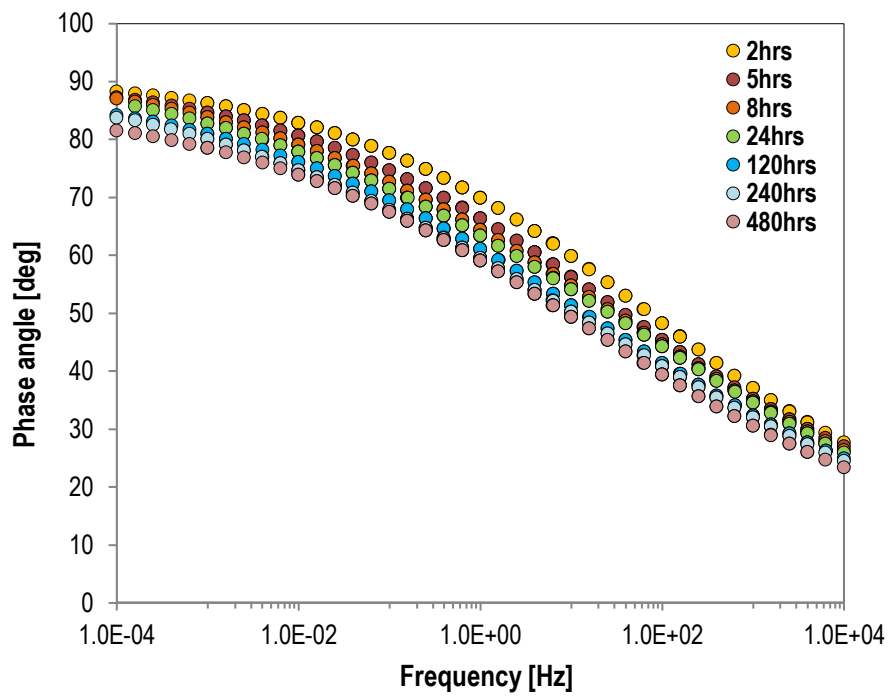


(b)

Figure 6.7 Master curves of (a) complex modulus and (b) phase angle of studied materials after oven-conditioning for 480 hrs at 100°C .

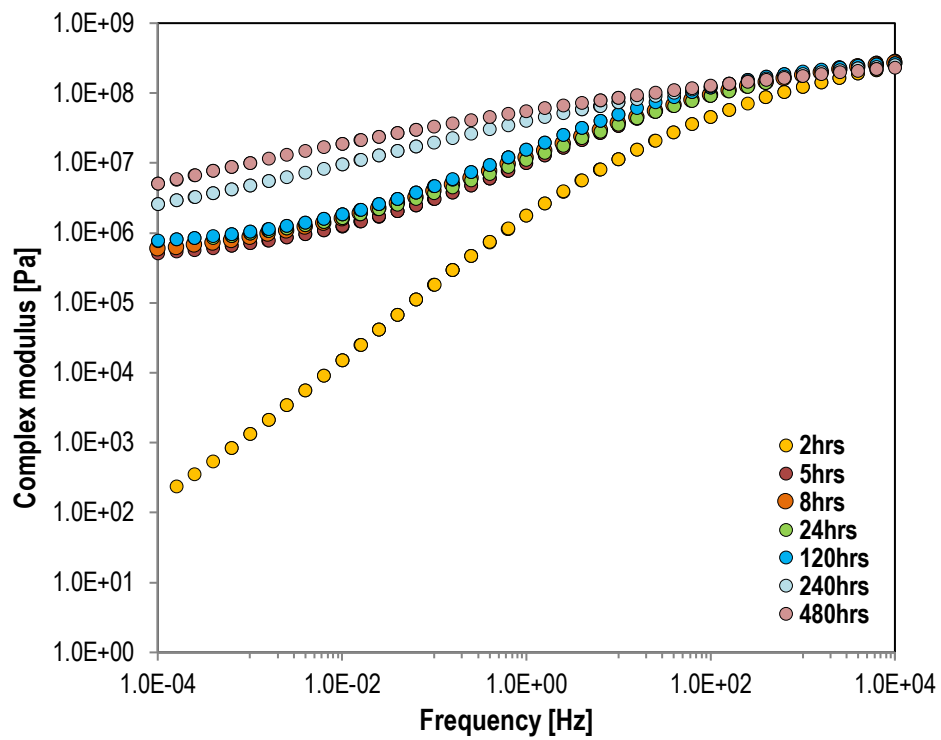


(i)

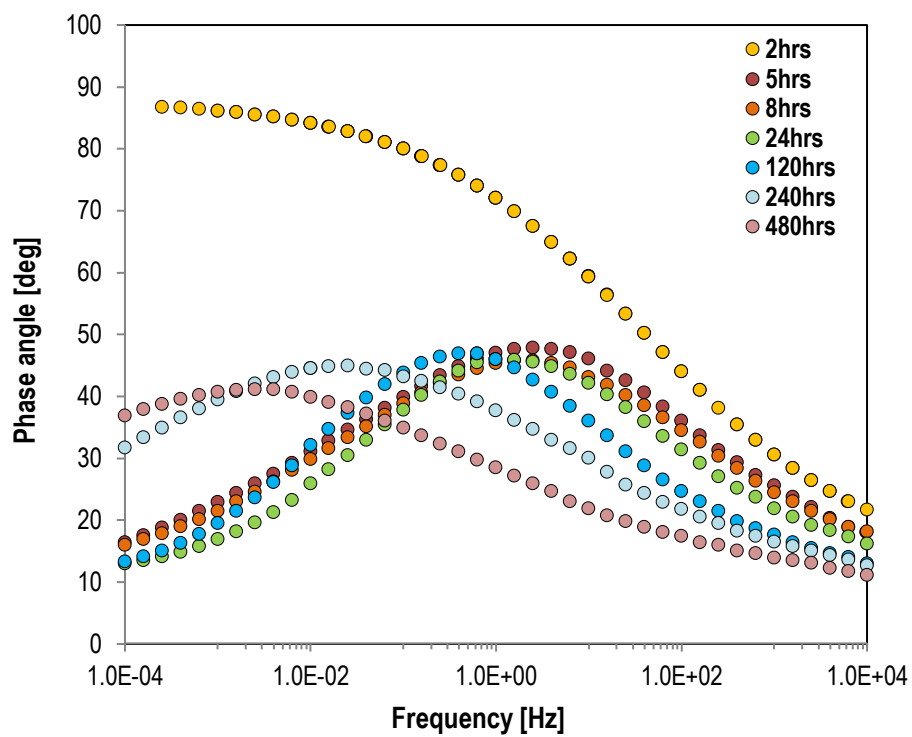


(ii)

(a)

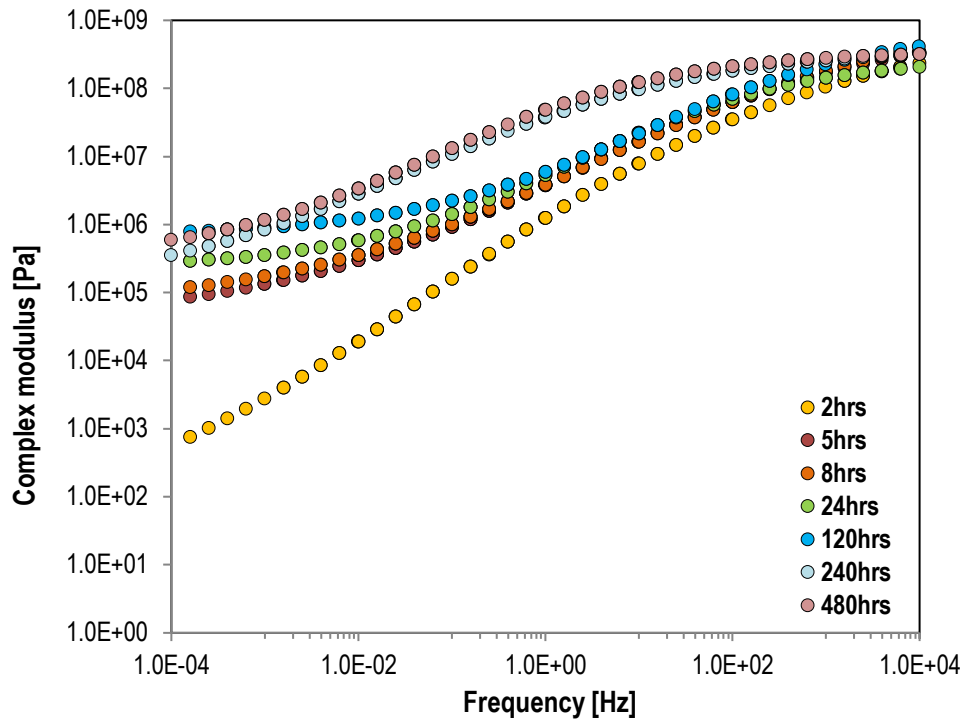


(i)

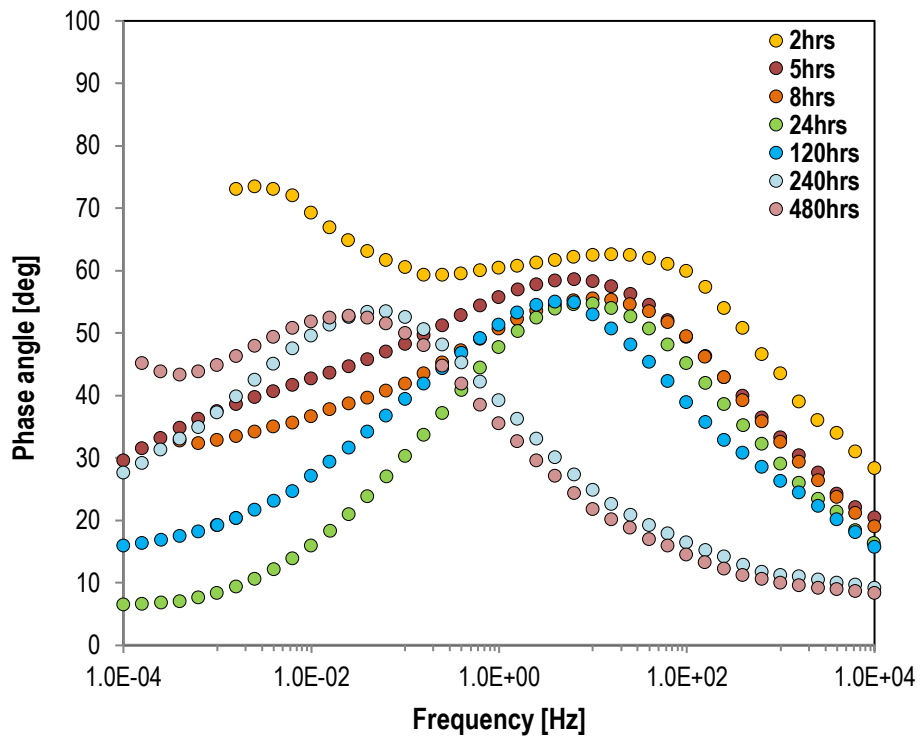


(ii)

(b)



(i)



(ii)

(c)

Figure 6.8 Master curves of (i) complex modulus and (ii) phase angle of (a) EAF20, (b) EAF50, and (c) EAF100 during oven-conditioning for different times.

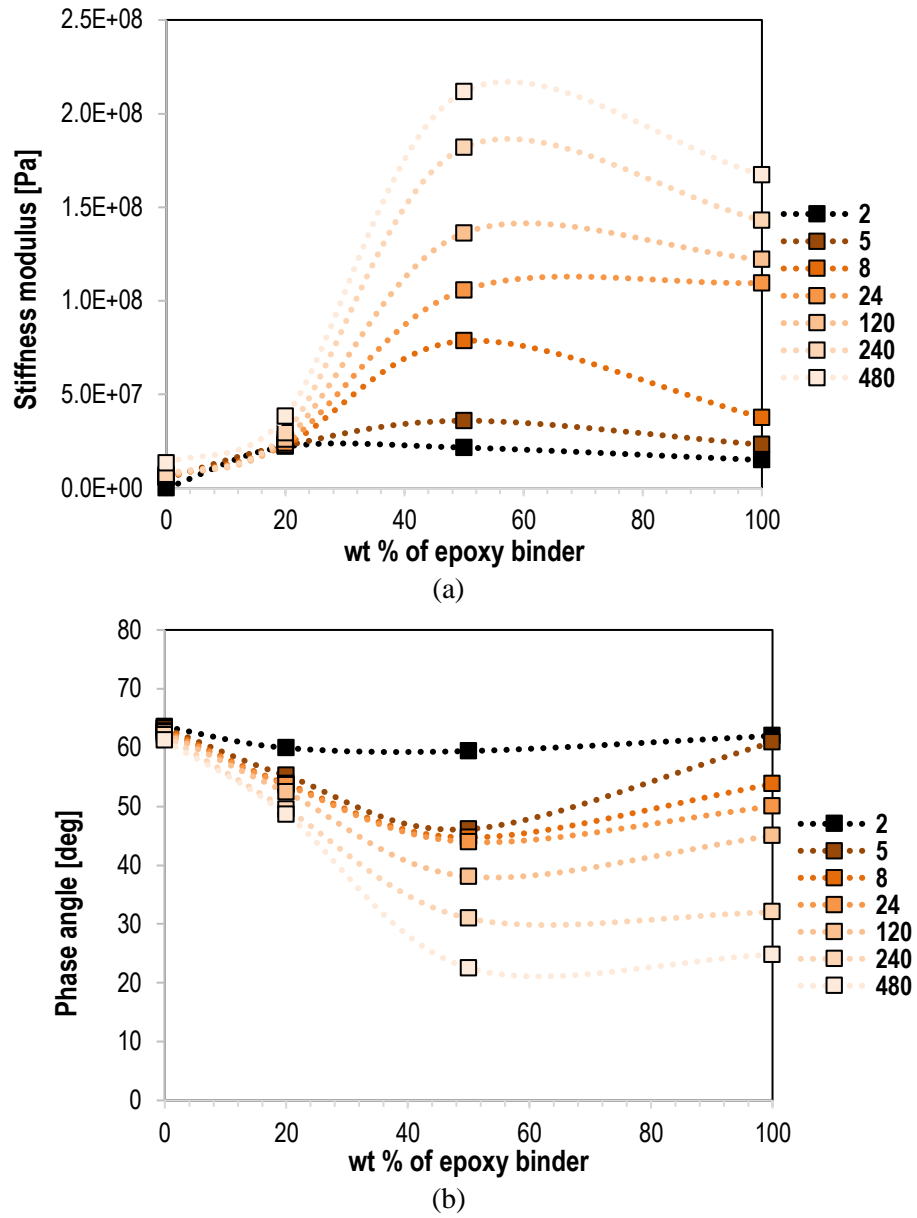


Figure 6.9 Composition dependence of (a) stiffness modulus and (b) phase angle at 10 Hz of epoxy asphalt mastics over oven-conditioning at 100°C (EAF0: 0 wt% and EAF100: 100 wt%).

Due to oven-aging, the phase angle over the whole frequency range tends to decrease. The elastic crosslinked network which offers the rubbery characteristics to the system becomes less effective and this region disappears. The decrease of phase angle together with the increase of stiffness modulus, which becomes considerably frequency-independent at all temperatures (frequencies), shows the development of a rubbery system of high modulus and elasticity at a very broad temperature range. With increasing oven-age time periods, the phase angle decreases and thus epoxy mastics with 50 and 100% of EA binder in them becomes more elastic. EAF20 demonstrates a stiffening process similar to an unmodified material without indicating any epoxy polymeric network in it, unlike EBF50 (see **Fig. 6.8(b)**). This suggests that the role of epoxy in EAF20 is not dominant.

Finally, the stiffness modulus and phase angle of oxidized mastics as function of epoxy proportion in asphalt were studied as well to elucidate the influence of epoxy on the oxidation extent and stiffening of asphalt. Stiffness modulus and phase angle values of mastics (i.e., EAF0, EAF20, EAF50 and EAF100) after different oven-aging time periods are provided in relation to the epoxy (% wt) in asphalt in **Fig. 6.9**. From the data provided on stiffness evolution of the mastics, the stiffness increases, and phase angle decrease appears related to the amount of epoxy in asphalt (EAF0: 0 % wt and EAF100: 100 % wt). This phenomenon is more apparent at high epoxy proportions in asphalt. The stiffness modulus increase and phase angle decrease with the increase of aging time lengths is more obvious in EAF50 and EAF100 after 24 hrs of aging. A remarkable change of these viscoelastic properties was observed as well between EAF20 and EAF50 indicating the existence of a threshold where the epoxy becomes the dominant phase in the material. The fact that the stiffness modulus of EAF50 was higher than of EAF100 may be related with the miscibility and the phase behavior of these materials, as discussed in the next sub-section.

6.6 Glass Transition Changes

The composition dependence of T_g and ΔC_p are plotted in **Fig. 6.10** for the epoxy-asphalt blends over the entire composition range. The T_g values of individual epoxy and asphalt binder are -22 and -20°C (see the top of **Fig. 6.10**). A positive deviation of the measured T_g from the predicted one (T_g^{eq}) based on the ideal mixing rule is also apparent in fresh blends. The black dash-line at the top of **Fig. 6.10** illustrates the profile predicted by the ideal mixing rule (see **Eq. 6.2**). This plot indicates the strong interactions in blends. Further, the ΔC_p values (lowerhand picture) of fresh blends shifts to negative deviations, as shown at the bottom of **Fig. 6.10**, with the ΔC_p values to yield to 0.35 and 0.37 J/(g °C) for the epoxy (EA100) and asphalt binder (EA0), respectively. The ΔC_p is the increment of heat capacity at glass transition. Although the two components are quite different in terms of chemistry, they showed comparable T_g and ΔC_p values.

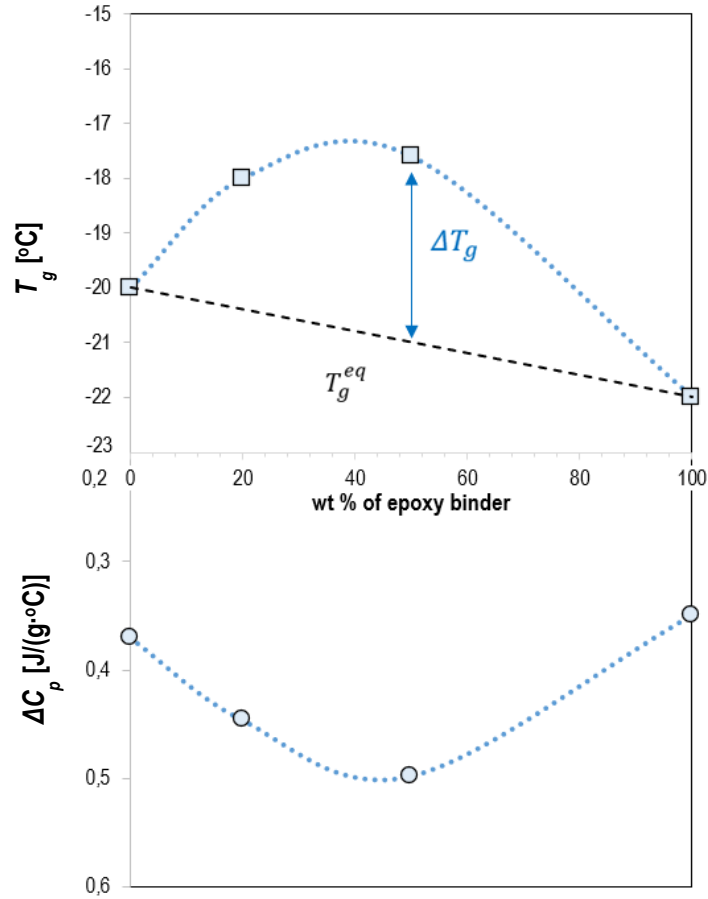
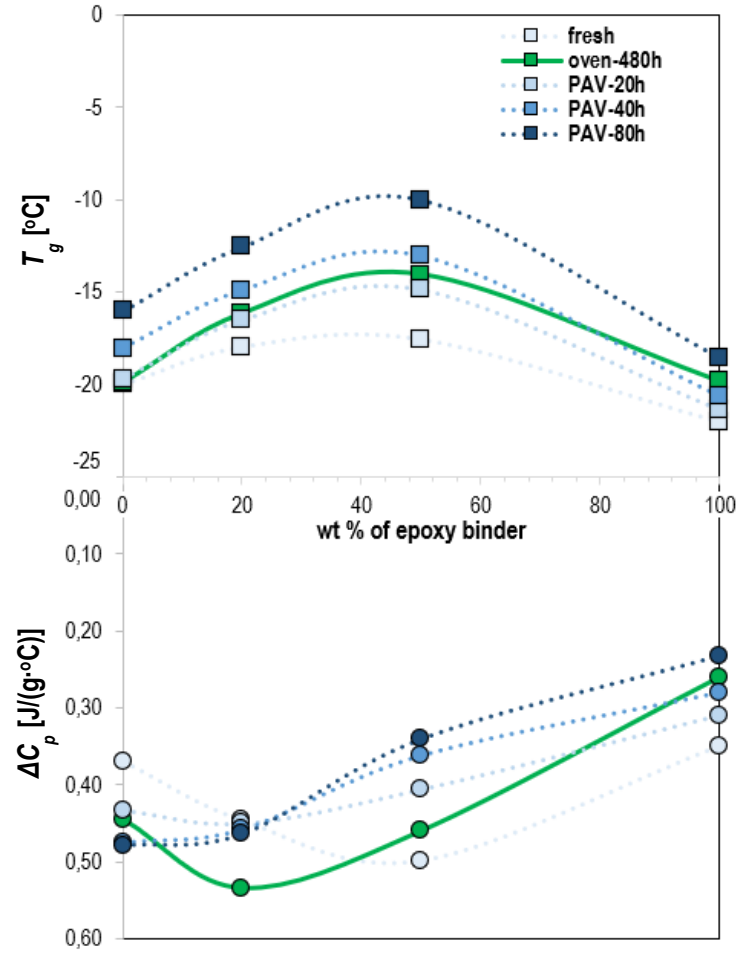
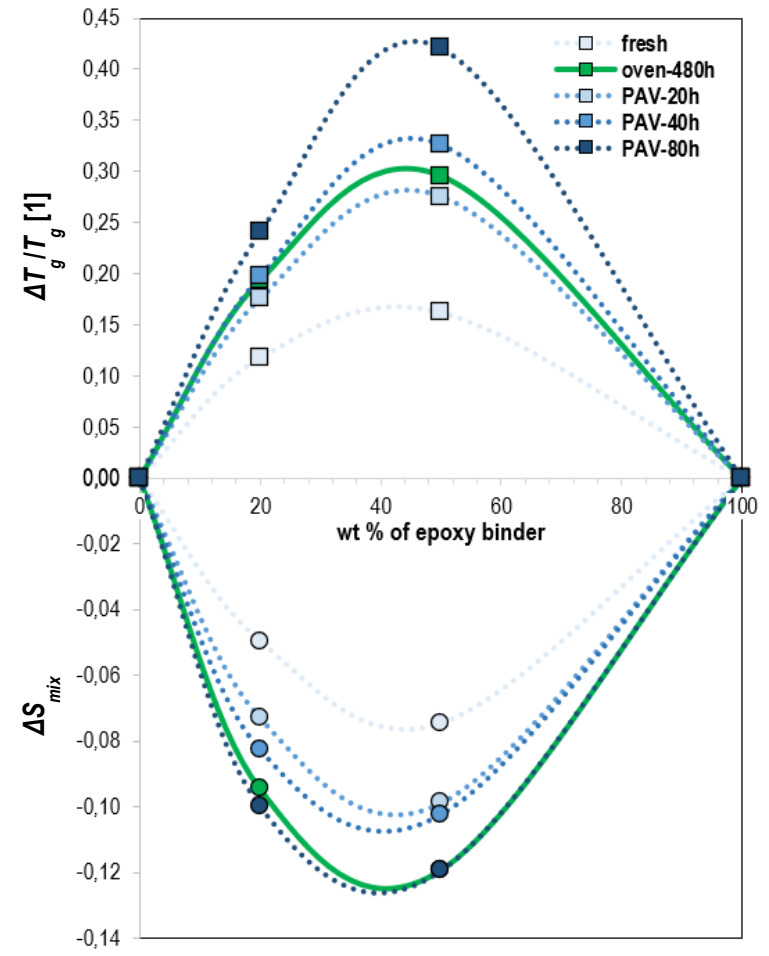


Figure 6.10 Composition dependence of the T_g (top) and ΔC_p (bottom) of fresh epoxy-asphalt blends.

Fig. 6.11a demonstrates the composition dependences of T_g (top) and ΔC_p (bottom) of blends after different aging time lengths, where a positive T_g deviation was observed after PAV and 480 hrs of oven-conditioning (see **Fig. 6.11a**, top). Regarding the heat capacity increment at glass transition over aging, the ΔC_p values show an increasing trend for the pure asphalt binder, EA0, (fresh: 0.37, oven-480h: 0.46, PAV-20h: 0.43, PAV-40h: 0.48, PAV-80h: 0.48 [J/(g °C)]) and lowering of the ΔC_p values for the epoxy binder, EA100 (fresh: 0.35, oven-480h: 0.26, PAV-20h: 0.31, PAV-40h: 0.28, PAV-80h: 0.23 [J/(g °C)]).



(a)



(b)

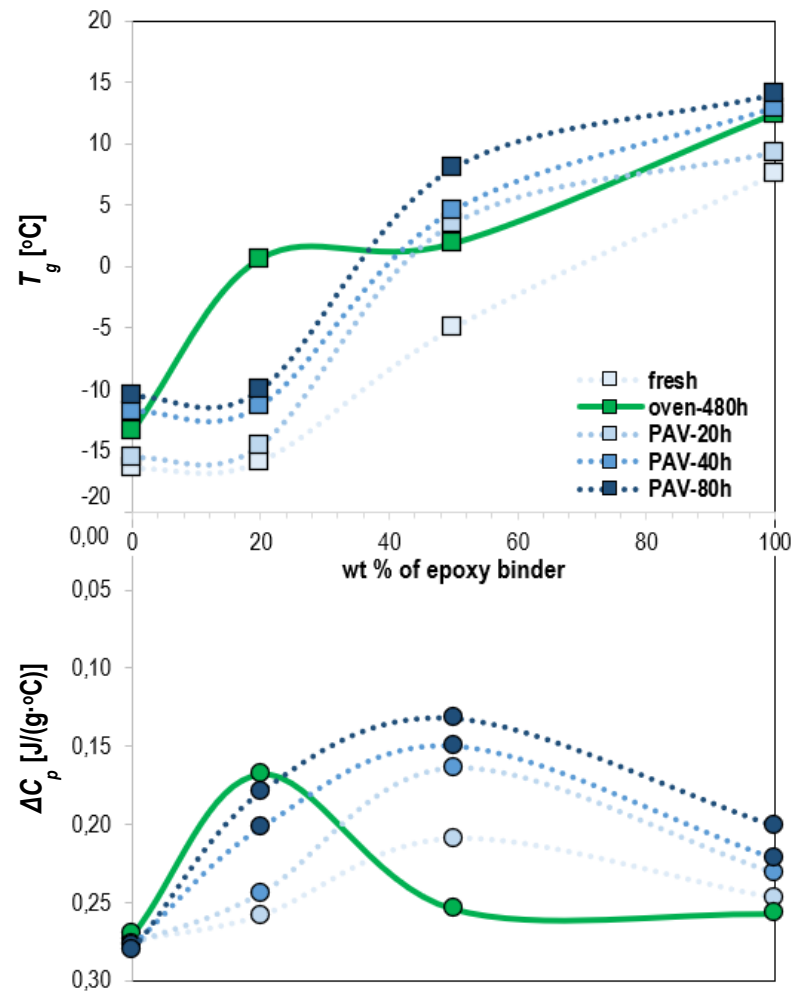
Figure 6.11 Composition and oxidative aging dependence of (a) the T_g (top) and ΔC_p (bottom), and (b) the relative T_g difference, $\Delta T_g/T_g$, (top) and the entropy of mixing contribution (bottom) of blends over different age conditions.

Moreover, the thermal behavior of blend with 20% of epoxy (EA20) demonstrates a slight increase as of asphalt binder (EA0), in comparison with the blend with 50% of epoxy (EA50) which shows a decreasing trend of ΔC_p similar to the epoxy binder (see at the bottom of **Fig. 6.11a**). The shape of the composition relationship of ΔC_p is quite different between the oven and PAV aged blends indicating the impact of the different aging schemes, and particularly of the pressure, on the oxidation mechanism of these materials.

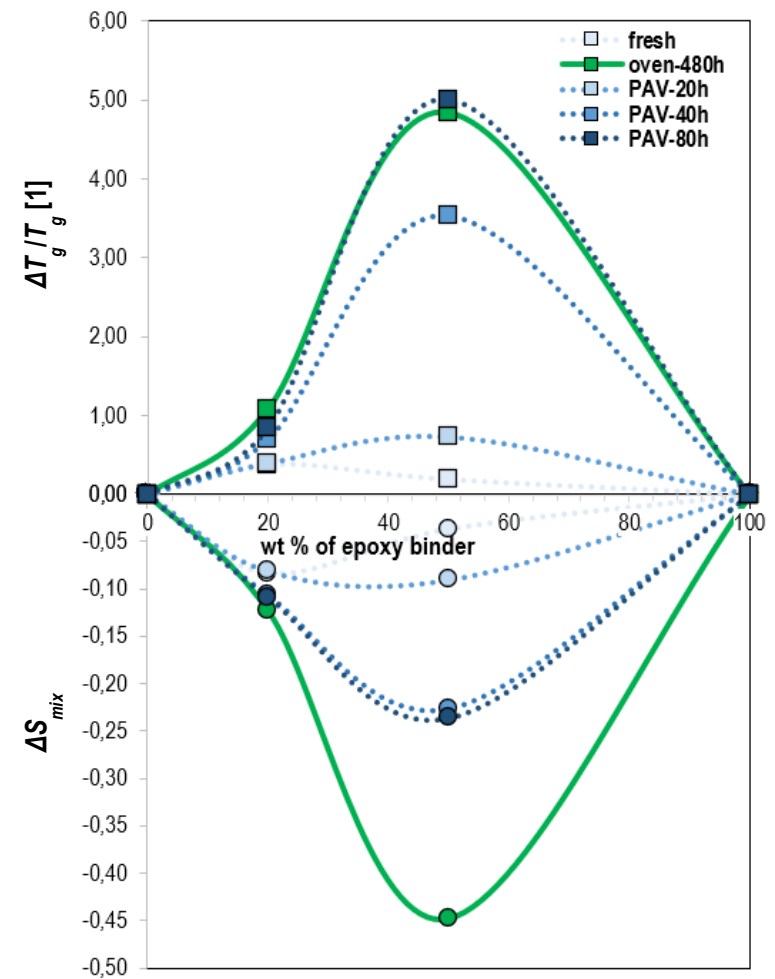
As mentioned previously, oxidative aging in asphalt binders is caused by the chemical reactions between specific asphalt species and oxygen (Branthaver et al., 1993; Petersen & Harnsberger 1998), and, apart from the material stiffening, is accompanied by embrittlement (Hesp et al., 2009). The oxidative aging in epoxy-asphalt blends leads to increase of the T_g of blends, a behavior which corresponds to the increase of intermolecular interactions, and the formation of glassy systems. The T_g values of amorphous mixes are generally interpreted in terms of the intermolecular interactions (Lesikar 1976; Kwei 1984; Painter et al., 1991), with the higher measured T_g values than those predicted by the ideal mixing rule to correspond to systems with strongly interacting components. The ΔT_g values, or the T_g difference between the measured values and those predicted by the GT equation (**Eq. 6.2**), are used to quantify the intermolecular strength developed due to the oxidation over the whole composition range (see **Fig. 6.11b**) and to provide an indication of brittleness.

The relative shift of T_g ($\Delta T_g/T_g$) for the blends over oxidative aging is shown in **Fig. 6.11b**, where ΔT_g is the T_g difference between the measured and predicted T_g values in terms of the ideal mixing rule (T_g^{eq}) (**Eq. 6.2**). Positive T_g deviation is shown in **Fig. 6.11b** with the values of $\Delta T_g/T_g$ to become continuously larger indicating stronger intermolecular interactions between the individual components (i.e., epoxy and asphalt binder). The highest values of $\Delta T_g/T_g$ were obtained after 80 hrs of PAV-aging, yielding 0.24 and 0.42 for the EA20 and EA50 blends. Similar values of $\Delta T_g/T_g$ as of the PAV-20h aged blends (0.18 and 0.28 for EA20 and EA50, respectively) were determined after 480 hrs of oven-conditioning at 100°C (0.19 and 0.29 for EA20 and EA50, respectively).

As mentioned, the miscibility of components or the phase stability of a system is guided by ΔG_{mix} with comprises ΔH_{mix} and ΔS_{mix} . When the ΔG_{mix} of a system is negative ($\Delta G_{mix} < 0$), miscibility is favored. The system tends to be phase-separated when the ΔG_{mix} is positive ($\Delta G_{mix} > 0$), implying a repulsion between the components of the system. To estimate the ΔG_{mix} values, the ΔH_{mix} has been typically perceived as the dominant quantity to enable predictions of miscibility. Positive and negative ΔH_{mix} indicates immiscible and miscible systems, respectively. The appearance of deviation in T_g values from the predicted by the ideal mixing rule is a consequence of the balance of ΔH_{mix} and ΔS_{mix} . However, when the ΔH_{mix} is shallow, as in apolar blends, the contribution of ΔS_{mix} can be considered equally important as a thermodynamic quantity in phase stability.



(a)



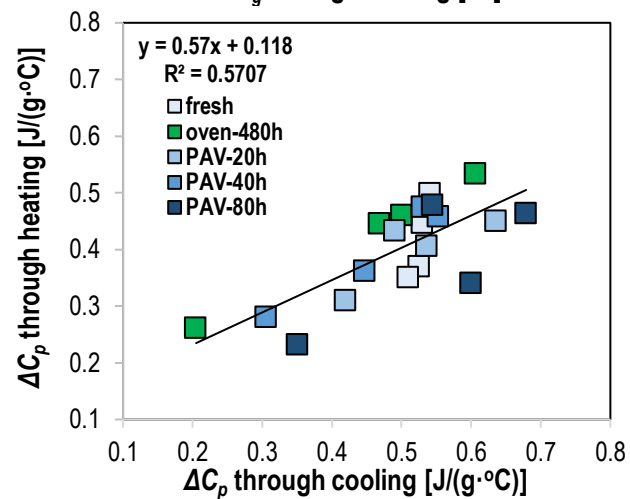
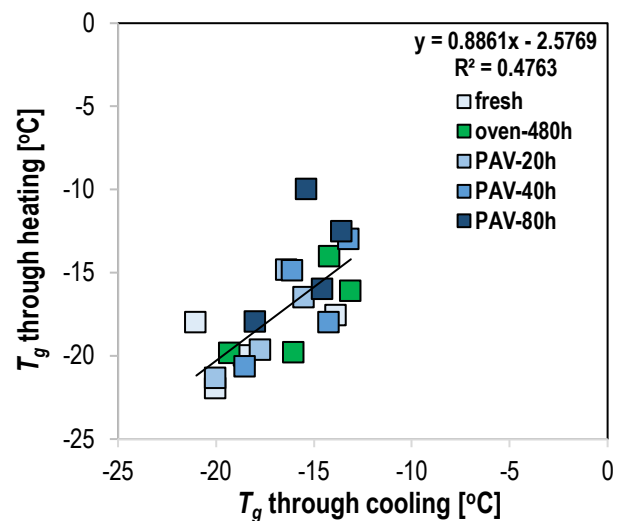
(b)

Figure 6.12 Composition and oxidative aging dependence of : (a) the T_g (top) and ΔC_p (bottom), and (b) the relative T_g difference, $\Delta T_g/T_g$, (top) and the entropy of mixing contribution (bottom) of blends with filler over different age conditions.

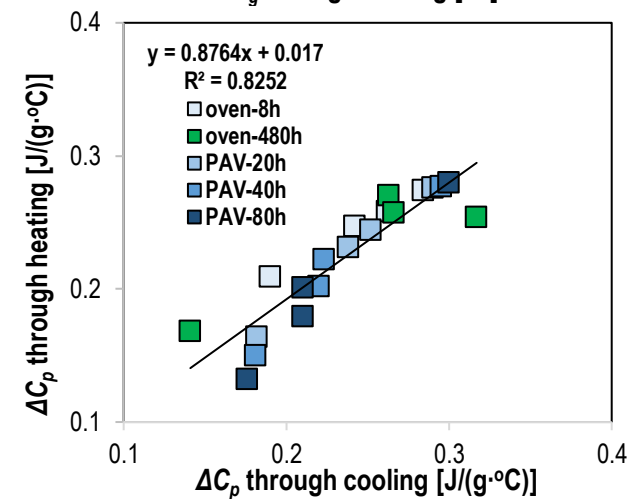
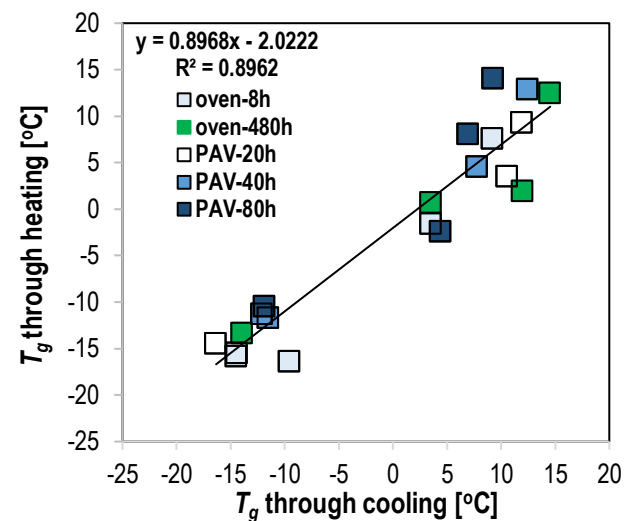
In this study, the accessible part of ΔS_{mix} was predicted based on **Eq. 6.5**. At the bottom of **Fig. 6.11b**, the colored circles represent the contribution of the configurational entropy of mixing (ΔS_{mix}^c). The ΔS_{mix}^c decreases with the increase of oxidative aging time. The age conditioning in the oven for 480 hrs (-0.09 and -0.12 [J/(mol °C)] for EA20 and EA50, respectively) could result in an equivalent embrittlement with the PAV for 80 hrs (-0.10 and -0.12 [J/(mol °C)] for EA20 and EA50, respectively). The shift to higher T_g deviations (shifting of T_g from the predicted values) indicates the decrease of ΔS_{mix}^c and consequently manifests the potential further increase of repulsive forces between components. Over aging, the reduction of ΔS_{mix}^c of blends give rise to a positive ΔG_{mix} attributing towards more thermodynamically unstable systems. The aging blends tend to break up spontaneously into two phases, mainly due to the increase of the molecular weight of individual components. Along these lines, this behavior illustrates the continuous enhancement of the repulsive internal forces in the already phase-separated blends and the irreversible transition to more brittle systems (see **Fig. 6.11b**).

Furthermore, the inclusion of fillers in asphalt binders might affect the rate of oxidation leading to materials of improved resistance against aging. The results of this study showed that the increase of epoxy proportion in asphalt led to decrease of activation energy and reaction rate of the formation of carbonyls, and thus more oxygen resistant materials were developed. The low values of activation energy of epoxy asphalt correspond to more temperature sensitive materials comparing the unmodified one. Moreover, the impact of filler on the oxidation kinetics was evaluated on these materials revealing a significant reduction of oxidation sensitivity with the addition of filler in both epoxy and asphalt binder. This phenomenon has been observed elsewhere as well when hydrated lime or limestone fillers were used believing that the oxygen diffusion in mastic and the binder-mineral sorption play the most important role during the material oxidation.

In this study, the oxidation effect on the glass transition of epoxy-asphalt mastics is investigated as well, and the change of T_g values induced by the fillers' addition in blends are shown in **Fig. 6.12a**. Particularly, a totally different relationship of T_g with the composition in mastics is depicted in **Fig. 6.12a** in comparison to the behavior plotted in **Fig. 6.10** and **6.11**. The S-shape increase of T_g values of mastics over increasing the aging time length in PAV is illustrated at the top of **Fig. 6.12a**. The unaged epoxy (EAF100) and asphalt mastics (EAF0) yield T_g values of 7.54 and -16.43°C, respectively, and those values to increase to 14 and -10.5 after 80 hrs of PAV-aging. At the bottom of **Fig. 6.12a**, the ΔC_p values of the individual components are measured for the unaged and aged (PAV-80h) epoxy (0.25 and 0.20 [J/(g °C)]) and asphalt mastics (0.27 and 0.28 [J/(g °C)]). The composition dependence on the stiffness modulus of blends with filler has been shown a similar shape, as shown in the previous sub-section. At higher proportions of epoxy in asphalt mastic, the modulus increases with increased oxidative aging time lengths, following a similar trend of composition dependence of T_g values. It is believed that the addition of apolar filler particles could toughen the blends, formulating strongly cross-linked mastics.



(a)



(b)

Figure 6.13 The relationship of the T_g [°C] values (top) through heating and cooling and the respective ΔC_p values [J/(g·°C)] (bottom) of (a) blends and (b) blends with filler.

In addition, as seen in blends, shifting the T_g values of mastics to higher values is observed in **Fig. 6.12a** corresponding to the positive T_g deviation in mastics from the ideal mixing rule (see **Fig. 6.12b**). Since the mastics have shown the S-shape of composition dependence with T_g , the Kwei equation has been used to predict the T_g values and to make the calculations from the ideal mixing mode (Gordon & Taylor 1952). The $\Delta T_g/T_g$ values are plotted in **Fig. 6.12b** depicting higher values with the increase of aging time lengths for the mastics (EAF20 and EAF50), a similar trend as of the same materials without filler (EA20 and EA50). At the bottom of the same figure, the colored circles also illustrate the change of entropy of mixing. As expected, the continuous decrease of ΔS_{mix}^c to negative values relates to the increase of the positive T_g deviation from the predicted T_g values, and ΔG_{mix} . The further decrease of negative ΔS_{mix}^c values imply the rise of repulsive forces between apolar fillers and blend, and the further separation of two components. Although the mastic systems were designed with adding limestone fillers, large values of $\Delta T_g/T_g$ and subsequently ΔS_{mix}^c were shown. The reduction of ΔS_{mix}^c causes large positive deviations of T_g in the systems with the rise in oxidative aging time lengths. The oven conditioning for 480 hrs at 100°C also resulted in mastics of dramatically smaller entropy values, particularly for EAF50, than those after 80 hrs in the PAV unit.

The changes in glass transition from the heating and cooling TM-DSC measurements in blends and mastics are studied here. The T_g and ΔC_p values through heating are correlated with those obtained through calorimetric cooling scans to indicate the impact of thermal history. Especially, slightly higher T_g values of blends with (i.e., EAF0, EAF20, EAF50 and EAF100) and without (i.e., EA0, EA20, EA50, EA100) filler are obtained through cooling than of heating for the different oven and PAV conditioning periods at 100°C, as shown at the top in **Fig. 6.13a** and **6.13b**. At the bottom of the figures, the ΔC_p values of studied materials obtained through cooling scans are provided in relation to the same values obtained through heating TM-DSC. The enthalpic values measured through heating agree with those values measured through cooling in binders with filler indicating that the mastics (R^2 is 0.8962 and 0.8252 for the T_g and ΔC_p , respectively) are less sensitive to the thermal history than the binders (R^2 is 0.4763 and 0.5707 for the T_g and ΔC_p , respectively).

Overall, the blends formulated by the epoxy and asphalt binder have shown higher T_g values than either of the T_g values of individual components, with the increase of T_g deviation from the ideal mixing rule and with the increase of oxidative aging time periods. This attempt to evaluate the relationship of T_g with the composition and in terms of oxidative aging could assist in the effort to establish a reliable characterization methodology to assess the brittleness of polymer-asphalt binders. Nevertheless, the usefulness of this method is not limited the brittleness studies but also can be utilized to determine the thermal behavior of various multiphasic systems.

6.7 Summary

To provide insight into the compositional changes due to oxidative aging of epoxy-asphalt, the FTIR spectroscopy was used, and the oxidation products were tracked at different temperatures over time. DSR studies have been performed as well to assess the oxidation-induced stiffening of studied mastics. Finally, these materials are expected to be more glassy and thus brittle after

aging, and thus more prone to thermal-induced cracking. Thus, the effect of oxidative aging on T_g was studied, and the deviation of T_g values from the ideal mixing rule was assessed to evaluate the glass forming tendency. The key findings of this **chapter** are as follows:

- When epoxy-asphalt is oxidized isothermally, the carbonyls and sulfoxides undergo a period of rapid decrease, which indicates the epoxy curing in asphalt binder. A time period of constant increase rate of these compounds was observed after curing, manifesting the oxidative aging. The incremental values of carbonyls of epoxy-asphalt materials were calculated through oxidative aging to estimate the oxidation kinetics parameters.
- The oxidation of carbon species of epoxy-asphalt materials was compositional dependent. Lower values of activation energy accompany in lower values of reaction rate were exhibited on mastics of high epoxy proportions in asphalt binder, with and without filler. The proportional increase of epoxy part in asphalt led to lower the oxidation reaction rates and thus carbonyls of lower reactivity, indicating the generation of materials with slow reacting carbon species, or materials of enhanced aging resistance.
- The different mastics have been subjected to DSR testing as well to provide sufficient data to evaluate the stiffening effect due to oxidation. Increase of modulus over a wide range of frequencies, decrease of frequency dependency of modulus and shifting of phase angle to lower values were some important observations noticed over oven-aging of epoxy-asphalt mastics. The S-shape of phase angle of both highly modified mastics indicates the presence of a strongly crosslinked polymer network and the rubbery characteristics of these materials at the whole frequency range. Mastics with higher proportions of epoxy in asphalt have shown higher stiffness modulus and elasticity over oxidative aging times.
- A positive deviation of the T_g values of epoxy-asphalt binders from the ideal mixing rule was observed indicating the existence of strong intermolecular interactions. In fact, the asphalt and epoxy binders are immiscible and thus strong repulsive forces are present when the two binders are mixed together. Over oxidative aging, the binders tend to break up spontaneously into two phases, as manifested with the increase of relative shift of T_g , or $\Delta T_g/T_g$. The Gordon and Taylor equation was used to predict the ideal mixing glass transition of binders.
- The values of heat capacity increment at glass transition, or ΔC_p , of epoxy-asphalt binders were determined as well. Although the T_g values indicated that oven conditioning for 480 hrs could result in an equivalent embrittlement with PAV for 80 hrs, a significantly different shape of the composition relationship of ΔC_p between the oven and PAV aged blends is observed. It is believed that the conditioning schemes affect the crosslinking degree of thermosetting binders and consequently the extent of oxidation over long-term oxidative aging.
- The S-shape of composition dependence of T_g values of mastics verifies an earlier study in which the composition dependence of modulus followed a similar trend. The T_g values of mastics were also higher than those of blends with the same epoxy proportion. The addition of fillers could toughen the blends formulating strongly crosslinked materials. The glass transition that corresponds to an ideal mastic, or a mastic without intermolecular forces, was predicted using Kwei equation.

- The negative configurational entropy of mixing ($\Delta S_{mix}^c < 0$) corresponds to the positive deviation of T_g from the ideal mixing rule ($\Delta T_g/T_g > 0$). In this study, the continuous decrease of ΔS_{mix}^c of both aging blends and mastics imply the further rise of repulsive internal forces between the individual components, attributing towards more thermodynamically unstable and brittle systems.

Future research is needed to link the parameters determined by DSC with the chemistry and fracture characteristics of asphalt binders. For instance, the T_g values of both blends and mastics were increased over oxidative aging, indicating the embrittlement of these materials with time. This could trigger an effort to establish a reliable characterization method to assess the brittleness of asphalt binders. The use of tools, such as Bending Beam Rheometer, Asphalt Binder Cracking Device, Direct Tension Tester, and others, in conjunction with DSC, will assist in understanding the thermal cracking of asphalt binders.

6.8 References

- Adam, G., J.H. Gibbs. On the Temperature Dependence of Cooperative Relaxation Properties in Glass Forming Liquids. *The Journal of Chemical Physics* 43, 1965, pp. 139-146.
- Airey, G.D. Rheological Properties of Styrene Butadiene Styrene Polymer Modified Road Bitumens. *Fuel* 82, 2003, pp. 1709-19.
- Airey, G.D., M.H. Mohammed, C. Fichter. Rheological Characteristics of Synthetic Road Binders. *Fuel* 87, 2008, pp. 1763-75.
- Apostolidis, P., X. Liu, S. Erkens, A. Scarpas. Evaluation of Epoxy Modification in Bitumen. *Construction and Building Materials* 208, 2019, pp. 361-368.
- Apostolidis, P., M. Elwardany, L. Porot, S. Vansteenkiste, E. Chailleux. Glass Transitions in Bituminous Binders. *Materials & Structures* 54:132, 2021.
- Bateman, L., K.R. Hargrave. Oxidation of Organic Sulfides, I: Interaction of Cyclohexylmethyl Sulfide with Hydroperoxides in Alcohols. *Proceedings of The Royal Society A224 (Part 1)*, 1954, pp. 389-398.
- Branthaver, J.R., J.C. Petersen, R.E. Robertson, J.J. Duvall, S.S. Kim, P.M. Harnsberger, T.Mill, E.K. Ensley, F.A. Barbour, J.R. Schabron. *Binder Characterization and Evaluation-Vol. 2: Chemistry*. SHRP Report A-368. Strategic Highway Research Program, National Research Council, Washington, D.C., 1993.
- Couchman, P.R., F.E. Karasz. A Classical Thermodynamic Discussion of the Effect of the Composition on Glass-Transition Temperatures. *Macromolecules* 11, 1978, pp. 117-119.
- Domke, C.H., R.R. Davison, C.J. Glover. Effect of Oxidation Pressure on Asphalt Hardening Susceptibility. *Transportation Research Record* 1661, National Research Council, Washington, D.C., 1999, pp. 114-121.
- Dorrence, S.M., F.A. Barbour, J.C. Petersen. Direct Evidence of Ketones in Oxidized Asphalts. *Analytical Chemistry* 46, 1974, pp. 2242-44.
- Durrieu, F., F. Farcas, V. Mouillet. The Influence of UV Aging of a Styrene/Butadiene/Styrene Modified Bitumen: Comparison between Laboratory and On Site Aging. *Fuel* 86(10-11), 2007, pp. 1446-51.

- Elder, A.C., M.M. Hatting, V.P. Servas, C.P. Marais. Use of Aging Tests to Determine the Efficiency of Hydrated Lime Additions to Asphalt in Retarding Its Oxidative Hardening. *Journal of the Association of Asphalt Paving Technologists*, Vol, 54, 1985, pp. 118–139.
- Farrar, M.J., T.F. Turner, J.-P. Planche, J.F. Schabron, P.M. Harnsberger. Evolution of the Crossover Modulus with Oxidative Aging: Method to Estimate Change in Viscoelastic Properties of Asphalt Binder with Time and Depth on the Road. *Transportation Research Record 2370*, National Research Council, Washington, D.C., 2013, pp. 76-83.
- Fox, T.G. Influence of Diluent and Copolymer Composition on the Glass Temperature of a Polymer System. *Bull. Am. Phys. Soc. 1*, 1956, pp. 123.
- Glaser, R.R., J.F. Schabron, T.F. Turner, J.-P. Planche, S.L. Salmans, J.L. Loveridge. Low-Temperature Oxidation Kinetics of Asphalt Binders. *Transportation Research Record 2370*, National Research Council, Washington, D.C., 2013, pp. 63-68.
- Glover, C.J., C.H. Domke. *Development of a New Method for Assessing Asphalt Binder Durability with Field Validation*. Texas Transportation Institute in Cooperation with the U.S. Department of Transportation Federal Highway Administration, Report 1872-2, 0-1872, 2005.
- Gordon, J.M., J.S. Taylor. Ideal Copolymers and the Second-Order Transitions of Synthetic Rubbers. I. Non-Crystalline Copolymers. *Journal of Applied Chemistry 2*, 1952, pp. 493.
- Gupta, P.K., J.C. Mauro. Composition Dependence of Glass Transition Temperature and Fragility. I. A Topological Model Incorporating Temperature Dependent Constraints. *The Journal of Chemical Physics 130*, 2009, 094503.
- Herrington, P. Thermal Decomposition of Asphalt Sulfoxides. *Fuel 74*(8), 1995, pp. 1232-35.
- Herrington, P. Diffusion and Reaction of Oxygen in Bitumen Films. *Fuel 94*, 2012, pp. 86-92.
- Herrington, P., D. Alabaster. Epoxy Modified Open-graded Porous Asphalt. *Road Materials and Pavement Design 9*(3), 2008, pp. 481-498.
- Herrington, P., B. James, T.F.P. Henning. Validation of a Bitumen Oxidation Rate Model. *Transportation Research Record 2632*, National Research Council, Washington, D.C., 2017.
- Hesp, S., A. Soleimani, S. Subramani, T. Phillips, D. Smith, P. Marks, K.K. Tam. Asphalt Pavement Cracking: Analysis of Extraordinary Life Cycle Variability in Eastern and Northeastern Ontario. *International Journal of Pavement Engineering 10*(3), 2009, pp. 209.
- Huang, S.-C., J.C. Petersen, R.E. Robertson, J.F. Branthaver. Effect of Hydrated Lime on Long-term Oxidative Aging Characteristics of Asphalt. *Transportation Research Record 1810*, National Research Council, Washington, D.C., 2002, pp. 17–24.
- Huang, S.-C., M. Zeng. Characterization of Aging Effect on Rheological Properties of Asphalt-Filler Systems. *International Journal of Pavement Engineering 8*(3), 2007, pp. 213-223.
- Huang, S.-C., W. Grimes. Influence of Aging Temperature on Rheological and Chemical Properties of Asphalt Binders. *Transportation Research Record 2179*, National Research Council, Washington, D.C., 2010, pp. 39-48.
- Huh, J.D., & R.E. Robertson. Modeling of Oxidative Aging Behavior of Asphalts from Short-Term High-Temperature Data as a Step Toward Prediction of Pavement Aging. *Transportation Research Record 1535*, National Research Council, Washington, D.C., 1996.
- International Transport Forum. *Long-life Surfacing for Roads: Field Test Results*. ITF Research Reports, OECD, Paris, France, 2017.

- Johansson, L., J.F. Branthaver, R.E. Robertson. A Study of Rheological Properties of Lime Treated Paving Asphalts Aged at 60°C in a Pressure Aging Vessel. *Fuel Science and Technology International*, Vol. 13, No. 10, 1995, pp. 1317–43.
- Johansson, L., J.F. Branthaver, R.E. Robertson. The Influence of Metal-Containing Compounds on Enhancement and Inhibition of Asphalt Oxidation. *Fuel Science and Technology International*, Vol. 14, No. 8, Sept. 1996, pp. 1143–59.
- Jin, X., R. Han, Y. Cui, C.J. Clover. Fast-Rate – Constant-Rate Oxidation Kinetics Model for Asphalt Binders. *Industrial & Engineering Chemistry Research* 50, 2011, pp. 13373-79.
- Jing, R., A. Varveri, X. Liu, A. Scarpas, S. Erkens. Rheological, Fatigue and Relaxation Properties of Aged Bitumen. *International Journal of Pavement Engineering* 2019a.
- Jing, R., A. Varveri, X. Liu, A. Scarpas, S. Erkens. Laboratory and Field Aging Effect on Bitumen Chemistry and Rheology in Porous Asphalt Mixture. *Transportation Research Record* 2673(3), National Research Council, Washington, D.C., 2019b, pp. 365-374.
- Jing, R., A. Varveri, X. Liu, A. Scarpas, S. Erkens. Ageing Effect on Chemo-Mechanics of Bitumen. *Road Materials and Pavement Design* 2019c, pp. 1-16.
- Jing, R. *Ageing of Bituminous Materials: Experimental and Numerical Characterization*. PhD Thesis, Delft University of Technology, 2019d.
- Kalogerias, I.M. Description and Molecular Interpretations of Anomalous Compositional Dependences of the Glass Transition Temperatures in Binary Organic Mixtures. *Thermochimica Acta* 509, 2010, pp. 135-146.
- Kauzmann, W. The Nature of the Glassy State and the Behavior of Liquids at Low Temperatures. *Chemical Reviews* 43, 1948, pp. 219-256.
- King, G.N. Oxycyclics: Understanding Catalyzed Oxidation Mechanisms in Bitumens and Other Related Petroleum Products. *Fuel Science and Technology* 11(1), 1993, pp. 201-238.
- Knotnerus, J. Oxygen Uptake by Bitumen Solutions as a Potential Measure of Bitumen Durability. *Division of Petroleum Chemistry, American Chemistry Society* 16(1), 1971.
- Kwei, T. The Effect of Hydrogen Bonding on the Glass Transition Temperature of Polymer Mixtures. *Journal of Polymer Science: Polymer Letters Edition* 22, 1984, pp. 307-313.
- Lamontagne, J. P. Dumas, V. Mouillet, J. Kister. Comparison by Fourier Transform Infrared (FTIR) Spectroscopy of Different Aging Techniques: Application to Road Bitumens. *Fuel* 80(4), 2001, pp. 483-488.
- Lau, C.K., K.M. Lunsford, C.J. Glover, R.R. Davidson, J.A. Bullin. Reaction Rates and Hardening Susceptibilities as Determined from Pressure Oxygen Vessel Aging of Asphalts. *Transportation Research Record* 1342, National Research Council, Washington, D.C., 1992.
- Lee, D.Y., R.J. Huang. Weathering of Asphalts as Characterized by Infrared Multiple Internal Reflectance Spectroscopy. *Applied Spectroscopy* 27, 1973, p. 435.
- Lesikar, A.V. Effect of Association Complexes on Glass Transition in Organic Halide Mixtures. *The Journal of Physical Chemistry* 80, 1976, pp. 1005-11.
- Lesueur, D., D.N. Little. Effect of Hydrated Lime on Rheology, Fracture, and Aging of Bitumen. In *Transportation Research Record* 1661, National Research Council, Washington, D.C., 1999, pp. 93–105.
- Lesueur, D., J. Petit, H.-J. Ritter. The Mechanisms of Hydrated Lime Modification of Asphalt Mixtures: a State-of-the-Art Review. *Road Materials and Pavement Design* 14(1), 2013.

- Lesueur, D., A. Teixeira, M.M. Lazaro, D. Andaluz, A. Ruiz. A Simple Test Method in order to Assess the Effect of Mineral Fillers on Bitumen Ageing. *Construction and Building Materials* 117, 2016, pp. 182-189.
- Liang, Y., R. Wu, J.T. Harvey, D. Jones, M.Z. Alavi. Investigation into the Oxidative Aging of Asphalt Binders. *Transportation Research Record* 2673(6), National Research Council, Washington, D.C., 2019, pp. 368-378.
- Lin, A.A., T.K. Kwei, A. Reiser. On the Physical Meaning of the Kwei Equation for the Glass Transition Temperature of Polymer Blends. *Macromolecules* 22, 1989, pp. 4112-19.
- Lin, M., R.R. Davidson, C.J. Glover, J.A. Bullin. Effects of Asphaltenes on Asphalt Recycling and Aging. *Transportation Research Record* 1507, National Research Council, Washington, D.C., 1995, pp. 86-95.
- Little, D.N., J.C. Petersen. Unique Effects of Hydrated Lime Filler on the Performance-related Properties of Asphalt Cements: Physical and Chemical Interactions Revisited. *Journal of Materials in Civil Engineering* 17(2), 2005, pp. 207-218.
- Liu, F., Z. Zhou, Y. Wang. Predict the Rheological Properties of Aged Asphalt Binders using a Universal Kinetic Model. *Construction and Building Materials* 195, 2019, pp. 283-291.
- Liu, G. C.J. Glover. A Study on the Oxidation Kinetics of Warm Mix Asphalt. *Chemical Engineering Journal* 280, 2015, pp. 115-120.
- Liu, M., K.M. Lunsford, R.R. Davison, C.J. Glover, J.A. Bullin. The Kinetics of Carbonyl Formation in Asphalt. *AIChE Journal* 42, 1996, pp. 1069-76.
- Lu, X., U. Isacson. Chemical and Rheological Evaluation of Aging Properties of SBS Polymer Modified Bitumen. *Fuel* 77(9-10), 1998, pp. 961-972.
- Lu, X. Y. Talon, P. Redelius. Aging of Bituminous Binders – Laboratory Tests and Field Data. *Proceedings of the 4th Eurasphalt and Eurobitumen Congress*, Copenhagen, Denmark, 2008.
- Lu, Q., J. Bors. Alternate Uses of Epoxy Asphalt on Bridge Decks and Roadways. *Construction and Building Materials* 78, 2015, pp. 18-25.
- Ma, T., X.M. Huang, E. Mahmoud, E. Garibaldy. Effect of Moisture on the Aging Behavior of Asphalt Binder. *International Journal of Minerals, Metallurgy and Materials* 18(4), 2011.
- Martin, K.G. Influence of Stabilizers on Bitumen Durability. *Journal of Applied Chemistry* 16, 1966, pp. 197-202.
- Martin, K.L., R.R. Davidson, C.J. Glover, J.A. Bullin. Asphalt Aging in Texas Roads and Test Section. *Transportation Research Record* 1269, National Research Council, Washington, D.C., 1990, pp. 9-19.
- Mill, T., D. Tse. Oxidation and Photooxidation of Asphalts. *Division of Petroleum Chemistry, American Chemistry Society* 35(3), 1990, pp. 483-489.
- Moraes, R., H.U. Bahia. Effect of Mineral Fillers on the Oxidative Aging of Asphalt Binders: Laboratory Study with Mastics. *Transportation Research Record* 2506, National Research Council, Washington, D.C., 2015a, pp. 19-31.
- Moraes, R., H.U. Bahia. Effect of Mineral Filler on Changes in Molecular Size Distribution of Asphalts during Oxidative Ageing. *Road Materials and Pavement Design* 16(2), 2015b.
- Mouillet, V. F. Farcas, S. Besson. Aging by UV Radiation of an Elastomer Modified Bitumen. *Fuel* 87(12), 2009, pp. 2408-19.
- Murthy, S.S.N. M. Tyagi. Dielectric Study of the Miscibility of Binary Liquids, One being an Alcohol. *Journal of Solution Chemistry* 31, 2002, pp. 33-58.

- National Academies of Sciences, Engineering and Medicine. *Long-Term Aging of Asphalt Mixtures for Performance Testing and Prediction*. NCHRP Research Report 871, Washington, D.C., 2017.
- Painter, P.C., J.F. Graf, M.M. Coleman. Effect of Hydrogen Bonding on the Enthalpy of Mixing and the Composition Dependence of the Glass Transition Temperature in Polymer Blends. *Macromolecules* 24, 1991, pp. 5630-38.
- Petersen, J.C., F.A. Barbour, S.M. Dorrence, Catalysis of Asphalt Oxidation by Mineral Aggregate Surfaces and Asphalt Components. *Association of Asphalt Paving Technologists* 43, 1974, pp. 162-177.
- Petersen, J.C., F.A. Barbour, S.M. Dorrence. Identification of Dicarboxylic Anhydrides in Oxidized Asphalts. *Analytical Chemistry* 47, 1975, pp. 107-111.
- Petersen, J.C. Oxidation of Sulfur Compounds in Petroleum Residues: Reactivity-Structural Relationships. *Division of Petroleum Chemistry, American Chemistry Society* 26(4), 1981.
- Petersen, J.C. Chemical Composition of Asphalt as Related to Asphalt Durability: State of the Art. *Transportation Research Record* 999, National Research Council, Washington, D.C., 1984, pp. 13-30.
- Petersen, J.C., H. Plancher, P.M. Harnsberger. Lime Treatment of Asphalt to Reduce Age Hardening and Improve Flow Properties. *Journal of the Association of Asphalt Paving Technologists*, Vol. 56, 1987, pp. 632–653.
- Petersen, J.C., J.F. Branthaver, R.E. Robertson, P.M. Harnsberger, J.J. Duvall, E.K. Ensley. Effects of Physicochemical Factors on Asphalt Oxidation Kinetics. *Transportation Research Record* 1391, National Research Council, Washington, D.C., 1993, pp. 1-10.
- Petersen, J.C., P.M. Harnsberger, R.E. Robertson. Factors Affecting the Kinetics and Mechanisms of Asphalt Oxidation and the Relative Effects of Oxidation Products on Age Hardening. *Division of Fuel Chemistry, American Chemical Society* 41(4), 1996.
- Petersen, J.C., P.M. Harnsberger. Asphalt Aging: Dual Oxidation Mechanism and Its Interrelationships with Asphalt Composition and Oxidative Age Hardening. *Transportation Research Record* 1638, National Research Council, Washington, D.C., 1998, pp. 47–55.
- Petersen, J.C. A Dual Sequential Mechanism for the Oxidation of Asphalts. *Petroleum Science and Technology* 16(9-10), 1998, pp. 1023-59.
- Petersen, J.C. *A Review of the Fundamentals of Asphalt Oxidation: Chemical, Physicochemical Property, and Durability Relationship*. Transportation Research Circular, Number E-C140, Transportation Research Board of National Academies, Washington, D.C., 2009.
- Pinal, R. Entropy of Mixing and the Glass Transition of Amorphous Mixtures. *Entropy* 10, 2008, pp. 207–223.
- Plancher, H., E.L. Green, J.C. Petersen. Reduction of Oxidative Hardening of Asphalts by Treatment with Hydrated Lime-A Mechanic Study. *Journal of the Association of Asphalt Paving Technologists*, Vol. 45, 1976, pp. 1–24.
- Schneider, H.A. Conformational Entropy Contributions to the Glass Temperature of Blends of Miscible Polymers. *Journal of Research of the National Institute of Standards and Technology* 102, 1997, pp. 229-248.
- Simha, R., R.F. Boyer. On a General Relation involving the Glass Temperature and Coefficients of Expansion of Polymers. *The Journal of Chemical Physics* 37, 1962, pp. 1003-07.

- Vallerga, B.A. Pavement Deficiencies Related to Asphalt Durability. *Association of Asphalt Paving Technologist* 50, 1981, pp. 481–491.
- Van Oort, W.P. Durability of Asphalt. *Industrial and Engineering Chemistry* 48, 1956.
- Wang, L.-M., Y.J. Tian, R.P. Liu, K.L. Ngai. Anomalous Component Dynamics of a Binary Mixture of Associating Glass-Forming Liquids. *The Journal of Physical Chemistry B* 115, 2011, pp. 719-724.
- Wei, J., & Y. Zhang. 2012. Study on the Curing Process of Epoxy Asphalt. *Journal of Testing and Evaluation* 40(7), 2012, pp. 1-8.
- Wu, J., G. Airey. The Influence of Aggregate Interaction and Aging Procedure on Bitumen Aging. *Journal of Testing and Evaluation* 37(5), 2009, pp. 1-8.
- Youtcheff, J., N. Gibson, A. Shenoy, G. Al-Khateeb. The Evaluation of Epoxy Asphalt and Epoxy Asphalt Mixtures. *Proceedings of the Canadian Technical Asphalt Association* 51, 2006.

7

Laboratory Tests on Epoxy modified Asphalt Concrete

7.1 Introduction

Epoxy-asphalt binders have captured the interest of road network administrations and infrastructure owners as an essential technology for flexible pavements specially designed for critical applications, such as airfields (Simpson et al., 1960; Burns 1694; Joseph 1965) and orthotropic steel deck bridges (Balala 1969; Touran & Okereke 1991; Gaul 1996; Hulsey et al., 1999; Hicks et al., 2000; Huang et al., 2003; Gaul et al., 2011; Lu & Bors 2015). As discussed in **Chapters 2, 3, and 4**, the epoxy modification of asphalt binders differs from the conventional thermoplastic block copolymers because once the reactive epoxy is fully cured in asphalt, a thermosetting system is created with limited possibilities to be re-melted. However, improved durability was observed when a reactive binder was blended with asphalt binder offering a new binder type with increased oxidative aging resistance, as discussed in **Chapter 6**.

In New Zealand (Herrington & Alabaster 2008; Herrington 2010; International Transport Forum 2017; Wu et al., 2019), and the United Kingdom (Widyatmoko et al., 2006; Widyatmoko & Elliott 2014; Dinnen et al., 2020), the epoxy-asphalt has been used for surfacing (wearing) pavement courses for high priority strategic roadways, such as open-graded porous asphalt roads. As a continuation of the international effort to assess the applicability of the epoxy-asphalt as a surfacing material for long-life roadway pavements, the effect of epoxy-asphalt on the performance of an asphalt concrete mix is discussed in this **chapter**. Emphasis will also be given on providing insights and recommendations for the large-scale surfacing applications of epoxy modified asphalt mixes. Finally, the interlayer bonding characteristics between pavement layers have a remarkable influence on the overall performance response during service life. Insufficient bonding could raise the risk of various distresses, such as slippage cracking. Thus, the potential use of epoxy-asphalt binder as tack coating is also explored by evaluating the interface shear strength of two-layer asphalt samples.

7.2 Epoxy-Asphalt as Surfacing Pavement Material

7.2.1 Laboratory experience

Materials and specimen preparation

The gradation of asphalt concrete of 8-mm nominal maximum aggregate size (SMA-NL 8B, RAW-2015) is given in **Table 7.1**. This asphalt type, which is designed with 5% air voids and 6.7% mass binder content, is commonly used as wearing course material in Dutch provincial roadways. To lower the cost of the designed epoxy modified asphalt mix, the effect of diluting the epoxy-asphalt binder with a neat asphalt binder (70/100 pengrade) was studied. 20 and 40 wt. % of the binder were substituted by the EA_{ref} binder, discussed in **Chapter 6**. The EA_{ref} was formulated by blending Part A with Part B. The two parts react together through an irreversible curing process, formulating a rubber-like elastomeric binder. By mixing the two parts of EA_{ref}, the curing process starts, and the viscosity of the binder increases over time up to gel point (see **Chapter 4**). According to the supplier, the typical lab curing process of this elastomeric binder is at 120°C for 4-5 hrs or 130°C for 3 hrs in the oven (ChemCo Systems Inc. 2015; 2016a & 2016b). Note that the strength gain predominantly occurs in several days and is initially dependent upon processing variables and later, substrate temperatures in the field.

Table 7.1 Aggregate gradation of SMA-NL 8B, RAW-2015.

Sieve size [mm]	min. [% m/m]	max. [% m/m]	Percentage passing [% m/m]
11.2	98.0	100.0	100
8	86.5	99.5	93
5.6	46.1	60.1	52
4			31
2	16.9	28.9	23
0.5	11.1	19.1	8.2
0.063	6.2	11.2	6.7
Binder content [% m/m]: 6.7			

Part A and B were oven-heated separately for 1 hr to 85 and 110°C, respectively. Afterward, they were mixed, and the EA_{ref} diluted in the already pre-heated (at 120°C) neat asphalt binder, based on the supplier's recommendations. Two diluted versions of epoxy modified asphalt concrete were studied, named ESMA-20 and ESMA-40. In other words, two epoxy modified binders were formed with the weight ratio of 20:80 and 40:60 of EA_{ref} and asphalt binder, respectively, and mixed with mineral particles at 135°C, producing loose mixes. A Hobart pan mixer and a spiral dough hook were used for mixing according to EN 12697. Immediately after mixing, slabs of loose mixes were rolling wheel compacted within a 500-mm by 500-mm steel mould. The target densities of control asphalt (ESMA-0) and epoxy modified asphalt (ESMA-20 and ESMA-40) samples were 2304 and 2310 kg/m³, respectively. Compacted slabs were cooled down to 20°C out of the mould and oven-cured at 85°C for a week. Four-point bending beams and cylindrical specimens were sawed and drilled from the slabs for further investigation. All specimens were conditioned at 12°C for two weeks. The determined values of mix density (NEN-EN 12697-5 method A) and air voids content (NEN-EN 12697-8) of the studied materials are given in **Table 7.2**. All mixes were evaluated by indirect tensile tests (ITT) according to NEN-EN 12697-12 to assess the water sensitivity and four-point bending (4PB) tests to assess the effect of epoxy modification on the mix stiffness and fatigue life.

Table 7.2 Physical properties of studied mixes designed for surfacing applications.

Property	Specification	ESMA-0 ^{*1}	ESMA-20 ^{*2}	ESMA-40 ^{*2}
Target density [kg/m ³]		2304	2310	2310
Mix density [kg/m ³]	NEN-EN 12697-5	2449	2435	2435
Air voids content [%]	NEN-EN 12697-8	5.9	5.1	5.3
production temperature range: 140-180°C ^{*1} and 125-145°C ^{*2}				

Indirect tensile tests

Cylindrical specimens of 100-mm diameter and 49.5-mm height were cored from the one-layer slabs to perform the ITTs. Tests were conducted at 15°C with a displacement-controlled loading speed of 50 mm/min, and a representative graph of the response of the three studied materials during ITT is shown in **Fig. 7.1**. The response of ESMA-20 appeared to be more brittle than of unmodified mix, ESMA-0, as it yields a faster drop in the overall force signal. Apart from higher brittleness, a higher level of epoxy modification leads to higher stiffness and strength, as depicted in **Fig. 7.1**. The ESMA-40 mix is the composite material of the highest strength and

stiffness, reflecting the impact of epoxy on developing surfacing materials of enhanced capacity to withstand forces against fracture.

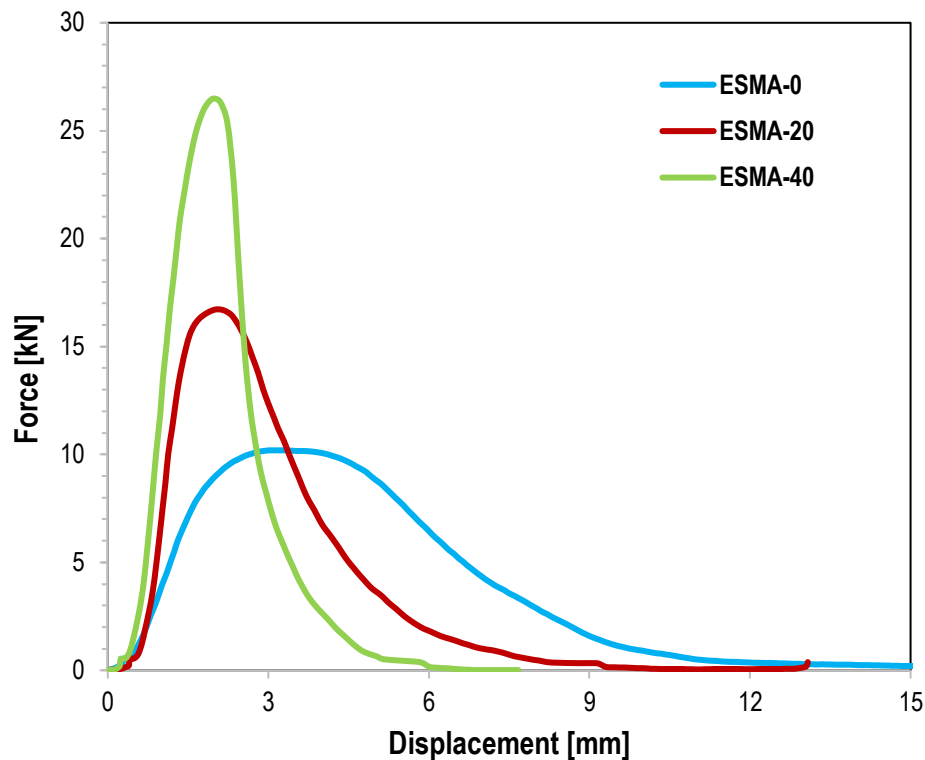


Figure 7.1 Representative force versus displacement curves of studied materials.

The influence of water on the ITT strength of studied mixes is shown in **Fig. 7.2**. The results presented in this figure were the mean (marker), maximum and minimum of four replicates. Without water conditioning, the mean indirect tensile strength of unmodified SMA (i.e., ESMA-0) was 1.28 MPa, almost 60% and 40% of the strength of ESMA-20 (2.02 MPa) and ESMA-40 (3.21 MPa), respectively (see **Fig. 7.2a**). Thus, the increase of epoxy proportion in asphalt resulted in an increase in material strength, with the ESMA-40 mix having the highest capacity to withstand the applied forces. By comparing the retained strength after water conditioning, the unmodified (control) mix (i.e., ESMA-0) has demonstrated the lowest water sensitivity, as it retained 100% of its original strength after conditioning. ESMA-20 and ESMA-40 had 95% and 85% water sensitivity fulfilling the requirement (80%) of RAW2015.

The total dissipated work is shown in **Fig. 7.2b**. The dissipated work, defined as the total area under force-displacement curve, is not part of the standard performance assessment of asphalt mixes and can be used as a measure of fracture resistance. The total dissipated work has marginally decreased with the 20% (by weight) epoxy addition in the mix (i.e., ESMA-20). Nevertheless, when the epoxy proportion in asphalt was increased to 40% by weight (i.e., ESMA-40), an increase of total dissipated work was noticed and thus an improvement of the fracture resistance of the asphalt mix. From the data presented in **Fig. 7.2b**, it can be seen that wet ESMA-20 and ESMA-40 mixes have shown almost the same wet total dissipated work compared with that of dry mixes, indicating that the fracture resistance of mixes remained almost unaffected due to water damage. Overall, the use of high proportions of epoxy in asphalt

improves both strength and fracture resistance without significantly sacrificing the material performance against the water.

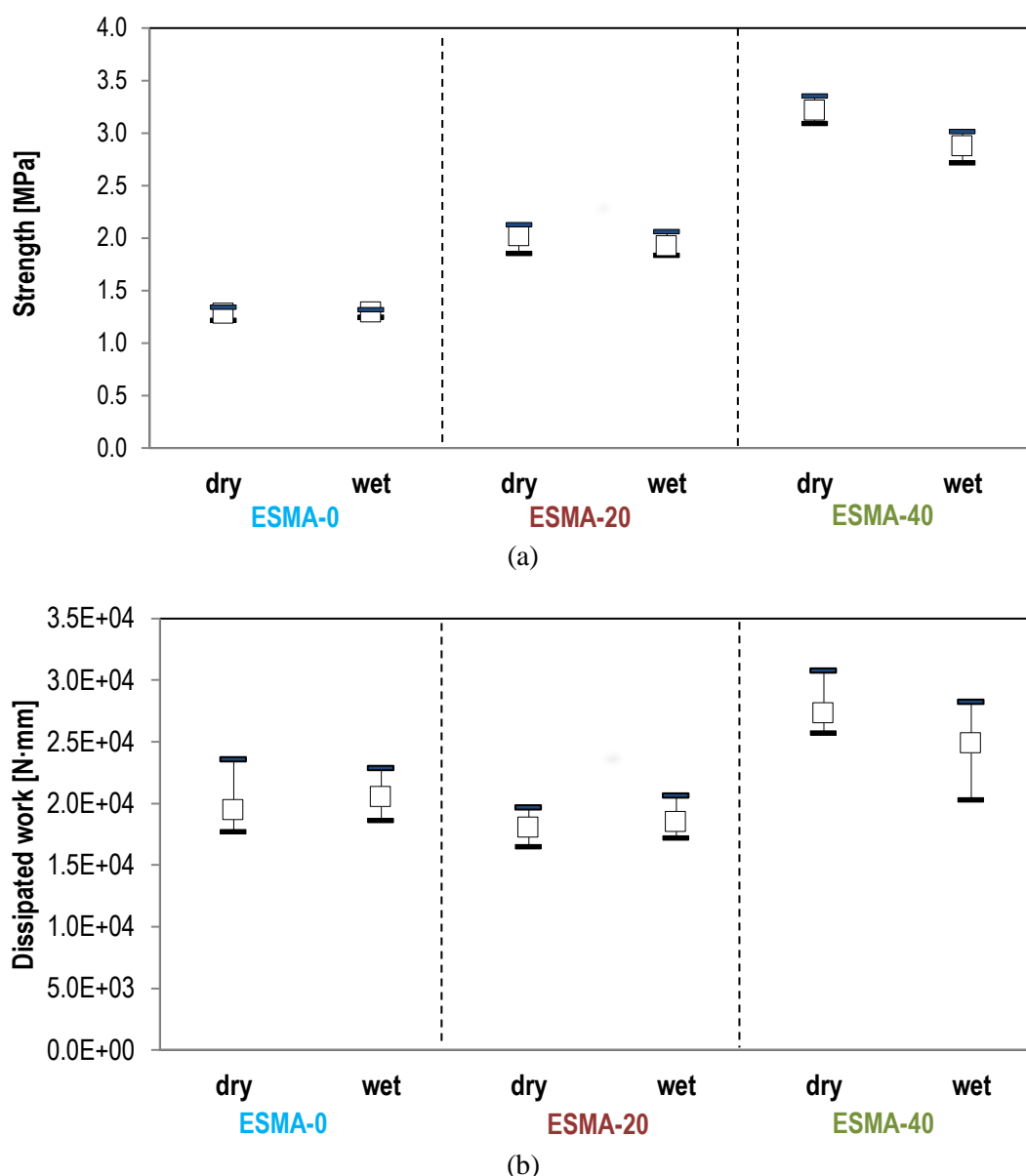


Figure 7.2 Indirect tensile test results; (a) tensile strength and (b) dissipated work of studied materials (dry: strength before moisture conditioning, wet: strength after moisture conditioning).

Four-point bending tests

The 4PB specimens flexural stiffness tests were performed at 10°C, assuming a Poisson's ratio of 0.35. The flexural stiffness and phase angle of 4PB specimens were measured at one strain level ($50 \pm 0.5 \mu\text{m/m}$), with 10 different loading frequencies; 0.1, 0.2, 0.5, 1, 2, 5, 8, 10, 20, and 30 Hz. 16 replicates were tested for each material.

The mean values of measured stiffness modulus and phase angle of studied materials are shown in **Fig. 7.3**. The stiffness modulus at 8 Hz of 4PB specimens was determined as 8330, 10490, and 13910 MPa for the ESMA-0, ESMA-20, and ESMA-40 mixes, respectively. Therefore, the

proportional substitution of asphalt binder with epoxy resulted in stiffer mixes with lower phase angle, indicating pavement materials with higher elasticity and capacity to resist traffic deformations in the field.

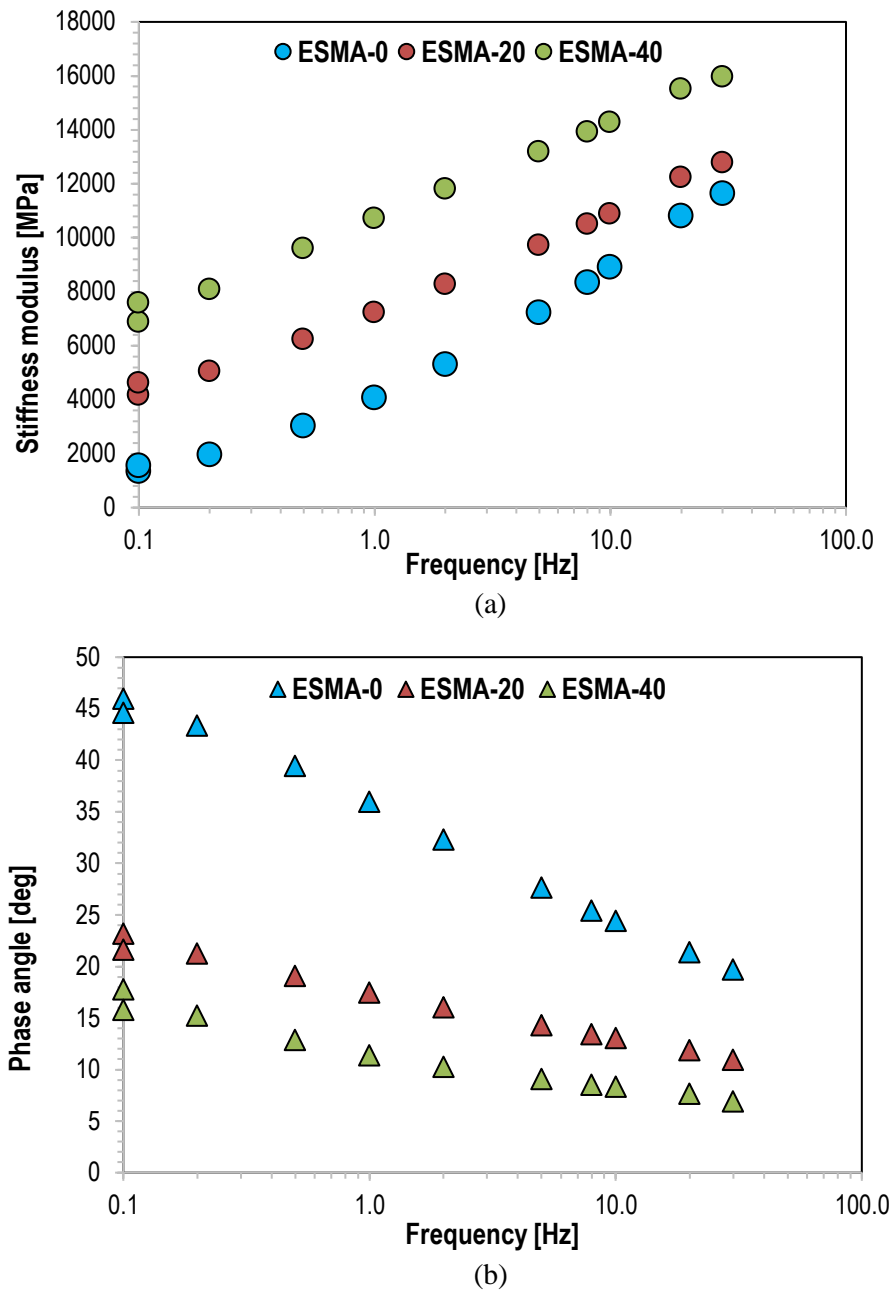


Figure 7.3 Frequency dependence of (a) stiffness modulus and (b) phase angle of the studied materials determined based on 4PB tests.

For the 4PB fatigue tests, the 50% reduction of the initial modulus was considered as fatigue life criteria. In other words, the fatigue test terminates when the flexural stiffness reaches half of its initial value. Three strain level were applied in 4PB beam specimens. **Fig. 7.4** demonstrates the fatigue life at the three different strain levels of the three different studied materials designed for surfacing applications. Both ESMA-20 and ESMA-40 have significantly higher fatigue resistance than the control mix. According to NEN-EN 12697-24, the 4PB fatigue resistance of ESMA-0, ESMA-20 and ESMA-40 was 111, 156 and 159, respectively.

As expected, the increase of epoxy modification level in asphalt leads to materials of high resistance to failure under cyclic loading, an observation which coincides with the fracture performance of epoxy modified asphalt mixes under monotonic loading.

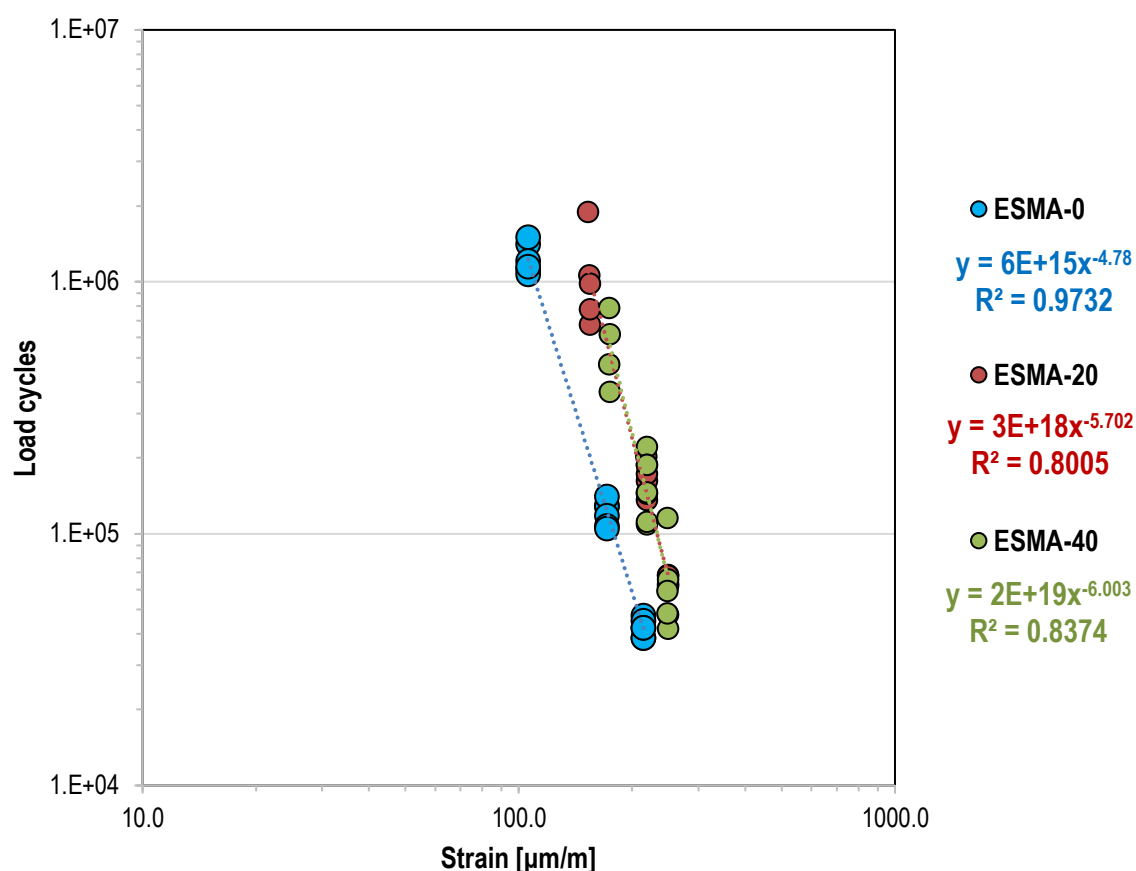


Figure 7.4 The relationship between applied strain and fatigue life of studied materials (at 10°C).

7.2.2 Field trials experience

Trials of epoxy modified asphalt concrete mixes have been carried out on various sections worldwide (International Transport Forum 2017). Due to the thermo-hardening nature of epoxy-asphalt binder, special care is needed to ensure complete mixing of all the components simultaneously through the in-plant production and prevent over-curing during the material transport and in-field operations (i.e., paving and compaction). The risk of in-plant output and construction failure is more significant than with conventional mixes. Thus, all the past experience of manufacturing pavements with epoxy-based materials should be taken into account for any further development.

In New Zealand, fatty acid-type epoxy modified asphalt mixes were studied at lab-scale and were applied in-field successfully with a turbulent-mass continuous-mix drum plant at a temperature range between 100 and 130°C (International Transport Forum 2017). Although some difficulties were encountered with the in-plant production and material delivery of epoxy modified asphalt mixes mainly because of the uncontrolled curing of an amine-type binder used, the implementation of a slow curing fatty acid-type epoxy-asphalt solved this issue

(International Transport Forum 2017). These field trials suggested using an automated distribution system to automatically blend the incorporating parts of epoxy-asphalt. Notably, Part A, which was heated to 85°C, entered the line carrying Part B, which was heated to 120°C, 4-m from the discharge point into the drum to ensure parts' pre-mixing before adding other constituents. Most installations use a stainless steel inline static mixer to ensure adequate shear of all components. After completion of in-plant manufacturing operations, cleaning the plant by blowing compressed air and special cleaning agents was also recommended. Special attention should be given to the storage tank, pumping systems, and transport lines involved in the plant production.

Despite the turbulent-mass drum mix plant and pugmill utilized in New Zealand and the United Kingdom, a (twin axle) batch mix plant was used in the Netherlands to produce an SMA-NL 8B mix with an epoxy binder for trial pavement sections in the Province of North Holland. More information about the in-plant and in-field operations performed in the Netherlands is provided below.

Batch plant production

To obtain complete control over the heating conditions of the liquid thermosetting parts of the epoxy binder, an in-line temperature system and a mass flow-control automated distribution system were installed to produce these components. Part B was pre-heated at 120°C and pumped from the distributor at ground level up to the mixing pugmill of the plant. In parallel, Part A was pre-heated at 75°C in its storage tank. Part A and Part B were pumped in the asphalt binder weighing vessel, and the asphalt binder injection pump achieved the pre-mixing of the two components. After pre-mixing, mineral particles (gradation of SMA-NL 8B) were added at 120°C, and the produced mix was discharged to trucks for transport to the trial pavement sections. Isolated Live Bottom Belt Asphalt trucks were used for the mix transport to prevent temperature segregation of the mix entering the paver.

In-plant trial

Although the ESMA mix may be handled similarly to normal asphalt mixes, time and temperature are even more critical to the successful manufacturing of the epoxy material than they are for regular asphalt concrete mixes. Thus, before manufacturing the trial surfacing road, a 100-m field trial was constructed at the plant to optimize the quality of the material via monitoring the development of mechanical properties of ESMA under controlled conditions. The development of properties demonstrates the curing profile of ESMA, and its optimization is essential to obtain the desired reaction rate of the epoxy system under local conditions.

A paver with vibrating/tamper screed and a three-wheel static roller followed by a tandem steel wheel vibratory roller were used for paving and compaction. The handling conditions in delivering trucks for the trial pavement sections, paving, and compaction of the newly produced mix were decided by the contractor in accordance with national standards. For example, the use of asphalt feeders or shuttle buggies are recommended to ensure continuous process without operational interruptions. Uniform material temperature could be achieved by having continuous operations and hence the undesired material over-curing will be avoided (see

Chapter 4). A mixer auger could also reduce the segregation minimizing the need for the paver to stop and the continuous feed in the paver hopper could minimize the cold spots.

In-field trials

The time between plant production and the start of paving was approximately 90 min. After delivering the material, ESMA was held in the truck before paving at 121°C with a standard deviation of 4°C. The total time between mixing and finishing of compaction was approximately 4 hrs. The compaction was done by a three-wheel static roller (10 metric tons) followed by a tandem steel wheel vibratory roller (7.5 metric tons). The mix compaction took approximately 30 min, and at the end of the compaction, the temperature was between 65 to 90°C, under sunny and dry weather conditions. It should be mentioned that a combination of rubber tire and steel wheel rollers is optimal for the compaction of dense-graded asphalt mixes according to the material supplier. Also, as noticed in (International Transport Forum 2017), large-scale mix production resulted in slower curing rates, leading to slower development of properties than was measured at lab-scale preliminary studies. This attribute could be explained by the fact that the laboratory activities performed under isothermal conditions compared to the uncontrolled temperature changes in the field. However, the curing rate was high enough, and thus the trial section was opened to traffic on the same afternoon.

As mentioned earlier, the structural performance of epoxy modified asphalt pavements depends not only on the mechanical properties of individual pavement layers but also on the interlayer bonding strength between them (Uzan et al., 1978; Romanoschi 1999). Thus, the use of epoxy-asphalt binder as tack coat to improve the interlayer bonding characteristics of pavements with epoxy modified asphalt surfacing layers is discussed in the following sub-section.

7.3 Epoxy-Asphalt as Tack Coat

Sufficient interlayer bonding of epoxy modified asphalt pavements will be critical to providing monolithic structural behavior. The interlayer shear strength depends on temperature, wetness and cleanliness of the surface, and pavement surface type and texture (West et al., 2005). Poor bonding could lead to various distresses (e.g., debonding, slippage, and fatigue cracking), decreasing thus the lifetime of epoxy modified asphalt pavements.

To ensure the interlayer bonding pavement characteristics, tack coats are applied by selecting the appropriate coat type under specific application rates and methods. Tack coat is a light application of asphalt-based emulsion or asphalt binder, which creates a bonding between the surface being paved and the wearing course to ensure adequate bonding strength (Canestrari & Santagata 2005). Tack coats of pure asphalt binders typically show higher bonding strength than emulsified binders. The emulsified binders, which are typically formulated with very soft cut asphalt binders, offer ease of handling, reduced energy consumption, and thus they are widely used as tack coats (Mohammad et al., 2008). However, these tack coats carry the risk of trapping water between pavement layers, particularly in surfaces with lower air void content, increasing the possibilities to delamination on a hot sunny day.

Different pavement surfaces require different application rates to achieve proper interface bonding strength (Scholar et al., 2004; Mohammad & Button 2005; Tashman et al., 2006;

Collop et al., 2009; Raab & Partl 2009; Mohammad et al., 2010; Mohammad et al., 2011; Raposeiras et al., 2013). In general, the application rate of tack coat is the amount of liquid asphalt sprayed by the distributor, and earlier studies have shown that it does not influence dominantly the interlayer bonding characteristics as other factors, such as temperature, texture as well as tack coat material. According to (Mohammad et al., 2011), the effect of tack coat material and application rate is more dominant in thin pavements. Low application rates of tack coat could also yield higher interlayer shear bonding when fine-graded asphalt mixes are studied (West et al., 2005). Thus, one of the main challenges related to the application of tack coat binders is the choice of the optimum quantity of additives to be applied at the interface to achieve an adequate level of interlayer bonding. Excessive tack coat may promote shear slippage at the interface. In contrast, insufficient tack coat may cause tensile stresses concentrated at the bottom of the surface layer, leading to the significant increase of tensile strains and crack generation (Mohammad et al., 2002; Leng et al., 2008 & 2009).

The interface shear strength of an epoxy modified asphalt concrete with a typical asphalt substrate was studied. The objective of the testing program was to quantify the interface shear bonding generated by using emulsion- and epoxy-type tack coats. Finally, recommendations on utilizing the epoxy-asphalt binder as a tack coat are provided.

7.3.1 Laboratory experience

Materials and specimen preparation

ESMA-20 was selected as the top layer material and was produced in the same way discussed in **section 7.2**. Hot-mix asphalt concrete with 65% RAP, named AC, was used as bottom layer material, and on the top of it, the tack coats were applied. For the compaction of the bottom layer, slab specimens were rolling wheel compacted. 500-mm by 500-mm steel moulds were used, and layers of 55-mm and 35-mm height were fabricated for AC bottom and ESMA-20 top materials, respectively. Without prior curing, the top ESMA-20 loose mix was applied and compacted on the top of an already compacted, cooled down, and tack coated bottom AC layer.

Two emulsion-type asphalt tack coats were selected in this study; emu-A and emu-B. These emulsion tack coats were heated to 40°C and brush applied on the top of AC with one application rate of 0.3 kg/m², 30 min before laying the ESMA-20. In the EA tack coat, Parts A and B were heated to 85 and 150°C, respectively (ChemCo Systems Inc. 2015). A few minutes before applying the top ESMA-20, the two parts of the EA tack coat were mixed at the mixing ratio A:B = 25:75, directly used on the bottom layer, and spread out evenly. As recommended by the material supplier, two application rates were applied on AC bottom layer: 0.45 kg/m² and 0.60 kg/m². To determine the contribution of the various tack coats, a system without tack coat (tackless) was produced as well. All samples have been oven-conditioned at 100°C for 5 hrs to accelerate the curing of tack coat and ESMA materials.

Table 7.3 shows the test factors of lab-prepared two-layer systems developed for this study. Eight replicate samples were prepared and tested for each condition. Overall, the lab-produced samples consisted of the top and bottom layers bonded with a tack coat at their interface. Two interface shear tests were performed to evaluate the contribution of different tack coats on interface shear bonding characteristics of two layers. Samples of 150-mm and 50-mm diameter

were cored out of two-layer slabs for shear testing. Details on testing methods and results are given in the following sub-section.

Table 7.3 Test factors for lab-prepared samples.

Variable	Content
Bottom layer material	AC
Top layer material	ESMA-20
Tack coat material	EA binder, emu-A, emu-B
Application rate [kg/m^2]	0 (tackless), 0.30 (for emuls. coat), 0.45 & 0.60 (for epoxy coat)
Wetness condition	Dry
Cleanliness conditions	Clean
Test temperature [$^{\circ}\text{C}$]	20
Test displacement rate [mm/min]	50

Interface shear tests

The shear test apparatus, developed originally by Leutner (Leutner 1979), was used here to determine the interlayer shear bonding strength between two pavement layers. Before testing, the shear zone of the samples was marked to be able to put them in the right position between the shear rings. Samples were conditioned in an insulated climate chamber with dimensions 0.6 x 0.5 x 0.6 m. Tests were performed on two-layer cylindrical samples of 150-mm diameter and under a displacement rate of 50 mm/min at 20°C according to CEN/TC 227 WG2 N 879E. According to this norm, there was a gap of 5-mm between the shear rings. The average of two external LVDTs, with a range of ± 10 -mm, was used to measure the shear velocity and the displacement between the shear rings. Five replicate samples were tested for each tack coat.

Fig. 7.5 shows the representative graphs of shear force versus displacement of the two-layer samples bonded with different tack coats. The effect of EA tack coat on bonding the two layers is evident for both application rate cases (i.e., 0.45 and 0.60 kg/m^2). Layers bonded with the EA binder have demonstrated a significantly higher shear strength and a more ductile fracture compared to samples bonded with emulsified tack coats.

According to **Fig. 7.6**, in where the average shear strength plotted versus displacement, the tackless samples showed the lowest average shear strength (0.50 MPa) with the minimum error bar, and the samples bonded with emulsified tack coat shown an improvement (emu-A: 0.97 MPa & emu-B: 0.96 MPa). Therefore, the shear bonding strength values of emulsion-type tack coats are of the same order of magnitude, significantly higher than the tackless system with an approximately 100% increase of strength.

The highest average shear bonding strength was obtained using EA tack coat (EA_0.45 kg/m^2 : 1.76 MPa & EA_0.60 kg/m^2 : 1.82 MPa), which finally did not result in interlayer fracture failure. It can be noticed that almost 200% higher shear bonding strength is obtained using EA binder than the two-layer systems with an emulsion-type tack coat. The use of epoxy-type binder as tack coat improves interlayer bonding for epoxy modified asphalt materials offering a potential solution for interfaces with high shear strength and more ductile response.

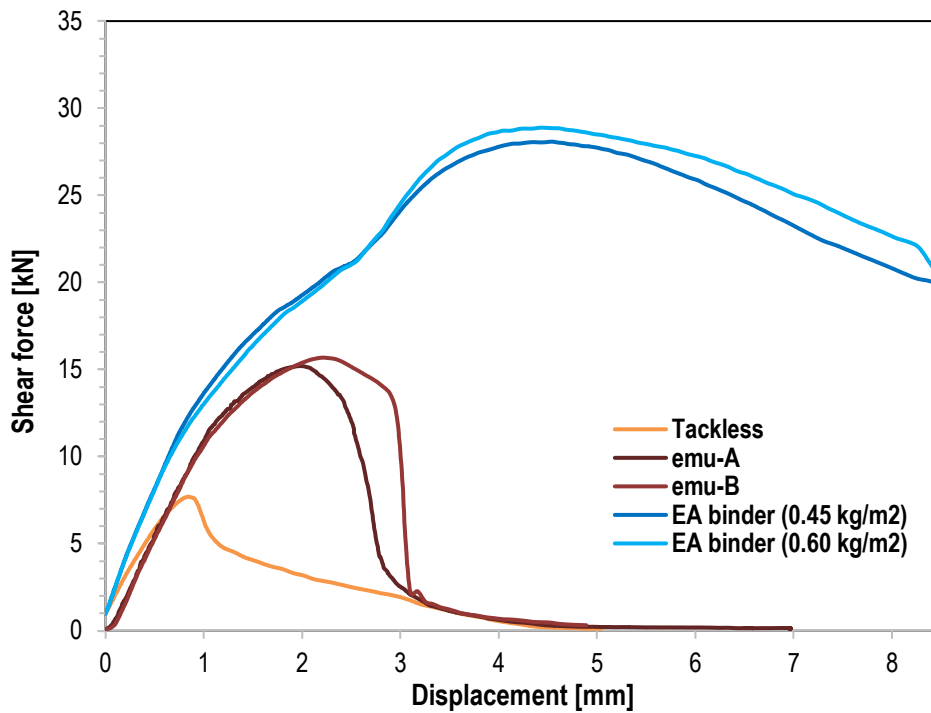


Figure 7.5 Representative shear force versus displacement curves of studied two-layer systems.

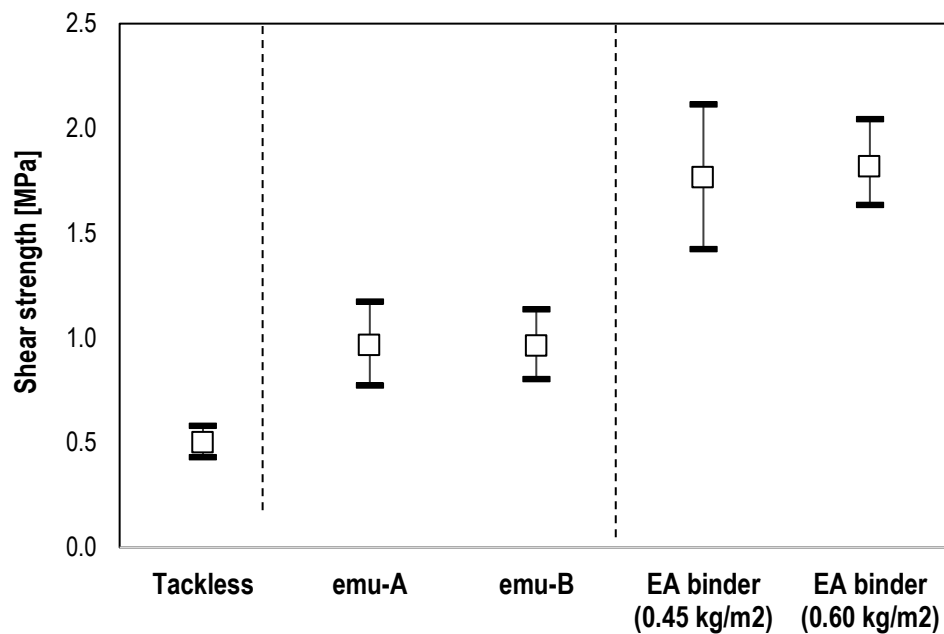


Figure 7.6 Effect of different tack coats on the interlayer shear bonding strength.

7.3.2 Recommendations for field trials

Overall, epoxy-asphalt can also enhance the interlayer shear bonding strength between pavement layers when applied or sprayed with a minimum residual application rate of 0.45 L/m² (Chen et al., 2018) or 0.68 L/m² (ChemCo Systems Inc. 2015). The application rates should be adjusted according to the specific mix design and surface smoothness (Wang et al., 2017). On steel decks, the epoxy-type tack coat serves as waterproofing, but still, an anti-corrosive treatment, such as a zinc silicate (inorganic primer) or a zinc epoxy (organic primer),

is needed (ChemCo Systems Inc. 2015). Note that the epoxy-type tack coat is fully able to bond to clean carbon steel but often in real applications, the steel is subjected to flash rusting which can undermine the potential to bond with any tack coat material. Moreover, as in epoxy modified asphalt surfacing layers, an essential aspect of using an epoxy-type tack coat is the curing time. During curing, covalent chemical bonds are generated between tack coat and contacting layers, and once these bonds are formed, it is very difficult to be broken even at high temperatures (e.g., 300°C and above). However, incomplete curing may occur when the construction temperature is too low. Another aspect that should be considered through the curing process of epoxy-type tack coats is to avoid moisture or humid environments. Usually, water changes the bond rupture site, resulting in possibly incomplete curing of the epoxy binder during construction and thus jeopardizes the build-up of mechanical properties (e.g., strength, stiffness modulus) (Bocci & Canestrari 2013; Jia et al., 2014). The construction conditions for EA materials are highly stringent; the presence of any unexpected factors may result in premature pavement defects, mainly cracking (Wang et al., 2017).

7.4 Summary

In this **chapter**, the epoxy-asphalt binder has been used to enhance asphalt mix's performance and prove that this binder can improve the interlayer bonding capacity between an epoxy modified asphalt and an unmodified one asphalt layer. The significant findings of this study are as follows:

- The laboratory results of performance testing confirm that increasing the epoxy modification level in asphalt leads to stronger and stiffer materials of improved fatigue resistance. The ITT results show that the epoxy modified asphalt mixes have higher tensile strength than control mixes (ESMA-0: 1.28; ESMA-20: 2.02 and ESMA-40: 3.25 MPa), while the 4PB tests demonstrate that the increase of stiffness modulus is accompanied by the proportional increase of the amount of epoxy in asphalt binder (ESMA-0: 8330; ESMA-20: 10490 and ESMA-40: 13910 MPa). The epoxy modification can also enhance the fatigue resistance of asphalt mixes designed for surfacing roadway applications. The epoxy modified asphalt mixes designed in the laboratory for a thin surface layer were produced in-plant, transported to the job site, paved, and compacted.
- The effect of an epoxy-type tack coat on interlayer shear bonding between an epoxy modified mix and an asphaltic substrate was also investigated. Two different emulsion-type tack coats of the same application rate (0.30 kg/m²) and one epoxy binder with two application rates (0.45 and 0.60 kg/m²) have been shear tested in a Leutner configuration. The shear bonding strength with the epoxy binder (≈ 1.82 MPa) was almost 2 and 3.5 times higher than that of emulsion coated (≈ 0.95 MPa) and tackless (0.50 MPa) systems, respectively. The test results confirmed that using an epoxy-type coat could improve the interlayer shear bonding strength, offering monolithic performance characteristics on epoxy modified asphalt pavements.

7.5 References

- Balala B. Studies Leading to Choice of Epoxy Asphalt for Pavement on Steel Orthotropic Bridge Deck of San Mateo-Hayward Bridge. *Highway Research Record* 287, 1969.
- Burns C.D. *Laboratory and Field Study of Epoxy-Asphalt Concrete*. Technical Report 3-368, US Army Engineer Waterways Experiment Station, US Corps of Engineers, 1964.
- Bocci, E., & F. Canestrari. Experimental Evaluation of Shear Resistance of Improved Steel-Asphalt Interfaces. In *Transportation Research Record: Journal of the Transportation Research Board*, No. 2370, TRB, Washington, D.C., 2013, pp. 145-150.
- Canestrari, F., & E. Santagata. Temperature Effects on the Shear Behaviour of Tack Coat Emulsions used in Flexible Pavements. *International Journal of Pavement Engineering* 6(1), 2005, pp. 39-46.
- ChemCo Systems, Inc. *Paving Contractor Information: Application of Epoxy Asphalt Bond (Tack) Coat*. Technical Report, 2015.
- ChemCo Systems, Inc. *Batch Plant Operator Information: Production of Epoxy Asphalt Paving Mix*. Technical Report, 2016a.
- ChemCo Systems, Inc. *Contractor Information: Paving Operation*. Technical Report, 2016b.
- Chen, C., W.O. Eisenhut, K. Lau, A. Buss, J. Bors. Performance Characteristics of Epoxy Asphalt Paving Material for Thin Orthotropic Steel Plate. *International Journal of Pavement Engineering* 21(3), 2020, pp. 397-407.
- Collop, A.C., M.H. Sutanto, G.D. Airey, R.C. Elliott. Shear Bond Strength between Asphalt Layers for Laboratory Prepared Samples and Field Cores. *Construction and Building Materials* 23, 2009, pp. 2251-58.
- CROW. *Standaard RAW Bepalingen*, 2015.
- Dinnen, J., J. Farrington, I. Widyatmoko. Experience with the Use of Epoxy-Modified Bituminous Binders in Surface Courses in England. *Asphalt Professional*, 2020, pp. 14-21.
- Gaul, R.W. Epoxy Asphalt Concrete – A Polymer Concrete with 25 Years' Experience. In *American Concrete Institute Publication Symposium 166(13)*, 1996, pp. 233-251.
- Gaul, R., S. Pence, W. Eisenhut, D. Donald. Accelerated Testing for Fatigue Crack Resistance of Pavement Systems on Orthotropic Steel Bridge Decks. *Proceeding of the GeoHunan Internation Conference*, 2011.
- Herrington, P., & D. Alabaster. Epoxy Modified Open-Graded Porous Asphalt. *Road Materials and Pavement Design* 9(3), 2008, pp. 481-498.
- Herrington, P.R. *Epoxy-modified Porous Asphalt*. NZ Transport Agency Research Report 410, 2010.
- Hicks, R.G., I.J. Dussek, C. Seim. Asphalt Surfaces on Steel Bridge Decks. In *Transportation Research Record: Journal of the Transportation Research Board* 1740, TRB, Washington, D.C., 2000, pp. 135-142.
- Huang, W., Z. Qian, G. Chen, J. Yang. Epoxy Asphalt Concrete Paving on the Deck of Long-Span Steel Bridges. *Chinese Science Bulletin* 48(21), 2003, pp. 2391-94.
- Hulsey, J.L., L. Yang, L. Raad. Wearing Surfaces for Orthotropic Steel Bridge Decks. In *Transportation Research Record: Journal of the Transportation Research Board* 1654, TRB, Washington, D.C., 1999, pp. 141-150.

- International Transport Forum. *Long-life Surfacing for Roads: Field Test Results*. ITF Research Reports, OECD, 2017, Paris, France.
- Jia, X., B. Huang, B.F. Bowers, T.E. Rutherford. Investigation of Tack Coat Failure in Orthotropic Steel Bridge Deck Overlay: Survey, Analysis, and Evaluation. In *Transportation Research Record: Journal of the Transportation Research Board*, No. 2444, TRB, Washington, D.C., 2014, pp. 28-37.
- Joseph, A.H. *Behavior of Epoxy-Asphalt Airfield Pavement, 1963 Inspections*. Technical Report 4-704, US Army Engineer Waterways Experiment Station, US Corps of Engineers, 1965.
- Leng, Z., H. Ozer, I.L. Al-Qadi, S.H. Carpenter. Interface Bonding Between Hot-Mix Asphalt and Various Portland Cement Surfaces: Laboratory Assessment. In *Transportation Research Record: Journal of the Transportation Research Board*, No. 2057, Transportation Research Board of the National Academies, Washington, D.C., 2008, pp. 46–53.
- Leng, Z., I.L. Al-Qadi, S.H. Carpenter, H. Ozer. Interface Bonding Between Hot-Mix Asphalt and Various Portland Cement Concrete Surfaces: Assessment of Accelerated Pavement Testing and Measurement of Interface Strain. In *Transportation Research Record: Journal of the Transportation Research Board*, No. 2127, Transportation Research Board of the National Academies, Washington, D.C., 2009, pp. 20–28.
- Leutner, R. Untersuchung des Schichtenverbundes Beim Bituminosen Oberbau (Investigation of the Adhesion of Bituminous Pavements). *Bitumen 3*, 1979, pp. 84-91.
- Lu, Q., & J. Bors. Alternate Uses of Epoxy Asphalt on Bridge Decks and Roadways. *Construction and Building Materials 78*, 2015, pp. 18-25.
- Luo, S., Q. Lu, Z. Qian. Performance Evaluation of Epoxy modified Open-graded Porous Asphalt Concrete. *Construction and Building Materials 79*, 2015, pp. 97-102.
- Mohammad, L.N., M.A. Raqib, B. Huang. Influence of Asphalt Tack Coat Materials on Interface Shear Strength. In *Transportation Research Record: Journal of the Transportation Research Board*, No. 1789, Transportation Research Board of the National Academies, Washington, D.C., 2002, pp. 56–65.
- Mohammad, L.N., & J. Button. *Optimization of Tack Coat for HMA Placement*. NCHRP Project 9-40. Phase I Report, Louisiana Transportation Research Center, Baton Rouge, 2005.
- Mohammad, L.N., S. Saadeh, Y. Qi, J.W. Button, J. Scherocman. Worldwide State of Practice on the Use of Tack Coats: A Survey. *Journal of the Association of Asphalt Paving Technologists 77*, 2008, pp. 1–26.
- Mohammad, L.N., A. Bae, M.A. Elseifi, J. Button, N. Patel. Effects of Pavement Surface Type and Sample Preparation Method on Tack Coat Interface Shear Strength. In *Transportation Research Record: Journal of the Transportation Research Board*, No. 2190, Transportation Research Board of the National Academies, Washington, D.C., 2010, pp. 93-101.
- Mohammad, L.N., M. Hassan, N. Patel. Effects of Tack Coat Shear Bond Characteristics on Pavement Performance at the Interface. In *Transportation Research Record: Journal of the Transportation Research Board*, No. 2209, Transportation Research Board of the National Academies, Washington, D.C., 2011, pp. 1-8.
- Raab, C., M.N. Partl. Interlayer Bonding of Binder, Base and Subbase Layers of Asphalt Pavements: Long-Term Performance. *Construction and Building Materials 23*, 2009.

- Raposeiras, A.C., D. Castro-Fresno, A. Vega-Zamanillo, J. Rodriguez-Hernande. Test Methods and Influential Factors for Analysis of Bonding between Bituminous Pavement Layers. *Construction and Building Materials* 43(3), 2013, pp. 372-381.
- Romanoschi, S.A. *Characterization of Pavement Layer Interfaces*. PhD dissertation. Louisiana State University, Baton Rouge, 1999.
- Sholar, G., G.C. Page, J.A. Musselman, P.B. Upshaw, H.L. Moseley. Preliminary Investigation of a Test Method to Evaluate Bond Strength of Bituminous Tack Coats. *Journal of the Association of Asphalt Paving Technologists* 73, 2004, pp. 771–801.
- Simpson, W.C., H.J. Sommer, R.L. Griffin, T.K. Miles. Epoxy Asphalt Concrete for Airfield Pavements. *Journal of the Air Transport Division, Proceedings of the American Society of Civil Engineer* 86, 1960, pp. 57–71.
- Tashman, L., K. Nam, T. Papagiannakis. *Evaluation of the Influence of Tack Coat Construction Factors on the Bond Strength between Pavement Layers*. Report WCAT 06-002. Washington Center for Asphalt Technology, Washington State University, Pullman, 2006.
- Touran, A., A. Okereke. Performance of Orthotropic Bridge Decks. *Journal of Performance of Constructed Facilities* 5(2), 1991, pp. 134-148.
- Uzan, J., M. Livneh, Y. Eshed. Investigation of Adhesion Properties between Asphaltic Concrete Layers. *Journal of the Association of Asphalt Paving Technologists* 47, 1978.
- Wang, J., F. Xiao, Z. Chen, X. Li, S. Amirkhanian. Application of Tack Coat in Pavement Engineering. *Construction and Building Materials* 152, 2017, pp. 856-871.
- West, R., J. Zhang, J. Moore. *Evaluation of Bond Strength Between Pavement Layers*. National Center for Asphalt Technology. Report 05-08. Auburn University, Auburn, Ala, 2005.
- Widyatmoko, I., B. Zhao, R.C. Elliott, W.G. Lloyd. Curing Characteristics and The Performance of Epoxy Asphalts. *Proceedings of the Canadian Technical Asphalt Association* 51, 2006.
- Widyatmoko, I., R.C. Elliott. Strength Characteristics and Durability of Epoxy Asphalts. *Proceedings of the Institution of Civil Engineers*, 1300029, 2014.
- Wu, J.P., P.R. Herrington, D. Alabaster. Long-term Durability of Epoxy-modified Open-graded Porous Asphalt Wearing Course. *International Journal of Pavement Engineering* 20(8), 2019, pp. 902-927.

8

Conclusions

8.1 Conclusions

The primary scope of this research was to provide fundamental understanding of curing and oxidative aging of epoxy-asphalt materials together with elucidating their phase behavior characteristics. To accomplish this scope, multi-physics models were developed and demonstrated in the present thesis in an effort to explain the various processes taking place in thermosetting epoxy-asphalt materials. An extensive experimental program has been adapted as well to determine the controlling parameters of curing and oxidation with the goal to guide the design of epoxy-asphalt materials based on fundamental knowledge.

In **Chapter 2**, the thermodynamic considerations regarding the phase behavior of binary binders are discussed on the basis of deploying miscible modified asphalt binders. Microstructure morphological analyses of various epoxy-asphalt binder formulations were also conducted in an atomic force microscopy (AFM) with a view to assess their homogeneity. When a proprietary protected binder was tested in AFM, the microstructure of a single-phase system was revealed with a relatively flat and smooth surface. Nevertheless, the morphological characteristics of binders formulated by simple mixing asphalt binders with epoxy resins were totally different. Asphalt binders with different epoxy proportions have shown limited dispersion of the epoxy phase through asphalt, indicating that such binders were phase separated. These AFM analyses reflect that the epoxy resins are generally immiscible in asphalt binders unless special formulations are used to allow co-association of individual phases. Partially miscible or immiscible binders are phase-separated systems of heterogeneous structures. As phase-separated binders are characterized by weak interfacial adhesion, the interfaces become the weak boundary between the polymer phases, leading mostly to insufficient mechanical properties. This is the reason why commercial epoxy formulations were selected as the case materials for the curing and aging analyses in this research.

In **Chapter 3**, calorimetric measurements were performed in two different epoxy formulations having the proprietary protected binder as a reference. DSC analyses specifically suggest that the proprietary protected binder demanded higher energy levels to initiate the curing process (i.e., the highest activation energy level) although it had higher curing rate than the other binders. The changes of glass transition temperature (T_g) are also shown to relate to the curing level of thermosetting binders. The T_g was shifting to higher temperatures as curing progresses. With the addition of epoxy in asphalt binder, reduction of the evolution rate of the T_g was obtained indicating that the pure epoxy polymers cures faster than the epoxy-asphalt binders. The effect of applied energy on the curing of pure epoxy was more pronounced than of the binders with those epoxy formulations. Furthermore, calorimetric measurements were conducted using the temperature modulated mode, however the exact evolution of the T_g of the thermosetting materials was hard to be obtained since a broad glass transition region was found. The binders were curing, and the glass transition regions were shifting during the temperature modulated calorimetric measurements. Hence, it was concluded that the linear temperature measurement mode is the most effective method to evaluate the curing parameters of binders.

As the epoxy-asphalt binders are thermosetting materials, it is of great importance to elucidate the phenomena that are involved to build-up their rheological properties during curing. Therefore, emphasis was given in **Chapter 4** on simulating the thermo-hardening behaviour of

epoxy-asphalt binders. A model implemented in a multi-physics tool to provide chemorheological predictions by linking the degree of conversion, or crosslinks degree, with the viscosity. Numerical predictions showed the impact of the curing kinetics parameters on the binder hardening. Lower levels of activation energy increase the rate of viscosity development. The curing rate is also highly dependent on the temperature with the increase of temperature the material viscosity increased. In short, the binders of different reactivity characteristics could show different flow responses under certain energy conditions.

Within the same framework, the inter-diffusion phenomena that take place over curing, because of the chemical interfacial interactions between the two contacting phases, were studied in **Chapter 5**. Two different models based on the free-volume theory were tested in a multi-physics tool to simulate the curing induced diffusion, and comparison of these two was performed to assess their effect on simulating the interfacial reactions. The numerical predictions demonstrated especially that lower values of activation energy result in the curing acceleration, as discussed in **Chapter 4**, leading to higher concentrations of newly produced species at the interface. Higher values of diffusion coefficient also lead to lower concentrations of newly produced species at the interface. Based on the analyses reported in **Chapter 5**, species of low diffusion coefficient and activation energy values are proposed to be incorporated in the reactive phases of epoxy-asphalt systems to allow an efficient phases co-association.

Both multi-physics models presented in **Chapter 4** and **5** can be utilized to demonstrate the various chemical and physical processes that involve in curing. Such models can assist in the effort to select the binder constituents and control the quality of binders by reducing the number of experiments.

As the high initial cost associated with the implementation of the epoxy-asphalt technology as pavement surfacing limited its wider use, asphalt binders are typically epoxy diluted to reduce the cost of binders formulated exclusively with epoxy. The idea to dilute the epoxy binder with conventional asphalt binders is not new as it has been adopted already in New Zealand as a feasible method to produce durable pavement materials. In **Chapter 6**, importance was placed on assessing the effect of epoxy on the oxidative aging mechanism of epoxy diluted asphalt binders and mastics. As the aging is accompanied by stiffening and embrittlement, Dynamic Shear Rheometer (DSR) and DSC studies have been performed to assess the oxidation induced compositional dependence of the rheological properties and glass transition of these systems, respectively. To track the oxidation products at different temperatures over time, the Fourier Transform Infrared spectroscopy was used as well providing insight into the chemical changes.

The oxidation of carbon species of epoxy modified asphalt materials was compositional dependent, which happened slowly leading to the conclusion that the incorporation of epoxy compounds in binders results in oxygen-resistant materials. In particular, the oxidation kinetic parameters were determined considering the carbonyl compounds as the aging index in the studied materials, and their incremental values were calculated to estimate the oxidation kinetics parameters based on a simple model. Lower values of activation energy of oxidation accompany in lower values of oxidation rate were exhibited on materials of high epoxy proportions in asphalt binder. The low values of activation energy in modified systems corresponded to more temperature sensitive systems in terms of carbonyls formation comparing

the unmodified ones. Reduction of oxidation sensitivity was demonstrated as well with the fillers in both pure epoxy and asphalt binders. The epoxy modified asphalt mastics were also tested in DSR to provide sufficient data to evaluate the stiffening effect due to oxidation. Mastics of higher epoxy proportions have shown higher stiffness and elasticity over oxidation.

Materials became glassier and thus more brittle over oxidation. The effect of oxidation on the T_g of epoxy-asphalt materials was studied, and the deviation of T_g values from the ideal mixing rule was assessed to evaluate the glass forming tendency. The contribution of entropy of mixing to the composition dependence of glass transition in epoxy modified asphalt was assessed giving special emphasis on the T_g deviation from the ideal mixing rule. A large and positive deviation of epoxy modified asphalt binders was observed, which was becoming more pronounced over oxidation. The T_g values of mastics were also higher than of binders with the same epoxy proportions. Another finding was that the continuous decrease of entropy of mixing caused the appearance of large positive deviations of T_g in the systems with the increase of oxidation time lengths.

In **Chapter 7**, the epoxy modified asphalt has been used to enhance the durability of a stone mastic asphalt mix, and to prove that the epoxy binder can improve the interlayer bonding capacity between two asphalt layers. The laboratory results of durability and performance testing confirmed that the increase of the epoxy proportion in asphalt led to stiffer and stronger surfacing mixes of high fatigue life. The use of epoxy binder as tack coating was explored as well by evaluating the interface shear strength of two-layer samples. The results of shear bonding indicated that the epoxy tack coat improves interlayer bonding for epoxy modified asphalt materials offering a potential solution for interfaces with high shear strength and more ductile response. Finally, insight and recommendations for the large-scale applications of epoxy modified asphalt mixes were discussed.

This thesis contributes to elucidate the factors that determine the curing and oxidation induced changes of chemical composition, physical and rheological properties of epoxy-asphalt materials which are utilized for flexible pavements. The modelling and experimental programs discussed throughout the thesis can help to provide the fundamental knowledge to design and develop new binders and binding systems of the desired properties and characteristics.

Summary

Pavements of enhanced longevity would be expected to withstand long-term traffic as well as varying environmental conditions reducing in this way the major maintenance needs. Considering also the adoption of long-term contracts by road authorities, long-life pavements have started to attract the interest of road contractors worldwide. New and relatively new binders specially designed to produce long-life pavements have been proposed to minimize the regular maintenance and reconstruction operations. Among others, one promising technology to reach this goal is the epoxy modified asphalt binder, or epoxy-asphalt.

Nevertheless, the addition of epoxy resins to asphalt binders may result in materials of inferior properties. Thermosetting epoxy resins may not mix homogeneously in asphalt binders leading to immiscible or partially miscible binders, which are mostly phase-separated materials. The phase-separated epoxy-asphalt binders can become brittle and thus more prone to cracking, leading the pavements to fail. Only a few epoxy products are applicable in asphalt binders, and the knowledge of incorporating chemistry to develop miscible epoxy binders remains unknown. For this to be the case, this thesis aims to provide a fundamental approach to elucidate the chemical and physical processes that determine the phase behavior of these binders.

A vital role in implementing the thermosetting epoxy-asphalt binders also plays the curing. To obtain fundamental insights into the material curing, multi-physics models and experimental methods are considered in this research to identify and assess the curing-induced changes of epoxy-asphalt. The development of rheological properties that reflect the material workability is determined by laboratory experiments and used as input to multi-physics simulations.

As the ultimate scope of implementing the epoxy-asphalt is to increase the longevity of pavements, the oxidation-induced changes of epoxy-asphalt materials as a function of time are evaluated as well in this research to prove their high aging resistance for wearing courses. Within the same framework, emphasis is also given to the effect of epoxy-asphalt on the durability and mechanical performance characteristics of an asphalt concrete mix.

In conclusion, this thesis contributes to elucidating the factors that determine the curing- and oxidation-induced changes of epoxy-asphalt and understanding what bears miscible binders. The modeling and experimental programs discussed throughout the thesis can help to provide the fundamental knowledge to design and develop new binders and binding systems of the desired properties and characteristics.

Curriculum Vitae

Panagiotis Apostolidis

1989 Born in Drama, Greece

2007-2012 Master of Engineering, School of Civil Engineering, Aristotle University of Thessaloniki

2013-2015 Master of Science, Civil Engineering and Geosciences, Delft University of Technology

since 2016 Research Engineer, Pavement Engineering Section, Delft University of Technology

2018-2022 Doctor of Philosophy, Civil Engineering and Geosciences, Delft University of Technology

Propositions

Chemo-mechanics of epoxy-asphalt of Panagiotis APOSTOLIDIS

1. A comprehensive understanding of the asphalt modification technologies is critical to protect the global roadway network for the decades to come. The epoxy-asphalt can be considered as a model binder for the roadway pavements of the future.
This proposition pertains to this dissertation [Chapter 8]
2. Roadways were primarily designed and built for the climatic conditions of the past. Nowadays, intense heatwaves and storms deteriorate the roadways faster, causing disasters of billion dollars losses. This situation is exacerbated by climate change.
3. The key for tuning the properties of asphalt binders is in asphaltenes.
4. An important part of being a PhD in engineering is to keep the gap between theory and practice as small as possible.
5. As people live longer, they are going to work 30, 40, 50 years or even longer. The education infrastructure should be prepared to cultivate the future workforce to develop more than one careers in a lifetime.
6. The ever-increasing inter-disciplinarity of the research enterprise demands more inter-agency collaborations within and across national borders.
7. Every change needs time to mature.
8. ‘More the knowledge - lesser the ego, lesser the knowledge – more the ego.’
Albert Einstein

These propositions are regarded as opposable and defensible, and have been approved as such by the promoters Prof.dr.ir S.M.J.G. Erkens and Prof.dr. A. Scarpas, and copromotor Dr. X. Liu.